Diploma Thesis IST-3.14

Geometric Analysis of the Formation Control Problem for Autonomous Robots

Florian Dörfler

Supervisor: Bruce Francis

University of Toronto

Systems Control Group (SCG)

Prof. Ph.D. M.Eng. B. Francis

University of Stuttgart

Institute for System Theory and Automatic Control (IST)

Prof. Dr.–Ing. F. Allgöwer

August 1, 2008

Erklärung

Ich erkläre hiermit, dass ich diese Diplomarbeit selbstständig verfasst, keine anderen als die angegebenen Hilfsmittel benutzt, sowie wörtliche und sinngemäße Zitate als solche gekennzeichnet habe.

Toronto, den 1. August 2008

Abstract

This thesis considers the formation control problem for autonomous robots, where the target formation is specified as an infinitesimally rigid formation. A general control law based on potential functions is derived from a directed sensor graph. The control law is distributed and relies on sensory information only. The resulting closed-loop dynamics contain various invariant sets and the stability properties of these sets are analyzed with Lyapunov set stability theory and differential geometric considerations.

By methods of inverse optimality a certain class of sensor graphs is identified, which is related to a cooperative behavior among the robots. These graphs are referred to as cooperative graphs, and undirected graphs, directed cycles, and directed open chain graphs can be identified as such graphs. Cooperative graphs admit a local stability result of the target formation together with a guaranteed region of attraction, which depends on the rigidity properties of the formation.

Moreover, in order to show instability of the undesired equilibria of the robots' closed-loop dynamics, a local stability and instability theorem is derived for differentiable manifolds. This theorem allows us to perform a global stability analysis for the benchmark example of three robots interconnected in a directed, cyclic sensor graph.

Kurzfassung

Die vorliegende Diplomarbeit beschäftigt sich mit dem Formationsproblem für autonome Roboter wobei die Zielformation als infinitesimal starre Formation vorgegeben wird. Ein allgemeines Regelgesetz basierend auf Potential Funktionen wird von einem gerichteten Sensorgraph abgeleitet. Dieses Regelgesetz ist verteilt und hängt nur von lokal zugänglichen Informationen ab. Die daraus resultierende Dynamik des geschlossenen Regelkreis beinhaltet verschiendene invariante Mengen deren Stabilitätseigenschaften mit Hilfe von Lyapunov Theorie für Mengen und mittels differentialgeometrischen Betrachtungen analysiert werden.

Mittels Methoden der inversen Optimalität wird eine Klasse von Sensorgraphen identifiziert, die ein kooperativen Verhalten der Roboter wiederspiegelt. Diese Graphen werden als kooperative Graphen bezeichnet und sowohl ungerichtete Graphen als auch gerichtetet zyklische Graphen und gerichtete offene Ketten können als solche identifiziert werden. Kooperative Graphen erlauben die Herleitung eines lokales Stabilitätsergebnis der Zielformation zusammen mit einem garantierten Einzugsbereich, der wiederum von den Starrheitseigenschaften der Formation abhängt.

Desweiteren, um Instabilität der ungewollten Ruhelagen des geschlossenen Kreises zu zeigen, wird ein lokales Stabilitäts- und Instabilitätstheorem für differenzierbare Mannigfalten hergeleitet. Dieses Theorem erlaubt es uns eine globale Stabilitätsanalyse für das Standardbeispiel von drei Robotern verbunden durch einem zyklischen Sensorgraph durchzuführen.

Acknowledgements

It is impossible to overstate my gratitude to my advisor Bruce Francis. I did not only get great research assistance and learned many skills from him, but also received wisdom about life in all perspectives. Under his guidance I made big progress both personally and academically and it has been simply a great time and a joy to work together with him.

I would like to thank all the people of the Systems Control Group at the University of Toronto. I received great support and technical advice from various group members and altogether they made my stay at the University of Toronto a very pleasant, joyful and productive time. I am also most thankful to the people who educated and supported me at the University of Stuttgart. Among others at the University of Stuttgart, I would like to acknowledge especially Prof. Frank Allgöwer and Prof. Michael Zeitz, who made it possible for me to spend one year at the University of Toronto

My greatest thanks goes to my family, my girlfriend Katrin and all my friends in Germany who helped and supported me during my one year adventure in Canada. I do not want to forget all the new and close friends that I made in Toronto, who accompanied me on various trips all over my host country and who made my year in Canada an unforgettable time.

Finally I would like to thank the Ontario/Baden-Württemberg Student Exchange Program and the Landesstiftung Baden-Württemberg, who organized my stay at the University of Toronto and who supported me financially.

Contents

Chapter 1

Introduction

Human beings have witnessed examples of collective behavior by groups of insects, schools of fish, herds of animals or flocks of birds since time immemorial. Such a behavior has arisen evolutionarily to permit sophisticated behavior of the group that would never be achievable by single members of the group. The behavior may serve the needs of defense against predators, or aggression against prey, of foraging for food, of mating, etc. Some creatures, fish and birds particularly, as part of their group behaviour, often display formation type behavior; in this sort of behavior while the whole formation moves as a cohesive whole, the relative positions of the fish or birds are preserved.

These remarkable biological phenomena have attracted human researcher ever since. The technology arising in the last 20 years made it possible to artificially imitate the behavior of of flocks of birds [1], fish schools [2], herds [3], insect swarms [4], and groups of people [5, 6], just to mention a few of various examples. The probably most famous artificial imitation of group behavior is Reynolds' distributed behavioural model "boids" [7]. The boids (or bird-oids) each obey a set of local interaction rules, which together result in a natural and appealing steady-state flocking behaviour for the group.

To some degree nature has probably been a conscious or unconscious motivator for human kind. Inspired by phenomena of nature researchers today try not only to understand and imitate the underlying mechanisms in biological systems, but also transfer them to technical systems. Today recent advances in communication and computation make it possible that

formations of robots, underwater vehicles and autonomous airborne vehicles are slowly being deployed to tackle problems in both civilian and defense spheres-for example, bush fire control, surveillance, mining, underwater exploration and the like.

1.1 Literature Review

Over the last years, the problem of coordinating the motion of multiple autonomous robots, has attracted significant attention. The robots are not controlled by a central unit and their behaviour is based exclusively on the local information that is provided by their sensors and the communication with their neighbouring robots. Among the numerous potential applications of such coordinated action through ad-hoc networks are search and recovery operations, manipulation in hazardous environments, exploration, surveillance, distributed sensing etc. All of these tasks hard or even impossible when carried out by a single robot, for example the surveillance of a wide area. Further advantages of solving a task by multiple autonomous robots compared to one central unit are the robustness of the overall system to failure of single robots or communication links, the ability of robots to adapt to the environment without centralized observation or computation, and the comparably low cost for sensor and communication.

The simplest task we can think of for autonomous robots is to meet at a common point. This is the so-called *rendezvous* problem [8, 9], which has, for example, been solved using pursuit strategies [10, 11] and the *circumcenter algorithm* [12, 13]. The opposite problem is referred to as *coverage control*. Here the robots should spread out in order to cover and surveil a certain area. This problem has first been solved in [14] using the concept of Voronoi cells. Since then coverage control has been extended into various directions and the most recent references include sensors with limited range [15] and an extension to a hybrid control algorithm applied to kinematic unicycles [16].

Another important aspect of motion coordination of a group of autonomous robots is

called *formation control*. The robots' task is to reach or maintain a certain formation, such as a line or a polygon, with only local information available. If each robot has an onboard Global Positioning System (GPS) device and there is an omniscient supervisor, then such a problem is routine: Each robot is simply assigned a location specified by global coordinates and stabilized to this location. However, this requires expensive sensors and communication devices for each robot and additionally the use of GPS has several problems: The precision of GPS depends on the number of satellites currently visible,. Thus in urban areas, under dense vegetation and during cloudy periods the GPS' precision may be very poor. In certain cases, such as mining or underwater robots, GPS it is not available at all.

These problems in obtaining global coordinates make it natural to study formation control in a distributed way, where each robot is only equipped with an onboard camera and can thus sense only the distance and heading relative to its neighbouring robots. Thus the action of one robot depends severely on the fact which other robots it is looking at. The resulting topology of information exchange between the robots is formalized in a so-called sensor graph.

There exists a vast literature on properties of the sensor graph including necessary conditions on directed and undirected graphs [17], time-varying sensor graphs [18], so-called rigid graphs [19, 20] and graph properties in three dimensional setups [21]. A non-technical survey over various research directions in formation control is given in [22]. Depending on this graph a formation control law for each robot are derived. Typically a potential function is constructed for each robot and each robot's control law is then obtained as a gradient control. Such an approach has first been undertaken for undirected graphs by Olfati-Saber [20] and Tanner [23] and more recently also by Arcak [24] and Smith [25]. The typical result of these references is that under the gradient control the robots will converge to a formation, where the potential function take their minimum value.

The work of Olfati-Saber [20] and Eren [19] shows that, if the desired target formation is described by a certain geometric configuration and the sensor graph is undirected, then a necessary graphical condition for the stability of this geometric configuration is a property called infinitesimal rigidity. In case of a directed graph an additional necessary graphical condition called constraint consistence has been introduced by Hendrickx [17].

Recently Krick [26] showed that infinitesimal rigidity is also a sufficient condition for local asymptotic stability of the target formation when specified by an undirected graph. Reference [26] also extends this result to acyclic directed graphs, which are infinitesimally rigid and constraint consistent. These remarkable results are only locally valid and their proofs are based on linearization and center manifold theory. In a global stability analysis various invariant sets of the robots' closed-loop dynamics have to be considered additionally.

A global stability analysis has so far only been performed for three robots which should form a triangle. This setup can be seen as a benchmark example in the formation control literature and has been explicitly addressed in various works, for example, with a directed cyclic sensor graph in [27, 28, 29], with an acyclic directed graph in [30] and with an undirected graph in [25, 24]. Also the work of the earlier mentioned references is applicable to this example. However, only Cao's [27, 28, 30] and Smith's [25] work solve the global stability problem rigorously, both in different ways.

In the author's personal opinion Krick's work [26] addressing the infinitesimal rigidity of the target formation is the best approach so far in the field of formation control and should be combined with Cao's [27, 28, 30] and Smith's [25] global stability proofs.

Before we address the contribution of the present work, we would like to point out the difficulties arising in a global stability analysis in a simple tutorial example.

1.2 Illustrative Example

The following tutorial example introduces the reader to the notation and the problem setup of formation control and points out the main difficulties arising in the stability analysis.

Example 1.2.1. Consider two wheeled robots that are fixed on a line and able to move along it. The two robots are labeled as robot 1 and robot 2 and are both modeled as simple one dimensional kinematic points with the dynamics

$$\dot{z}_1 = u_1 \tag{1.1}$$

$$\dot{z}_2 = u_2\,, \tag{1.2}$$

where $z_1, z_2 \in \mathbb{R}$ are the positions of the robots on the line and $u_1, u_2 \in \mathbb{R}$ are direct velocity commands that are used as control inputs to steer the robots. The setup is illustrated in Figure 1.1. The robots are equipped with no other sensors than onboard cameras and have

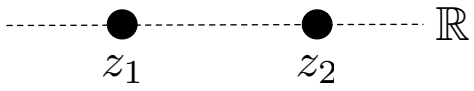

Figure 1.1: Two one dimensional kinematic points

no GPS or any communication devices. Thus each robot has only local sensory information, that is, robot 1 can see robot 2 and vice versa. This setup is formalized in the so-called *sensor graph* $\mathcal{G}$, which is illustrated in Figure 1.2. The nodes 1 and 2 of the graph $\mathcal{G}$ correspond to the robots, the directed edge e_1 from 1 to 2 means that robot 1 can sense robot 2, and the edge e_2 has the analogous meaning. If robot 1 sees robot 2, then it can see the direction and relative distance to robot 2, that is, it can sense the relative position $z_2 - z_1$; similarly for robot 2.

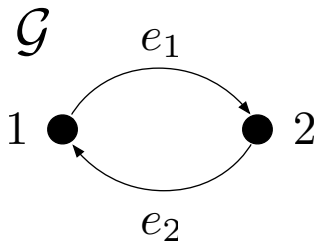

Figure 1.2: Sensor graph $\mathcal{G}$ associated with Example 1.2.1

The robots should now perform a task that we denote as *formation control*, that is, the two robots should move to a stationary position where they are a specified distance $d > 0$ apart and to do so each robot is allowed to use only the information given by its camera. Although this task seems to be a fairly easy problem its solution will turn out to be not trivial. If we use the concatenated vectors $z = [z_1, z_2]^T$ for the state and $u = [u_1, u_2]^T$ for the control input, the equations (1.1)-(1.2) can be written compactly as $\dot{z} = u$ and with this notation the formation control problem can be formulated as follows:

Problem. *Formation control of two kinematic points:*
Given the dynamics $\dot{z} = u$, the graph $\mathcal{G}$, and a specified distance $d > 0$, find control laws u_1 and u_2 such that

(i) $u_1 = u_1(z_2 - z_1)$, $u_2 = u_2(z_1 - z_2)$

(ii) $z(t) \underset{t\to\infty}{\to} \mathcal{E}_z := \{ z \in \mathbb{R}^2 |\ |z_2 - z_1| = d\}$

(iii) $z(t) \underset{t\to\infty}{\to}$ *const.*

Note that the conditions *(ii)* and *(iii)* could have also been lumped together by saying that a trajectory $z(t)$ converges for $t \to \infty$ to some finite point $z_* \in \mathcal{E}_z$, where z_* is not necessarily unique and might depend on the initial condition $z(0)$. For example, if robot 1 starts left of robot 2 then, under a certain control, the two robots approach a point z_* where they have the desired distance d. Assume their initial positions are exchanged and possibly also translated, then the robots will probably also converge to a point where they are a distance d apart, but this point is not necessarily the same z_*. The reason why the stability problem $z(t) \underset{t\to\infty}{\to} z_* \in \mathcal{E}_z$ is split up in *(ii)* and *(iii)* is that the analysis of these two points is severely different as the reader will see in this example. Another issue is that the formation control problem might not be solvable for all initial conditions $z(0) \in \mathbb{R}^{2n}$. Our task is then to find the maximum region of attraction from which a trajectory $z(t)$ converges to $\mathcal{E}_z$.

Typically a potential function approach is used to construct a control law that is capable of solving the formation control problem. For each robot a potential function is constructed which has the property that it is zero whenever the robot has the desired distance from the other and it is positive otherwise. Such a potential function can be interpreted as a cost that the robot has to pay if it does not satisfy its distance constraint. For simplicity we choose the smooth potential functions

$$\Phi_1(z) = \frac{1}{4}\left(|z_2 - z_1|^2 - d^2\right)^2 \tag{1.3}$$

$$\Phi_2(z) = \frac{1}{4}\left(|z_1 - z_2|^2 - d^2\right)^2 . \tag{1.4}$$

From the heuristic argument that each robot wants to minimize its cost, we apply the *steepest descent control law*

$$u_i \;=\; -\frac{\partial}{\partial z_i}\,\Phi_i(z) \tag{1.5}$$

which makes sure that each robot minimizes its potential function. The resulting *z-dynamics* under this control law are

$$\begin{bmatrix}\dot{z}_1\\ \dot{z}_2\end{bmatrix} \;=\; \begin{bmatrix}(z_2-z_1)\,\left(|z_2-z_1|^2-d^2\right)\\ (z_1-z_2)\,\left(|z_1-z_2|^2-d^2\right)\end{bmatrix} \;=\; \begin{bmatrix}u_1(z_2-z_1)\\ u_2(z_1-z_2)\end{bmatrix}. \tag{1.6}$$

The control inputs u_i indeed satisfy condition *(i)* and can be interpreted as follows: The velocity vector of each robot is always directed towards the other one, which means that they are pursuing each other, and the speed by which they do this depends on their distance. They are pushing away from each other if they are too close and they approach each other if they are too far apart. The equilibria of the z-dynamics are unfortunately not only constituted by the points where the robots meet their distance constraint, that is, $z \in \mathcal{E}_z$, but also by the points where the robots are collocated, that is,

$$z \in \mathcal{X}_z := \left\{ z \in \mathbb{R}^2 \middle|\; z_2 = z_1 \right\}. \tag{1.7}$$

The state space, containing the sets $\mathcal{E}_z$ and $\mathcal{X}_z$, is illustrated in Figure 1.3. It can be seen that $\mathcal{E}_z$ is the union of two disjoint sets, one where robot 1 is a distance d to the left of robot 2 and also the other way round. Furthermore, the sets $\mathcal{E}_z$ and $\mathcal{X}_z$ have infinite extent and are thus not compact. This is because these sets are defined by the relative distance of the robots and not by their exact positions. Thus all possible translations are included in the problem setup and therefore we end up with non-compact sets.

Besides specification *(iii)* we are actually interested only in the relative positions of the robots. Therefore we try to reformulate and solve stability problem *(ii)* in terms of relative positions. Let us associate these with the edges e_1 and e_2 of the sensor graph $\mathcal{G}$, that is,

$$\begin{bmatrix}e_1\\ e_2\end{bmatrix} \;=\; \begin{bmatrix}z_2-z_1\\ z_1-z_2\end{bmatrix} \;=\; \begin{bmatrix}-1 & 1\\ 1 & -1\end{bmatrix}\begin{bmatrix}z_1\\ z_2\end{bmatrix}. \tag{1.8}$$

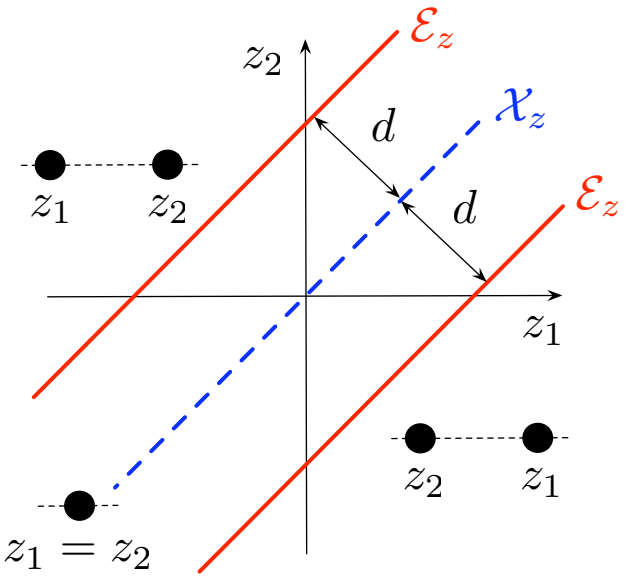

Figure 1.3: The state space of Example 1.2.1

Let us for simplicity say that e_1 and e_2 are *links* whether we are referring to the edges of the graph or to the relative positions. The matrix appearing in (1.8) relating the links to the positions is called the *incidence matrix* of the graph $\mathcal{G}$ and will be abbreviated by the symbol H. With the concatenated vector $e = [e_1, e_2]^T$ equation (1.8) in vector form is simply $e = H\, z$ and we define the *link space* as $H(\mathbb{R}^2)$, namely, the image of $\mathbb{R}^2$ under H. The matrix H is square and has a nontrivial kernel, namely $\ker(H) = \operatorname{span}\left\{[1,1]^T\right\}$. Therefore the links are not independent. The link space has the underlying algebraic constraint $e_1 + e_2 = 0$. Let us map the state space to the link space $H(\mathbb{R}^2)$ and denote the sets $H(\mathcal{E}_z)$ and $H(\mathcal{X}_z)$ by

$$\mathcal{E}_e := H(\mathcal{E}_z) = \left\{e \in H\left(\mathbb{R}^2\right) \middle|\ |e_1| = d\right\} \tag{1.9}$$

$$\mathcal{X}_e := H(\mathcal{X}_z) = \left\{e \in \mathbb{R}^2 \middle|\ e_1 = 0\right\}. \tag{1.10}$$

This map is illustrated in Figure 1.4. The map H factors out all translations, that is $\operatorname{span}\left\{[1,1]^T\right\}$, and we are left over with the compact sets $\mathcal{E}_e$ and $\mathcal{X}_e$. The link space $H(\mathbb{R}^2)$ itself is the line defined by $e_1 + e_2 = 0$ and is a subspace. The resulting dynamics in the link space are by definition $\dot{e} = H\,\dot{z}$. Since the right-hand side of the z-dynamics depends only on

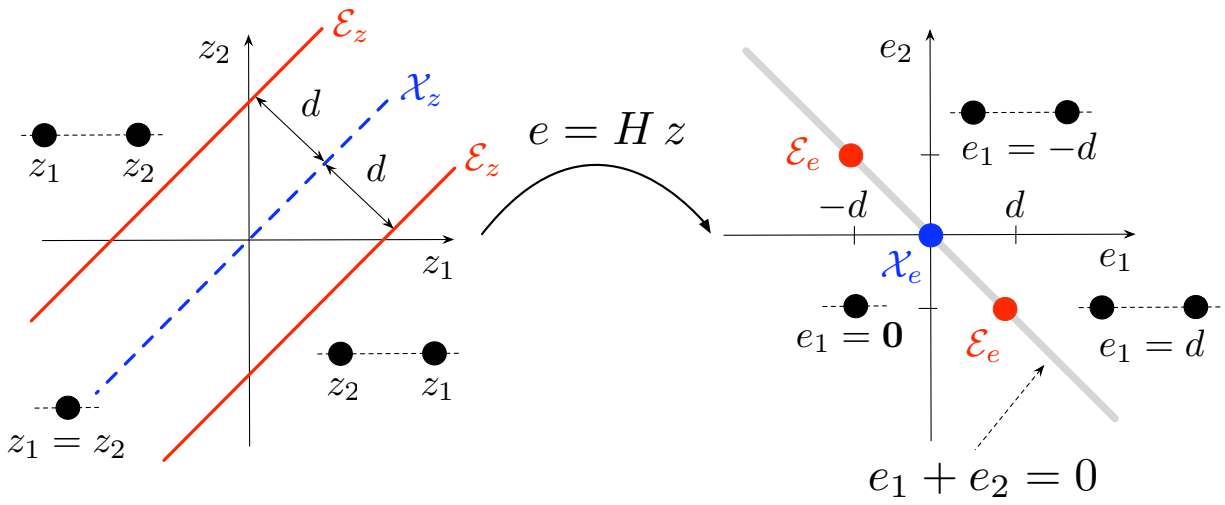

Figure 1.4: Map H from state space to link space

the relative distance, the *link dynamics* are obtained as the self-contained dynamical system

$$\begin{bmatrix} \dot{e}_1 \\ \dot{e}_2 \end{bmatrix} = \begin{bmatrix} e_2 \left(|e_2|^2 - d^2\right) - e_1 \left(|e_1|^2 - d^2\right) \\ e_1 \left(|e_1|^2 - d^2\right) - e_2 \left(|e_2|^2 - d^2\right) \end{bmatrix}, \tag{1.11}$$

which evolves on the line $e_1 + e_2 = 0$.

Instead of analyzing the behavior of the z-dynamics we rather analyze the link dynamics because their equilibria $\mathcal{E}_e$ and $\mathcal{X}_e$ are compact and they admit a Lyapunov based stability analysis. An obvious Lyapunov function candidate in order to prove stability of $\mathcal{E}_e$ is given by the sum of the two potential functions when the links are taken as arguments:

$$\begin{aligned} V: \quad & H\left(\mathbb{R}^2\right) \to \mathbb{R} \\ V(e) = & \frac{1}{4}\left(|e_1|^2 - d^2\right)^2 + \frac{1}{4}\left(|e_2|^2 - d^2\right)^2 = \begin{cases} = 0 & \forall\, e \in \mathcal{E}_e \\ > 0 & \text{else} \end{cases} \end{aligned} \tag{1.12}$$

Due to compactness of the set $\mathcal{E}_e$ the level sets $V^{-1}(c) := \{e \in H\left(\mathbb{R}^2\right) |\ V(e) = c\}$ are also compact sets. The derivative of $V(e)$ along trajectories of (1.11) yields

$$\dot{V}(e) = -\Big(e_1 \left(|e_1|^2 - d^2\right) - e_2 \left(|e_2|^2 - d^2\right)\Big)^2 \tag{1.13}$$

$$= \begin{cases} = 0 & \forall\, e \in \{\mathcal{E}_e \cup \mathcal{X}_e\} \\ < 0 & \text{else}\,, \end{cases} \tag{1.14}$$

which is clearly negative semidefinite. Because of this and because the level sets $V^{-1}(c)$ are compact we can conclude existence, uniqueness, and stability for the link dynamics. In a standard Lyapunov analysis we would now invoke the invariance principle and conclude that $e(t)$ converges to either $\mathcal{E}_e$ or $\mathcal{X}_e$, which are the two equilibria of the link dynamics. However we cannot prove attractivity of the set $\mathcal{E}_e$ by standard methods, and the open question is whether a convergence to $\mathcal{X}_e$ can be ruled out and, if so, how this can be done. Let us sketch two possible solution schemes for how to go on.

One solution approach might be to exploit the redundancy of the link dynamics since e_1 and e_2 are coupled via $e_1 + e_2 = 0$. If we solve for $e_2 = -e_1$ we can reduce the link dynamics to a scalar nonlinear differential equation. This is illustrated in Figure 1.5. The remaining

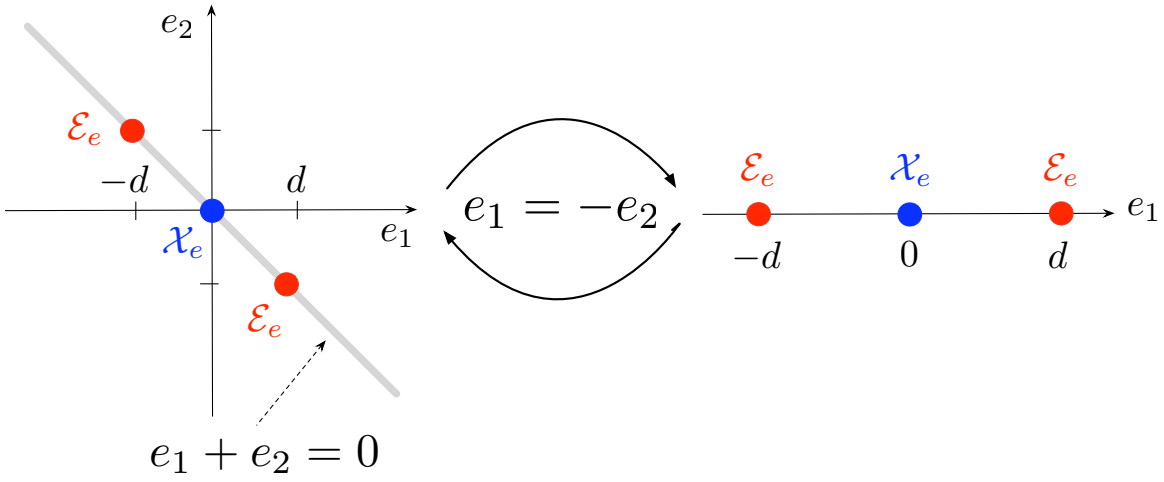

Figure 1.5: Reduction of the link dynamics

dynamics then are

$$\dot{e}_1 \;=\; -2\,e_1\,\left(|e_1|^2 - d^2\right) \tag{1.15}$$

and the stability can be analyzed either by linearization or graphically in the $(e_1, \dot{e}_1)$-diagram shown in Figure 1.6. The obvious result then is that $\mathcal{X}_e$ is an unstable equilibrium and $\mathcal{E}_e$ consists of two stable equilibria, with regions of attraction $e_1 \in (0, \pm\infty)$. This shows that the robots cannot cross $\mathcal{X}_e$, that is spoken loosely, "jump above each other." However it is

questionable whether or not a model reduction might be advantageous in a more complicated example where the reduced model is not a scalar differential equation.

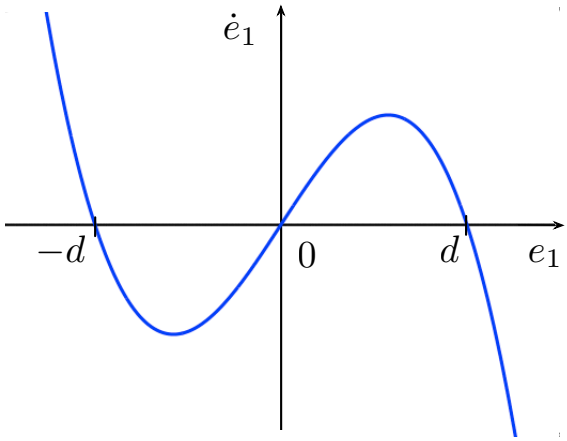

Figure 1.6: $(e_1, \dot{e}_1)$-diagram of the reduced link dynamics

Another solution approach might be an extension of the prior Lyapunov based approach. Although the Lyapunov method did not yield a satisfying stability result, it can still be used to derive a local result. Consider a sublevel set

$$\Omega(c) \quad = \quad \left\{ e \in H\left(\mathbb{R}^2\right) \,|\, V(e) \leq c \right\} \tag{1.16}$$

where c is small enough such that $\Omega(c)$ excludes the set $\mathcal{X}_e$. Such a level set is illustrated in Figure 1.7. Note that $\Omega(c)$ is invariant and that for every initial condition within $\Omega(c)$ the derivative $\dot{V}(e)$ is zero if and only if $e \in \mathcal{E}_e$. Therefore the set $\mathcal{E}_e$ is locally asymptotically stable. However this result is only local and a global stability result could be obtained if we can show that the vector field is always pointing away from $\mathcal{X}_e$ as illustrated on Figure 1.7. For our example this can of course be verified by plotting the vector field in the link space.

Assume we can prove by one of the two prior approaches that the link dynamics indeed converge to $\mathcal{E}_e$. This implies that the robots converge to the desired formation. But then we are still left over with showing property *(iii)* of the control, namely that the robots

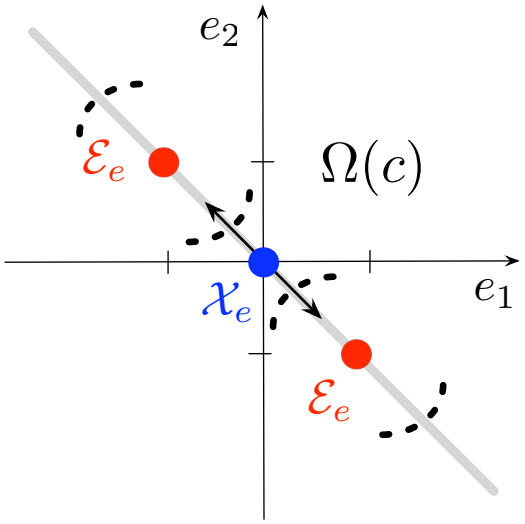

Figure 1.7: Idea for a local and global stability result to Example 1.2.1

actually stop and do not slide along the real axis. Since convergence of the links implies only that the *point-to-set distance* to $\mathcal{E}_z$ converges to zero, one of two possible cases can happen. Either the positions converge to stationary values or the they do not. Two possible trajectories illustrating the two cases are shown in Figure 1.8. For both the solid and the dotted trajectory the point-to-set distance to $\mathcal{E}_z$ is converging to zero, but only the solid trajectory converges to a finite point in $\mathcal{E}_z$.

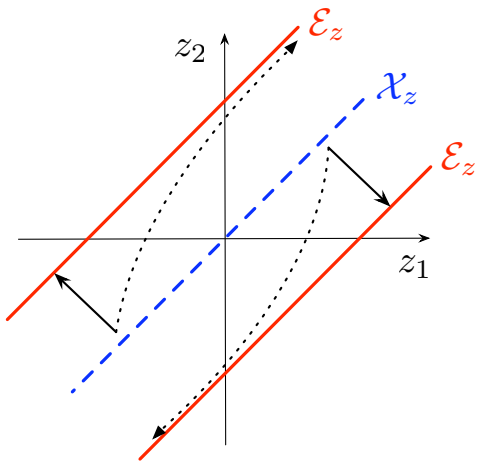

Figure 1.8: Possible behavior of solutions which are converging to $\mathcal{E}_z$.

In our example the state space is two dimensional and the *vector field*, the right hand side of the dynamics (1.6), is always orthogonal to span $\left\{[1,1]^T\right\}$. The trajectories are always tangential to the vector field and thus parallel to the vector $[-1,1]^T$. Therefore trajectories approach the equilibrium set $\mathcal{E}_z$ orthogonally as shown by the solid line in Figure 1.8. The final conclusion after this extensive stability analysis is that the gradient control (1.5) solves the formation control problem iff the the two robots are initially not collocated.

Example 1.2.1 introduced the reader to the formation control problem and showed that the solution to an apparently simple problem is by no means not straightforward. In fact, the example was only solvable because of the low dimension of the state which gave us the necessary geometric insight, and allowed us to plot the invariant sets of the closed loop dynamics and the vector field. It is indeed questionable whether a higher dimensional example involving more than two robots with two dimensional coordinates might be solvable.
However we have gained some insight from this example, namely first of all, that a potential function based control law might indeed be a suitable solution to a formation control problem. Furthermore, we have seen that the analysis in the link space was superior to an analysis in the state space, because the equilibrium set $\mathcal{E}_e$ was compact and additionally the potential functions served as Lyapunov functions and admitted a local stability result. The main obstacle in the analysis were the multiple equilibria for which a convergence could not be ruled out by standard methods. In the very end, after having proved the stability of the formation, we were left over with showing that the robots indeed converge to stationary points. Another possible obstacle, which we did not encounter in Example 1.2.1, might be that each equilibrium has a stable manifold and a certain region of attraction which complicates a global stability analysis. Furthermore, the specific choice of the potential functions was somewhat arbitrary and additional features such as an repulsive behavior between the robots could be considered.

This example actually leaves us with more questions than it answers. But after all we have now some intuition and look at a more general setup with an arbitrary number of robots

in the plane. In a general setup we still face the same problems but now lack the geometric insight to the formation control problem. Additionally the formation control problem might not be solvable for any arbitrary sensor graph and the solvability of the problem might depend heavily on initial positions of the robots.

1.3 Contribution of the Thesis

In this work the target formation is specified as an infinitesimally rigid and constraint consistent formation. In the spirit of [26] a potential function based gradient control law is derived for a general directed sensor graph. The resulting closed-loop dynamics have a compact form and depend only on matrices related to the sensor graph.

The formation control problem is not approached in the space of the positions of the robots, but in the space of relative positions given by the links of the sensor graph. In this space the formation control problem is illustrated from a game theoretic viewpoint and it is shown that in the undirected graph case the overall control law is inverse optimal w.r.t. a cost functional depending on the target formation and on rigidity properties of the evolving formation. In order to transfer such a behavior of the overall system to directed graphs, we define the class of cooperative graphs via a dissipation equality which reflects the cost-to-go function of the inverse optimal control problem that we identified for undirected graphs. Besides undirected graphs, this dissipation equality allows us to identify also directed cyclic graphs and directed open chain graphs as cooperative graphs. Moreover, for cooperative graphs we can establish the exponential stability of the target formation together with a guaranteed region of attraction via Lyapunov set stability theory.

In order to obtain a global result we have to rule out a convergence to the various other invariant sets of the closed-loop dynamics. For this reason a stability and instability theorem for differentiable manifolds is derived, which allows to perform a global stability analysis of three robots in a directed cyclic graph and to confirm Cao's results [27, 28].

The thesis is organized as follows. In Chapter 2 the necessary background on algebraic

graph theory and rigidity is given. This allows us to formulate the formation control problem in Chapter 3 and to derive a controller that is capable of solving this problem. In Chapter 4 we provide the necessary background on Lyapunov set stability theory, optimal control, inverse optimality and on the interconnection of these topics. With these tools we show in Chapter 5 the relationship of the overall control obtained for undirected graphs to an optimal control problem. Additionally we define the class of cooperative graphs in this chapter and derive our first main result on the stability of the target formation. All the results will be illustrated at the example of three robots interconnected in a directed cyclic sensor graph which should form a triangle. In Chapter 6 we introduce the reader to the necessary background in differential geometry and to the geometrical viewpoint of a dynamical system. We make use of this in Chapter 7 to derive a manifold stability theorem that helps us to perform a global stability analysis of a directed triangular formation. And finally, in the last chapter a summary and discussion of the results of this thesis is given together with possible future extensions.

Chapter 2

Preliminaries and Definitions I

The purpose of this chapter and later chapters with similar title is to introduce the basic mathematical notions and background information used throughout this thesis. These definitions and facts will be completed in later parts of the thesis where needed.

2.1 Graph Theory

2.1.1 Algebraic Graph Theory

This section introduces the reader to the basic notations of algebraic graph theory, which can be found in [31, 32]. All the following definitions and results on graphs will be related to the example graph $\mathcal{G}$ in Figure 2.1.

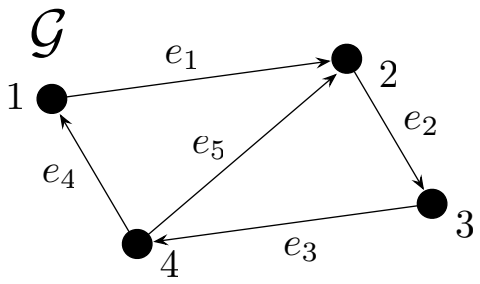

Figure 2.1: Graph $\mathcal{G}$ with n=4 nodes with m=5 links

A *directed graph* $\mathcal{G} = (V, E)$ is an ordered pair consisting of a finite set of *nodes* $V =$

$\{1, \ldots, n\}$ and *edges* $E \subset V \times V$. We assume the edges are ordered, that is, $E = \{e_1, \ldots, e_m\}$ where $m \in \{1, n\,(n-1)\}$ and exclude the possibility of self loops. The *neighbour set* N_i of a node i is the set of all nodes j where there is an edge e_k from i to j. In this case we denote the node i as the *source node* of the edge e_k and j as the *sink node*. The edge e_k is then also called an *outgoing edge* of node i, respectively, an *ingoing edge* of node j.

Example 2.1.1. The graph $\mathcal{G}$ in Figure 2.1 is parametrized by the node set $V = \{1, 2, 3, 4\}$ and the edge set $E = \{e_1, e_2, e_3, e_4, e_5\}$. The neighbour sets are given by $N_i = \{i + 1\}$ for $i \in \{1, 2, 3\}$ and $N_4 = \{1, 2\}$. The edge e_5, for example, is an outgoing edge of node 4 and an ingoing edge of node 2. Edge e_5's sink node is node 2 and its source node is node 4.

A graph is said to be *undirected* or *symmetric* if, whenever there is an edge e_{k_1} from node i to node j, then there is also an edge e_{k_2} from node j to node i. An undirected graph can either be represented as a directed graph or by lumping the edges e_{k_1} and e_{k_2} together in one bidirectional edge e_k. The graph has then m bidirectional edges, where $m \in \left\{1, \frac{n\,(n-1)}{2}\right\}$. This is illustrated at the undirected triangular graph in Figure 2.2. In order to avoid confusion the edges of the directed graph representation in Figure 2.2(a) were not labeled. For the remainder of this chapter, when we refer to a directed graph, we will always think of a graph with bidirectional edges as in Figure 2.2(b).

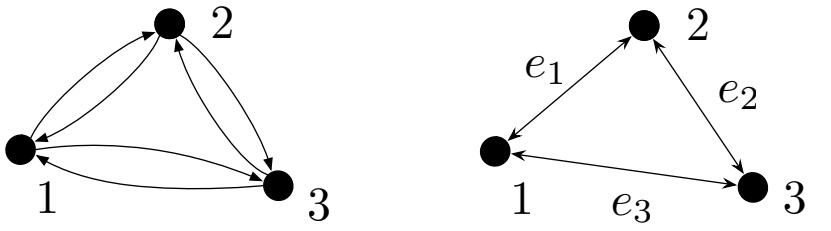

(a) An undirected graph represented as a directed graph

(b) An undirected graph represented with bidirectional edges

Figure 2.2: Equivalent representations of an undirected graph

With a graph $\mathcal{G}$ we associate different matrices. The matrix relating the nodes to the

edges is called the *incidence matrix* $H = \{h_{ij}\} \in \mathbb{R}^{m \times n}$ of the graph and is defined as

$$h_{ij} := \begin{cases} +1 & \text{if node } j \text{ is the sink node of edge } e_i \\ -1 & \text{if node } j \text{ is the source node of edge } e_i \\ 0 & \text{else .} \end{cases}$$

Example 2.1.1 (continued)**.**

$$H = \begin{bmatrix} -1 & 1 & 0 & 0 \\ 0 & -1 & 1 & 0 \\ 0 & 0 & -1 & 1 \\ 1 & 0 & 0 & -1 \\ 0 & 1 & 0 & -1 \end{bmatrix} \tag{2.1}$$

For the sake of an intuitive understanding we take a closer look at the rows and the columns of H. The rows of H correspond to the links e_i of the graph $\mathcal{G}$ and are obtained by permutations of the elements of the vector $[-1, 1, 0, \ldots, 0]$. By the definition of the incidence matrix, the vector $\mathbf{1}$ lies in the kernel of H, where $\mathbf{1}$ is a n dimensional vector with a 1 in each component. Furthermore $\operatorname{rank}(H) = n - 1$ iff $\mathcal{G}$ is connected ([32], Proposition 4.3) and thus in this $\ker(H) = \operatorname{span}\{\mathbf{1}\}$. For the remainder of this work we will assume that all graphs are connected. In the jth column of H all ingoing and outgoing edges e_i of node j can be identified by $h_{ij} = 1$, respectively $h_{ij} = -1$. The *co-rank* of H, that is, $\text{co-rank}(H) = \dim\left(\ker\left(H^T\right)\right) = m - \operatorname{rank}(H)$, depends on the cycles contained in the graph. Let Q be a cycle in the graph $\mathcal{G}$ and consider the vector $\xi_Q = \left\{\xi_{Q_j}\right\}$ with the components

$$\xi_{Q_j} = \begin{cases} +1 & \text{if } e_j \text{ belongs to } Q \text{ and its cycle orientation} \\ & \text{coincides with its orientation } \mathcal{G} \\ -1 & \text{if } e_j \text{ belongs to } Q \text{ and its cycle orientation} \\ & \text{is reverse of its orientation } \mathcal{G} \\ 0 & \text{if } e_j \text{ does not belong to } Q \text{ .} \end{cases}$$

Hence ξ_Q contains one of two possible cycle-orientations of the edges and furthermore $\xi_Q \in \ker\left(H^T\right)$ ([32], Theorem 4.5). For the Example 2.1.1 we have the two clockwise oriented cycles $(1,2,3,4)$ and $(1,2,4)$ which lead to

$$\text{rowspan}\left\{\begin{bmatrix} 1 & 1 & 1 & 1 & 0 \\ 1 & 0 & 0 & 1 & -1 \end{bmatrix}\right\} \;=\; \ker\left(H^T\right).$$

The incidence matrix can also be defined for an undirected graph by introducing arbitrary orientations for the bidirectional links and will be denoted by H_u. If we introduce a clockwise orientation to the undirected triangular graph in Figure 2.2(b) H_u is given by

$$H_u \;=\; \begin{bmatrix} -1 & 1 & 0 \\ 0 & -1 & 1 \\ 1 & 0 & -1 \end{bmatrix}. \tag{2.2}$$

In addition to the incidence matrix, of interest for us are also the *ingoing edge matrix* $U = \{u_{ij}\} \in \mathbb{R}^{n\times m}$ and the *outgoing edge matrix* $O = \{o_{ij}\} \in \mathbb{R}^{n\times m}$ with components

$$u_{ij} \;:=\; \begin{cases} 1 & \text{if node } i \text{ has ingoing edge } j \text{ (sink node)} \\ 0 & \text{else} \end{cases}$$

$$o_{ij} \;:=\; \begin{cases} -1 & \text{if node } i \text{ has outgoing edge } j \text{ (source node)} \\ 0 & \text{else}. \end{cases}$$

Example 2.1.1 (continued)**.**

$$U = \begin{bmatrix} 0 & 0 & 0 & 1 & 0 \\ 1 & 0 & 0 & 0 & 1 \\ 0 & 1 & 0 & 0 & 0 \\ 0 & 0 & 1 & 0 & 0 \end{bmatrix}, \quad O = \begin{bmatrix} -1 & 0 & 0 & 0 & 0 \\ 0 & -1 & 0 & 0 & 0 \\ 0 & 0 & -1 & 0 & 0 \\ 0 & 0 & 0 & -1 & -1 \end{bmatrix} \tag{2.3}$$

Note that from the definitions of H, U and O it follows directly $O + U = H^T$. Since we will later relate the nodes of the graph to robots and the outgoing edges to the sensory information accessible by the robots, the outgoing-edge matrix will be of special interest for us.

Additional graph matrices which are related to control theory are the *adjacency matrix* $A \in \mathbb{R}^{n\times n}$, the *out-degree matrix* $D \in \mathbb{R}^{n\times n}$ and the *Laplacian* $L := D - A$. For undirected graph, L is related to the incidence matrix via $L = H_u^T H_u$ ([32], Proposition 4.8). These matrices play an important role in control tasks such as *consensus/rendezvous* and we will later refer back to them as special cases of *formation control*.

2.1.2 Graph Rigidity

Graph rigidity is a mathematical concept which emerged from mechanical and civil engineering [33, 34] in order to analyze scaffolds and frameworks. The concept of rigidity and frameworks entered the domain of formation control for the first time in [19, 20] as a design tool to construct undirected graphs and has since been continuously extended. More recent references extend the rigidity concept to directed graphs [17] and higher dimensions [21] or employ it as an analysis tool for the stability of an undirected formation [26]. For an non-technical overview of the applications of rigidity in formation control we refer the reader to [35]. This section gives a comprehensive introduction to graph rigidity and its directed counterpart persistence.

Rigidity of Undirected Graphs

Rigidity is a property that refers to undirected graphs. In order to introduce the notion of graph rigidity, we view the undirected graph $\mathcal{G}$ as a framework embedded in the plane. Let $\mathcal{G} = (V, E)$ be an undirected graph with n nodes and m edges. We embed the graph $\mathcal{G}$ into the plane $\mathbb{R}^2$ by assigning to each node i a location $z_i \in \mathbb{R}^2$. A *framework* is then a pair $(\mathcal{G}, z)$ where $z = [z_1, \ldots, z_n]^T \in \mathbb{R}^{2n}$. The edges of the graph can then be interpreted as two dimensional links connecting the points z_i. We associate the edge e_k connecting the nodes i and j with the relative position $e_k = z_j - z_i$. In the sequel we will not distinguish between the edge e_k or the relative position e_k and denote both simply as *link* e_k, where the meaning will be clear from the context. Now after having embedded the nodes and the edges of the graph $\mathcal{G}$ in the plane we can address rigidity. Therefore, we define the *rigidity function* $r_{\mathcal{G}}(z)$

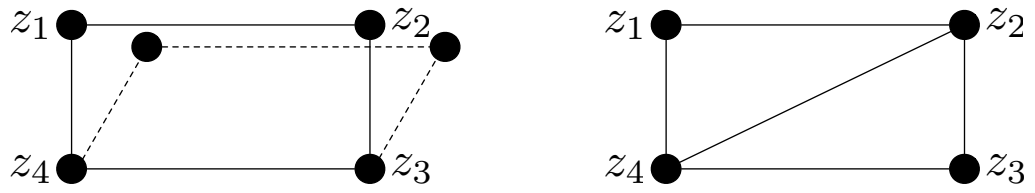

(a) A flexible framework (b) A rigid framework

Figure 2.3: Rigidity properties of a framework with four points

as

$$\begin{aligned} r_{\mathcal{G}} : \quad & \mathbb{R}^{2n} \rightarrow \mathbb{R}^m \\ r_{\mathcal{G}}(z) \quad = \quad & \frac{1}{2}\left[\ldots, \left\|z_j - z_i\right\|^2, \ldots\right]^T \end{aligned} \tag{2.4}$$

where the kth component in $r_{\mathcal{G}}(z)$ corresponds the length of link e_k and $\|\cdot\|$ denotes the standard euclidean norm. Let us now define rigidity.

Definition 2.1.1. A framework $(\mathcal{G}, z)$ is said to be *rigid* if there is an open neighbourhood $\mathcal{U}$ of z such that if $q \in \mathcal{U}$ and $r_{\mathcal{G}}(z) = r_{\mathcal{G}}(q)$, then $(\mathcal{G}, z)$ is congruent to $(\mathcal{G}, q)$.

The concept of rigidity can be illustrated graphically as shown in the example in Figure 2.3, where, for simplicity, the links are neither labeled nor is their bidirectional orientation indicated to avid clutter. The framework in Figure 2.3(a) is not rigid since a slight perturbation of the upper two points of the framework results in a framework that is not congruent to the original one although their rigidity functions coincide. If we add an additional cross link to the framework as shown in Figure 2.3(b), small perturbations that do not change the rigidity function will result in a congruent framework. Thus the framework in Figure 2.3(b) is rigid.

Infinitesimal and Minimal Rigidity

Although rigidity is a very intuitive concept, its definition does not provide a condition that is easy to check, especially if one is interested in finding the exact neighbourhood $\mathcal{U}$ where the framework is rigid. Luckily there is a linearized version of the rigidity concept which breaks it

down to an algebraic condition. The idea is to allow an infinitesimally small perturbation ∂z of the framework $(\mathcal{G}, z)$ while keeping the rigidity function constant up to first order. Then the first order Taylor series of the rigidity function $r_{\mathcal{G}}$ about z is

$$r_{\mathcal{G}}(z+\partial z) \;=\; r_{\mathcal{G}}(z) + \frac{\partial r_{\mathcal{G}}(z)}{\partial z}\,\partial z + \mathcal{O}^2(\partial z)\,. \tag{2.5}$$

The rigidity function then remains constant up to first order if $\partial z \in \ker\left(\frac{\partial r_{\mathcal{G}}(z)}{\partial z}\right)$. The matrix $\frac{\partial r_{\mathcal{G}}(z)}{\partial z} \in \mathbb{R}^{m\times 2n}$ is called the *rigidity matrix* of the graph $\mathcal{G}$. If the perturbation ∂z is a rigid body motion, that is a translation and rotation of the framework, then, by Definition 2.1.1, the framework is still rigid. Thus it is possible to argue that the dimension of the kernel of the rigidity matrix is at least 3, which corresponds to the three degrees of freedom of planar rigid body motions. The idea that rigidity is preserved under infinitesimal perturbations motivates the following definition of infinitesimal rigidity.

Definition 2.1.2. ([33]) A framework $(\mathcal{G}, z)$ is said to be *infinitesimally rigid* if $\dim\left(\ker\left(\frac{\partial r_{\mathcal{G}}(z)}{\partial z}\right)\right) = 3$ or equivalently if $\operatorname{rank}\frac{\partial r_{\mathcal{G}}(z)}{\partial z} = 2n-3$.

If a framework is infinitesimally rigid, then it is also rigid but the converse is not necessarily true. Also note that a infinitesimally rigid framework must have at least $2n-3$ links. If it has exactly $2n-3$ links the we denote it as a *minimally rigid* framework. Let us illustrate these concepts with an example.

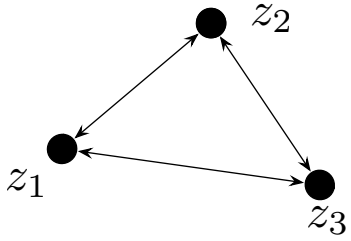

(a) A rigid and infinitesimally rigid framework

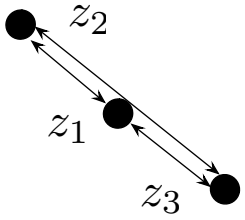

(b) A rigid but not infinitesimally rigid framework

Figure 2.4: Infinitesimal rigidity properties of a framework with three points

Example 2.1.2. Consider the triangular framework in Figure 2.4(a) and the collapsed triangular framework in Figure 2.4(b) which are both embeddings of the same graph. The rigidity function for both frameworks is given by

$$r_{\mathcal{G}}(z) \;=\; \frac{1}{2}\begin{bmatrix} \|z_2 - z_1\|^2 \\ \|z_3 - z_2\|^2 \\ \|z_1 - z_3\|^2 \end{bmatrix}. \tag{2.6}$$

Clearly both frameworks are rigid but only the left framework will turn to be minimally rigid. To see this, consider therefore the rigidity matrix

$$\frac{\partial r_{\mathcal{G}}(z)}{\partial z} \;=\; \begin{bmatrix} z_1^T - z_2^T & z_2^T - z_1^T & \mathbf{0} \\ \mathbf{0} & z_2^T - z_3^T & z_3^T - z_2^T \\ z_1^T - z_3^T & \mathbf{0} & z_3^T - z_1^T \end{bmatrix} \tag{2.7}$$

and note that its rank at a collinear point is $2 < 2\,n - 3$. Therefore, the collapsed triangle in Figure 2.4(b) is not minimally rigid.

Example 2.1.2 leads to the conclusion that the triangular framework in Figure 2.4(a) is minimally rigid for almost every $z \in \mathbb{R}^6$, just not in a thin set of measure zero. A lot of frameworks $(\mathcal{G}, z)$ turn out to be minimally rigid for a generic $z \in \mathbb{R}^{2n}$. Thus one might argue that infinitesimal rigidity depends almost only on the graph $\mathcal{G}$ and not on the points z. This property is called *generic rigidity* of the graph $\mathcal{G}$ [36] and throughout the literature (infinitesimally, minimally) rigid frameworks are often denoted as (infinitesimally, minimally) rigid graphs. We will also use this term in the following paragraph on the construction of minimally rigid graphs. We do this only for the sake of notational convenience and remind the reader that infinitesimal rigidity is not a global property of a framework but depends on the rigidity function and thus on the links of the framework.

Construction of Minimally Rigid Graphs

A state of the art review regarding rigid graphs is provided in [34] where also methods to construct minimally rigid graphs are presented. Among the main results we mention the following one about Henneberg sequences: A *Henneberg sequence* is a sequence of graphs

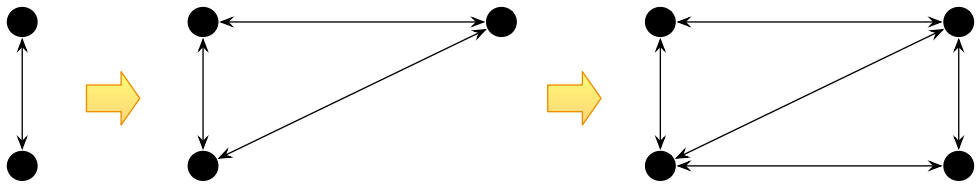

Figure 2.5: Subsequent node additions leading to the minimally rigid graph of Figure 2.3(b)

beginning with a minimally rigid graph, for example, two nodes with a bidirectional edge connecting them. Next either an *edge splitting* or a *node addition* is performed. For simplicity, we just illustrate the latter case: A new node is added to the minimally rigid graph with two bidirectional edges connecting the new node to two distinct nodes of the prior graph. By subsequent node additions the minimal rigidity of the graph is maintained, and one can even show that every minimally rigid graph can be obtained by a sequence of node additions and edge splittings. The node addition is illustrated in Figure 2.5, where we start from simplest undirected graph containing two edges and end up with the graph from Figure 2.3(b) while minimal rigidity is preserved. Again we omitted a labeling of the graph to avoid clutter.

Formations and Target Formations

Let us now think of the points $z_i \in \mathbb{R}^2$ of the framework not as a set of fixed points in the plane, but rather as the positions of wheeled robots. The robots can move freely in the plane and their task is to form a prescribed geometric formation. When we say the robots are in a formation we do not think of a geometric structure such as a framework fixed at a specific location z in the plane, but rather defined independently of translations and rotations of the framework.

Formation: We define a *formation* by the pair $(\mathcal{G}, e)$ where $\mathcal{G}$ is the graph and $e = [e_1, \ldots, e_m]^T$ is the vector containing the links of the framework $(\mathcal{G}, z)$. Note that by defining the link e_k as $e_k = z_j - z_i$, we have introduced an artificial orientation to an actually undirected link. This somewhat arbitrary orientation allows us to fix the incidence matrix H_u of the undirected graph. Let us introduce the composite vector $e = [e_1, \ldots, e_m]^T \in \mathbb{R}^{2m}$ and

the notation $\hat{A} := A \otimes I_2$, where A is a matrix, I_2 is the two dimensional identity matrix and $\otimes$-operator is the *Kronecker product*, that is, the element wise multiplication. With this notation and the the incidence matrix H_u the positions z can be related to the links e by

$$e \;=\; \hat{H}_u\, z\,. \tag{2.8}$$

Keep in mind that the links are actually bidirectional and that the orientation introduced by the incidence matrix is abritrary.

Infinitesimal Rigidity of a Formation: The rigidity function $r_{\mathcal{G}}(z)$, which maps the positions to the link lengths, can then also be defined as a function $v(e)$ with the domain $\hat{H}_u\,(\mathbb{R}^{2n})$:

$$\begin{aligned} v\;:\quad & \hat{H}_u\left(\mathbb{R}^{2n}\right) \;\to\; \mathbb{R}^m \\ v(e) \;=\; & \frac{1}{2}\left[\|e_1\|^2\,,\,\ldots\,,\,\|e_m\|^2\right]^T \end{aligned} \tag{2.9}$$

We then have the relationship $r_{\mathcal{G}}(z) = v(\hat{H}_u\, z)$ and obtain the following simple form for the rigidity matrix:

$$\frac{\partial r_{\mathcal{G}}(z)}{\partial z} \;=\; \frac{\partial v(\hat{H}_u\, z)}{\partial z} \;=\; \frac{\partial v(e)}{\partial e}\,\frac{\partial e}{\partial z} \tag{2.10}$$

$$\;=\; \operatorname{diag}\left\{e_i^T\right\}\,\hat{H}_u \tag{2.11}$$

The matrix $R_{\mathcal{G}}(e) := \operatorname{diag}\left\{e_i^T\right\}\,\hat{H}_u \in \mathbb{R}^{m\times 2n}$ is the *rigidity matrix* of the formation $(\mathcal{G}, e)$. Infinitesimal rigidity is a property of a framework, but since it obviously depends only on the links, we can equivalently talk about the infinitesimal rigidity of a formation. All the subsequent definitions and theorems will have the property that they can be equivalently formulated in terms of frameworks or formations and we omit this distinction from now on.

Target Formation: Let us go back to to the idea of wheeled robots in the plane and assign them a task, namely the robots should move to a prescribed formation. We denote this desired formation as the *target formation* and specify it by the pair $\left(\mathcal{G}, v^{-1}(\mathbf{d})\right)$. Here $\mathbf{d} \in \mathbb{R}^m$ is a vector with components d_i^2 specifying the desired squared length of the link

e_i, that is, $\|e_i\|^2 = d_i^2$ or in vector form $v(e) = \mathbf{d}$. Note that a target formation could be equivalently defined by the pair $\big(\mathcal{G}, r_{\mathcal{G}}^{-1}(\mathbf{d})\big)$.

It will in the later analysis be beneficial for us to choose $\big(\mathcal{G}, v^{-1}(\mathbf{d})\big)$ as an infinitesimally rigid formation. Let us run one possible scenario to motivate this. Consider four robots and the target formation specified via the graph in Figure 2.3(a), arbitrarily labeled links and $\mathbf{d} = \mathbf{1}$. Assume that the robots have converged to the target formation and note that the target formation is not a rigid formation. In this case the robots could move slightly without leaving the target formation, as indicated in Figure 2.3(a). But clearly the geometric configuration of the robots is then not congruent to the initial configuration. Moreover, in the extreme case the positions of the robots can even be made collinear without leaving the target formation, and, under the control law that we later derive, once collinear robots will stay collinear for all time. If we want to prevent such a scenario, we have to choose a graph that leads to an infinitesimally rigid target formation, for example, the one in Figure 2.3(b).

Remark 2.1.1. It is worth to mention that the concept of infinitesimal rigidity can also be derived as a necessary and sufficient condition to prevent exactly this scenario [19, 37].

Persistence of Directed Graphs

Let us generalize the ideas of the preceding paragraphs to directed graphs and see which additional problems arise. Consider again a set of wheeled robots with positions z_i in the plane. With each robot we associate a set of neighbours and with each neighbour a distance constraint which the robot has to meet with respect to that neighbour. This setup can again be formalized by a framework $(\mathcal{G}, z)$ and a target formation $\big(\mathcal{G}, r_{\mathcal{G}}^{-1}(\mathbf{d})\big)$, where $\mathcal{G}$ is now a directed graph and the points of the framework correspond again to the positions of the robots $z_i \in \mathbb{R}^2$. Each node i has outgoing edges e_k to other nodes $j \in N_i$ which correspond to the neighbours. The outgoing edges e_k are again links connecting the robots, that is, $e_k = z_j - z_i$ or in vector form

$$e \;=\; \hat{H}\, z\,, \tag{2.12}$$

where H is the incidence matrix of the directed graph $\mathcal{G}$. The pair $(\mathcal{G}, e)$ is then a formation and we say that the framework, respectively the formation, is (minimally) rigid if the corresponding undirected framework is (minimally) rigid. The target formation is the pair $\left(\mathcal{G}, r_{\mathcal{G}}^{-1}(\mathbf{d})\right)$ where the components of the vector $\mathbf{d}$ are the squared distance constraints. Likewise the target formation is said to be (minimally) rigid if the corresponding undirected target formation is (minimally) rigid. In the following example we want to point out a problem that occurs in directed graphs.

Example 2.1.3. Consider the setup in Figure 2.6(a) with three robots with positions $z_i \in \mathbb{R}^2$ and where robot 1 wants to be a desired distance away from robots 2,3 and 4. In our formalism we have a framework $(\mathcal{G}, z)$ where $\mathcal{G}$ is a directed graph with $N_1 = \{2, 3, 4\}$. The links of this framework are e_1,e_2 and e_3 and the desired target formation is $\left(\mathcal{G}, v^{-1}(\mathbf{d})\right)$ with $\mathbf{d} = [1, 1, 1]^T$. Let us fix the positions z_i as shown in Figure 2.6(a) and assume that robot 1

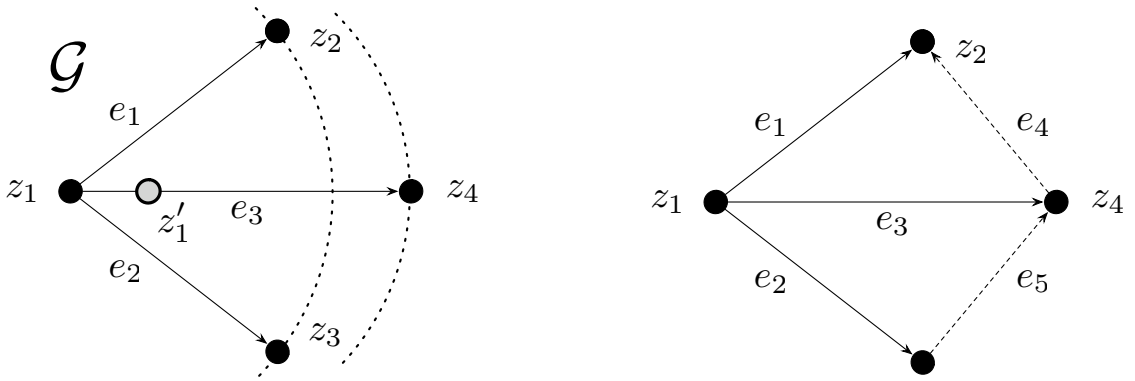

(a) Example of a not constraint consistent framework

(b) Framework from Figure 2.6(b) embedded in a rigid framework

Figure 2.6: Two frameworks that are not constraint consistent

in position z_1 meets its distance constraint w.r.t. link e_1 and link e_2. In order to satisfy its distance constraint w.r.t. link e_3 robot 1 has to move, for example, to position z_1'. Clearly robot 1 cannot move without violating its other two distance constraints. We then say the framework $(\mathcal{G}, z)$ is not constraint consistent. Note that the framework in Figure 2.6(a) is not an artificial example and the underlying graph $\mathcal{G}$ could be a subgraph of the graph of the rigid framework in Figure 2.6(b).

If a situation such as the one in Example 2.1.3 cannot happen the framework is said to be *constraint consistent*. The precise definition of constraint consistence can be found in [17] and is beyond the realm of this thesis. Instead we use the following sufficient characterization of constraint consistence.

Definition 2.1.3. ([17], Lemma 1): A directed framework $(\mathcal{G}, z)$ is constraint consistent if each node of $\mathcal{G}$ has fewer than two outgoing edges.

Note that Definition 2.1.3 could equivalently be given for a formation $(\mathcal{G}, e)$. Finally we call a framework or formation *(minimally) persistent* if it is constraint consistent and (minimally) rigid. Whether or not a directed graph is persistent is a fairly tough question to answer and just recently an algorithm was published which allows to check persistence in polynomial time [38]. For minimally persistent frameworks the following theorem gives a checkable condition.

Theorem 2.1.1. *([17], Theorem 4) A rigid framework is minimally persistent if and only if the underlying graph $\mathcal{G}$ has either*

(i) three nodes that have one outgoing edge and the remaining nodes have two outgoing edges, or

(ii) one node that has no outgoing edge, one node that has one outgoing edge and the remaining vertices have two outgoing edges.

The graph in Figure 2.1 at the beginning of this chapter is an example for a graph that satisfies condition *(i)* of Theorem 2.1.1. We can construct minimally persistent frameworks that satisfy condition *(ii)* by a modification of the Henneberg sequence by which we constructed minimally rigid graphs. Start with a single node at position z_1 and add a second node at position z_2 and the directed link $e_1 = z_1 - z_2$. All remaining nodes are added at positions z_i and are connected to two distinct nodes of the framework by two outgoing edges of z_i. The resulting framework will be *acyclic*, that is, it contains no cycles. An example of a of a Henneberg sequence resulting in minimally persisten graph is given in Figure 2.7 where omitted a labeling of the links of the framework.

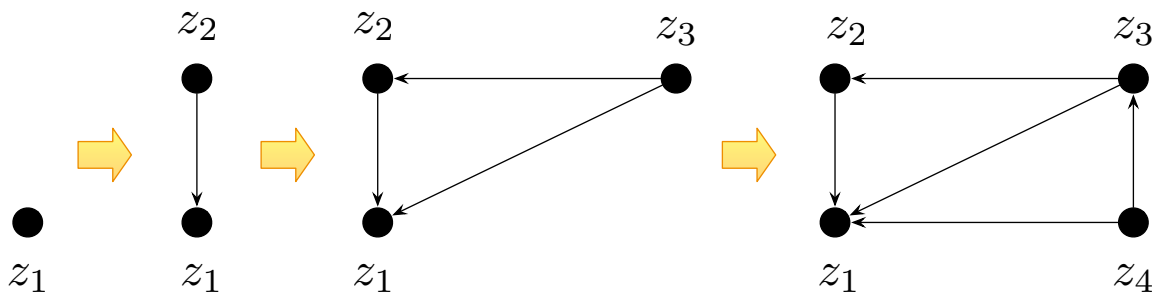

Figure 2.7: A Henneberg sequence leading to a minimally persistent graph.

The nodes of the framework can of course be labeled arbitrary, but if they are labeled as proposed by us then the framework has a so called *leader follower structure*. This term emphasizes the fact that, if we interpret nodes of the graph as moving robots, then each robot has either zero, one or two leaders. By topological sorting algorithms [39] it is even possible to label every constraint consistent and acyclic framework in a such a way that it has a leader follower structure.

Chapter 3

Problem Setup

This chapter motivates and formulates the formation control problem for autonomous robots based on distributed control. Furthermore, a gradient control law is developed which is capable of solving this problem. Based on this control law the dynamic equations of the closed loop are derived and are dependent only on the graph matrices.

3.1 Control Structure

Let us start this section by motivating, explaining and delimiting the terms autonomous agents, multi-agent system and centralized or distributed control of such a system. Then we move on to the specific control problem of autonomous wheeled vehicles.

3.1.1 A Distributed Control Approach to a Multi-Agent System

For our purposes an *autonomous agent* is a dynamical systems whose action relies on its own perception and strategy only and not on commands from outside. A dynamical system consisting of autonomous agents as subsystems is then called a *multi-agent system*. The multi-agent system consists of either homogenous or heterogeneous agents where each agent has incomplete capabilities to solve a problem. We refer to the strategy of a single agent as its control and the to the collection of the strategies of all agents in the multi-agent system as

the overall control. The multi-agent system can a priori be interconnected, and, depending on the interconnection structure, the action of one agent might influence certain other agents. Let us illustrate these concepts at the following two examples:

Example 3.1.1. A system of power plants interconnected by a grid is a multi-agent system. The power plants correspond to the autonomous agents and their task is to maintain a constant voltage on the power grid. This task cannot be handled by one single power plant alone but each power plant can do its share by injecting power to the grid, which again affects the other power plants.

Example 3.1.2. As second example consider different manufacturing robots working on a production line. We assume the robots are not controlled from a central computer. With the robots as agents the production line constitutes a heterogeneous multi-agent system and it is obvious that a single manufacturing robot is not able to execute all tasks involved in the production. The production line forms a cascade system, where the action of one robot influences only its successors.

Depending on the information which is accessible by the agents we refer to the overall control as either a *centralized control* or a *decentralized control*. In the first case the control strategy of each agent can make use of central information, which means that each agent has the knowledge of all the other agents and the controlled multi-agent system is not necessarily structured. In the second case the control strategy of each agent is based on local sensory information, which is also referred to as *distributed control*. There are no leaders and at least one agent does not know what all the others are doing. Thus the controlled multi-agent system is structured and the agents work separately and independently of each other but still achieve a common goal. These two concepts are again illustrated at the Examples 3.1.1 and 3.1.2.

Example 3.1.1. (continued): Interconnected power plants are a typical application for a distributed control approach. Each power plant can locally measure voltage fluctuations on the grid and tries to sustain them by injecting power. Each power plant does so independently of the others but altogether they guarantee a stable voltage on the grid.

Example 3.1.2. (continued): The easiest and probably most effective solution to optimize the performance of the production line is a centralized control of the manufacturing robots. The robots can all be linked by communication devices and synchronize by sharing their information.

A multi-agent system either arises naturally by interconnecting a priori given subsystems (e.g. power plants) or is designed. The advantages of the latter are that the complexity of a problem or the effort to solve it can both be reduced by splitting the problem up to easier subtasks (e.g. manufacturing robots). A distributed control approach to a multi-agent system is obviously harder and might not produce the same performance results as a centralized control. On the other hand it might be robust to failure of single agents and the individual control strategies of the agents might not have to be changed if the number of agents changes. Additionally the costs of sensors grows only proportionally to the number of agents since no communication network among the agents is needed. For these reasons and the obvious theoretic challenge we look at distributed control of a multi-agent system.

3.1.2 Distributed Control of Autonomous Wheeled Robots

For our purposes an autonomous agent is a wheeled and actuated robot in the plane, which has no communication devices and is only equipped with an onboard camera. Using methods of feedback linearization or flattening [40] a lot of standard models for wheeled vehicles can be transformed to a *kinematic point*. A kinematic point is a robot whose motion is fully actuated, that is, it has dynamics

$$\dot{z}_i \;=\; u_i\,, \tag{3.1}$$

where $z_i \in \mathbb{R}^2$ is the position of robot i in the plane and $u_i \in \mathbb{R}^2$ is a direct velocity command and serves as control input. In a total we consider n robots and the index i is evaluated for $i \in \{1,\dots,n\}$. With the concatenated vectors $z = [z_1,\dots,z_n]^T \in \mathbb{R}^{2n}$ and $u = [u_1,\dots,u_n]^T \in \mathbb{R}^{2n}$ the dynamics of the overall system are given by

$$\dot{z} \;=\; u \tag{3.2}$$

and constitute a diagonal multi-agent system. The topology of information exchange between the single robots is expressed in a graph $\mathcal{G}$ which we refer to as the *sensor graph* or the *visibility graph*. The sensor graph $\mathcal{G}$ has m edges which we denote by e_j with $j \in \{1, \dots, m\}$. Let us for the moment consider directed sensor graphs and later specify the results of this chapter to undirected graphs. We can do this without loss of generality since we noted in Section 2.1.1 that every undirected graph can be represented as either a directed graph or equivalently with bidirectional edges. The nodes of the sensor graph $\mathcal{G}$ correspond to robot i's position z_i, and a directed edge j from robot i to robot $k \in N_i$ means that robot i can sense robot k via its onboard camera. Thus robot i can sense the relative distance and direction of robot k and therefore the relative position, respectively link, $e_j = z_k - z_i$. If we consider the concatenated vector $e = [e_1, \dots, e_m]^T$ and the incidence matrix H of the graph $\mathcal{G}$, then the links are obtained by

$$e \;=\; \hat{H}\, z\,. \tag{3.3}$$

Thus the sensor graph $\mathcal{G}$ and the positions z define the framework $(\mathcal{G}, z)$ with the links $e \in \hat{H}\,(\mathbb{R}^{2n})$. Suppose the robots should now perform certain tasks and, in order to do so, a distributed control is designed for each robot. In a distributed control approach the control input u_i of robot i is depending exclusively on sensory information, which are the links $e_j = z_k - z_i$ with $k \in N_i$. That is to to say, $u_i = u_i\,(e_j)$ where $e_j = z_k - z_i$ with $k \in N_i$.

3.1.3 The Formation Control Problem

The precise task the robots should perform is called *formation control* and is specified as follows. Given the sensor graph $\mathcal{G}$ we define a desired and realizable formation, that is, a set of distance constraints $d_i > 0$, where $i \in \{1, \dots, m\}$, such that a formation $(\mathcal{G}, e)$ with $\|e_i\| = d_i$ is realizable in the plain. This can be formalized by the target formation $\big(\mathcal{G}, r_{\mathcal{G}}^{-1}(\mathbf{d})\big)$ with $r_{\mathcal{G}}^{-1}(\mathbf{d}) \neq \emptyset$. We have seen in the previous section that persistence of the formation is a beneficial if not even necessary condition for the robots to attain a desired formation. That's why we specify the target formation to be a persistent formation, that is, it has to be constraint consistent and the corresponding undirected formation has to be

infinitesimally rigid. The formation control problem is then to find a distributed control law u such that the robots converge to a stationary target formation. This can also be formulated as a set stabilization problem:

Problem. *Formation Control:*
Given the dynamics $\dot{z} = u$, the sensor graph $\mathcal{G}$ and a persistent target formation $\left(\mathcal{G}, r_{\mathcal{G}}^{-1}(\mathbf{d})\right)$ such that $r_{\mathcal{G}}^{-1}(\mathbf{d}) \neq \emptyset$, find a control law u such that

(i) $u_i = u_i(z_j - z_i)$, $j \in N_i$

(ii) $z(t) \underset{t\to\infty}{\to} r_{\mathcal{G}}^{-1}(\mathbf{d})$

(iii) $z(t) \underset{t\to\infty}{\to}$ *const.*

In condition *(ii)* we appeal to the reader's intuition what convergence of a point to a set means and formalize it mathematically in the next chapter. As we have already mentioned in the introductory example (Example 1.2.1), the conditions *(ii)* and *(iii)* can be lumped together into the condition

$$z(t) \underset{t\to\infty}{\to} z_* \text{ with } z_* \in r_{\mathcal{G}}^{-1}(\mathbf{d})\,. \tag{3.4}$$

We do not formulate the problem this way since the later analysis will clearly distinguish between convergence to $r_{\mathcal{G}}^{-1}(\mathbf{d})$ and convergence to a finite point $z_* \in r_{\mathcal{G}}^{-1}(\mathbf{d})$. Additionally the formation control problem will not be solvable for every initial condition $z(0) \in \mathbb{R}^{2n}$, as we have seen in Example 1.2.1. In Chapter 5 we will present conditions under which the formation control problem is solvable locally, and in Chapter 7 we try to find the exact region of initial conditions from where the the problem is guaranteed to be feasible. We conclude this section with the example of three robots in formation control.

Example 3.1.3. Directed triangle:
Consider three robots modeled as kinematic points $\dot{z}_i = u_i$ which should form a triangle based on a distributed control law. The three robots are interconnected in the directed cyclic sensor graph $\mathcal{G}$ shown in Figure 3.1. The three nodes of the graph are labeled clockwise and are interconnected by the three edges e_1, e_2, e_3 which are also oriented and labeled clockwise.

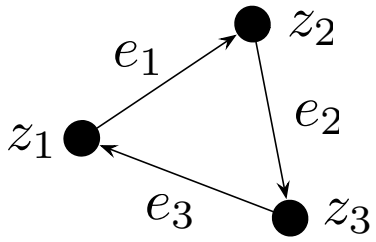

Figure 3.1: The *directed triangle*.

In the remainder of this thesis we will refer to this example as the *directed triangle*. The incidence matrix of the directed triangle is given by

$$H = \begin{bmatrix} -1 & 1 & 0 \\ 0 & -1 & 1 \\ 1 & 0 & -1 \end{bmatrix} \tag{3.5}$$

and we obtain the links as $e = \hat{H}\, z$ and the rigidity matrix of the formation $(\mathcal{G}, e)$ as $R_{\mathcal{G}}(e) = \operatorname{diag}\left\{e_i^T\right\} \hat{H}$. We have already shown in Example 2.1.2 that the corresponding undirected formation is infinitesimally rigid whenever the the robots' positions z are not collinear, or equivalently, whenever the three links are not collinear. Additionally each node of $\mathcal{G}$ has only one outgoing edge, and thus, by Definition 2.1.3, the formation is constraint consistent. Let us specify a target formation by the vector $\mathbf{d} = [d_1^2, d_2^2, d_3^2]^T$, such that the d_i are positive and fulfill the triangle inequalities

$$d_1 < d_2 + d_3\,, \quad d_2 < d_1 + d_3\,, \quad d_3 < d_1 + d_2\,. \tag{3.6}$$

By the triangle inequalities two unique and non collapsed triangles are defined, where one of the two is the triangle with clockwise labeled nodes as shown in Figure 3.1. The other one results if the triangle in Figure 3.1 is flipped over. Both triangles are non collapsed and thus the formation $(\mathcal{G}, e)$ is minimally rigid and and consequently also minimally persistent. Each robot i has the outgoing link e_i, which connects robot i to its leader $(i+1) \bmod 3$. From condition *(i)* the control input u_i of each robot may only depend on its outgoing link $e_i = z_{(i+1) \bmod 3} - z_i$, that is $u_i = u_i(e_i)$. Robot i's task is then to meet the distance constraint

$\|e_i\| = d_i$, and at the same time to converge to a stationary position, which corresponds to the conditions *(ii)* and *(iii)*.

The triangle is a popular example in the literature on formation control. It has, for example, been analyzed in combination with a directed cyclic sensor graph in [27, 28, 29], with an acyclic directed graph in [30] and with an undirected graph in [20, 25, 24] to name only a few examples. Also the results of [26, 23] are applicable to an undirected triangle and the results of [26] additionally to a directed acyclic triangle. Each of these mentioned references uses similar controllers to solve the formation control problem. However the analysis concepts are extremely different for each reference and thus hit other obstacles. Among the approaches are Lyapunov theory, passivity, the invariance principle in different versions, a cascade analysis and linearization combined with center manifold theory. We will refer back to the directed triangle and the referenced solution approaches in the following chapters.

3.2 Derivation of the Dynamic Equations

This section will propose a control law that is capable of solving the formation control problem. The closed-loop equations under this control can then be directly derived from the specific target formation.

3.2.1 A Potential Function Approach

The key idea to derive a control law that is both distributed and that guarantees local stability of the target formation can be motivated from physics. Consider an undirected graph and think for a moment of the robots as point masses and of the links interconnecting the point masses as springs, as it is illustrated in Figure 3.2(a). Each point mass connected to a spring has then a potential energy which takes its minimum iff the spring is in equilibrium. The force exerted by a spring on the mass corresponds to the gradient of its potential energy. Two point masses connected by a spring are then subject to either cohesion or separation forces exerted by the spring. The orientation and the magnitude of these forces depend on

the distance the two point masses are apart, as shown in Figure 3.2(b). Naturally each point mass moves into a position where the external forces acting on it take a minimum value and, if there is additional damping involved, the entire system of point masses comes to a stationary state where the overall potential energy takes a minimum.

(a) Point masses interconnected by springs

(b) Free body picture of Figure 3.2(b)

Figure 3.2: Point masses interconnected by springs and the forces exerted on the masses

This physical picture motivates a potential function based control design for undirected graphs, where the control inputs are designed to mimic the forces exerted by the springs. Early references applying this approach are [20, 23] and more recent ones are [26, 24]. Other approaches first construct a control law and then later relate it to a potential function [27, 28, 25]. Historically the idea of potential functions emerged for undirected graphs. We follow the approach of [26] and derive a control law for a general directed visibility graph $\mathcal{G}$. For each link e_i of the graph $\mathcal{G}$ a desired link length $d_i > 0$ is specified by the target formation $\big(\mathcal{G}, v^{-1}(\mathbf{d})\big)$. For each link we define a so-called potential function:

Definition 3.2.1. A function

$$V_i : \quad \big(-d_i^2, \infty\big) \rightarrow \mathbb{R} \tag{3.7}$$

is said to be a *potential function* if it has the following properties:

(i) V_i is defined and twice continuously differentiable on $(-d_i^2, \infty)$

(ii) $V_i(\omega) = 0 \Leftrightarrow \omega = 0$

(iii) $\nabla V_i(\omega) := \frac{\partial V_i(\omega)}{\partial \omega} = 0 \Leftrightarrow \omega = 0$

(iv) $\nabla V_i(\omega)$ is strictly monotone increasing

Hereby the notation ∇ denotes the gradient of a function. To arrive at an intuitive understanding of a potential function, we invoke again the physical interpretation and view the link as a spring which has to be designed. The potential function $V_i\big(\|e_i\|^2 - d_i^2\big)$ associated with the link e_i and also the force applied by the potential function $\nabla V_i\big(\|e_i\|^2 - d_i^2\big)$ take their minimum value iff $\|e_i\| = d_i$, that is, iff the link is in equilibrium. Otherwise the potential function is always positive and the force $\nabla V_i\big(\|e_i\|^2 - d_i^2\big)$ is always strictly growing depending on the stress applied to the link. The potential function itself may "blow off" if the spring is either stretched out infinitely or compressed to zero length, that is, $V_i(\omega) \to \infty$ if either $\omega \to 0$ or if $\omega \to \infty$. Two typical potential functions and their gradients are shown in Figure 3.3. Some references such as [26, 27] take simply a quadratic function (solid line in Figure 3.3), other literature, for example [20, 23, 24], requires the potential function to grow infinitely at the boundaries of its definition intervals (dashed line in Figure 3.3), and again others just require an infinitely steep slope at the left boarder of the interval of existence [29, 25]. Reference [28] establishes a result for the special case of a directed triangular formations considering general potential functions as in Definition 3.2.1.

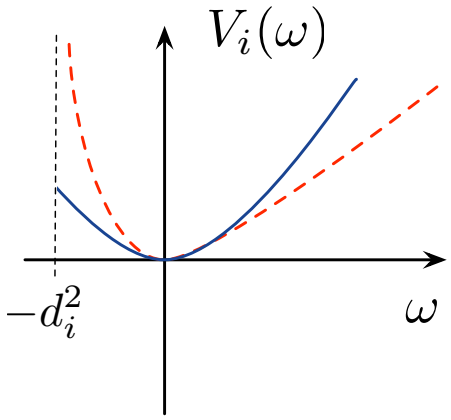

(a) Two typical potential functions used in the literature

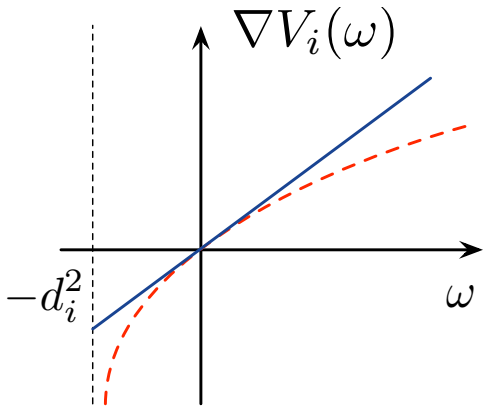

(b) The gradients of the two potential functions in Figure 3.3(b)

Figure 3.3: Examples of potential functions and their gradients

The control law for robot i can then be derived heuristically by the following argumentation. Robot i is subject to the forces acting on it by its outgoing links, that is to say, the position z_i of robot i is subject to the forces of created by the potential

$$\begin{aligned} \Phi_i : \quad & \mathcal{Z} \to \mathbb{R} \\ \Phi_i(z) \;=\; & \sum_{j \text{ with } o_{ij}\neq 0} V_j\big(\|e_j\|^2 - d_j^2\big)\,. \end{aligned} \tag{3.8}$$

Here $\mathcal{Z} \subset \mathbb{R}^{2n}$ is the domain where the potential functions are defined, that is, where no two robots connected by a link are collocated. A geometric definition of $\mathcal{Z}$ will be given in Chapter 5. The term o_{ij} is the jth element of the ith row of the outgoing edge matrix O and takes the value $o_{ij} = -1$ if e_j is an outgoing link of node i in the sensor graph; otherwise o_{ij} takes the value zero. In order to minimize the forces acting on it, robot i moves in the direction of the steepest descent of the potential function. Therefore, the velocity of robot i, which is the control input u_i, is given by the *gradient control*

$$u_i = -\left[\frac{\partial}{\partial z_i}\,\Phi_i(z)\right]^T \tag{3.9}$$

$$= -\sum_{j \text{ with } o_{ij}\neq 0} \left[\frac{\partial}{\partial z_i} V_j\big(\|e_j\|^2 - d_j^2\big)\right]^T \tag{3.10}$$

$$= -\sum_{j \text{ with } o_{ij}\neq 0} \left[\frac{\partial}{\partial \omega}\, V_j(\omega)\Big|_{\|e_j\|^2 - d_j^2} \frac{\partial\big(\|e_j\|^2 - d_j^2\big)}{\partial e_j}\, \frac{\partial e_j}{\partial z_i}\right]^T \tag{3.11}$$

$$= \sum_{j \text{ with } o_{ij}\neq 0} \big[\nabla V_j\big(\|e_j\|^2 - d_j^2\big)\, 2\, e_j^T\, (-1)\big]^T\,. \tag{3.12}$$

Note that u_i is indeed a distributed control law, that is, it depends only on outgoing links $e_j = z_k - z_i$ with $k \in N_i$. With $o_i^T = [0, \ldots, 0, -1, 0, \ldots, 0]\, O$ denoting the ith row of O and the vector $\mathbf{\Psi}(e) \in \mathbb{R}^m$ containing the gradients of the potential functions

$$\mathbf{\Psi}(e) \;:=\; 2 \begin{bmatrix} \nabla V_1\big(\|e_1\|^2 - d_1^2\big) \\ \vdots \\ \nabla V_m\big(\|e_m\|^2 - d_m^2\big) \end{bmatrix} \tag{3.13}$$

the closed-loop dynamics of robot i can be written in vector form as

$$\dot{z}_i \;=\; -\hat{o}_i^T\, \mathrm{diag}\,\{e_i\}\; \mathbf{\Psi}(e) \tag{3.14}$$

and the overall *z-dynamics* are then obtained as

$$\begin{aligned} \dot{z} &= -\hat{O}\,\mathrm{diag}\,\{e_i\}\;\boldsymbol{\Psi}(e) \\ z(0) &= z_0 \in \mathcal{Z}\,. \end{aligned} \tag{3.15}$$

Example 3.1.3. Directed triangle (continued):
For the directed triangle the outgoing edge matrix is simply $O = -I_3$ and we obtain the control input of robot i as

$$u_i = 2\,e_i\,\nabla V_i\big(\|e_i\|^2 - d_i^2\big) = u_i(e_i) \tag{3.16}$$

and the overall z-dynamics as

$$\begin{bmatrix}\dot{z}_1\\ \dot{z}_2\\ \dot{z}_3\end{bmatrix} = \begin{bmatrix}2\,e_1\,\nabla V_1\big(\|e_1\|^2 - d_1^2\big)\\ 2\,e_2\,\nabla V_2\big(\|e_2\|^2 - d_2^2\big)\\ 2\,e_3\,\nabla V_3\big(\|e_3\|^2 - d_3^2\big)\end{bmatrix} \tag{3.17}$$

$$= \begin{bmatrix}2\;(z_2 - z_1)\;\nabla V_1\big(\|(z_2 - z_1\|^2 - d_1^2\big)\\ 2\;(z_3 - z_2)\;\nabla V_2\big(\|z_3 - z_2\|^2 - d_2^2\big)\\ 2\;(z_1 - z_3)\;\nabla V_3\big(\|z_1 - z_3\|^2 - d_3^2\big)\end{bmatrix}. \tag{3.18}$$

The closed loop behavior of the three robots is analogous to the one in the introductory example of the two points on a line (Example 1.2.1). Each robot i has leader robot $(i+1) \bmod 3$ and each robot i pursues its leader. The speed by which robot i is pursuing its leader has a nonlinear gain, namely the force $2\,\nabla V_i\big(\|e_i\|^2 - d_i^2\big)$ exerted by the potential function $V_i\big(\|e_i\|^2 - d_i^2\big)$.

3.2.2 A General Distributed Control Structure for Autonomous Robots

Although this control law seems fairly special compared to the class of admissible distributed control laws, it is very general and captures a wide variety of formation and consensus control laws. To see this generality, let us introduce the diagonal operator C as

$$\begin{aligned} C:\quad & \hat{H}\left(\mathbb{R}^{2n}\right) \to \mathbb{R}^{2m} \\ C(e) &= \mathrm{diag}\,\{e_i\}\;\boldsymbol{\Psi}(e)\,. \end{aligned} \tag{3.19}$$

With the operator C, the incidence matrix H and the outgoing edge matrix O of the graph $\mathcal{G}$ the overall control law can be formulated as

$$u \;=\; -\hat{O}\, C\left(\hat{H}\, z\right) \tag{3.20}$$

and the resulting closed-loop z-dynamics are given by

$$\dot{z} \;=\; -\hat{O}\, C\left(\hat{H}\, z\right) \tag{3.21}$$

and are illustrated in Figure 3.4. The open-loop dynamics $\dot{z} = u$ constitute a diagonal multi-agent system. The output of this system are the positions z, which are mapped to the links e via $\hat{H}$. The links e enter the diagonal operator C, which can be seen as a controller. The output of the controller is then negatively fed back to the robot dynamics via the outgoing edge matrix $\hat{O}$, which makes sure that the control law is indeed distributed. The only external input to the controlled multi-agent system is the initial condition $z(0) = z_0$.

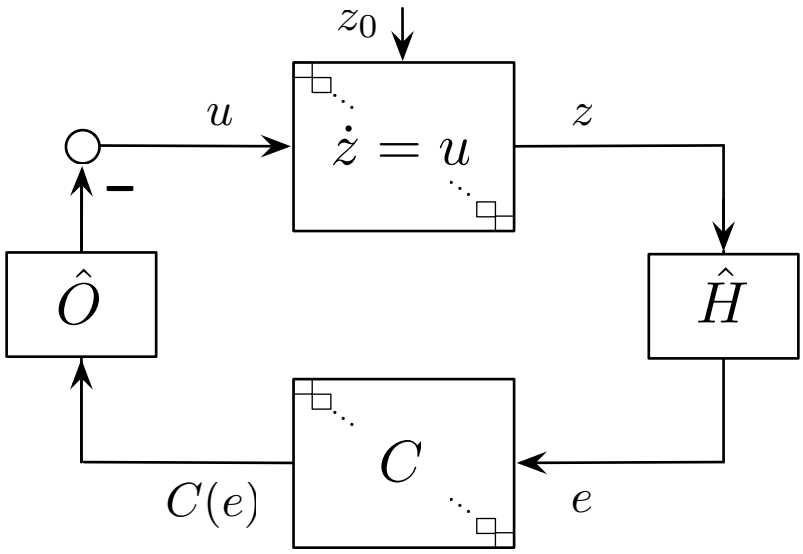

Figure 3.4: Autonomous robots under distributed control

The control setup from Figure 3.4 can of course be found in formation control with directed graphs [26, 27, 28, 29, 30], but besides that also in certain *consensus/rendezvous* problems [41, 42, 10, 11, 43], where the control objective is a convergence of the robots to a common position. We illustrate this in the case of a control strategy called *cyclic pursuit*.

Example 3.2.1. Consider a cyclic graph with clockwise labeled nodes corresponding to robots, for example, the directed triangle. If we set C to be the identity map, that is $C = I_{2m}$, then the closed-loop dynamics are simply

$$\dot{z} = -\hat{O}\,\hat{H}\,z = \hat{H}\,z \tag{3.22}$$

$$= \begin{bmatrix} -I_2 & I_2 & 0 \\ 0 & -I_2 & I_2 \\ I_2 & 0 & -I_2 \end{bmatrix} z\,. \tag{3.23}$$

If we write the equations out in components, for example $\dot{z}_1 = z_2 - z_1$, we see that the robots pursue each other in a cyclic way. Note that the centroid of the robots, which is the vector $\frac{1}{n}\,(\mathbf{1} \otimes I_2)^T\,z = \frac{1}{n}\,\mathbf{I}_2^T\,z$, is stationary since $\mathbf{I}_2^T\,\dot{z} = \mathbf{0}$. The matrix $\hat{H}$ has two zero eigenvalues and the remaining ones are negative. Thus the robots converge to the zero eigenspace of the matrix $\hat{H}$ which is span $\{\mathbf{I}_2\}$, that is, the robots meet at a common point. Note that this control could also have been derived from the potential function $V_i(e_i) = \frac{1}{2}\,\|e_i\|^2$, that is, $u_i = -\left[\nabla V_i(e_i)\right]^T$.

Undirected Graphs

Let us now specify the results from the previous paragraphs to undirected graphs. We can of course treat any undirected graph $\mathcal{G}$ as a directed graph, but then we actually consider two times the same directed graph, with different orientations of the edges. This might simplify the control structure from Figure 3.4 tremendously as we see in the following example.

Example 3.2.2. An extension of the cyclic pursuit strategy presented in the previous example to a more general rendezvous strategy, where the graph is not necessarily a directed cycle, can be obtained by setting again $C = I_{2m}$. The robots in the resulting closed-loop system $\dot{z} = -\hat{O}\,\hat{H}\,z$ converge to a common point iff the graph has a globally reachable node [42]. The control law in [42] is originally derived from the adjacency matrix A and the out-degree matrix D of the graph as $u = -\hat{L}\,z$, where $L := D - A$ is the Laplacian of the graph. We noted in Section 2.1.1 that for an undirected graph we have the identity $\hat{L} = \hat{H}_u^T\,\hat{H}_u$, where H_u is the incidence matrix of the undirected graph. The dynamics for an undirected graph

are then given by $\dot{z} = -\hat{H}_u^T \hat{H}_u z$, that is, the very same dynamics as for a directed graph, but now $\hat{O}$ is replaced by $\hat{H}_u^T$.

If we look at an undirected graph $\mathcal{G}$ as a directed graph with m links, where each link appears twice in different orientations, then the links can then be labeled in such a way that the edge set E of the graph $\mathcal{G} = (V, E)$ is given by

$$E \;=\; \{e_{1_1}\,,\, e_{2_1}\,,\, \ldots\,,\, e_{m_1}\,,\, e_{1_2}\,,\, e_{2_2}\,,\, \ldots\,,\, e_{m_2}\}\,, \tag{3.24}$$

where $e_{i_1} = -e_{i_2}$, that is e_{i_1} and e_{i_2} have opposite directions. The undirected graph $\mathcal{G}_u$ can be split up in two directed graphs $\mathcal{G}_1 = (V, E_1)$ and $\mathcal{G}_2 = (V, E_2)$ where $E_i = \{e_{1_i}\,,\, e_{2_i}\,,\, \ldots\,,\, e_{m_i}\}$. By the definition of the matrices H, U and O in Section 2.1.1 we get the following relation between the graphs $\mathcal{G}, \mathcal{G}_1, \mathcal{G}_2$:

$$O \;=\; \Big[O_1 \,|\, O_2\Big]\;,\; O_1 \;=\; -U_2 \quad\text{and}\quad O_2 \;=\; -U_1 \tag{3.25}$$

$$H \;=\; \begin{bmatrix} H_1 \\ - - - - \\ H_2 \end{bmatrix} \;=\; \begin{bmatrix} H_1 \\ - - - - \\ -H_1 \end{bmatrix} \tag{3.26}$$

$$H_1^T \;=\; O_1 + U_1 \;=\; O_1 - O_2 \tag{3.27}$$

The controller $C(e)$ from (3.20) is then given by

$$C(e) \;=\; \operatorname{diag}\{e_i\}\;\boldsymbol{\Psi}(e) \;=\; \begin{bmatrix} \operatorname{diag}\{e_{i_1}\} & \mathbf{0} \\ \mathbf{0} & \operatorname{diag}\{e_{i_2}\} \end{bmatrix} \boldsymbol{\Psi}(e) \tag{3.28}$$

$$= \; 2 \begin{bmatrix} \operatorname{diag}\{e_{i_1}\} & \mathbf{0} \\ \mathbf{0} & \operatorname{diag}\{e_{i_2}\} \end{bmatrix} \begin{bmatrix} \nabla V_{1_1}\big(\|e_{1_1}\|^2 - d_1^2\big) \\ \vdots \\ \nabla V_{m_1}\big(\|e_{m_1}\|^2 - d_m^2\big) \\ - - - - - - - - - - - - \\ \nabla V_{1_2}\big(\|e_{1_2}\|^2 - d_1^2\big) \\ \vdots \\ \nabla V_{m_2}\big(\|e_{m_2}\|^2 - d_m^2\big) \end{bmatrix} \tag{3.29}$$

$$= 2 \begin{bmatrix} \text{diag}\{e_{i_1}\} & \mathbf{0} \\ \mathbf{0} & -\text{diag}\{e_{i_1}\} \end{bmatrix} \left[\begin{array}{c} \nabla V_{1_1}\left(\|e_{1_1}\|^2 - d_1^2\right) \\ \vdots \\ \nabla V_{m_1}\left(\|e_{m_1}\|^2 - d_m^2\right) \\ \hline \nabla V_{1_1}\left(\|e_{1_1}\|^2 - d_1^2\right) \\ \vdots \\ \nabla V_{m_1}\left(\|e_{m_1}\|^2 - d_m^2\right) \end{array}\right] \tag{3.30}$$

$$= \begin{bmatrix} C_1(e_1) \\ -C_1(e_1) \end{bmatrix} \tag{3.31}$$

where $e_1 = [e_{1_1}\ ,\ e_{2_1}\ ,\ \ldots\ ,\ e_{m_1}]^T = \hat{H}_1\, z$ and $C_1(e_1) = C_1\left(\hat{H}_1\, z\right)$ is the control applied to graph $\mathcal{G}_1$. The overall control u input is then

$$u = -\hat{O}\, C\left(\hat{H}\, z\right) = -\left[\hat{O}_1 \mid \hat{O}_2\right] \begin{bmatrix} C_1(e_1) \\ -C_1(e_1) \end{bmatrix} \tag{3.32}$$

$$= -\left[\hat{O}_1 \mid \hat{O}_1 - \hat{H}_1^T\right] \begin{bmatrix} C_1(e_1) \\ -C_1(e_1) \end{bmatrix} \tag{3.33}$$

$$= -\hat{H}_1^T\, C_1(e_1) = -\hat{H}_1^T\, C_1\left(\hat{H}_1\, z\right). \tag{3.34}$$

We now go back to the representation of the undirected graph $\mathcal{G}$ with $\frac{m}{2}$ bidirectional links e. Let us choose an arbitrary orientation of the links e, such that $e = \hat{H}_u\, z$. Without loss of generality we can choose the orientation such that $H_u = H_1$ and thus the overall z-dynamics for an undirected graph are

$$\dot{z} = u = -\hat{H}_u^T\, C\left(\hat{H}_u\, z\right), \tag{3.35}$$

that is, the same dynamics that we obtain for a directed graph just with $\hat{O}$ replaced by $\hat{H}_u^T$. The closed loop is illustrated in Figure 3.5. Examples where the setup from Figure 3.5 appears in formation control are formation control with rigid graphs [26], where we have in the notation of [26] $C(e) = J_v(e)^T\,(v(e) - d^2)$, and formation control with undirected graphs [25, 20, 23, 24]. Additionally, as mentioned in Example 3.2.2, the control structure with C as identity map also appears in the rendezvous problem with undirected graphs [43, 41, 42].

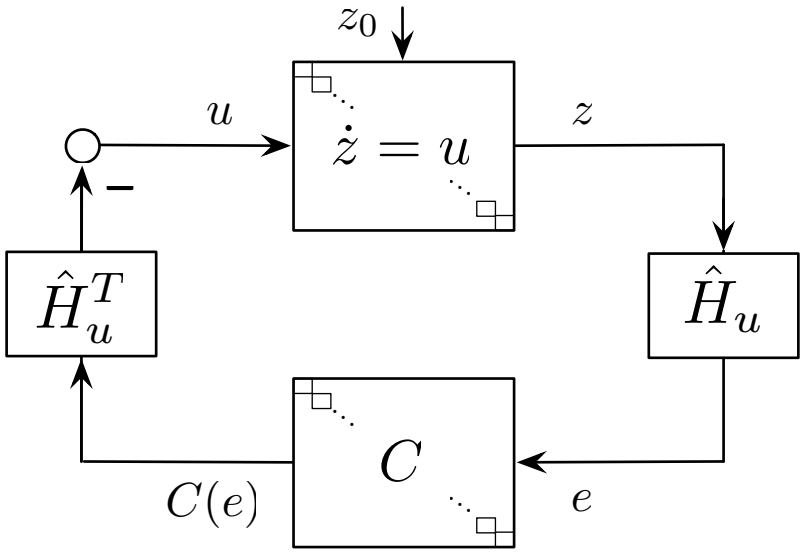

Figure 3.5: Autonomous robots under distributed control with an undirected sensor graph

Properties of the Gradient Control

Reference [44] proves that the control law (3.20) when applied to undirected graphs with the special the potential functions $V_i(\omega) = \frac{1}{2}\omega^2$ is independent of rotations and translations of the framework in the plane ([44], Lemma 5.2). This result follows from the fact that the argument of the potential function is the deviation of the link length from its desired length. This result directly transferable to the case of a more general potential function as defined in Definition 3.2.1 and to directed graphs. We omit the simple proofs and refer the interested reader to [44].

Another result of [44], which is extendable to directed graphs, is that under the control (3.20) initially collinear robots stay collinear $\forall\, t \geq 0$ ([44], Lemma 5.3). We again omit the proof and will show it later for the specific example of the directed triangle (Example 3.1.3).

For undirected graphs the control law (3.35) has the additional interesting property that the vector $\frac{1}{n}\,\mathbf{I}_2^T\, z$, which is the centroid of the robots, is stationary ([44], Lemma 5.1). This result follows directly from the fact that $\mathbf{I}_2^T\, \dot{z} = \mathbf{0}$ because $\mathbf{I}_2 \in \ker\left(\hat{H}\right)$.

Extensions of the General Distributed Control Framework

This short section diverges from the thesis and points out different control algorithms from the literature which can be seen as extensions of the control structure in Figure 3.4.

External Inputs If we admit additional external inputs the control structure of Figure 3.4 also captures different extensions of formation and consensus control laws, for example, so-called *linear formations* [41, 10]. The idea is that, if each robot is equipped with an additional onboard compass, it can determine a global direction. In this case a robot can do more than simply pursuing another one as in cyclic pursuit. A robot can now pursue a relative displacement $c_i \in \mathbb{R}^2$ of the other robot, for example, $\dot{z}_1 = (z_2 + c_1) - z_1$. Written out in vector form the dynamics then are $\dot{z} = \hat{H}\, z + c$, where $c = [c_1, \ldots, c_n]^T \in \mathbb{R}^{2n}$ is the displacement vector. Additionally for the displacement vector $\mathbf{1}^T c = 0$ must hold for the centroid to be stationary. The system with the external input c is illustrated in Figure 3.6(a). Consider now a vector a vector $d \in \mathbb{R}^{2n}$ and let us apply the following trick:

$$\frac{d}{d\,t}\,(z - d) \;=\; \dot{z} \;=\; \hat{H}\, z + c \;=\; \hat{H}\,(z - d) + \hat{H}\, d + c \tag{3.36}$$

If we choose d uniquely from $\hat{H}\, d + c = \mathbf{0}$ and $\mathbf{1}^T d = 0$, we regain the cyclic pursuit dynamics with the new variable $z - d$. The position z_i of robot i will then converge to the centroid displaced by d_i. Thus the robots altogether converge to a formation. The algebraic trick which we applied corresponds to shifting the displacement vector c around the loop as indicated in Figure 3.6(b).

With external inputs we can also extend formation (respectively consensus) control laws to moving robots, which besides their actual tasks also track a continuously differentiable curve $z_{ref}(t) \in \mathbb{R}^2$. If we extend the control structure as shown in Figure 3.7(a), the error variable $z - z_{ref}(t)\mathbf{1}$ then follows the dynamics

$$\frac{d}{d\,t}\left(z - z_{ref}(t)\mathbf{1}\right) \;=\; -\hat{O}\, C\left(\hat{H}\left(z - z_{ref}(t)\mathbf{1}\right)\right). \tag{3.37}$$

The controller C, which is originally designed to stabilize a stationary formation (respectively consensus) problem, then also stabilizes the error dynamics (3.37). Note that $\mathbf{1} \in \ker\left(\hat{H}\right)$

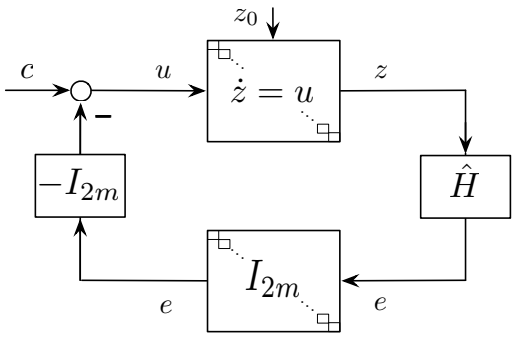

(a) Control structure for linear formations

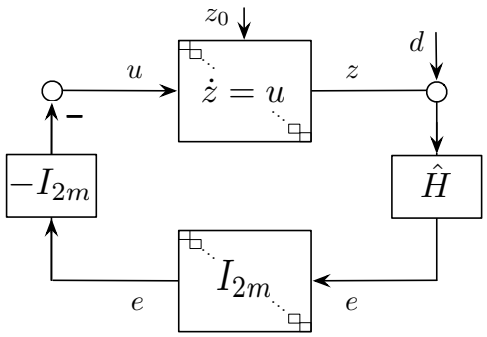

(b) The vector d is the displacement vector c shifted around the loop

Figure 3.6: Linear formations

and thus the control structure simplifies to the one in Figure 3.7(b). Thus each robots needs to know the global velocity vector $z_{ref}(t)$ and the tracking "comes for free." This structure was for example exploited by [24, 23], but has the clear drawback, that every robot needs to know the global velocity vector. If only one leader robot knows the global velocity vector and the other robots should track this leader, then the they need an adaptive control algorithm to guess the leader's velocity vector. This is the outline of the main idea of [45, 46].

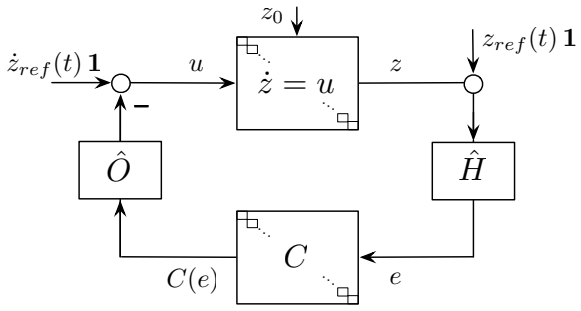

(a) The controller C guarantees stable error dynamics

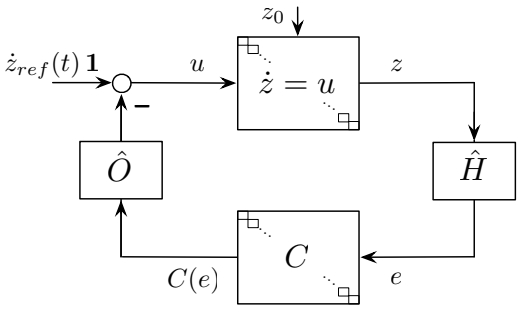

(b) A global velocity vector is sufficient for distributed control combined with tracking

Figure 3.7: Distributed Control combined with tracking

Time-varying sensor graph The control structure of Figure 3.4 can also be extended to a time-varying sensor graph $\mathcal{G}(t)$, where the matrices $H(t)$ and $O(t)$ are time-varying. Formation control based on potential functions [18] and also the concensus problem [24] can then be extended to a time-varying sensor graph. The conditions on the matrices $H(t)$ and $O(t)$, under which this is possible, turn out to correspond to connectivity properties of the sensor graph $\mathcal{G}(t)$. This time-varying setup has so far been only considered for undirected graphs, but the author firmly believes that the results of this thesis also allow a straightforward extension to a certain class of directed graphs, so-called cooperative graphs which will be presented in Chapter 5.

Thus the control structure in Figure 3.4 includes a wide variety of formation and consensus control laws, even for time-varying graphs. However it does for example not include the *circumcentre control law*, a consensus control law which was first introduced in the discrete time case in [47, 13] and later also extended to the continuous time case [12] and to sampled-data systems [48]. Nevertheless, we propose control law (3.20) as a standard control structure which might be extendable to a more general diagonal multi-agent system where the agents themselves have higher order dynamics. This has for example been shown in [24], where the undirected graph control law (3.35) has been successfully applied to strictly passive agents.

Chapter 4

Preliminaries and Definitions II

This chapter gives the necessary preliminaries on set stability theory and inverse optimality, which will be the key tools to prove the results in Chapter 5.

4.1 Set Stability Theory

Set stability theory is an extension of the well known Lyapunov stability concepts w.r.t. to an equilibrium point, which is treated extensively in [49, 50]. In particular all common definitions and theorems can be extended from the equilibrium point case to stability of closed, invariant sets if the solutions are well defined. Set stability theory is extensively discussed in [50, 51, 52] and this section introduces the necessary definitions and results, which we will make use of in Chapter 5.

In this section we consider the autonomous ordinary differential equation

$$\dot{x} \;=\; f(x)\,, \tag{4.1}$$

where $f : D \to \mathbb{R}^n$ is a locally Lipschitz continuous function of x and $D \subset \mathbb{R}^n$ is a domain. The variable $x \in D$ is the *state* and $x(0) = x_0 \in D$ is the *initial condition* of the system (4.1). Due to its local Lipschitz property a unique solution $x(t)$ to (4.1) is defined on some maximum interval of existence $I_0 = (T_{x0}^-, T_{x0}^+)$ with $-\infty \leq T_{x0}^- < 0 < T_{x0}^+ \leq +\infty$. The

mapping

$$\Phi \,:\, I_0 \times D \to D\,, \tag{4.2}$$

where $\Phi(t, x_0)$ satisfies the differential equation for an initial condition $x_0 \in D$, is called the *flow* of (4.1). The flow is usually defined as a one-parameter group [53], but for our purposes it is sufficient to think of the flow $\Phi(t, x_0)$ as the solution $x(t)$ of (4.1) at time $t \in I_0$ and with initial condition x_0. The system (4.1) is said to be *forward complete* if $\forall\, x_0 \in D$, $T^+_{x0} = +\infty$, it is *backward complete* if $\forall\, x_0 \in D$, $T^-_{x0} = -\infty$, and it is *complete* if it is both forward and backward complete.

We say that a nonempty, closed set $\mathcal{A} \subseteq D$ is a *positively invariant set* w.r.t. (4.1) if

$$(\forall\, x_0 \in \mathcal{A})\ T^+_{x0} = +\infty \quad \text{and} \quad (\forall\, t \geq 0)\ \Phi(t, x_0) \in \mathcal{A}\,, \tag{4.3}$$

$\mathcal{A}$ is a *positively invariant set* w.r.t. (4.1) if

$$(\forall\, x_0 \in \mathcal{A})\ T^-_{x0} = -\infty \quad \text{and} \quad (\forall\, t \leq 0)\ \Phi(t, x_0) \in \mathcal{A}\,, \tag{4.4}$$

and $\mathcal{A}$ is *invariant* if it is both positively and negatively invariant. Without loss of generality the set $\mathcal{A}$ is closed because if $\mathcal{A}$ is invariant, the closure $\bar{\mathcal{A}} := \mathcal{A} \cup \partial\mathcal{A}$ is also invariant ([50],Theorem 16.3). A special invariant set is the *equilibrium set* $f^{-1}(\mathbf{0})$, where $\dot{x} = \mathbf{0}$.

There exist various stability and attractivity concepts for invariant sets and especially for non-compact invariant sets (see [52], Chapter VI. for an overview). However the way we define set stability is a straightforward extension of the well known definition for an equilibrium point, and thus the stability theorems will also be based on standard Lyapunov theory. In order to continue we define the *point to set distance* for each nonempty $\mathcal{A} \subseteq D$ and each $x \in D$ as

$$\|x\|_{\mathcal{A}} \;:=\; \operatorname{dist}(x, \mathcal{A}) \;=\; \inf_{\xi \in \mathcal{A}} \|x - \xi\|\ . \tag{4.5}$$

The point to set distance allows us to define stability of a closed set. The following definition of set stability is taken from [50], but can be found under different names also in [51, 52].

Definition 4.1.1. Consider system (4.1) and the nonempty, closed invariant set $\mathcal{A} \subseteq D$. The set $\mathcal{A}$ is said to be *stable* w.r.t. (4.1) if (4.1) is forward complete and

$$(\forall\, \epsilon > 0)\ (\exists\, \delta > 0)\ \ \|x_0\|_{\mathcal{A}} < \delta \ \ \Rightarrow\ \ (\forall\, t \geq 0)\ \|x(t)\|_{\mathcal{A}} < \epsilon\,. \tag{4.6}$$

Otherwise $\mathcal{A}$ is *unstable*. The set $\mathcal{A}$ is said to be *attractive* w.r.t. (4.1) if

$$(\exists\, \gamma > 0)\ \|x_0\|_{\mathcal{A}} < \gamma \ \ \Rightarrow\ \ \lim_{t\to\infty} \|x(t)\|_{\mathcal{A}} \to 0\,. \tag{4.7}$$

The *region of attraction* Ω is given by the set of all points $x_0 \in D$ with the property

$$\Omega \ = \ \left\{ x_0 \in D \,\middle|\, \lim_{t\to\infty} \|\Phi(t, x_0)\|_{\mathcal{A}} \ = \ 0 \right\}. \tag{4.8}$$

The set $\mathcal{A}$ is *asymptotically stable* w.r.t. (4.1) if it is both stable and attractive, and it is *exponentially stable* w.r.t. (4.1) if there exist positive constants c_1, c_2 and c_3 such that

$$(\forall\, t \geq 0)\ (\forall\ \|x_0\|_{\mathcal{A}} < c_1)\ \ \|x(t)\|_{\mathcal{A}} \ \leq \ c_2\, \|x_0\|_{\mathcal{A}}\, e^{-c_3\, t}\,. \tag{4.9}$$

If $D = \mathbb{R}^n$ and $\Omega = \mathbb{R}^n$, then $\mathcal{A}$ is said to be *globally asymptotically stable*, respectively *globally exponentially stable*, w.r.t. (4.1).

Observe that when $\mathcal{A}$ is compact the assumption of forward completeness is redundant, since in that case property (4.6) implies that solutions are bounded on a compact invariant set which again implies by standard arguments existence and uniqueness $\forall\, t \geq 0$ ([49], Theorem 3.3). Note that the right-hand side of (4.9) constitutes a function which is increasing w.r.t. $\|x_0\|_{\mathcal{A}}$ and exponentially decreasing in time. This idea can be generalized to so-called comparison functions which were introduced in [50]. With the help of comparison functions an equivalent characterization of stability and asymptotically stability can be obtained, which will turn out to be mathematically more convenient. The following definitions of comparison functions are directly taken from ([49], Definitions 4.2,4.3) and ([50], Definitions 2.5-2.6, 36.1-36.3).

Definition 4.1.2. *Comparison functions*:

- A continuous function $\alpha : [0, a) \to [0, \infty)$ is said to belong to class $\mathcal{K}$ if it is strictly increasing and $\alpha(0) = 0$. It is said to belong to the class $\mathcal{K}_\infty$ if additionally $a = \infty$ and $\lim_{r\to\infty} \alpha(r) \to \infty$.

- A continuous function $\sigma : [0, \infty) \to [0, \infty)$ is said to belong to class $\mathcal{L}$ if it is strictly decreasing and $\lim_{r \to \infty} \sigma(r) \to 0$.
- A continuous function $\beta : [0, a) \times [0, \infty) \to [0, \infty)$ is said to belong to class $\mathcal{KL}$ if, for each fixed s, the mapping $\beta(r, s)$ belongs to class $\mathcal{K}$ w.r.t. r and, for each fixed r, the mapping $\beta(r, s)$ is decreasing w.r.t. s and $\lim_{s \to \infty} \beta(r, s) \to 0$.

With the help of comparison functions the concept of set stability defined in Definition 4.1.1 can be equivalently formulated in a more general way, which extends to stability properties of non-autonomous systems ([49], Lemma 4.5).

Lemma 4.1.1. *The set $\mathcal{A}$ is stable w.r.t. (4.1) if and only if it is forward complete and there exists a $\mathcal{K}$-function α and a positive constant c, such that*

$$(\forall\, t \geq 0)\ (\forall\, \|x_0\|_{\mathcal{A}} < c)\ \ \|x(t)\|_{\mathcal{A}} \ \leq\ \alpha\left(\|x_0\|_{\mathcal{A}}\right), \tag{4.10}$$

the set $\mathcal{A}$ is asymptotically stable w.r.t. (4.1) if and only if it is forward complete and there exists a $\mathcal{KL}$-function β and a positive constant c, such that

$$(\forall\, t \geq 0)\ (\forall\, \|x_0\|_{\mathcal{A}} < c)\ \ \|x(t)\|_{\mathcal{A}} \ \leq\ \beta\left(\|x_0\|_{\mathcal{A}}, t\right), \tag{4.11}$$

and $\mathcal{A}$ is globally asymptotically stable if and only if $D = \mathbb{R}^n$ and (4.11) holds for any $x_0 \in \mathbb{R}^n$.

Note that, if in (4.11) we can find $\beta\left(\|x_0\|_{\mathcal{A}}, t\right) = c_2\ \|x_0\|_{\mathcal{A}}\ e^{-c_3\, t}$ with positive constants c_2 and c_3, then we have the definition of exponentially stability.

In Chapter V.2 of [51] it is shown in various theorems and examples that (asymptotic) stability of a closed set $\mathcal{A}$ is equivalent to the existence of a continuous function $V(x)$, where $V(\Phi(t, x_0))$ is (strictly) decreasing $\forall\, t \geq 0$ and which takes its minimum value iff $x \in \mathcal{A}$. Unfortunately this characterization of stability requires the knowledge of the flow $\Phi(t, x_0)$ of the system, which we do in general not have. If we additionally require smooth differentiability of the function $V(x)$, then the condition that $V(\Phi(t, x_0))$ is (strictly) decreasing reduces to an algebraic condition on the derivative of $V(x)$ along trajectories of (4.1). Such a function is called a Lyapunov function.

Definition 4.1.3. A *Lyapunov function* for the system (4.1) w.r.t. a nonempty, closed invariant set $\mathcal{A} \subseteq D$ is a continuously differentiable function $V : D \to \mathbb{R}$, such that there exist two class $\mathcal{K}$ functions α_1, α_2 and a continuous positive semidefinite function α_3 such that $\forall\, x \in D$ and $\forall\, t \geq 0$

$$\alpha_1 \left(\|x\|_{\mathcal{A}} \right) \;\leq\; V(x) \;\leq\; \alpha_2 \left(\|x\|_{\mathcal{A}} \right) \tag{4.12}$$

$$\dot{V}(x) \;:=\; \frac{\partial V(x)}{\partial x} f(x) \;\leq\; -\alpha_3 \left(\|x\|_{\mathcal{A}} \right) . \tag{4.13}$$

Since we defined set stability in terms of comparison functions, the well known Lyapunov stability theorems for the equilibrium point case and also their proofs extend almost one-to-one to the set stability case, where we need only the additional assumption of forward completeness. A summary of various theorems on set stability which can be found in [50, 51, 52] is given in the next theorem.

Theorem 4.1.1. *Assume that system (4.1) is forward complete. Let $\mathcal{A} \subseteq D$ be a nonempty, closed invariant set for this system and assume there exists a Lyapunov function for (4.1). Then*

*(i) $\mathcal{A}$ is **stable** w.r.t. (4.1),*

*(ii) if α_3 is a positive definite function then $\mathcal{A}$ is **asymptotically stable** w.r.t. (4.1), and*

(iii) if there exists positive constants k_1, k_2, k_3 and a s.t.

$$\alpha_1 = k_1 \, \|x\|_{\mathcal{A}}^a \;,\; \alpha_2 = k_2 \, \|x\|_{\mathcal{A}}^a \;,\; \alpha_3 = k_3 \, \|x\|_{\mathcal{A}}^a \tag{4.14}$$

*then $\mathcal{A}$ is **exponentially stable** w.r.t. (4.1).*

*(iv) In case (ii) and (iii) the guaranteed **region of attraction** is given by the sublevel set*

$$\Omega(c) \;=\; \{x \in D \,|\, V(x) \leq c\} \tag{4.15}$$

*where (ii) or (iii) hold. If $D = \mathbb{R}^n$, (ii) (respectively (iii)) hold on $\mathbb{R}^n$, and α_1 and α_2 are $\mathcal{K}_\infty$ functions, the system is **globally asymptotically** (respectively **globally exponentially stable**).*

Remark 4.1.1.

- Observe that when $\mathcal{A}$ is compact, forward completeness is again a redundant property, since in that case property (4.10) implies that solutions are bounded.

- We should note that concepts such as Lasalle's invariance principle ([49], Theorem 4.4) require compact, invariant sets. For a non-compact set $\mathcal{A}$ the sublevel set $\Omega(c)$ is not compact and thus the corollaries of the invariance principle (Barbashin's and Krasovskii's Theorem) cannot be applied to the set where $\dot{V}(x) = 0$.

- According to ([50],Theorem 25.6) a sufficient condition for local exponential stability is that the three comparison functions α_i are of the same order of magnitude, that is,

$$a_{ij}\,\alpha_i \;\leq\; \alpha_j \;\leq\; b_{ij}\alpha_i \quad i \neq j \tag{4.16}$$

  for some constants a_{ij} and b_{ij} and $i, j \in \{1, 2, 3\}$. We introduce some conservatism in Theorem 4.1.1 by restricting the comparison functions to be proportional to $\|x\|^a_{\mathcal{A}}$. However, we will later refer back to this idea in Chapter 5, where we find the Lyapunov function itself to be exponentially decreasing in time.

- Theorem 4.1.1 generalizes the well known Lyapunov stability theorem w.r.t. an equilibrium point. A very interesting generalization of this theorem to differential inequalities and discrete time systems can be found in [54].

Note that Definition 4.1.3 does not require that we indeed know upper and lower bounding class $\mathcal{K}$ functions on the Lyapunov function, these just have to exist. The following definition and lemma are useful for relating a function to upper and lower bounding class $\mathcal{K}$ functions with the point to set distance as argument.

Definition 4.1.4. Let $D \subset \mathbb{R}^n$ be a domain, $\mathcal{A} \subseteq D$ be a nonempty and closed set, and let $V : D \to \mathbb{R}$ be a continuous function. The function V is said to be *positive semidefinite* (p.s.d.) w.r.t. $\mathcal{A}$ if

$$V(x) \;=\; \begin{cases} = 0 & \forall\, x \in \mathcal{A} \\ \geq 0 & \forall\, x \in D \setminus \mathcal{A}\,. \end{cases} \tag{4.17}$$

If the upper inequality is a strict inequality, then V is *positive definite* (p.d.) w.r.t. $\mathcal{A}$. If $(-V)$ is p.d. (respectively p.s.d.) w.r.t. $\mathcal{A}$, then V is said to be *negative definite* (n.d.) (respectively *negative semidefinite* (n.s.d.)) w.r.t. $\mathcal{A}$. Otherwise V is *indefinite*.

Lemma 4.1.2. *Let $D \subset \mathbb{R}^n$ be a domain, $\mathcal{A} \subseteq D$ be a nonempty and closed set, and let $V : D \to \mathbb{R}$ be a continuous function. Let V be positive definite w.r.t. $\mathcal{A}$ and let*

$$B_r(\mathcal{A}) \;=\; \{x \in \mathbb{R}^n \,|\, \|x\|_{\mathcal{A}} \leq r\} \subset D \tag{4.18}$$

for some $r > 0$. Then, there exist class $\mathcal{K}$ functions α_1 and α_2 defined on $[0, r]$, such that $\forall\, x \in B_r(\mathcal{A})$

$$\alpha_1\left(\|x\|_{\mathcal{A}}\right) \;\leq\; V(x) \;\leq\; \alpha_2\left(\|x\|_{\mathcal{A}}\right). \tag{4.19}$$

If $D = \mathbb{R}^n$, the functions α_1 and α_2 will be defined on $[0, \infty)$ and the foregoing inequality will hold $\forall\, x \in \mathbb{R}^n$. Moreover, if $V(x)$ is radially unbounded, then α_1 and α_2 can be chosen to belong to class $\mathcal{K}_\infty$.

For a constructive proof of Lemma 4.1.2 we refer the reader to the proof of Lemma 4.3 from [49], which is given for $\mathcal{A} \equiv \mathbf{0}$. However, for our later needs in Chapter 5 we will have to explicitly construct the comparison functions.

A clear obstacle is that Theorem 4.1.1 is only sufficient and we have to find a function $V(x)$ with a negative (semi)definite derivative. The recent references [55, 56] show that for a complete system the existence of a radially unbounded Lyapunov function with a negative definite derivative is both necessary and sufficient for global asymptotic stability, but this function still has to be found. The next section on optimal control allows us to obtain an "optimal" Lyapunov function candidate as solution of a PDE.

4.2 Optimal Control and Inverse Optimality

One way to rather calculate than guess a Lyapunov function for a nonlinear system is to solve an optimal control problem, that is, to find a controller which optimizes certain performance

specifications on the system. An optimal control problem is an infinite dimensional optimization problem on the control input $u(t)$ and an analytic solution to this problem is in general hard to obtain. However, the idea of an inverse optimal controller allows to relate certain gradient based control laws to the solution of an optimal control problem and thus provides a natural Lyapunov candidate for the controlled system. Following these ideas, the first two subsections of this section give a brief introduction to optimal control and its relations to stability. The second subsection introduces the reader to the ideas of inverse optimality.

4.2.1 Optimal Control

For an introduction to nonlinear optimal control, consider the textbooks [57, 58] and for a simple overview the lecture notes [59]. An optimal control aims at finding a control input $u(t)$ to the system $\dot{x}(t) = f(x(t), u(t))$ which optimizes a cost functional related to the state $x(t)$, control input $u(t)$ and time t. For the purpose of this work we seek at finding a solution the optimization problem

$$\begin{aligned} \min_u J(x_0, u) \;&=\; \int_0^{T_f} L(x,u)\, d\tau + \Phi(T_f, x(T_f)) \\ &\text{with}\;\; T_f \geq 0\,,\; L : \mathbb{R}^n \times \mathbb{R}^p \to \mathbb{R}\,,\; L(x,u) \in \mathcal{C}^0 \text{ w.r.t. } x \text{ and } u\,,\; L(x,u) \text{ p.s.d. w.r.t. } x \\ &\text{and p.d. w.r.t. } u\,,\; \Phi : \mathbb{R} \times \mathbb{R}^n \to \mathbb{R}\,,\; \Phi(T_f, x(T_f)) \geq 0 \text{ and } \Phi \in \mathcal{C}^0 \\ \text{s. t.}\quad &\text{state constraint: } x \in \mathbb{R}^n \\ &\text{input constraint: } u \in \mathbb{R}^m \\ &\text{dynamic constraint: } \dot{x} \;=\; f(x,u) \;\;,\; x(0) = x_0 \in \mathbb{R}^n \\ &\text{with}\;\; f : \mathbb{R}^n \times \mathbb{R} \to \mathbb{R}^n\,,\; f(x,u) \in \mathcal{C}^0 \text{ w.r.t. } u \text{ and locally Lipschitz continuous in } x\,. \end{aligned} \tag{4.20}$$

We refer to $J(x_0, u)$ as the *cost functional* and to $T_f \geq 0$ as *terminal time*, which can either be a fixed or a free variable. In the second case the terminal time can be seen as an additional control parameter to minimize the cost, that is, $J(x_0, u, T_f)$. In the language of optimal control the setup (4.20) is called a finite horizon optimization problem with terminal cost Φ,

integral penalty L on state and control effort, without time penalty, with an unconstrained control input, and without state constraint. Suppose a feedback control input $u(t)$ is optimal, that is, it minimizes $J(x_0, u)$, then we denote it by $u^*(t)$, the corresponding optimal closed-loop trajectory by $x^*(t)$, and the corresponding cost functional as $J^*(x_0) = J(x_0, u^*(t))$.

In principle there are two approaches to solve an optimal control problem like (4.20). First of all there is *variational calculus* which transforms an optimal control problem into a two point boundary value problem and gives a necessary condition on an optimal solution. Variational calculus peaks in the celebrated Pontryagin Maximum Principle [60] and results in a locally optimal feedforward control input $u^*(t)$. Its counterpart *dynamic programming* [61] relates the optimal control problem to the solution of of a PDE, the so-called Hamilton-Jacobi-Bellman equation. This PDE is in the general nonlinear case very hard to solve, but the advantage of the latter approach is that we end up with a globally optimal feedback control law. We will give a brief introduction to both approaches with special emphasis of the latter since it will be the main tool to derive inverse optimality of a feedback control law.

Variational Calculus

Variational calculus follows the ideas of constrained static optimization and eliminates the dynamic constraint with the Langrange multiplier $\lambda \in \mathbb{R}^n$, the so-called *costate*. This leads to the modified cost functional

$$\tilde{J}(x_0, u) = \int_0^{T_f} L(x, u) + \lambda^T \left(f(x, u) - \dot{x} \right) d\tau + \Phi(T_f, x(T_f)) \,, \tag{4.21}$$

where we fix the terminal time T_f for the moment. The variational calculus approach now follows the simple observation, that the optimal trajectory should be such that neighbouring trajectories do not lead to a smaller cost than the optimal cost $\tilde{J}^*(x_0)$. Thus along an optimal trajectory small variations of the control strategy ∂u, the state ∂x, the costate $\partial \lambda$, and the terminal state $\partial x(t_f)$ do not change the optimal cost functional, that is, $\partial \tilde{J}^*(x_0) = 0$. If $\partial \tilde{J}^*(x_0)$ is integrated by parts and is set to zero for all independent variations we arrive at

necessary conditions for optimality. If we define the *Hamiltonian*

$$\begin{aligned} H &: \quad \mathbb{R}^n \times \mathbb{R}^p \times \mathbb{R}^n \ \rightarrow \ \mathbb{R} \\ H(x,u,\lambda) &= L(x,u) + \lambda^T \big(f(x,u)\big) \end{aligned} \tag{4.22}$$

then the necessary conditions on an optimal control input $u^*(t)$, on an optimal closed loop trajectory $x^*(t)$, and on optimal costate trajectory $\lambda^*(t)$ read for a fixed T_f as in Table 4.1 (see, for example, [62], Theorem 5.3).

Description	**Equation**		
state equation:	$\dot{x}$	$= \left[\frac{\partial H(x,u,\lambda)}{\partial \lambda}\right]^T$	$= f(x,u)$
costate equation:	$\dot{\lambda}$	$= -\left[\frac{\partial H(x,u,\lambda)}{\partial x}\right]^T$	
input stationarity:	$\frac{\partial H(x,u,\lambda)}{\partial u}$	$= \mathbf{0}$	
initial condition:	$x(0)$	$= x_0$	
transversality condition:	$\lambda(T_f)$	$= \left.\frac{\partial \Phi(x,t)}{\partial x}\right\vert_{T_f}$	

Table 4.1: Necessary conditions for optimality with a fixed terminal time T_f

Note that in Table 4.1 the arguments and superscripts of $u^*(t)$, $x^*(t)$, and $\lambda^*(t)$ are dropped to avoid clutter. The state equation and the costate equation constitute together with the initial condition and the transversality condition a two point boundary value problem, where the control input u is obtained by the input stationarity equation. In the instance that the terminal time T_f is a free variable to optimize the cost $J(x_0, u, T_f)$, a variation in the terminal time ∂T_f leads to the condition

$$H(x^*(t), u^*(t), \lambda^*(t)) + \left.\frac{\partial \Phi(x^*(t),t)}{\partial t}\right|_{T_f} = 0\,, \tag{4.23}$$

which gives the optimal terminal time T_f. Condition (4.23) must hold additionally to the formulas of Table 4.1, since the control $u^*(t)$ of course also solves the control problem if we fix the optimal terminal time T_f ([57], Section 2.7).

The conditions derived by variational calculus in Table 4.1 are only necessary conditions on the optimality of the control law $u^*(t)$ and the optimal closed loop trajectory $x^*(t)$. A

sufficient condition for local (respectively global) optimality is that $u^*(t)$ locally (respectively globally) minimizes the Hamiltonian $H\left(x^*(t), u(t), \lambda^*(t)\right)$. Sufficient for this again is the local (respectively global) positive definiteness of the Hessian $\frac{\partial^2 H(x,u,t)}{\partial u^2}$. Summarizing we can say that the variational calculus approach is an extension of static optimization to an optimal control problem. It results for each initial condition in a two point boundary value problem for the feedforward control input $u^*(t)$, which fulfills the necessary conditions on optimality. However, from the viewpoint of control it is desirable to obtain a feedback control law which is guaranteed to be optimal for every initial condition. Dynamic programming is a clever trick, which provides such a feedback control law and even more.

Dynamic programming

For the dynamic programming approach we have to extend the optimization problem (4.20) slightly and introduce some additional smoothness assumptions. Let us fix the terminal time T_f and assume that the optimal control problem is feasible with the piecewise continuous optimal control input $u^*(t)$. We define the *value function* (optimal cost-to-go function) as

$$\begin{aligned} V \; : \qquad & [0, T_f] \times \mathbb{R}^n \; \rightarrow \; \mathbb{R} \\ V(t,x) \;\; = \;\; & \min_{u \in \mathbb{R}^m, u \in C^0} \int_t^{T_f} L(x(\tau), u(\tau))\, d\tau + \Phi(T_f, x(T_f))\,, \end{aligned} \tag{4.24}$$

where $x(\tau)$ is the solution of

$$\dot{x}(\tau) \;\; = \;\; f(x(\tau), u(\tau))\;,\; t \leq \tau \leq T_f \tag{4.25}$$

$$x(t) \;\; = \;\; x\,. \tag{4.26}$$

It is easy to see that the value function satisfies the condition

$$V(T_f, x) \;\; = \;\; \Phi(T_f, x)\,. \tag{4.27}$$

Besides piecewise continuity of $u^*(t)$ we additionally assume continuous differentiability of the value function $V(t,x)$, which allows us to give an heuristic derivation of the solution of the optimal control problem (4.20). Bellman's principle of optimality [61] loosely speaking

says that "end pieces of optimal trajectories are optimal." This idea can be formulated by considering the value function $V(t,x)$ as the optimum of an optimal end trajectory and a control input over an initial time interval Δt of sufficiently small positive length:

$$V(t,x) = \min_{u\in\mathbb{R}^m, u\in C^0} \int_t^{T_f} L(x(\tau),u(\tau))\,d\tau + \Phi(T_f,x(T_f)) \tag{4.28}$$

$$= \min_{u\in\mathbb{R}^m, u\in C^0} \left\{ \int_t^{t+\Delta t} L(x(\tau),u(\tau))\,d\tau + V(t+\Delta t, x(t+\Delta t)) \right\} \tag{4.29}$$

Since we assumed continuous differentiability of $V(t,x)$ we can expand the right hand side of the prior equation into a first order Taylor series about t:

$$V(t,x) = \min_{u\in\mathbb{R}^m, u\in\mathcal{C}^0} \left\{ L(x,u)\,\Delta t + V(t,x) + \frac{\partial V(t,x)}{\partial t}\,\Delta t + \frac{\partial V(t,x)}{\partial x} f(x,u)\,\Delta t + \mathcal{O}^2(\Delta t) \right\} \tag{4.30}$$

If we divide equation (4.30) by Δt and let Δt approach zero we arrive at the so-called *Hamilton-Jacobi-Bellman equation*:

$$0 = \frac{\partial V(t,x)}{\partial t} + \min_{u\in\mathbb{R}^m, \mathcal{C}^0} \left\{ L(x,u) + \frac{\partial V(t,x)}{\partial x} f(x,u) \right\} \tag{4.31}$$

Equation (4.31) delivers the feedback

$$u = k(t,x) = \operatorname*{argmin}_{u\in\mathbb{R}^m, \mathcal{C}^0} \left\{ L(x,u) + \frac{\partial V(t,x)}{\partial x} f(x,u) \right\} \tag{4.32}$$

and results in the equation

$$0 = \frac{\partial V(t,x)}{\partial t} + L(x,k(t,x)) + \frac{\partial V(t,x)}{\partial x} f(x,k(t,x))\,, \tag{4.33}$$

which constitutes a PDE for the optimal cost-to-go function function $V(t,x)$ with the boundary condition (4.27). If we can find a solution $V(t,x)$ to the PDE (4.33) then the so-called verification theorem states that the feedback $k(t,x)$ obtained from (4.32) is the optimal control input $u^*(t)$ and $V(t,x)$ is the value function.

Theorem 4.2.1. *Verification Theorem ([63], Section 9.2, Theorem 1):*
Consider the optimization problem (4.20). *Suppose there exists a differentiable function* V :

$[0, T_f] \times \mathbb{R}^n \to \mathbb{R}$ which satisfies equation (4.31) with the boundary condition (4.27), and furthermore, there exists a function $k : [0, T_f] \times \mathbb{R}^n \to \mathbb{R}$ with $k(t, x)$ piecewise continuous in t and locally Lipschitz in x satisfying (4.32), then $k(t, x)$ is an optimal feedback control for the optimization problem(4.20) and $V(t, x)$ is the value function.

We will later have the case that the terminal constraint Φ is time-invariant. In this case also the value function V is time-invariant [64] and, accordingly also the optimal control input obtained from (4.32), that is, $u^*(t) = k(x(t))$.

Although variational calculus and and dynamic programming are presented here as separate and independent concepts, they can in fact be linked to each other via the Hamiltonian $H(x, u, \lambda)$, which was defined in (4.22) and corresponds to the integral cost and the dynamic constraint. If we set $\lambda = \left[\frac{\partial V(t,x)}{\partial x}\right]^T$, then the Hamilton-Jacobi-Bellman equation can be formulated in terms of the Hamiltonian as

$$0 = \frac{\partial V(t, x)}{\partial t} + \min_{u \in \mathbb{R}^m, \mathcal{C}^0} H\left(x, u, \left[\frac{\partial V(t, x)}{\partial x}\right]^T\right). \tag{4.34}$$

From here also the necessary conditions obtained by variational calculus can be derived ([57]). Note that equation (4.34) evaluated for $t = T_f$ gives us the free terminal time condition (4.23) obtained by variational calculus. Indeed, the free terminal time conditions in dynamic programming read as the transversality condition $\left.\frac{\partial V(t,x)}{\partial x}\right|_{T_f} = \left.\frac{\partial \Phi(x,t)}{\partial x}\right|_{T_f}$ and $\left.\frac{\partial V(t,x)}{\partial t}\right|_{T_f} = -\left.\frac{\partial \Phi(x,t)}{\partial t}\right|_{T_f}$ and can be derived independently from variational calculus [65].

Equations (4.32)-(4.33) can be further simplified to a form, which allows to identify optimal control laws by their structure. This then paves the way to identify a control law as being "inverse optimal". Therefore, we look at the input affine system $\dot{x} = f(x) + g(x)\, u$ and specify the integral penalty as $L(x, u) = q(x) + u^T R(x)\, u$, where $q(x) \geq 0$ and $R(x) \succ 0$. Equation (4.32) may be written with the Hamiltonian $H\left(x, u, \left[\frac{\partial V(t,x)}{\partial x}\right]^T\right)$ as

$$u^*(t) = \operatorname*{argmin}_{u \in \mathbb{R}^m, \mathcal{C}^0} H\left(x, u, \left[\frac{\partial V(t, x)}{\partial x}\right]^T\right). \tag{4.35}$$

The minimizing $u^*(t)$ can be obtained by static minimization:

$$(i) \quad \text{necessary condition:} \quad \frac{\partial}{\partial u} H\left(x, u, \left[\frac{\partial V(t,x)}{\partial x}\right]^T\right) \stackrel{!}{=} \mathbf{0} \tag{4.36}$$

$$\Rightarrow u = k(x) = -\frac{1}{2} R^{-1}(x)\, g(x)^T \left[\frac{\partial V(t,x)}{\partial x}\right]^T \tag{4.37}$$

$$(ii) \quad \text{sufficient condition:} \quad \frac{\partial^2}{\partial u^2} H\left(x, u, \left[\frac{\partial V(t,x)}{\partial x}\right]^T\right) = R(x) \succ 0 \tag{4.38}$$

Thus $u^*(t) = k(t,x)$ is the optimal feedback control law and PDE (4.33) simplifies to

$$0 = \frac{\partial V(t,x)}{\partial t} + q(x) + \frac{\partial V(t,x)}{\partial x} f(x) - \frac{1}{4} \frac{\partial V(t,x)}{\partial x} g(x) R^{-1}(x) g(x)^T \left[\frac{\partial V(t,x)}{\partial x}\right]^T . \tag{4.39}$$

Thus for an input affine system and for a quadratic penalty of the control effort the optimal control may be identified as the gradient control law (4.37).

To conclude this section we can say that, if we can find a solution $V(t,x)$ to the Hamilton-Jacobi-Bellman equation, then $V(t,x)$ is the value function and provides an optimal feedback control $k(t,x)$. Besides these nice properties, dynamic programming has three additional benefits in the time-invariant case. The first one is the well known robustness of an optimal feedback control law $k(x)$ w.r.t. input uncertainties. As we will see in the next paragraph, the value function can in certain cases be used as Lyapunov function to derive stability conditions on the closed loop. Furthermore, we have seen that the optimal control takes sometimes the form of a gradient control. Thus it might also be possible to relate a gradient control law to an optimal control problem, as we will show in the paragraph after the next.

Optimal Control and Stability

In this section we consider, for simplicity, a so-called *infinite horizon* optimal control problem, that is, we set in the setup (4.20) the terminal time $T_f = \infty$ and let the terminal cost Φ be zero. Thus both the value function and the optimal feedback control law obtained from (4.31)-(4.32) are time-invariant. The value function for an infinite horizon problem is then

$$\begin{aligned} V &: \quad \mathbb{R}^n \to \mathbb{R} \\ V(x) &= \min_{u \in \mathbb{R}^m, u \in C^0} \int_t^\infty L(x(\tau), u(\tau))\, d\tau \,, \end{aligned} \tag{4.40}$$

where $x(\tau)$ the solution of $\dot{x}(\tau) = f(x(\tau), u(\tau))\,,\ x(t) = x$. Under the additional assumption, that the value function $V(x)$ is positive definite w.r.t. a closed, invariant set $\mathcal{A}$, $V(x)$ serves as a suitable control Lyapunov function candidate. If we make use of the time-invariant Hamilton-Jacobi-Bellman equation (4.33), the derivative of $V(x)$ along trajectories of the closed-loop dynamics is obtained as

$$\dot{V}(x) \;=\; \frac{\partial V(x)}{\partial x}\, f(x, k(x)) \;=\; -L(x, k(x))\,. \tag{4.41}$$

Note that the definiteness properties of $L(x, k(x))$ render $\dot{V}(x)$ negative semidefinite and thus establish stability of $\mathcal{A}$ w.r.t. to the closed loop dynamics. In the case, that $\dot{V}(x)$ is n.d. w.r.t. $\mathcal{A}$, asymptotic stability of $\mathcal{A}$ can be concluded and in the case, that $\mathcal{A}$ is compact, the invariance principle ([49], Theorem 4.4) guarantees convergence of the closed-loop system to the largest invariant set contained in the set where $\dot{V}(x) = 0$.

More can be said by theory of *Integral-Invariance* [66], which basically states that the convergence of the integral on the right-hand side of $V(x)$ implies that the integrand itself converges to zero. If additionally $L(x, 0)$ is $\mathcal{A}$-detectable w.r.t. the unforced system, that is,

$$L(x,0) \equiv 0 \ \text{ implies } \ \Phi(t,x) \to \mathcal{A}\,, \text{ where } \Phi(t,x) \text{ is the solution of } \begin{cases} \dot{x}(\tau) = f(x(\tau), 0) \\ x(t) = x\,, \end{cases}$$

then the closed-loop system converges to $\mathcal{A}$. If we combine this convergence result together with the prior stability result, we get asymptotic stability of $\mathcal{A}$.

For detailed proof on this and further references and stability results on infinite horizon optimal control consider [66, 67]. We only use these observation to motivate the fact, that a stabilizing gradient control law, such as (4.37), which was not necessarily derived by dynamic programming, can a posteriori be related to optimality, it is so to say inverse optimal.

4.2.2 Inverse Optimality

Optimal stabilization guarantees several desirable properties of the closed-loop system but also requires the Hamilton-Jacobi-Bellman equation (4.31), which, in general, is not a feasible task. On the other hand, the robustness and stability achieved as a result of optimality is

largely independent of the particular choice of the integral cost. This gives the motivation to pursue the development of controller design methods which solve the "inverse problem of optimal stabilization", or short, the problem of *inverse optimality*. The textbook [68] gives an excellent introduction to the concept of inverse optimality and its benefits in nonlinear control. For further reading consider the standard paper [69] or the corresponding book [70]. This short section introduces the reader to the basic idea of inverse optimality.

In the inverse approach, a stabilizing feedback for the set $\mathcal{A}$ is designed first and then shown to be optimal for an infinite horizon cost functional of the form $J(x_0, u) = \int_0^\infty q(x) + u^T R(x)\, u\, d\tau$. The problem is inverse because the functions $q(x)$ and $R(x)$ are a posteriori determined by the stabilizing feedback, rather than a priori chosen by the designer.

A control law $u = k(x)$ solves an inverse optimal problem for the input affine system $\dot{x} = f(x) + g(x)\, u$ if it can be expressed as

$$u = k(x) = -\frac{1}{2} R^{-1}(x)\, g(x)^T \left[\frac{\partial V(x)}{\partial x}\right]^T \tag{4.42}$$

with $R(x) \succ 0$ and $V : \mathbb{R}^n \to \mathbb{R}$, $V(x)$ p.d. w.r.t. $\mathcal{A}$, and such that the negative semidefiniteness of $\dot{V}(x)$ is achieved with the control $u = \frac{1}{2} k(x)$, that is,

$$\dot{V}(x) = \frac{\partial V(x)}{\partial x} f(x) + \frac{1}{2} \frac{\partial V(x)}{\partial x} g(x)\, k(x) \leq 0\,. \tag{4.43}$$

When the function $-q(x)$ is set to be the right-hand side of (4.43), that is,

$$q(x) = -\frac{\partial V(x)}{\partial x} f(x) - \frac{1}{2} \frac{\partial V(x)}{\partial x} g(x)\, k(x) \geq 0 \tag{4.44}$$

then $V(x)$ is a solution to the Hamilton-Jacobi-Bellman equation

$$0 = q(x) + \frac{\partial V(x)}{\partial x} f(x) - \frac{1}{4} \frac{\partial V}{\partial x} R^{-1}(x)\, g(x)^T \left[\frac{\partial V(x)}{\partial x}\right]^T . \tag{4.45}$$

That means that $V(x)$ is the value function corresponding to the cost functional

$$J(x_0, u) = \int_0^\infty q(x) + u^T R(x)\, u\, d\tau \tag{4.46}$$

and $k(x)$ is the optimal control input. We will call a control law of the form (4.42) satisfying (4.43) an *inverse optimal control law*. In the sequel we will see that in the directed graph case the formation control laws obtained by gradient control are inverse optimal.

Chapter 5

Main Result I

This chapter shows, that for a certain class of graphs the gradient control law (3.20) is indeed capable of solving the formation control problem posed in Chapter 3, that is, for a certain class of sensor graphs the robots indeed converge to the desired target formation. The main idea to derive this result is the inverse optimality of the overall system's dynamics in the link space, that is, the space where the links e_i of the sensor graph $\mathcal{G}$ live. The relation to optimality will provide us a natural set Lyapunov function candidate to guarantee stability of the target formation.

5.1 The Different Spaces

The formation control problem is the problem of stabilizing a group of autonomous robots to a specified formation and is obviously a geometric problem arising in the plane $\mathbb{R}^2$, the physical space where the agents are acting. However, in order to perform a full stability analysis of the problem we have to consider the dynamics of each agent, that is, the state $z_i \in \mathbb{R}^2$ with $i \in \{1, \dots, n\}$. Therefore the overall dynamics are located in the $\mathbb{R}^{2n}$. In this space we face the problem that all possible rotations and translations of a formation in the plane are included. So a priori all sets which are related to the formation are not compact. Since a formation control is specified in terms of links which should attain a specific length, it is quite conclusive to approach the problem in the link space. The link space has the nice

property that most relevant sets are either compact or can be compactified by a Lyapunov function. This section introduces the reader to the different spaces and their properties, and illustrates these at the example of the directed triangle (Example 3.1.3).

5.1.1 The Physical Space $\mathbb{R}^2$

No matter how far we will later diverge from the real physical problem into abstract mathematics, we should not forget that the original problem is posed in the plane $\mathbb{R}^2$, which we call the *physical space*. Each robot's position z_i and its dynamics $\dot{z}_i = u_i = -\left[\frac{\partial}{\partial z_i}\Phi_i(z)\right]^T$ are located in $\mathbb{R}^2$, and so is each link e_i of the sensor graph $\mathcal{G}$. This is for the directed triangle (Example 3.1.3) illustrated in Figure 5.1.

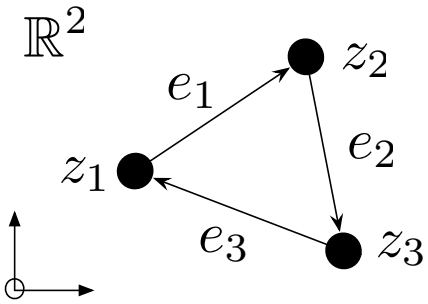

Figure 5.1: The three autonomous robots from Example 3.1.3 are acting in the plane $\mathbb{R}^2$

5.1.2 The State Space $\mathcal{Z}$

As already mentioned, a stability analysis of the closed-loop z-dynamics

$$\dot{z} \;=\; u \;=\; -\hat{O}\,\mathrm{diag}\,\{e_i\}\;\boldsymbol{\Psi}(e) \tag{5.1}$$

requires the entire state $z_i \in \mathbb{R}^2$ of each agent, that is, a stability problem posed in the $\mathbb{R}^{2n}$. We already noted in Section 3.2 that the initial condition $z(0) = z_0$ of the z-dynamics is not allowed to be anywhere in $\mathbb{R}^{2n}$, since then the potential functions V_i and their gradients contained in the vector $\boldsymbol{\Psi}(e)$ are not properly defined whenever two robots interconnected

by a link of $\mathcal{G}$ are collocated. Let us define the set $\mathcal{X}_z^i$ as the set where the two robots interconnected by the link e_i are collocated, that is,

$$\mathcal{X}_z^i \;=\; \left\{ z \in \mathbb{R}^{2n} \middle|\; e_i = \mathbf{0}\,,\; e = \hat{H}\, z \right\}\,. \tag{5.2}$$

The *state space* $\mathcal{Z}$ is then defined as an open subset of $\mathbb{R}^{2n}$ given by

$$\mathcal{Z} \;=\; \mathbb{R}^{2n} \setminus \bigcup_{i=1}^{m} \mathcal{X}_z^i \tag{5.3}$$

and we will also refer to it as the *z-space*. The state space of Example 3.1.3 is thus

$$\mathcal{Z} \;=\; \mathbb{R}^6 \setminus \left\{ z \in \mathbb{R}^{2n} \middle|\; z_i = z_{i+1}\,,\; i \in \{1,2,3\} \mathrm{mod} 3 \right\}\,, \tag{5.4}$$

that is, the set of all robot positions where no two robots are collocated. In order to see that in this space the z-dynamics are well defined, we state the following preliminary lemma on the potential functions.

Lemma 5.1.1. *Every potential function and its gradient are locally Lipschitz on* $(-d_i^2, \infty)$.

Proof. Consider a potential function $V_i(\omega)$ as in Definition 3.2.1. By definition the gradient $\nabla V_i(\omega)$ and also the second derivative $\frac{\partial^2}{\partial \omega^2} V_i(\omega)$ are continuous on $(-d_i^2, \infty)$ and thus $V_i(\omega)$ and $\nabla V_i(\omega)$ are locally Lipschitz ([49], Lemma 3.2). □

Lemma 5.1.1 guarantees that $\forall\, z \in \mathcal{Z}$ the right-hand side of the z-dynamics is locally Lipschitz. Thus $\forall\, z_0 \in \mathcal{Z}$ exists a maximum time interval T_{z0}^+ where a solution $\Phi(t, z_0) > 0$ of the z-dynamics is defined. In the case that the limit $\lim_{\omega \downarrow -d_i^2} \nabla V_i(\omega)$ exists, the proper state space of the z-dynamics might be extendable from $\mathcal{Z}$ to all of $\mathbb{R}^{2n}$. That's why we classify potential functions as either regular or irregular potential functions.

Definition 5.1.1. A potential function V_i is said to be *regular* if the limits

$$\lim_{\omega \downarrow -d_i^2} V_i(\omega) \quad , \quad \lim_{\omega \downarrow -d_i^2} \nabla V_i(\omega) \tag{5.5}$$

both exist. If both limits do not exist V_i is said to be *irregular*.

The classification of potential functions to regular and irregular functions does not include all possible potential functions as the following example shows.

Example 5.1.1. Consider the function

$$V_i(\omega) \;=\; -\frac{1}{2}\frac{(\omega+d_i^2)^{1-1/n}}{1-1/n}+\frac{1}{2}\frac{\omega}{d_i^{2/n}}+\frac{1}{2}\frac{d_i^{2-2/n}}{1-1/n} \tag{5.6}$$

with $d_i > 0$, $n > 1$ and its gradient

$$\nabla V_i(\omega) \;=\; -\frac{1}{2}\frac{1}{(\omega+d_i^2)^{1/n}}+\frac{1}{2}\frac{1}{d_i^{2/n}}\,. \tag{5.7}$$

The function V_i and its gradient are defined and continuously differentiable on $(-d_i^2,\infty)$, take the value zero for $\omega = 0$, and additionally $\nabla V_i(\omega)$ is strictly monotone increasing. This makes V_i a suitable potential function, which is illustrated together with its gradient for the parameters $d_i = 1$ and $n = 2$ in Figures 5.2(a) and 5.2(b). If we compare the plots in Figure 5.2, we see that in this case the limit $\lim_{\omega\downarrow -d_i^2} V_i(\omega) = \frac{1}{2}$ exists, but for the gradient the limit $\lim_{\omega\downarrow -d_i^2} \nabla V_i(\omega)$ does not exist.

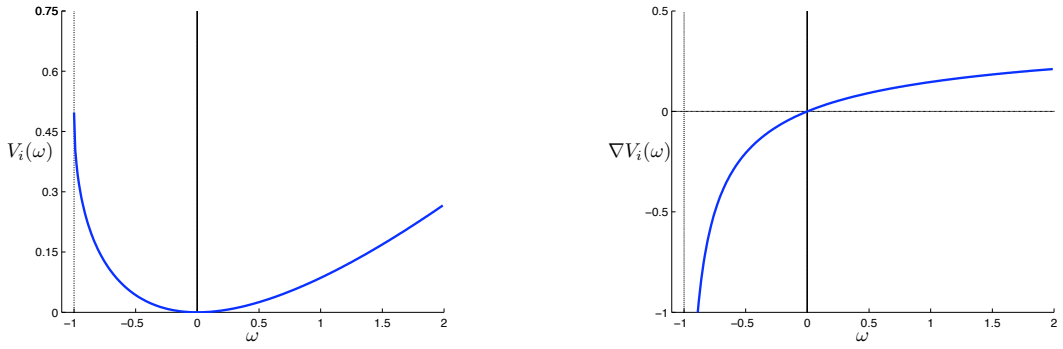

(a) Potential function $V_i(\omega)$ (b) Gradient of potential function $\nabla V_i(\omega)$

Figure 5.2: Illustration of the potential function $V_i(\omega)$ from Example 5.1.1 and its gradient $\nabla V_i(\omega)$ for the parameters $d_i = 1$ and $n = 2$.

We will not consider potential functions as in Example 5.1.1, which are neither regular nor irregular. The reason therefore is, that we are not able to guarantee forward completeness of the z-dynamics in this case. This will be clear after the results in Section 5.4 at the end of this chapter. Let us state the following lemma on regular potential functions which allows us to extend the state space $\mathcal{Z}$ to all of $\mathbb{R}^{2n}$.

Lemma 5.1.2. *For every regular function the domain of continuity and Lipschitz continuity of the potential function and its gradient can be extended to the interval* $[-d_i^2, \infty)$.

Proof. Consider a regular potential function $V_i(\omega)$ and its gradient $\nabla V_i(\omega)$ which are by Lemma 5.1.1 Lipschitz continuous on $(-d_i^2, \infty)$. For simplicity, this lemma is only proved for $V_i(\omega)$ since the proof for $\nabla V_i(\omega)$ is analogous. For a regular potential function the limit $\lim_{\omega \downarrow -d_i^2} V_i(\omega)$ exists and we can continuously extend $V_i(\omega)$ by defining

$$\begin{aligned} \tilde{V}_i : \quad & [-d_i^2, \infty) \to \mathbb{R} \\ \tilde{V}_i(\omega) = & \begin{cases} = V_i(\omega) & \forall\, \omega \in (-d_i^2, \infty) \\ = \lim_{\omega \downarrow -d_i^2} V_i(\omega) & \text{for } \omega = -d_i^2\,. \end{cases} \end{aligned} \tag{5.8}$$

We already know that $\tilde{V}_i(\omega)$ is locally Lipschitz continuous $\forall\, \omega \in (-d_i^2, \infty)$. Consider $\omega_1 = -d_i^2$, $\omega_2 \in (-d_i^2, \infty)$ and $\delta > 0$, such that $\delta < \omega_2 - \omega_1$. Then the Lipschitz condition is

$$\frac{\left|\tilde{V}_i(\omega_1 + \delta) - \tilde{V}_i(\omega_2)\right|}{|\omega_1 - \omega_2|} \leq L \tag{5.9}$$

where L is a positive constant. The left-hand side of (5.9) is a continuous function of δ which we denote by F:

$$\begin{aligned} F : \quad & \mathbb{R} \to \mathbb{R} \\ F(\delta) = & \frac{\left|\tilde{V}_i(\omega_1 + \delta) - \tilde{V}_i(\omega_2)\right|}{|\omega_1 - \omega_2|} \end{aligned} \tag{5.10}$$

Note that $F(\delta) \leq L$ for every $\delta > 0$ and that the limit $\lim_{\delta \downarrow 0} F(\delta)$ exists. Since L does not depend on δ, it also holds that $F(0) \leq L$. Thus Lipschitz continuity of $\tilde{V}_i(\omega)$ is also guaranteed at $\omega = -d_i^2$. □

By Lemma 5.1.2 the right-hand side of the z-dynamics is Lipschitz continuous for regular potential functions. In this case the state space $\mathcal{Z}$ can be extended to all of $\mathbb{R}^n$.

The formation control problem posed in Section 3.1.3 contains under *(ii)* a set stability problem, namely $z(t) \underset{t \to \infty}{\to} r_{\mathcal{G}}^{-1}(\mathbf{d})$. The set $r_{\mathcal{G}}^{-1}(\mathbf{d})$, which we referred to as the target

formation, can also be formulated as

$$r_{\mathcal{G}}^{-1}(\mathbf{d}) \;=\; \left\{ z \in \mathcal{Z} \;\middle|\; \|e_i\| = d_i \,,\, i \in \{1,\ldots,m\} \,,\, e = \hat{H}\, z \right\} \;=:\; \mathcal{E}_z \tag{5.11}$$

and will from now on be denoted by $\mathcal{E}_z$. Since every d_i is positive it holds that $\mathcal{E}_z \subset \mathcal{Z}$. Unfortunately the target formation $\mathcal{E}_z$ is not bounded in the state space, since the robots' positions can be located anywhere in the plane. Thus $\mathcal{E}_z$ is not a compact set, but it has the nice property that, when $\mathcal{Z} = \mathbb{R}^{2n}$, $\mathcal{E}_z$ constitutes a three dimensional submanifold of $\mathbb{R}^{2n}$ ([26], Lemma 11). In order to overcome the unboundedness of the target formation, we illuminate the set stability problem $z(t) \underset{t\to\infty}{\to} \mathcal{E}_z$ from the links' side.

5.1.3 The Link Space $\hat{H}(\mathcal{Z})$

If we approach the formation control problem in the state space, we also consider translations and rotations of the robot's positions z, but the target formation $\left(\mathcal{G}, r_{\mathcal{G}}^{-1}(\mathbf{d})\right)$ itself is invariant under translations and rotations. By allowing these motions, even a simple set, such as the set of collocated robots

$$\mathcal{X}_z \;:=\; \left\{ z \in \mathbb{R}^{2n} \,|\, z \in \mathrm{Im}\,(\mathbf{I}_2) \right\} \,, \tag{5.12}$$

has infinite extent. However, in terms of the links e this set can be simply parametrized by $e = \mathbf{0}$. So probably a better way to approach the set stability problem $z(t) \underset{t\to\infty}{\to} \mathcal{E}_z$ is via the space of all links e, which also makes sense because the right-hand side of the z-dynamics depends only on the links e and is therefore independent of translations in z-space.

The links are defined via the incidence matrix $e = \hat{H}\, z$. Thus the *link space*, or more briefly the *e-space*, is obtained by the mapping of $\mathcal{Z}$ under the incidence matrix $\hat{H}$, that is,

$$\hat{H}(\mathcal{Z}) \;=\; \hat{H}\left(\mathbb{R}^{2n} \setminus \bigcup_{i=1}^{m} \mathcal{X}_z^i \right) \,. \tag{5.13}$$

An alternative description of the link space can be derived if we parametrize the sets $\hat{H}(\mathcal{X}_z^i) \subset \hat{H}(\mathbb{R}^{2n})$ as the subspaces

$$\mathcal{X}_e^i \;:=\; \hat{H}\left(\mathcal{X}_z^i\right) \;=\; \left\{ e \in \hat{H}\left(\mathbb{R}^{2n}\right) \middle|\; e_i = \mathbf{0} \right\} \,. \tag{5.14}$$

The link space is then obtained as $\hat{H}\left(\mathbb{R}^{2n}\right)$ if additionally the subspaces $\mathcal{X}_e^i$ are subtracted:

$$\hat{H}\left(\mathbb{R}^{2n} \setminus \bigcup_{i=1}^{m} \mathcal{X}_z^i\right) \;=\; \hat{H}\left(\mathbb{R}^{2n}\right) \setminus \bigcup_{i=1}^{m} \mathcal{X}_e^i \,. \tag{5.15}$$

The relationship of the two parameterizations (5.13) and (5.15) is illustrated in the commutative diagram in Figure 5.3.

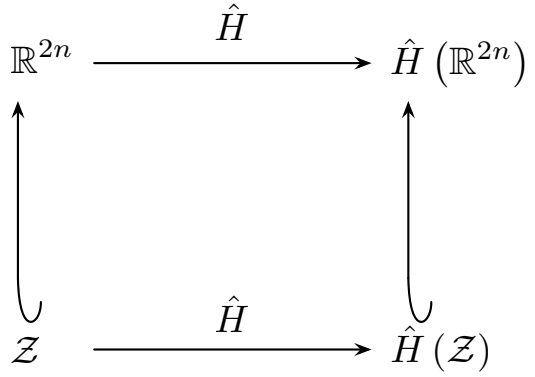

Figure 5.3: Illustration of the state space and the link space where the vertical arrows are insertion maps [71]

For a connected graph $\mathcal{G}$ the incidence matrix $\hat{H}$ does not have full rank. As mentioned in Section 2.1, the incidence matrix always has rank $2n-2$ and $\ker\left(\hat{H}\right) = \operatorname{span}\{\mathbf{I}_2\}$, which means that the mapping $\hat{H}$ from e-space to z-space cancels out all translations. This achieves the compactness of the target formation $\hat{H}\left(\mathcal{E}_z\right)$ in the link space, that is,

$$\mathcal{E}_e \;:=\; \hat{H}\left(\mathcal{E}_z\right) \;=\; \left\{ e \in \hat{H}(\mathcal{Z}) \,|\, \|e_i\| = d_i \;\; \forall\, i \in \{1,\ldots,m\} \right\} \tag{5.16}$$

is a compact set. This becomes immediately clear because $\mathcal{E}_e$ is closed and it can be bounded within the cube $\left\{ e \in \hat{H}(\mathcal{Z}) \middle|\; \|e\|_\infty = \max\limits_{i\in\{1,\ldots,m\}} d_i \right\}$.

Let us give a geometric definition of the link space which can be related to the sensor graph $\mathcal{G}$. For simplicity, let us again assume that $\mathcal{Z} = \mathbb{R}^{2n}$. If we have at least as many links as nodes in the graph ($m \geq n$), then the incidence matrix $\hat{H}$ has a nontrivial kernel and thus the link space $\hat{H}(\mathcal{Z}) = \hat{H}\left(\mathbb{R}^{2n}\right)$ is not all of $\mathbb{R}^{2m}$. The linear system $e = \hat{H}\, z$ has

$2m - \text{rank}\left(\hat{H}\right) = 2m - 2(n-1)$ linearly dependent equations, or equivalently, there exists a matrix $E \in \mathbb{R}^{2m \times (2m-2(n-1))}$ with full column rank such that

$$\mathbf{0} \;=\; E^T e \;=\; E^T \hat{H}\, z\,. \tag{5.17}$$

We have that

$$\text{Im}\left(\hat{H}\right) \;=\; \ker\left(E^T\right) \;\Leftrightarrow\; \ker\left(\hat{H}^T\right) \;=\; \text{Im}\,(E) \tag{5.18}$$

and thus the link space can be formulated as

$$\hat{H}\left(\mathbb{R}^{2n}\right) \;=\; \left\{ e \in \mathbb{R}^{2m} \middle|\; E^T e = \mathbf{0} \right\}, \tag{5.19}$$

which is a hyperplane in the $\mathbb{R}^{2m}$ with the columns of E as normal vectors. From Section 2.1.1 we know that $\ker\left(\hat{H}^T\right)$ is spanned by vectors corresponding to the loops in the graph $\mathcal{G}$. Since $\ker\left(\hat{H}^T\right)$ is the orthogonal complement of the link space, the link space can be seen a hyperplane whose normal vectors correspond to the loops in the graph. In the case $\mathcal{Z} \neq \mathbb{R}^{2m}$ the subspaces $\mathcal{X}_e^i$ have to be subtracted from this hyperplane.

Let us conclude this section with an illustration at the example of the directed triangle.

Example 3.1.3. Directed triangle (continued):
Let us at the beginning assume that the control laws of the three robots are obtained from regular potential functions. The links of the directed triangle are given by

$$\begin{bmatrix} e_1 \\ e_2 \\ e_3 \end{bmatrix} \;=\; \begin{bmatrix} -I_2 & I_2 & 0 \\ 0 & -I_2 & I_2 \\ I_2 & 0 & -I_2 \end{bmatrix} \begin{bmatrix} z_1 \\ z_2 \\ z_3 \end{bmatrix}. \tag{5.20}$$

The three links are not independent and we have the underlying geometric constraint

$$\mathbf{0} \;=\; \begin{bmatrix} I_2 & I_2 & I_2 \end{bmatrix}^T e \;=\; e_1 + e_2 + e_3\,. \tag{5.21}$$

The constraint implies that the three links constitute a hyperplane passing through the origin of $\mathbb{R}^6$ with the normal vectors $[I_2\ I_2\ I_2]^T$, which corresponds to the loop $(1,2,3)$ in the graph. A qualitative picture of the link space $\hat{H}\left(\mathbb{R}^6\right)$ embedded in $\mathbb{R}^6$ is given in Figure 5.4. In the

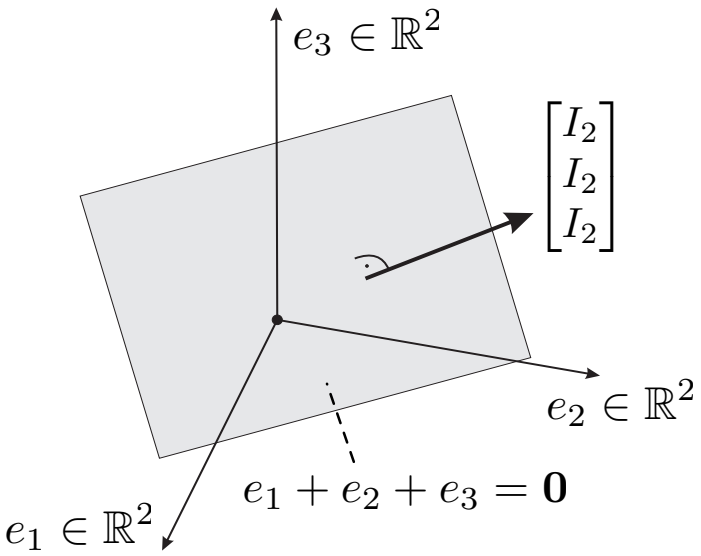

Figure 5.4: Qualitative picture of the link space embedded in $\mathbb{R}^6$

case of irregular potential functions we have to subtract the subspaces

$$\mathcal{X}_e^i \;=\; \left\{ e \in \hat{H}\left(\mathbb{R}^{2n}\right) \middle|\; e_i = \mathbf{0} \right\} \tag{5.22}$$

from the hyperplane $\hat{H}\left(\mathbb{R}^6\right)$. The subspace $\mathcal{X}_e^1$, for example, is the plane $e_1 = \mathbf{0}$ intersected with the hyperplane defined by $e_1 + e_2 + e_3 = 0$. This gives the subspace $e_2 + e_3 = \mathbf{0}$.

5.2 The Link Dynamics

The dynamics in the link space can be obtained simply by the dynamics in the z-space as

$$\dot{e} \;=\; \hat{H}\,\dot{z} \;=\; -\hat{H}\,\hat{O}\,\mathrm{diag}\left\{e_i\right\}\,\mathbf{\Psi}(e) \tag{5.23}$$

with initial condition $e(0) = e_0 \in \hat{H}(\mathcal{Z})$. In the following the dynamical system (5.23) will be referred to as the *link-dynamics* or the *e-dynamics* and its flow will be denoted by $\Phi_e(t, e_0)$. The e-dynamics define a self contained dynamical system evolving in the link space, which will later turn out to be an invariant set. Just as the z-dynamics the e-dynamics are locally Lipschitz continuous $\forall\, e \in \hat{H}(\mathcal{Z})$ and thus $\forall\, e_0 \in \hat{H}(\mathcal{Z})$ exists a maximum time interval $T_{e0}^+ > 0$ where a unique solution $\Phi_e(t, e_0)$ is defined.

Example 3.1.3. Directed triangle (continued):

Let us for notational convenience introduce the term ψ_i for the ith component of the vector $\mathbf{\Psi}(e)$, that is $\psi_i = 2\,\nabla V_i\big(\|e_i\|^2 - d_i^2\big)$. The e-dynamics of the directed triangle then read as

$$\dot{e} \;=\; \begin{bmatrix} \dot{e}_1 \\ \dot{e}_2 \\ \dot{e}_3 \end{bmatrix} \;=\; \hat{H}\,\dot{z} \;=\; \begin{bmatrix} \dot{z}_2 - \dot{z}_1 \\ \dot{z}_3 - \dot{z}_2 \\ \dot{z}_1 - \dot{z}_3 \end{bmatrix} \;=\; \begin{bmatrix} e_2\,\psi_2 - e_1\,\psi_1 \\ e_3\,\psi_3 - e_2\,\psi_2 \\ e_1\,\psi_1 - e_3\,\psi_3 \end{bmatrix} . \tag{5.24}$$

If the potential functions are regular, then the link space $\hat{H}(\mathcal{Z})$ is the entire hyperplane with normal vector $[I_2\,,\,I_2\,,\,I_2]^T$. The underlying constraint $e_1(t) + e_2(t) + e_3(t) = \mathbf{0}$ makes sure that this hyperplane is invariant. In the case of irregular potential functions, additionally a convergence of $\Phi_e(t, e_0)$ to the sets $\mathcal{X}_e^i$ has to be ruled out in order to guarantee invariance of the link space.

Alternatively, we could define the e-dynamics (5.23) together with the algebraic equation (5.17) as a descriptor system. The drawback of the latter approach is, that we regard (5.23) and (5.17) as a redundant system. If we eliminate the algebraic constraint (5.17) and thereby reduce the system order, the equations (5.23) loose the relationship to the graph $\mathcal{G}$. That's why we will not follow this approach and just illustrate its drawbacks at the directed triangle.

Example 3.1.3. Directed triangle (continued):

The dynamic equations (5.24) are of sixth order and form together with the algebraic equations (5.21) a descriptor system. By eliminating the algebraic constraint, that is, solving for $e_3 = -e_1 - e_2$, the system can be reduced to the fourth order system

$$\begin{aligned} \begin{bmatrix} \dot{e}_1 \\ \dot{e}_2 \end{bmatrix} \;&=\; \begin{bmatrix} e_2\,\psi_2 - e_1\,\psi_1 \\ -\,(e_1 + e_2)\;\psi_3 - e_2\,\psi_2 \end{bmatrix} \\ e_3 \;&=\; -e_1 - e_2\,, \end{aligned} \tag{5.25}$$

where $\psi_3 = 2\,\nabla V_3\left((e_1 + e_2)^2 - d_3^2\right)$. System (5.25) is evolving in the (e_1, e_2)-space. The mapping of the link space to the $(e_1\,,\,e_2)$-space is bijective, since it is only rotation of the plane $e_1 + e_2 + e_3 = \mathbf{0}$ in the $\mathbb{R}^6$ as shown in Figure 5.5. Therefore the dynamics which

we obtain for the reduced system (5.25) are diffeomorphic to those of the full system (5.24). Unfortunately this model reduction does not simplify the analysis of the link dynamics, quite the contrary, equations (5.24) loose their symmetry when being reduced.

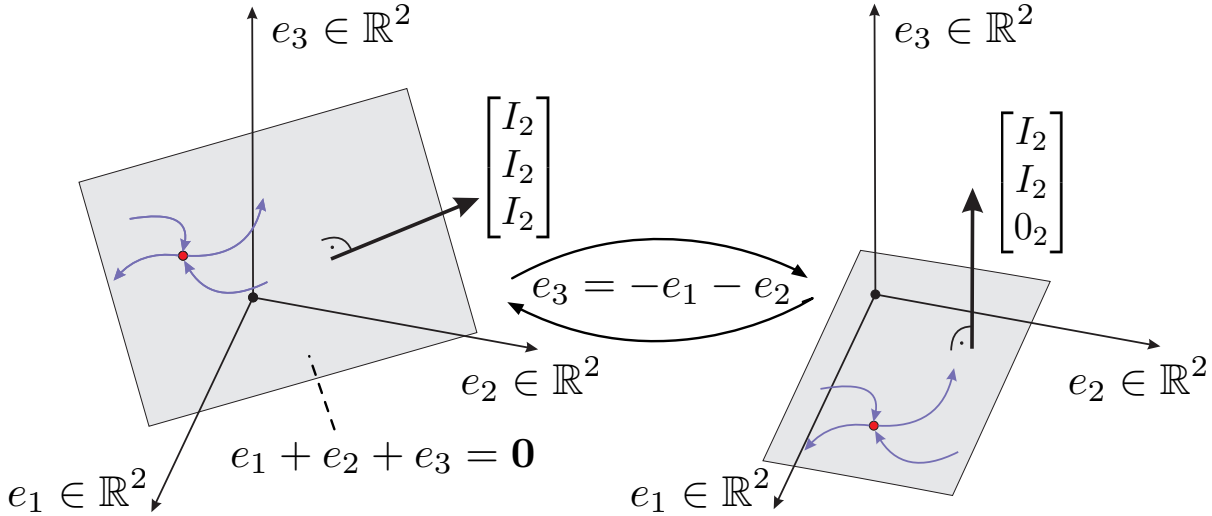

Figure 5.5: Qualitative picture of the dynamics in the e-space and in the reduced e-space

5.2.1 The Right Perspective on the Formation Control Problem

The link dynamics provide a better approach to solve the set stability problem $z(t) \underset{t\to\infty}{\to} \mathcal{E}_z$, which reads in the link space as $e(t) \underset{t\to\infty}{\to} \mathcal{E}_e$. The reasons therefore is the compactness of $\mathcal{E}_e$. If we find a set Lyapunov function to guarantee stability of $\mathcal{E}_e$, then the link dynamics are a priori bounded within a compact sublevel set of this Lyapunov function. This a priori compactness of the link dynamics allows us then to establish forward completeness, to apply invariance concepts, and will also be of help in the geometrical considerations in Chapter 7.

For these reasons we perform the stability analysis in the e-space and think of the solution $e(t)$ of the e-dynamics as input to the z-dynamics. The entire system is then a cascade system which is strongly dependent on the initial condition z_0, which is the only external input to the overall system. This is illustrated in the block diagram in Figure 5.6. There is also an obstacle arising in this approach, which becomes clear in Figure 5.6. The convergence

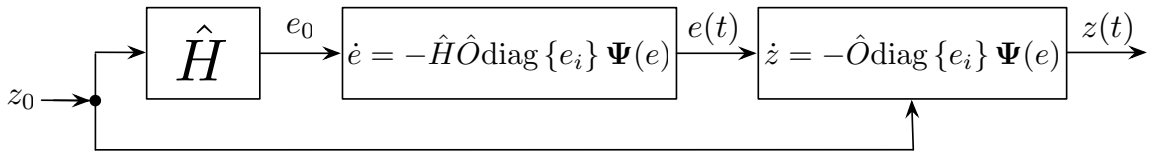

Figure 5.6: Cascade interpretation of the e and the z-dynamics

$e(t) \underset{t\to\infty}{\to} \mathcal{E}_e$ in the link space does not imply convergence of the z-dynamics to a finite point $z_* \in \mathcal{E}_z$. Convergence of the links guarantees only, that the point to set distance $\|z(t)\|_{\mathcal{E}_z}$ converges to zero, but $z(t) \underset{t\to\infty}{\to} z_* \in \mathcal{E}_z$ is part of the problem specification posed in Section 3.1. To overcome this obstacle we look at the z-dynamics as shown in Figure 5.7, namely as an integrator with the input $f(t) := -\hat{O}\,\text{diag}\{e_i(t)\}\;\mathbf{\Psi}(e(t))$. The dynamics $\dot{z} = f(t)$ with initial condition $z(0) = z_0$ can then be written in integrated form as

$$z(t) \;=\; z_0 + \int_0^t f(\tau)\,d\tau\,. \tag{5.26}$$

A sufficient conditions that $\lim_{t\to\infty} z(t) = z^* = const.$, or equivalently, that the integral converges, is $f \in \mathcal{L}_1$. A sufficient condition for this again would be that $f(t)$ is an exponentially decreasing function, that is, $\text{diag}\{e_i(t)\}\;\mathbf{\Psi}(e(t)) \sim e^{-\lambda t}$ with some $\lambda > 0$. So additionally to $e(t) \underset{t\to\infty}{\to} \mathcal{E}_e$, we want to show that the rate of convergence of the link dynamics is exponential. In the author's opinion the block diagram in Figure 5.7 is the right perspective on the

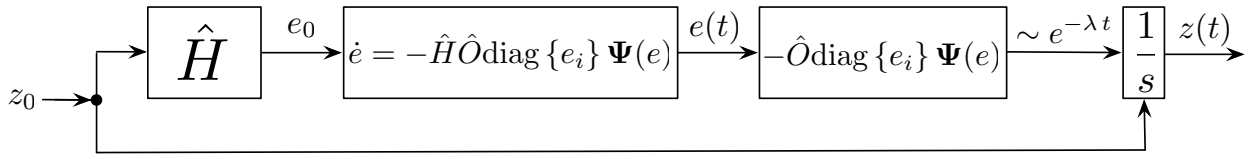

Figure 5.7: Exponential stability serves as bridge between e and z-dynamics

formation control problem and the link dynamics are in fact the dynamics to be analyzed. Before we move on the actual stability analysis, the next section discusses invariant sets of both z and the e-dynamics, which additionally complicate the stability analysis.

5.2.2 Invariant sets

The equilibria of the e-dynamics

$$\dot{e} \;=\; \hat{H}\,\dot{z} \;=\; -\hat{H}\,\hat{O}\,\mathrm{diag}\,\{e_i\}\;\boldsymbol{\Psi}(e) \tag{5.27}$$

are given by the set

$$\mathcal{M}_e \;=\; \left\{ e \in \hat{H}\left(\mathcal{Z}\right) \,\middle|\, \hat{H}\,\dot{z} = \mathbf{0}\,,\; z \in \hat{H}^{-1}\left(\mathcal{Z}\right) \right\}. \tag{5.28}$$

We refer to the set $\mathcal{M}_e$ as the set of equal velocities, since $e \in \mathcal{M}_e$ implies $\dot{z}_1 = \dot{z}_2 = \cdots = \dot{z}_n$. The set $\mathcal{M}_e$ contains besides the set of robots moving with equal velocity also the set of equilibria of the z-dynamics, that is, where the robots are stationary. The following two sections will show that the e-dynamics contain no other positive limit sets other than their equilibria. Let us look more closely at a subset of $\mathcal{M}_e$, namely the equilibria of the z-dynamics

$$\dot{z} \;=\; -\hat{O}\,\mathrm{diag}\,\{e_i\}\;\boldsymbol{\Psi}(e)\,. \tag{5.29}$$

These are of course the target formation $\mathcal{E}_z$ where $\boldsymbol{\Psi}(e) = \mathbf{0}$, and, if $\mathcal{Z} = \mathbb{R}^{2n}$, also the set of collocated robots $\mathcal{X}_z = \mathrm{span}\,\{\mathbf{I}_2\}$ where $e = \mathbf{0}$. Additionally the outgoing edge matrix $\hat{O}$ can have a nontrivial kernel if at least one node of the graph $\mathcal{G}$ has multiple outgoing links, that is, there are two nonzero components in a row of $\hat{O}$. Then an equilibrium arises if $\mathrm{diag}\,\{e_i\}\;\boldsymbol{\Psi}(e) \in \ker\left(\hat{O}\right)$, that is, some links are zero, some are in equilibrium and others form a closed vector sum. In the directed triangle example (Example 3.1.3) the graph $\mathcal{G}$ is a cycle, thus $O = -I_3$ and these equilibria do not exist.

In the case of an undirected graph with bidirectional links, the matrix $\hat{O}$ is replaced by $\hat{H}_u^T$ and we can write the z-dynamics as

$$\dot{z} \;=\; -\hat{H}_u^T\,\mathrm{diag}\,\{e_i\}\;\boldsymbol{\Psi}(e) \;=\; -R_{\mathcal{G}}(e)^T\boldsymbol{\Psi}(e) \tag{5.30}$$

where $R_{\mathcal{G}}(e)$ is the rigidity matrix. Thus for an undirected graph an equilibrium at $\bar{z} \in \mathcal{Z}$ arises whenever $R_{\mathcal{G}}\left(\hat{H}\,\bar{z}\right)$ has a rank loss, that is, the the framework $(\mathcal{G}, \bar{z})$ is infinitesimally not rigid, or if $\bar{z} \in \mathcal{E}_z$, which is the target formation. For an undirected triangular framework a collinear and thus not infinitesimally rigid equilibrium is illustrated in Figure 5.8.

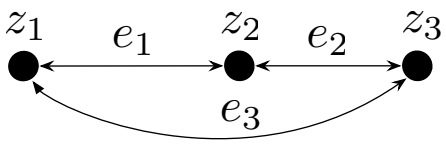

Figure 5.8: Collinear equilibrium of three robots with a undirected visibility graph.

Let us conclude this section by taking a closer look at the equilibria of the directed triangle.

Example 3.1.3. Directed triangle (continued):
The equilibria of z-dynamics of the directed triangle are the desired equilibrium set $\mathcal{E}_z$ and for regular potential functions also the set of collocated robots $\mathcal{X}_z$. We have already mentioned that the matrix $\hat{O}$ introduces no additional equilibria. The equilibria of the e-dynamics are then besides $\mathcal{E}_e$ and $\mathcal{X}_e = \hat{H}(\mathcal{X}_z)$ also the set where all robots move with equal velocity in the same direction, that is, $\dot{z}_1 = \dot{z}_2 = \dot{z}_3$. But this again implies $e_1 \psi_1 = e_2 \psi_2 = e_3 \psi_3$, which means that the links e_i must be collinear . Therefore, $\mathcal{M}_e \setminus \{\mathcal{E}_e \cup \mathcal{X}_e\}$ corresponds in the physical space to collinear robots moving with the same velocity and fulfilling $e_1 \psi_1 = e_2 \psi_2 = e_3 \psi_3 \neq \mathbf{0}$. The three equilibria are shown in Table 5.1.

link space	$\mathcal{E}_e$	$\mathcal{X}_e$	$\mathcal{M}_e \setminus \{\mathcal{E}_e \cup \mathcal{X}_e\}$
physical space	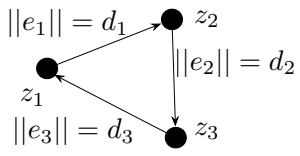	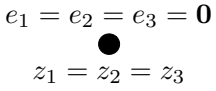	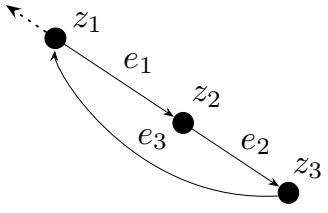

Table 5.1: Overview over the different invariant sets of the directed triangle

5.3 Cooperative Graphs

In the specification of the formation control problem we demanded certain properties of the sensor graph $\mathcal{G}$. We can lump these properties together under the term persistence and regard it as a necessary condition on formation control. We attack the formation control problem in a distributed way by assigning a potential function to each robot. Each robot's control law aims then at a steepest descent of its potential function. By letting each robot do so, we hope to solve the overall problem.

Let us illuminate this idea from a game theoretic viewpoint. Each robot has its own individual strategy, which consists of minimizing its potential function, that is, optimizing all its outgoing links to the desired length. On the other hand the robots do not communicate with each other, which leads to the fact that each robot follows its own strategy regardless of what the other robots are doing. A valid question to ask is wheter or not the robots indeed act cooperatively and achieve a common goal. If we look at the example in Figure 5.9 it does not necessarily seem so. Figure 5.9 shows two distinct robots which are embedded in a larger network, have positions z_1 and z_2, and are interconnected by a directed link e_1 from robot 1 to robot 2. While as the strategy of robot 1 is to pursue robot 2 to meet its distance

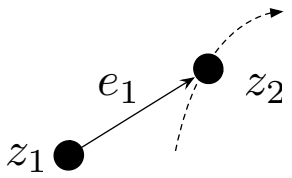

Figure 5.9: Robots do not necessarily act cooperatively.

constraint on the link e_1, robot 2 follows its own strategy, which does not involve link e_1. In fact, the overall graph could be set up, such that robot 2 is moving away from robot 1, as it is illustrated by the dashed line. Thus the robots do not act in a way that we would call cooperative.

5.3.1 Inverse Optimality of a Symmetric Graph

Intuitively such a scenario cannot happen in a symmetric graph, where each link is bidirectional. Loosely speaking, a bidirectional link between two robots implies that both robots take care about the link, that is, the strategy of both robots involves optimizing the link to its desired length. Therefore, robots interconnected in a symmetric graph should altogether pursue a common goal, or spoken differently, the overall system should be inverse optimal w.r.t. a meaningful cost functional. The following theorem establishes this inverse optimality and is for simplicity stated only for regular potential functions.

Theorem 5.3.1. *In a symmetric graph the gradient control law (3.35) based on regular potential functions is an inverse optimal control law and optimizes the cost functional*

$$J(e_0, u) \;=\; \frac{1}{2}\int_0^{T_f} \boldsymbol{\Psi}(e)^T\, R_{\mathcal{G}}(e)\, R_{\mathcal{G}}(e)^T\, \boldsymbol{\Psi}(e) + u^T u \; d\tau + V(e(T_f)) \tag{5.31}$$

for any fixed terminal time $T_f \geq 0$ and where $V(e) = \sum_{i=1}^{m} V_i\big(\|e_i\|^2 - d_i^2\big)$ is the sum of the potential functions of all links. The value function is for $0 \leq t \leq T_f$ given by

$$\int_t^{T_f} \boldsymbol{\Psi}(e)^T\, R_{\mathcal{G}}(e)\, R_{\mathcal{G}}(e)^T\, \boldsymbol{\Psi}(e)\, d\tau + \frac{1}{4}\, V(e(T_f)) \;=\; V(e)\,. \tag{5.32}$$

Before we come to the proof of Theorem 5.3.1 we want to emphasize the significance of this result. Theorem 5.3.1 states that, although each robot's strategy u_i is independent of the other robots' strategies, the overall strategy u optimizes the cost functional (5.31). The robots do so up to any arbitrary but fixed terminal time $T_f \geq 0$.

Before move on to the implications of the optimality of the overall strategy u, we want to clarify two technical questions, which obviously arise. The first is whether or not there exists an optimal terminal time, since T_f is specified as arbitrary but fixed. We will later show that the gradient control (3.35) and the value function $V(e)$ also solve the corresponding free terminal time problem $J(e_0, u, T_f)$, and it turns out that any arbitrary terminal time T_f is the optimal terminal time. The second and now even more intriguing question is about this finite horizon T_f. If we fix any $T_f \geq 0$, then neither the value function $V(e)$ nor the gradient

control law (3.35) reflect this bounded horizon T_f in any way, and, moreover, the robots' control remains the same also for $t \geq T_f$. The reason therefore lies in a structural property of the optimal control problem (5.31). This can be equivalently represented by the infinite horizon cost functional

$$J(e_0, u) \;=\; \frac{1}{2} \int_0^\infty \mathbf{\Psi}(e)^T \, R_{\mathcal{G}}(e) \, R_{\mathcal{G}}(e)^T \, \mathbf{\Psi}(e) + u^T u \; d\tau \tag{5.33}$$

and the terminal set $\mathcal{E}_e$ to which an optimal solution has to converge to. The reader might have already guessed that the gradient control (3.35) is the optimal control and $V(e)$ is the value function of the infinite horizon problem (5.33). Thus the problem (5.31) can be seen as a finite part of the infinite horizon problem (5.33), and the terminal cost $V(e(T_f))$ of the finite horizon problem is simply the optimal cost-to-go to the terminal set $\mathcal{E}_e$. Therefore, the optimal control u^* and the value function $V(e)$ are the same for any horizon T_f and are obviously independent of this horizon.

The implications of the optimality of the overall strategy u become clear from the value function $V(e)$, which describes the optimal cost-to-go from any $e \in \hat{H}_u\,(\mathbb{R}^{2n})$ at time t and, interestingly enough, corresponds to the sum of the potential functions of all links. Since $V(e)$ is independent of T_f, the left-hand side of (5.32) is constant for any T_f and thus the functional exists even for the limit $T_f \to \infty$. By *Barbalat's Lemma* ([49], Lemma 8.2), we conclude that in this case the integrand itself has to converge to zero. The integrand is a quadratic form, which is related to the equilibrium set $\mathcal{E}_e$ via the vector $\mathbf{\Psi}(e)$ and to rigidity of the formation via the rigidity matrix $R_{\mathcal{G}}(e)$. The integrand converges to zero if either the solution $\Phi(t, e_0)$ converges to a set where the rigidity matrix has a permanent rank loss or if $\mathbf{\Psi}(\Phi_e(t, e_0)) \to 0$, or equivalently $\Phi_e(t, e_0) \to \mathcal{E}_e$. In the second case also the terminal cost takes the value zero, while it is positive in the first one. The terminal cost measures the final deviation from the equilibrium set and thus the robots either converge to the desired target formation, which corresponds to a global minimum of $V(e)$, or "get stuck" in a formation that is not rigid and that can be interpreted as a local minimum of $V(e)$. From the viewpoint of the infinite horizon problem (5.33) with terminal set $\mathcal{E}_e$, the two cases correspond simply to initial condition from where the optimal control problem is either feasible or not.

Before we go to the actual proof of Theorem 5.3.1, let us motivate the cost functional (5.31). In the undirected graph case the e-dynamics are given by

$$\dot{e} \;=\; \hat{H}_u\, u(e) \;=\; -\hat{H}_u\, \hat{H}_u^T\, \mathrm{diag}\,\{e_i\}\; \boldsymbol{\Psi}(e) \tag{5.34}$$

with initial condition $e(0) = e_0$. Consider the sum of all potential functions $V(e)$ defined as in the statement of Theorem 5.3.1. For a symmetric graph references [26, 37] derive the overall control $u(e)$ from the function $V(e)$. This can a posteriori be justified as follows:

$$u(e) \;=\; -\hat{H}_u^T\, \mathrm{diag}\,\{e_i\}\; \boldsymbol{\Psi}(e) \;=\; -\hat{H}_u^T \begin{bmatrix} 2\, e_1\, \nabla V_1\big(\|e_1\|^2 - d_1^2\big) \\ \vdots \\ 2\, e_m\, \nabla V_m\big(\|e_m\|^2 - d_m^2\big) \end{bmatrix} \tag{5.35}$$

$$= \; -\hat{H}_u^T \begin{bmatrix} \frac{\partial}{\partial e_1}\, \nabla V_1\big(\|e_1\|^2 - d_1^2\big) \\ \vdots \\ \frac{\partial}{\partial e_m}\, \nabla V_m\big(\|e_m\|^2 - d_m^2\big) \end{bmatrix} \;=\; -\hat{H}_u^T \left[\frac{\partial}{\partial e} \sum_{i=1}^{m} V_i\big(\|e_i\|^2 - d_i^2\big) \right]^T \tag{5.36}$$

$$= \; -\hat{H}_u^T \left[\frac{\partial}{\partial e} V\,(e) \right]^T . \tag{5.37}$$

The control law is of the form of an inverse optimal control law, which we derived for an infinite horizon problem in (4.42). The difference between our case and a standard inverse optimality approach is that we do not know yet whether the control law is indeed stabilizing the links to $\mathcal{E}_e$. Let us nevertheless follow the approach outlined in Section 4.2.2. In the notation of Section 4.2.2 the matrix penalizing the control effort is simply $R(e) = \frac{1}{2}\, I_m$ and the state cost $q(e)$ is

$$q(e) \;=\; -\frac{1}{2}\, \frac{\partial V(e)}{\partial e}\, \hat{H}_u\, u(e) \;=\; \frac{1}{2}\, \boldsymbol{\Psi}(e)^T\, \mathrm{diag}\left\{e_i^T\right\}\; \hat{H}_u\, \hat{H}_u^T\, \mathrm{diag}\,\{e_i\}\; \boldsymbol{\Psi}(e) \tag{5.38}$$

$$= \; \frac{1}{2}\, \boldsymbol{\Psi}(e)^T\, R_{\mathcal{G}}(e)\, R_{\mathcal{G}}(e)^T\, \boldsymbol{\Psi}(e)\,. \tag{5.39}$$

This motivates us to set up the optimal control problem with the cost functional (5.31), the fixed terminal time $T_f \geq 0$, and where both state and input are unconstrained. We do not set up an infinite horizon control problem without terminal cost since we do not know whether the control law is indeed stabilizing. After these important observations follows now the proof of Theorem 5.3.1.

Proof of Theorem 5.3.1. We derive a solution to the optimal control problem with cost functional (5.31) via dynamic programming. The Hamiltonian corresponding to the cost functional is given by

$$H\left(e,u,\lambda\right) \;=\; \frac{1}{2}\,\mathbf{\Psi}(e)^T\,R_{\mathcal{G}}(e)\,R_{\mathcal{G}}(e)^T\,\mathbf{\Psi}(e) + \frac{1}{2}\,u^T\,u + \lambda^T\,\hat{H}_u\,u\,. \tag{5.40}$$

The Hamilton-Jacobi-Bellman equation corresponding to the optimal control problem (5.31) is then given by

$$0 \;=\; \frac{\partial \tilde{V}(t,e)}{\partial t} + \min_{u\in\mathbb{R}^{2m},\mathcal{C}^0} H\left(e,u,\left[\frac{\partial \tilde{V}(t,e)}{\partial e}\right]^T\right)\,, \tag{5.41}$$

where $\tilde{V}:\,[0,T_f]\times\hat{H}\left(\mathbb{R}^{2n}\right)\to\mathbb{R}$ is the value function that fulfills the boundary condition

$$\tilde{V}(T_f,e(T_f)) \;=\; V(e(T_f))\,. \tag{5.42}$$

The minimizing control input is then according to equation (4.37) given by

$$u^* \;=\; -\hat{H}_u^T\left[\frac{\partial \tilde{V}\left(t,e\right)}{\partial e}\right]^T\,. \tag{5.43}$$

If we plug u^* into the Hamilton-Jacobi-Bellman equation (5.41), we arrive at the PDE

$$0 \;=\; \frac{\partial \tilde{V}(t,e)}{\partial t} + \frac{1}{2}\,\mathbf{\Psi}(e)^T R_{\mathcal{G}}(e)\,R_{\mathcal{G}}(e)^T\mathbf{\Psi}(e) - \frac{1}{2}\,\frac{\partial \tilde{V}\left(t,e\right)}{\partial e}\,\hat{H}_u\,\hat{H}_u^T\left[\frac{\partial \tilde{V}\left(t,e\right)}{\partial e}\right]^T\,. \tag{5.44}$$

An intriguing solution for $\tilde{V}(t,e)$ which fulfills the PDE (5.44) and also the boundary condition (5.42) is a time-invariant function, namely the sum of the potential functions $V(e)$. By the verification theorem (Theorem 4.2.1) the optimal control law is given by (5.37) and $V(e)$ is the value function. Since both $V(e)$ and u^* are time-invariant and independent of T_f, they constitute the value function and optimal control for any arbitrary but fixed $T_f\geq 0$.

□

We already mentioned, that the control law solves two other inverse optimal control problems, which we would like to state as corollaries of Theorem 5.3.1.

Corollary 5.3.1. *The gradient control law (3.35) is also the solution to the optimal control problem (5.32) with a free terminal time T_f. The sum of all potential functions $V(e)$ is the value function and any terminal time $T_f\geq 0$ is optimal.*

Proof. In the free terminal time problem we have the same Hamilton-Jacobi-Bellman equation with the additional boundary conditions $\left.\frac{\partial \tilde{V}(t,e)}{\partial e}\right|_{T_f} = \frac{\partial V(e)}{\partial e}$ and $\left.\frac{\partial \tilde{V}(t,e)}{\partial t}\right|_{T_f} = 0$. These boundary conditions are for any T_f trivially satisfied by $\tilde{V}(t,e) = V(e)$. Thus any terminal time $T_f \geq 0$ is optimal, $V(e)$ is the value function, and u^* is the optimal control. □

Remark 5.3.1. A necessary condition for the optimality of the control law can also can be derived via variational calculus and results in the two point boundary value problem

$$\begin{array}{lccl}
\text{state equation:} & \dot{e} & = & \left[\frac{\partial H(e,u,\lambda)}{\partial \lambda}\right]^T = \hat{H}_u\, u \\
\text{costate equation:} & \dot{\lambda} & = & -\left[\frac{\partial H(e,u,\lambda)}{\partial e}\right]^T = -\left[\frac{\partial q(e)}{\partial e}\right]^T \\
\text{input stationarity:} & \frac{\partial H(e,u,\lambda)}{\partial u} & = & \mathbf{0} \;\Leftrightarrow\; u = -H_u^T\,\lambda \\
\text{initial condition:} & e(0) & = & e_0 \\
\text{transversality condition:} & \lambda(T_f) & = & \operatorname{diag}\{e_i\}\; \boldsymbol{\Psi}(e)\big|_{e(T_f)} = \left[\frac{\partial V(e)}{\partial e}\right]^T\Bigg|_{e(T_f)}.
\end{array}$$

It can easily be checked that the control law (5.37) and $\lambda = \left[\frac{\partial V(e)}{\partial e}\right]^T$ solve the two point boundary value problem, which is a necessary condition for optimality. The sufficiency can be established by $\frac{\partial^2 H(e,u,\lambda)}{\partial u^2} \succ 0$. Therefore, the control law (5.37) optimizes the optimal control problem (5.31) for any arbitrary but fixed $T_f \geq 0$. Moreover, the condition for a free terminal time is satisfied for any $T_f \geq 0$, that is, $H\left(e, u^*, \lambda\right) = 0$ for any T_f.

Corollary 5.3.2. *The gradient control law* (3.35) *is also the solution to the infinite horizon optimal control problem* (5.33) *with the terminal set* $\mathcal{E}_e$*, and* $V(e)$ *is the value function.*

Proof. In the infinite horizon problem with the terminal set $\mathcal{E}_e$ we have the Hamilton-Jacobi-Bellman equation (5.41) in its time-invariant version and with the boundary conditions

$$\tilde{V}(e) = 0 \;\Leftrightarrow\; e \in \mathcal{E}_e \;\Leftrightarrow\; V(e) = 0 \;\; ([72], \text{Section } 10.23)\,. \tag{5.45}$$

An obvious solution is given by $\tilde{V}(e) = V(e)$ and results in the same control u^* as before. □

In the general directed graph case each robot has its own potential function which it is trying to optimize and we will not be able to derive the overall control law from the function

$V(e)$. However the robots might still work together and optimize a common cost functional. We try to capture this behavior by the definition of a cooperative graph in the next section.

5.3.2 Definition of a Cooperative Graph

We have seen in the preceding section that for a directed graph the control law (3.35) based on regular potential functions is inverse optimal and minimizes a meaningful cost functional, which can be interpreted in terms of rigidity. Unfortunately, the concept of inverse optimality does not generalize to directed graphs. However, an idea that might generalize is that the robots act cooperatively in the sense that they behave as if the sensor graph was undirected. That is to say, the closed-loop link dynamics optimize the common cost functional (5.32), and they do so at every time point t and for every $e \in \hat{H}(\mathcal{Z})$. We refer to such graphs as cooperative graphs and define them in analogy to the inverse optimality result as follows:

Definition 5.3.1. A graph $\mathcal{G}$ is said to be *cooperative* if

$$V(e) = \int_t^{T_f} \boldsymbol{\Psi}(e(\tau))^T R_{\mathcal{G}}(e(\tau)) R_{\mathcal{G}}(e(\tau))^T \boldsymbol{\Psi}(e(\tau)) \, d\tau + V(e(T_f)) \tag{5.46}$$

with $e(\tau)$ from the dynamical system

$$\dot{e}(\tau) = -\hat{H}\hat{O} \operatorname{diag}\left\{e_i(\tau)^T\right\} \boldsymbol{\Psi}(e(\tau)) \quad , \quad \tau \in [t, T_f] \tag{5.47}$$

$$e(t) = e \tag{5.48}$$

holds for any $e \in \hat{H}(\mathcal{Z})$ and for any $t \leq T_f$ s.t. solutions to (5.47)-(5.48) exist on $[t, T_f]$.

The term cooperative graph is at the first glance a little misleading because it is actually the link dynamics which are cooperative. However, once the graph is fixed the link dynamics are completely determined and that's why cooperativeness corresponds to the interconnection structure. We already discussed the interpretation of the functional on the right-hand side of (5.46) if the link dynamics are forward complete and we can set $T_f = \infty$. Equation (5.46) is called an *integral dissipation (in)equality* [73] for the function $V(e)$. Similar to Lyapunov's stability condition the solution $e(t)$ is not needed and Definition 5.3.1 can be equivalently represented by an algebraic equation called a *differential dissipation (in)equality*.

Lemma 5.3.1. *A graph $\mathcal{G}$ is cooperative if and only if for any $e \in \hat{H}(\mathcal{Z})$ $V(e)$ satisfies*

$$\frac{\partial V(e)}{\partial e}\,\dot{e} \;=\; -\boldsymbol{\Psi}(e)^T\, R_{\mathcal{G}}(e)\, R_{\mathcal{G}}(e)^T\, \boldsymbol{\Psi}(e)\,. \tag{5.49}$$

Proof. $\Rightarrow$: Let $e \in \hat{H}(\mathcal{Z})$ be arbitrary. Since $V(e) \in \mathcal{C}^1$, we can take the time derivative of $V(e) = V(e(t))$ along trajectories of the dynamics (5.47)-(5.48). This results in

$$\dot{V}(e(t)) \;=\; \frac{\partial V(e)}{\partial e}\,\dot{e}(t) \;=\; -\boldsymbol{\Psi}(e(t))^T\, R_{\mathcal{G}}(e(t))\, R_{\mathcal{G}}(e(t))^T\, \boldsymbol{\Psi}(e(t))\,. \tag{5.50}$$

With the identity $e(t) = e$ from (5.48) the statement is (5.49) is true for any $e \in \hat{H}(\mathcal{Z})$.

$\Leftarrow$: Let $e \in \hat{H}(\mathcal{Z})$ be arbitrary and note that the left-hand side of (5.49) can be replaced with $\dot{V}(e(\tau))$ and the argument e on the right-hand side by $e(\tau)$. Thus we obtain

$$\dot{V}(e(\tau)) \;=\; -\boldsymbol{\Psi}(e(\tau))^T\, R_{\mathcal{G}}(e(\tau))\, R_{\mathcal{G}}(e(\tau))^T\, \boldsymbol{\Psi}(e(\tau))\,. \tag{5.51}$$

Now let $t \leq T_f$ be such that solutions of (5.47)-(5.48) are well defined on $\tau \in [0, T_f]$. An integration of equation (5.51) within the time interval $\tau \in [0, T_f]$ leads to Definition 5.3.1. □

Since $V(e)$ is positive definite w.r.t. the compact invariant set $\mathcal{E}_e$ and its derivative $\dot{V}(e)$ is clearly negative semidefinite, $V(e)$ serves as a natural set Lyapunov function candidate for cooperative graphs. This directly allows us to derive a result on forward completeness, stability and convergence of the link dynamics.

Theorem 5.3.2. *Consider a cooperative graph $\mathcal{G}$ and the resulting link dynamics (5.23) which are obtained by irregular potential functions. For every initial condition $e_0 \in \hat{H}(\mathcal{Z})$ the sublevel set*

$$\Omega(V(e_0)) \;=\; \left\{ e \in \hat{H}\left(\mathcal{Z}\right) \,|\, V(e) \leq V(e_0) \right\} \tag{5.52}$$

is a compact invariant set, the link dynamics are forward complete, the set $\mathcal{E}_e$ is stable w.r.t. them, and their solution $\Phi_e(e_0, t)$ converges to the largest invariant set contained in

$$\mathcal{W}_e \;=\; \left\{ e \in \Omega(V(e_0)) \,\middle|\, \boldsymbol{\Psi}(e)^T\, R_{\mathcal{G}}(e)\, R_{\mathcal{G}}(e)^T\, \boldsymbol{\Psi}(e) = 0 \right\}. \tag{5.53}$$

Moreover, in the case of regular potential functions all results hold with $\mathcal{Z} = \mathbb{R}^{2n}$.

Proof. Note that in the case of irregular potential functions the initial condition is restricted to $e_0 \in \hat{H}(\mathcal{Z})$. The definition interval for every irregular potential function V_i and its gradient ∇V_i is given by $D_i = -(d_i^2, \infty)$. This defines the sets $\mathcal{X}_i^e$ and thus the state space $\mathcal{Z}$. By Lemma 5.1.2 the right-hand side of the link dynamics is locally Lipschitz continuous on the open cube $D = D_1 \times \cdots \times D_m$. Thus existence and uniqueness of the solution $\Phi_e(e_0, t)$ are guaranteed $\forall\, t \in [0, \delta)$ with $\delta > 0$ ([49], Theorem 3.1).

Consider the function $V(e)$ where e is evaluated as solution of (5.23), that is $e = \Phi_e(e_0, t)$ $\forall\, t \in [0, \delta)$. Note that for irregular potential functions the limit $\lim\limits_{\omega \downarrow -d_i^2} V_i(\omega) = \infty$ holds. This fact and property *(iv)* of Defintion 3.2.1 imply that the sum of all potential functions $V(e)$ is a proper function, that is,

$$V(\omega) \underset{\omega \to \partial \hat{H}(\mathcal{Z})}{\to} \infty\,. \tag{5.54}$$

Therefore every sublevel set

$$\Omega(c) \;=\; \left\{ e \in \hat{H}(\mathcal{Z}) \,|\, V(e) \leq c \right\} \tag{5.55}$$

excludes the complement of $\hat{H}(\mathcal{Z})$, that is $\Omega(c) \cap \bigcup\limits_{i=1}^{m} \mathcal{X}_e^i = \emptyset$. Thus $\Omega(c)$ can be equivalently formulated as

$$\Omega(c) \;=\; \left\{ e \in \hat{H}\left(\mathbb{R}^{2n}\right) \,|\, V(e) \leq c \right\}, \tag{5.56}$$

which shows that $\Omega(c)$ is closed. The set $\mathcal{E}_e$ is compact and thus $\Omega(c)$ is compact. The derivative of the Lyapunov function $V(e)$ along trajectories of (5.23) is for $t \in [0, \delta]$ given by (5.49) and is clearly negative semidefinite. Therefore, $\Omega(V(e_0))$ is an invariant set, that is,

$$(\forall\, e_0 \in \Omega(V(e_0)))\;\; (\forall\, t \in [0, \delta))\;\;\; \Phi_e(e_0, t) \in \Omega(V(e_0))\,. \tag{5.57}$$

The compactness and invariance of $\Omega(c)$ and the fact that it is a subset of the domain D guarantee the boundedness, existence and uniqueness of $\Phi_e(t, e_0)$ $\forall\, e_0 \in \hat{H}(\mathcal{Z})$ and $\forall\, t \geq 0$ ([49],Theorem 3.3). By Theorem 4.1.1 the set $\mathcal{E}_e$ is stable w.r.t. the link dynamics and additionally the assumptions for the invariance principle ([49],Theorem 4.4) are also satisfied. Thus $\Phi_e(e_0, t)$ converges to the largest invariant set contained in

$$\mathcal{W}_e \;=\; \left\{ e \in \Omega(V(e_0)) \,\middle|\, \dot{V}(e) = \mathbf{\Psi}(e)^T\, R_{\mathcal{G}}(e)\, R_{\mathcal{G}}(e)^T\, \mathbf{\Psi}(e) = 0 \right\}. \tag{5.58}$$

For regular potential functions the state space can be extended to $\hat{H}(\mathcal{Z}) = \hat{H}(\mathbb{R}^{2n})$: By Lemma 5.1.2 the domain of Lipschitz continuity of a regular potential function V_i and its gradient can be continuously extended to the set $\bar{D}_i = [-d_i^2, \infty)$. The right-hand side of (5.23) is thus locally Lipschitz on $\bar{D} = \bar{D}_1 \times \dots \bar{D}_m$ and due to continuity also in a domain containing $\bar{D}$. Thus we can consider initial conditions $e_0 \in \hat{H}(\mathbb{R}^{2n})$ and the argumentation is analogous as for irregular potential functions. □

Remark 5.3.2. Note that we have no requirements on the potential functions V_i in Theorem 5.3.2 besides them all being of either regular or irregular nature. Moreover, by an appropriate definition of the state space we could also consider a system that contains both regular and irregular potential functions. We omit this here for the sake of a transparent notation.

Remark 5.3.3. It is clear now why potential functions V_i such as the one from Example 5.1.1 are not be addressed. If we allow such a potential function V_i, the right-hand side of the link dynamics is not well defined whenever the gradients ∇V_i are not well defined, that is, $e \in \mathcal{X}_e^i$. Additionally the function $V(e)$ is then not proper in the sense that it does not take an infinite value whenever the ∇V_i is not well defined. Thus we cannot rule out a convergence of the solution $\Phi_e(t, e_0)$ to $\mathcal{X}_e^i$, where the right-hand side of the link dynamics is singular.

An important implication of Theorem 5.3.2 is that the solution $\Phi_e(t, e_0)$ can only converge to a subset of $\mathcal{W}_e$. But since $\frac{\partial V(e)}{\partial t} = \mathbf{\Psi}(e)^T \operatorname{diag}\{e_i\}\, \dot{e}$ holds, we have that $\mathcal{W}_e \subset \mathcal{M}_e$. Therefore, the link dynamics have no other positive limit sets than their equilibria.

The idea to make use of the sum of all potential functions in combination with the invariance principle is not astonishing. References [20, 23, 24, 25] follow similar approaches but only for undirected graphs. However, the approach using the definition of a cooperative graph is superior because it reflects the relationship to rigidity and optimality and is also extendable to certain directed graphs as we will see in the next section. Moreover, the concept of cooperative graphs in combination with infinitesimal rigidity will lead us to a local stability result. But before that we want to give examples of cooperative and non-cooperative graphs.

5.3.3 Examples for Cooperative Graphs

Lemma 5.3.1 gives us a checkable condition for a cooperative graphs. If the potential functions are either regular or irregular, we simply have to check the derivative $\dot{V}(e)$ and see wether or not it matches (5.49). Of course, the definition of a cooperative graph can be extended to give additional degrees of freedom in $\dot{V}(e)$. We do not want to do this and rather conserve the idea that we have from undirected graphs, namely that two robots interconnected by a link both care about this link and optimize it together to its desired length. Interestingly enough, we can find the exactly same behavior also for certain directed graphs, where the robots are not meant to cooperate and one robot is not even part of the other's strategy.

Theorem 5.3.3. *Every undirected graph, every directed cycle and every open chain is a cooperative graph.*

Before we state the proof the reader should consider the following real world example to gain an intuitive understanding of Theorem 5.3.3.

Example 5.3.1. Consider an aerobic group consisting of 10 people standing in a circle who had just performed a partner exercise. Now they should all step backward such that everybody has enough space for the next exercise. Normally each of them would do so by stretching both his arms and stepping backward until he can just touch the shoulders of both his neighbours. This way the people line up in a wider circle. An implication of Theorem 5.3.3 is that each group member could alternatively just reach for his right neighbour's shoulder and step backwards as long as he can still touch it. The resulting circle will by Theorem 5.3.3 be exactly the same as in the first case.

Let us now present the proof of Theorem 5.3.3.

Proof of Theorem 5.3.3. For this proof we have to introduce some additional notation to characterize graphs. This notation will be only used within this proof and the corresponding graphs will be illustrated at the examples in Figure 5.10.

In general the derivative of $V(e)$ along trajectories of (5.23) is given by

$$\dot{V}(e) = \frac{\partial V(e)}{\partial e}\dot{e} = -\mathbf{\Psi}(e)^T \operatorname{diag}\left\{e_i^T\right\} \hat{H}\hat{O} \operatorname{diag}\{e_i\} \mathbf{\Psi}(e) \tag{5.59}$$

$$= -\frac{1}{2}\,\mathbf{\Psi}(e)^T \operatorname{diag}\left\{e_i^T\right\}\,\left(\hat{H}\,\hat{O}+\hat{O}^T\,\hat{H}^T\right)\,\operatorname{diag}\left\{e_i\right\}\,\mathbf{\Psi}(e)\,. \tag{5.60}$$

In a first step we reconsider the results for an undirected graph and then reduce the properties of directed cycles and directed open chains to those of an undirected graph. Case *(i)*: For an undirected graph with bidirectional links e we have to replace $\hat{H}$ and $\hat{O}$ by $\hat{H}_u$ and $\hat{H}_u^T$ in order to obtain the dynamics of the bidirectional links e. Note that we introduce an arbitrary orientation by defining $\hat{H}_u$. The derivative of $V(e)$ along trajectories then simplifies to

$$\dot{V}\,(e) = -\mathbf{\Psi}(e)^T \operatorname{diag}\left\{e_i^T\right\}\,\hat{H}_u\,\hat{H}_u^T \operatorname{diag}\left\{e_i\right\}\,\mathbf{\Psi}(e) \tag{5.61}$$

$$= -\mathbf{\Psi}(e)^T\,R_{\mathcal{G}}(e)\,R_{\mathcal{G}}(e)^T\,\mathbf{\Psi}(e) \tag{5.62}$$

and thus by Lemma 5.3.1 every undirected graph is a cooperative graph. Case *(ii)*: A directed cyclic graph $G_{c,m}^d$ is illustrated in Figure 5.10(a). The subscripts c and m stand for "cyclic graph" with m nodes and the superscript d stands for "directed." For such a graph we have the same number of nodes as links ($n = m$) and the matrices

$$H_{c,m} = P_m - I_m \in \mathbb{R}^{m\times m} \quad \text{and} \quad O_{c,m} = -I_m \in \mathbb{R}^{m\times m}\,, \tag{5.63}$$

where P_m is the companion matrix, that is, a circulant matrix defined as

$$P_m = \operatorname{circ}\begin{bmatrix}0 & 1 & 0 & \dots & 0\end{bmatrix} := \begin{bmatrix}0 & 1 & 0 & \dots & 0\\ 0 & 0 & 1 & \dots & 0\\ \vdots & & \ddots & & \vdots\\ 0 & \dots & 0 & 0 & 1\\ 1 & 0 & \dots & 0 & 0\end{bmatrix} \in \mathbb{R}^{m\times m}\,. \tag{5.64}$$

Obviously P_m is orthogonal, that is $P_m\,P_m^T = I_m$. For $H_{c,m}$ and $O_{c,m}$ we have the relationship

$$O_{c,m}^T\,H_{c,m}^T + H_{c,m}\,O = -H_{c,m}^T - H_{c,m} = -\left(P_m - I_m\right)^T - \left(P_m - I_m\right) \tag{5.65}$$

$$= -P_m^T + I_m - P_m + I_m = P_m\,P_m^T - P_m - P_m^T + I_m \tag{5.66}$$

$$= \left(P_m - I_m\right)\left(P_m - I_m\right)^T = H_{c,m}\,H_{c,m}^T\,. \tag{5.67}$$

If we define the rigidity matrix of the corresponding undirected graph $G_{c,m}^u$ as $R_{\mathcal{G}}(e) = \operatorname{diag}\left\{e_i^T\right\}\,\hat{H}_u$ with $H_u = H_{c,m}$, then $\dot{V}(e)$ simplifies to

$$\dot{V}\,(e) = -\frac{1}{2}\,\mathbf{\Psi}(e)^T \operatorname{diag}\left\{e_i^T\right\}\,\left(\hat{O}_{c,m}^T\,\hat{H}_{c,m}^T + \hat{H}_{c,m}\,\hat{O}_{c,m}\right)\,\operatorname{diag}\left\{e_i\right\}\,\mathbf{\Psi}(e) \tag{5.68}$$

$$= -\frac{1}{2}\operatorname{diag}\{e_i^T\}\left(\hat{H}_u\,\hat{H}_u^T\right)\operatorname{diag}\{e_i\} \tag{5.69}$$

$$= \frac{1}{2}\,\mathbf{\Psi}(e)^T\,R_{\mathcal{G}}(e)\,R_{\mathcal{G}}(e)^T\,\mathbf{\Psi}(e)\,. \tag{5.70}$$

Again by Lemma 5.3.1 every directed cycle is a cooperative graph. Case *(iii)*: A directed open chain graph $\mathcal{G}^d_{oc,m+1}$ is illustrated in Figure 5.10(c). The subscripts oc and $m+1$ stand for "open chain" and for the total number of nodes and the subscript d again for "directed." Such a graph has m links and $n = m+1$ nodes and the graph matrices

$$H_{oc,m+1} = \begin{bmatrix} -1 & 1 & 0 & \dots & 0 \\ 0 & -1 & 1 & \dots & 0 \\ \vdots & & \ddots & & \vdots \\ 0 & \dots & 0 & -1 & 1 \end{bmatrix} \in \mathbb{R}^{m\times m+1} \tag{5.71}$$

$$O_{oc,m+1} = \begin{bmatrix} -1 & 0 & 0 & \dots & 0 \\ 0 & -1 & 0 & \dots & 0 \\ \vdots & & \ddots & & \vdots \\ 0 & 0 & \dots & 0 & 0 \end{bmatrix} \in \mathbb{R}^{m+1\times m}\,. \tag{5.72}$$

The idea is now that the graph $\mathcal{G}^d_{oc,m+1}$ is almost the same graph as the cycle $\mathcal{G}^d_{c,m}$ with only one link missing. Note that $H_{oc,m+1}$ corresponds to $H_{c,m+1}$ with last line erased and $O_{oc,m+1}$ corresponds to $O_{c,m+1}$ with last column erased. We know from *(ii)* that the symmetric part of $H_{c,m+1}\,O_{c,m+1}$ corresponds to

$$H_{c,m+1}\,H_{c,m+1}^T = \operatorname{circ}\begin{bmatrix} 2 & -1 & 0 & \dots & 0 & -1 \end{bmatrix}. \tag{5.73}$$

Therefore the symmetric part of $H_{oc,m+1}\,O_{oc,m+1}$ corresponds to $H_{c,m+1}\,H_{c,m+1}^T$ when erasing the last row and last column. Thus for a directed open chain we have

$$O_{oc,m+1}^T\,H_{oc,m+1}^T + H_{oc,m+1}\,O_{oc,m+1} = \begin{bmatrix} 2 & -1 & 0 & \dots & 0 \\ -1 & 2 & -1 & \dots & 0 \\ \vdots & & \ddots & & \vdots \\ 0 & \dots & -1 & 2 & -1 \\ 0 & \dots & 0 & -1 & 2 \end{bmatrix} \in \mathbb{R}^{m\times m}\,, \tag{5.74}$$

which again corresponds to $H_{oc,m+1}\, H_{oc,m+1}^T$. If we let the orientation of the corresponding undirected graph $\mathcal{G}_{oc,m+1}^u$ be determined by $H_u = H_{oc,m+1}$, the remaining argument is analogous to case *(ii)*.

□

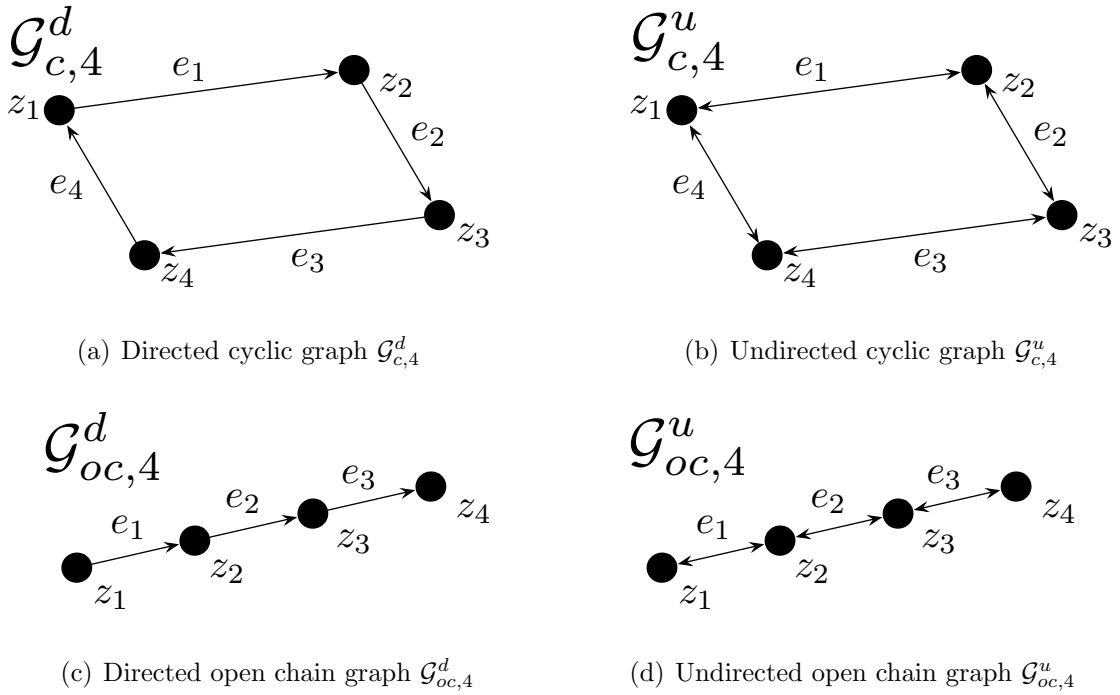

(a) Directed cyclic graph $\mathcal{G}_{c,4}^d$

(b) Undirected cyclic graph $\mathcal{G}_{c,4}^u$

(c) Directed open chain graph $\mathcal{G}_{oc,4}^d$

(d) Undirected open chain graph $\mathcal{G}_{oc,4}^u$

Figure 5.10: Four robots interconnected in cooperative graphs

In the light of Theorem 5.3.3 both a directed cyclic graph $\mathcal{G}_{c,m}^d$ as in Figure 5.10(a) and an undirected cyclic graph $\mathcal{G}_{c,m}^u$ as in Figure 5.10(b) are cooperative. For both graphs $V(e)$ is equivalent to the same cost functional. Since we already proved the inverse optimality in the undirected graph case, this is not surprising for the graph $\mathcal{G}_{c,m}^u$. In the case of an undirected cycle, each robot focuses on its leader robot only. However, this leader does not care about the interconnecting link to its follower but only about the one to its own leader. Nevertheless, the robots behave as if there would be no leader follower structure but rather an information flow in both directions. So from the viewpoint of optimality, both setups in Figure 5.10(a) and Figure 5.10(b) optimize the very same cost functional, although the robots in Figure 5.10(a) are not meant to do so. This quite astonishing fact also can be found

for undirected and directed open chains which are shown for four robots in Figure 5.10(c) and Figure 5.10(d). It is clear that we will not be able to find such a relationship for every undirected graph as the next paragraph shows.

5.3.4 Non-Cooperative Graphs

The condition for cooperative graphs given in Lemma 5.3.1 is given in terms of a dissipation inequality for the sum of the potential functions. Therefore, the question of cooperativeness is fairly easy to answer by looking at $\dot{V}(e)$. On the other hand, the stability and convergence result in Theorem 5.3.2 follows directly from Lemma 5.3.1 and motivates the question whether or not we can find a function $\tilde{V} : \hat{H}(\mathcal{Z}) \to \mathbb{R}$, such that $\tilde{V}(e)$ is positive definite w.r.t. $\mathcal{E}_e$ and such that the derivative along trajectories of the link dynamics satisfies

$$\begin{aligned} \dot{\tilde{V}}(e) &= \frac{\partial \tilde{V}(e)}{\partial e}\,\dot{e} = -\frac{\partial \tilde{V}(e)}{\partial e}\,\hat{H}\,\hat{O}\,\mathrm{diag}\left\{e_i^T\right\}\,\boldsymbol{\Psi}(e) && (5.75)\\ &\stackrel{!}{=} -\boldsymbol{\Psi}(e)^T\,R_{\mathcal{G}}(e)\,R_{\mathcal{G}}(e)^T\,\boldsymbol{\Psi}(e) && (5.76)\\ &= -\boldsymbol{\Psi}(e)^T\,\mathrm{diag}\left\{e_i^T\right\}\,\hat{H}_u\,\hat{H}_u^T\,\mathrm{diag}\left\{e_i^T\right\}\,\boldsymbol{\Psi}(e)\,. && (5.77)\end{aligned}$$

The existence of such a function implies by the arguments of Theorem 5.3.2 that the solution of the link dynamics converges to the largest invariant set of

$$\left\{ e \in \Omega(\tilde{V}(e_0)) \,\middle|\, \hat{H}_u^T\,\mathrm{diag}\left\{e_i^T\right\}\,\boldsymbol{\Psi}(e) = 0 \right\}, \tag{5.78}$$

where $\Omega(\tilde{V}(e_0))$ is a sublevel set bounded by $\tilde{V}(e) = \tilde{V}(e_0)$. However, in general the set of equilibria for the link dynamics is given by

$$\left\{ e \in \hat{H}(\mathcal{Z}) \,\middle|\, \hat{H}\,\hat{O}\,\mathrm{diag}\left\{e_i^T\right\}\,\boldsymbol{\Psi}(e) = \mathbf{0} \right\} \tag{5.79}$$

and therefore we arrive at the following necessary condition for a graph to be cooperative.

Lemma 5.3.2. *Consider a function $\tilde{V} : \hat{H}(\mathcal{Z}) \to \mathbb{R}$, where $\tilde{V}(e)$ is p.d. w.r.t. $\mathcal{E}_e$. If its derivative along the trajectories of the link dynamics satisfies (5.77), then it must hold that*

$$\ker\left(\hat{H}\,\hat{O}\right) \subseteq \ker\left(\hat{H}_u^T\right). \tag{5.80}$$

Before we go to the proof, note that Lemma 5.3.2 of course captures the case when $\tilde{V}(e) = V(e)$ but also the more general case.

Proof. By the preceding arguments it is clear that, if a function such as $\tilde{V}(e)$ exists, then every equilibrium point $\bar{e} \in \hat{H}(Z)$ of the link dynamics, that is, every $\bar{e} \in \hat{H}(Z)$ in the set (5.79), must also be in the positive limit set (5.78). Therefore, it must hold that

$$\ker\left(\hat{H}\,\hat{O}\right) \;\subseteq\; \ker\left(\hat{H}_u^T\right). \tag{5.81}$$

□

The undirected graphs we have identified in Theorem 5.3.3 fulfill of course the condition of Lemma 5.3.2. We omit the simple proof and conclude this section with an example of a non-cooperative graph, namely an acyclic triangular graph.

Example 5.3.2. Consider the example of three robots in a directed Henneberg graph. The graph is illustrated in Figure 5.11 and the graph matrices are

$$H = \begin{bmatrix} 1 & -1 & 0 \\ 1 & 0 & -1 \\ 0 & 1 & -1 \end{bmatrix} = H_u \quad \text{and} \quad O = \begin{bmatrix} 0 & 0 & 0 \\ -1 & 0 & 0 \\ 0 & 1 & -1 \end{bmatrix}. \tag{5.82}$$

The equilibria of the link dynamics are with $\psi_i := 2\,\nabla V_i\big(\|e_i\|^2 - d_i^2\big)$ given by

$$\mathbf{0} \;=\; \hat{H}\,\hat{O}\,\mathrm{diag}\left\{e_i^T\right\}\,\mathbf{\Psi}(e) \;=\; \begin{bmatrix} e_1\,\psi_1 \\ e_2\,\psi_2 + e_3\,\psi_3 \\ -e_1\,\psi_1 + e_2\,\psi_2 + e_3\,\psi_3 \end{bmatrix} \tag{5.83}$$

$$\Rightarrow \qquad \mathrm{diag}\left\{e_i^T\right\}\,\mathbf{\Psi}(e) \;=\; c\begin{bmatrix} 0 & 0 & 1 & 1 & -1 & -1 \end{bmatrix}^T \tag{5.84}$$

with $c \in \mathbb{R}$. This vector must then also be a solution of

$$\mathbf{0} \;=\; \hat{H}_u^T\,\mathrm{diag}\left\{e_i^T\right\}\,\mathbf{\Psi}(e)\,. \tag{5.85}$$

But we have that $c\begin{bmatrix} 0 & 0 & 1 & 1 & -1 & -1 \end{bmatrix}^T \notin \ker\left(H_u^T\right)$ and thus the graph is not cooperative. Stability for of the target formation with an acyclic graph follows by the results of [26, 30], but these results are based on the cascade structure of the z-dynamics. Indeed, we have

already mentioned in Section 2.1.2 that the Henneberg sequence always results in leader follower graph, such as in Figure 5.11, and thus also the z-dynamics will have a triangular structure. The leader follower structure is also evident in the link dynamics (5.83) which suggests a cascade analysis of the system. The robots do not act cooperatively in this case. For example, robot 3 only stops if both robot 2 and robot 1 are stationary. But robot 2 again does not care about robot 3 but only about its link to robot 1. The entire system only converges because robot 1 is stationary. This non cooperativeness is even more evident in

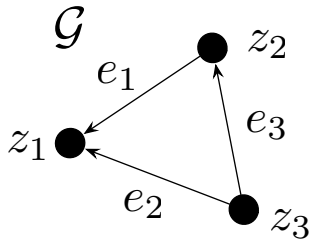

Figure 5.11: Three robots in a directed graph which is obtained by a Henneberg sequence

the acyclic graph in Figure 5.12 which was also obtained by a Henneberg sequence. Here robot 5 tries to meet its distance constraint w.r.t. robot 2 and robot 4. But these both go away in different directions and robot 5 has to pursue them.

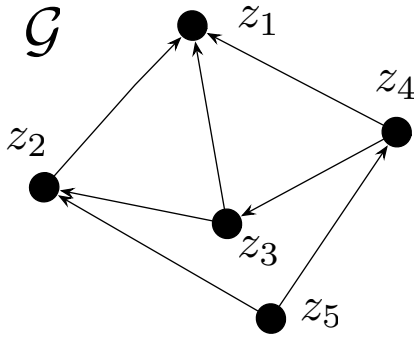

Figure 5.12: Directed acyclic graph for five robots

5.4 Stability Results on Cooperative and Rigid Graphs

5.4.1 Stability of the e-Dynamics

By Theorem 5.3.2 the link dynamics resulting of a cooperative graph are stable and their solution converges to an equilibrium contained in the set $\mathcal{W}_e$, as specified in (5.53). Unfortunately Theorem 5.3.2 does not enable us to draw a conclusion about the asymptotic stability of $\mathcal{E}_e$, that is, whether or not the robots converge to the target formation. Note that $\mathcal{E}_e \subset \mathcal{W}_e$. By the definition of $\mathcal{W}_e$ we have that for every $e \in \mathcal{W}_e \setminus \mathcal{E}_e$ the matrix $R_{\mathcal{G}}(e)^T$ must have a rank loss, and thus the formation $(\mathcal{G}, e)$ is not infinitesimally rigid. However, the target formation $(\mathcal{G}, v^{-1}(\mathbf{d}))$ is specified as infinitesimally rigid formation and this fact is the key point which allows us to derive local asymptotic stability of $\mathcal{E}_e$. The following theorem states this result for any potential functions, not just regular or irregular ones.

Theorem 5.4.1. *For every cooperative graph the set $\mathcal{E}_e$ is locally asymptotically stable w.r.t. the link dynamics (5.23). A guaranteed region of attraction is given by the compact invariant level set*

$$\Omega(\rho) \;=\; \left\{ e \in \hat{H}(\mathcal{Z}) \,|\, V(e) \leq \rho \right\}, \tag{5.86}$$

where ρ is sufficiently small, such that for every $e \in \Omega(\rho)$, $(\mathcal{G}, e)$ is infinitesimally rigid.

Proof. Due to infinitesimal rigidity of the target formation $(\mathcal{G}, v^{-1}(\mathbf{d}))$ the matrix $R_{\mathcal{G}}(e)^T \in \mathbb{R}^{2n \times m}$ has full rank $m \;\forall\, e \in \mathcal{E}_e$, or spoken differently $R_{\mathcal{G}}(e)\, R_{\mathcal{G}}(e)^T$ has no zero eigenvalues $\forall\, e \in \mathcal{E}_e$. The eigenvalues of $R_{\mathcal{G}}(e)\, R_{\mathcal{G}}(e)^T$ are continuous functions of the matrix elements ([74], Corollary VI.1.6) and thus of $e \in \hat{H}\,(\mathcal{Z})$. Since the minimal eigenvalue of $R_{\mathcal{G}}(e)\, R_{\mathcal{G}}(e)^T$ is positive $\forall\, e \in \mathcal{E}_e$, then due to continuity also in a neighbourhood of $\mathcal{E}_e$. Therefore, the matrix $R_{\mathcal{G}}(e)\, R_{\mathcal{G}}(e)^T$ has full rank in an open set containing the set $\mathcal{E}_e$ in its interior. Let $\mathcal{Q}$ be the set where the matrix $R_{\mathcal{G}}(e)^T$ has a rank loss and thus the matrix $R_{\mathcal{G}}(e)\, R_{\mathcal{G}}(e)^T$ has a zero eigenvalue. In order to continue, consider a level set

$$\Omega(\rho) \;=\; \left\{ e \in \hat{H}(\mathcal{Z}) \,|\, V(e) \leq \rho \right\}. \tag{5.87}$$

where ρ is small enough such that $\Omega(\rho)$ does not intersect the set $\mathcal{Q}$. The sets $\mathcal{E}_e$, $\mathcal{Q}$ and $\Omega(\rho)$ are illustrated in Figure 5.13. The sum of all potential functions $V(e)$ is a suitable Lyapunov

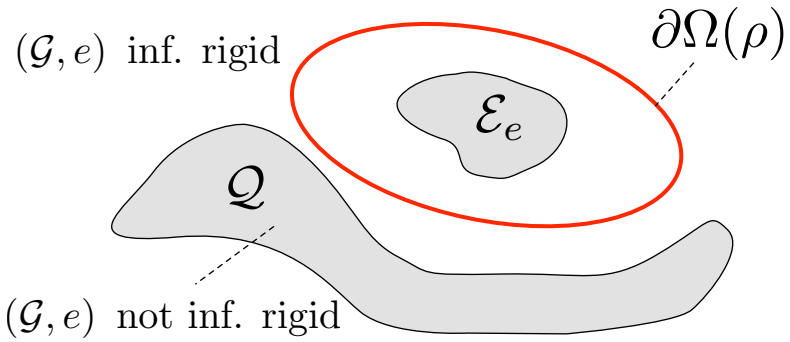

Figure 5.13: Illustration of the sets $\mathcal{E}_e$, $\mathcal{Q}$ and $\Omega(\rho)$.

function candidate, which has for cooperative graphs the derivative along trajectories

$$\dot{V}(e) \;=\; -\mathbf{\Psi}(e)^T\, R_{\mathcal{G}}(e)\, R_{\mathcal{G}}(e)^T\, \mathbf{\Psi}(e)\,. \tag{5.88}$$

Every potential function and its gradient are locally Lipschitz $\forall\, e \in \Omega(\rho)$ which is a compact and invariant set. Therefore, existence, uniqueness and boundedness of the solution $\Phi_e(e_0, t)$ are guaranteed $\forall\, t \geq 0$ and $\forall\, e_0 \in \Omega(\rho)$ ([49],Theorem 3.3). Since the eigenvalues of a matrix are continuous functions of the matrix elements and $\Omega(\rho)$ is compact we define λ as

$$\lambda \;:=\; \min_{e\in\Omega(\rho)} \operatorname{eig}\left(R_{\mathcal{G}}(e)\, R_{\mathcal{G}}(e)^T\right) \;>\; 0\,, \tag{5.89}$$

that is, as minimum singular value of the rigidity matrix. We then have

$$(\forall\, e \in \Omega(\rho)) \;\; \dot{V}(e) \;\leq\; -\lambda\, \|\mathbf{\Psi}(e)\|^2 \tag{5.90}$$

and thus $\forall\, e_0 \in \Omega(\rho)$ $\dot{V}(e)$ is negative definite w.r.t. e. Therefore, by Theorem 4.1.1 the set $\mathcal{E}_e$ is asymptotically stable with region of attraction $\Omega(\rho)$. □

Theorem 5.4.1 gives no information about the the rate of convergence. From Subsection 5.2.1 it is clear that the rate of convergence should be such that a trajectory $\Phi(t, e_0)$ which is converging to $\mathcal{E}_e$ is a $\mathcal{L}_1$ signal. Otherwise we cannot conclude that the z-dynamics attain stationary values. The next theorem will give us an exponential convergence rate, but prior

to that we have to derive a result on the Lyapunov function $V(e)$. We already know by Lemma 4.1.2 that there exists two class $\mathcal{K}$ functions $\alpha_1(\cdot)$ and $\alpha_2(\cdot)$, such that

$$\alpha_1\left(\|e\|_{\mathcal{E}_e}\right) \;\leq\; V(e) \;\leq\; \alpha_2\left(\|e\|_{\mathcal{E}_e}\right). \tag{5.91}$$

We will now construct these two comparison functions simply as a sum of quadratic potential functions $V_i\big(\|e_i\|^2 - d_i^2\big) = \frac{1}{2}\left(\|e_i\|^2 - d_i^2\right)^2$. For notational convenience we define the vector containing the gradients of quadratic potential functions by

$$\bar{\boldsymbol{\Psi}}(e) \;=\; \begin{bmatrix}\bar{\psi}_1 & \dots & \bar{\psi}_m\end{bmatrix}^T \;=\; \begin{bmatrix}\|e_1\|^2 - d_1^2 & \dots & \|e_m\|^2 - d_m^2\end{bmatrix}^T. \tag{5.92}$$

The following lemma relates arbitrary potential functions to quadratic potential functions. The idea for the lemma and its proof are taken from [28], Lemma 3.

Lemma 5.4.1. *Let $\nu < \min\limits_{i\in\{1,\dots,m\}} d_i^2$ be a positive number. There exist positive numbers α_1 and α_2 such that $\forall\, e \in \hat{H}(\mathcal{Z})$ with $\left\|\bar{\boldsymbol{\Psi}}(e)\right\| \leq \nu$ we have that*

$$\frac{\alpha_1}{\sqrt{m}}\left\|\bar{\boldsymbol{\Psi}}(e)\right\| \;\leq\; \|\boldsymbol{\Psi}(e)\| \;\leq\; \alpha_2\sqrt{m}\,\left\|\bar{\boldsymbol{\Psi}}(e)\right\| \tag{5.93}$$

$$\frac{\alpha_1}{2}\,\bar{\boldsymbol{\Psi}}(e)^T\,\bar{\boldsymbol{\Psi}}(e) \;\leq\; V(e) \;\leq\; \frac{\alpha_2}{2}\,\bar{\boldsymbol{\Psi}}(e)^T\,\bar{\boldsymbol{\Psi}}(e). \tag{5.94}$$

The basic idea of the proof is that due to strict monotony and local Lipschitz continuity we can upper and lower bound the slope of the gradient of the potential function. This will then also lead to bounds on the potential functions.

Proof. Consider $\sigma \in \mathbb{R}$, $\omega \in \mathbb{R}$ and assume that $|\sigma| \leq \nu$ and $|\omega| \leq \nu$. Let

$$\alpha_1^i \;=\; \min_{|\sigma|\leq\nu} \frac{\partial \nabla V_i(\sigma)}{\partial \sigma} \quad,\; i \in \{1,\dots,m\}. \tag{5.95}$$

Every α_1^i is strictly positive because, by Definition 3.2.1, each $\nabla V_i(\sigma)$ is continuously differentiable $\forall\, \sigma \in (-d_i^2, \infty)$ and strictly monotone increasing. From this and from $\nabla V_i(0) = 0$ it follows that

$$|\nabla V_i(\sigma)| \;\geq\; \alpha_1^i\,|\sigma| \quad,\; i \in \{1,\dots,m\}. \tag{5.96}$$

If we integrate $\nabla V_i(\sigma)$ and apply the preceding inequality we get

$$V_i(\omega) \;=\; \int_0^\omega \nabla V_i(\sigma)\,d\sigma \;\geq\; \frac{\alpha_1^i}{2}\,\omega^2 \quad,\; i \in \{1,\dots,m\}. \tag{5.97}$$

By Lemma 5.1.1 $\nabla V_i(\sigma)$ is locally Lipschitz continuous and there exists for every $i \in \{1,\dots,m\}$ a positive constant α_2^i, such that

$$|\nabla V_i(\sigma)| \;\leq\; \alpha_2^i\,|\sigma| \;\;,\;\; i \in \{1,\dots,m\}\,. \tag{5.98}$$

It follows from this that

$$V_i(\omega) \;=\; \int_0^{\omega} \nabla V_i(\sigma)\,d\sigma \;\leq\; \frac{\alpha_2^i}{2}\,\omega^2 \;\;,\;\; i \in \{1,\dots,m\}\,. \tag{5.99}$$

The norm of the vector containing the gradients of the potential functions, that is, $\|\boldsymbol{\Psi}(e)\|$, can then be related to $\left\|\bar{\boldsymbol{\Psi}}(e)\right\|$ the following way:

$$\|\boldsymbol{\Psi}(e)\| \;\geq\; \|\boldsymbol{\Psi}(e)\|_\infty \;\geq\; \min_{i=1,\dots,m} \alpha_1^i \left\|\bar{\boldsymbol{\Psi}}(e)\right\|_\infty \;\geq\; \min_{i=1,\dots,m} \alpha_1^i \frac{1}{\sqrt{m}} \left\|\bar{\boldsymbol{\Psi}}(e)\right\| \tag{5.100}$$

$$\|\boldsymbol{\Psi}(e)\| \;\leq\; \sqrt{m}\,\|\boldsymbol{\Psi}(e)\|_\infty \;\leq\; \max_{i=1,\dots,m} \alpha_2^i \sqrt{m}\,\left\|\bar{\boldsymbol{\Psi}}(e)\right\|_\infty \tag{5.101}$$

$$\leq\; \max_{i=1,\dots,m} \alpha_2^i \sqrt{m}\,\left\|\bar{\boldsymbol{\Psi}}(e)\right\|\,. \tag{5.102}$$

The lower and upper bound from the statement of the lemma follow by $\alpha_1 = \min\limits_{i=1,\dots,m} \alpha_1^i$ and $\alpha_2 = \max\limits_{i=1,\dots,m} \alpha_2^i$. The function $V(e)$ is the sum of the potential functions, that is,

$$V(e) \;=\; \sum_{i=1}^{m} V_i\big(\|e_i\|^2 - d_i^2\big)\,, \tag{5.103}$$

The lower and upper bound on $V(e)$ follow by bounding each addend $V_i\big(\|e_i\|^2 - d_i^2\big)$ and setting again $\alpha_1 = \min\limits_{i=1,\dots,m} \alpha_1^i$ and $\alpha_2 = \max\limits_{i=1,\dots,m} \alpha_2^i$. □

With the help of Lemma 5.4.1 we can extend Theorem 5.4.1 such that the rate of convergence is exponential. The following corollary states the exponential stability of $\mathcal{E}_e$.

Corollary 5.4.1. *For every cooperative graph the set $\mathcal{E}_e$ is locally exponentially stable w.r.t. the link dynamics (5.23) with guaranteed region of attraction $\Omega(\rho)$, as in Theorem 5.4.1.*

Proof. From the proof of Theorem 5.4.1 we have that for a sufficiently small $\rho > 0$

$$(\forall\, e \in \Omega(\rho)) \;\; \dot{V}(e) \;\leq\; -\lambda\,\|\boldsymbol{\Psi}(e)\|^2\,. \tag{5.104}$$

We now invoke Lemma 5.4.1. Let ν denote a number such that

$$(\forall\, e \in \Omega(\rho)) \;\; \left\|\bar{\boldsymbol{\Psi}}(e)\right\| \leq \nu\,. \tag{5.105}$$

Note that $e \in \Omega(\rho)$ implies that $\nu < \min_{i\in\{1,\dots,m\}} d_i^2$. Thus we have by Lemma 5.4.1

$$(\forall\, e \in \Omega(\rho))\ (\exists\, \alpha_1, \alpha_2 > 0) \qquad \frac{\alpha_1}{\sqrt{m}} \left\|\bar{\boldsymbol{\Psi}}(e)\right\| \ \leq\ \|\boldsymbol{\Psi}(e)\| \ \leq\ \alpha_2 \sqrt{m}\, \left\|\bar{\boldsymbol{\Psi}}(e)\right\| \tag{5.106}$$

$$\frac{\alpha_1}{2}\, \bar{\boldsymbol{\Psi}}(e)^T\, \bar{\boldsymbol{\Psi}}(e) \ \leq\ V(e) \ \leq\ \frac{\alpha_2}{2}\, \bar{\boldsymbol{\Psi}}(e)^T\, \bar{\boldsymbol{\Psi}}(e)\,. \tag{5.107}$$

We can combine the derivative $\dot{V}(e)$ with the previous inequalities to

$$(\forall\, e \in \Omega(\rho))\ \ \dot{V}(e) \ \leq\ -\lambda \boldsymbol{\Psi}(e)^T\, \boldsymbol{\Psi}(e) \tag{5.108}$$

$$-\frac{\alpha_1^2}{m}\, \lambda \bar{\boldsymbol{\Psi}}(e)^T\, \bar{\boldsymbol{\Psi}}(e) \ \leq\ -2\, \frac{\alpha_1^2}{\alpha_2\, m}\, \lambda\, V(e)\,. \tag{5.109}$$

To avoid clutter we define $\sigma := 2\, \frac{\alpha_1^2}{\alpha_2\, m}$. A solution for the differential inequality (5.109) is given by the *Bellman-Gronwall Lemma* ([49], Lemma A.1) as

$$(\forall\, e \in \Omega(\rho))\ \ V(e(t)) \ \leq\ V(e_0)\, e^{-\sigma\, t}\,. \tag{5.110}$$

Since $V(e(t))$ measures the distance to equilibrium set $\mathcal{E}_e$ the point-to-set distance $\|e(t)\|_{\mathcal{E}_e}$ should also be exponentially decreasing. In order to show this, we relate $V(e(t))$ to the quadratic potential function

$$\frac{\alpha_1}{2}\, \left\|\bar{\boldsymbol{\Psi}}(e(t))\right\|^2 \ \leq\ V(e(t)) \ \leq\ V(e_0)\, e^{-\sigma\, t} \ \leq\ \frac{\alpha_2}{2}\, \left\|\bar{\boldsymbol{\Psi}}(e_0)\right\|^2\, e^{-\sigma\, t}\,. \tag{5.111}$$

Consider the following set of inequalities

$$\left\|\bar{\boldsymbol{\Psi}}(e(t))\right\|^2 \ \leq\ \frac{2}{\alpha_1}\, V(e(t)) \ \leq\ \frac{\alpha_2}{\alpha_1}\, \left\|\bar{\boldsymbol{\Psi}}(e_0)\right\|^2\, e^{-\sigma\, t} \tag{5.112}$$

$$\Rightarrow\ \left\|\bar{\boldsymbol{\Psi}}(e(t))\right\|_\infty^2 \ \leq\ \left\|\bar{\boldsymbol{\Psi}}(e(t))\right\|^2 \ \leq\ \frac{\alpha_2}{\alpha_1}\, \left\|\bar{\boldsymbol{\Psi}}(e_0)\right\|^2\, e^{-\sigma\, t} \ \leq\ m\, \frac{\alpha_2}{\alpha_1}\, \left\|\bar{\boldsymbol{\Psi}}(e_0)\right\|_\infty^2\, e^{-\sigma\, t} \tag{5.113}$$

$$\Rightarrow\ (\forall\, i \in \{1,\dots,m\})\ \ \left(\|e_i(t)\|^2 - d_i^2\right)^2 \ \leq\ m\, \frac{\alpha_2}{\alpha_1}\, \left(\|e_i(0)\|^2 - d_i^2\right)^2\, e^{-\sigma\, t} \tag{5.114}$$

$$\Rightarrow\ \left|\|e_i(t)\|^2 - d_i^2\right| \ \leq\ \sqrt{m\, \frac{\alpha_2}{\alpha_1}}\, \left|\|e_i(0)\|^2 - d_i^2\right|\, e^{-\sigma\, t/2} \tag{5.115}$$

$$\Leftrightarrow\ \left|\|e_i(t)\| - d_i\right|\, \left(\|e_i(t)\| + d_i\right) \ \leq\ \sqrt{m\, \frac{\alpha_2}{\alpha_1}}\, \left|\|e_i(0)\|^2 - d_i^2\right|\, e^{-\sigma\, t/2} \tag{5.116}$$

$$\Rightarrow\ \left|\|e_i(t)\| - d_i\right| \ \leq\ \frac{\sqrt{m\, \frac{\alpha_2}{\alpha_1}}}{\left(\|e_i(t)\| + d_i\right)}\, \left|\|e_i(0)\|^2 - d_i^2\right|\, e^{-\sigma\, t/2}$$

$$\leq\ \frac{\sqrt{m}}{d_i}\, \sqrt{\frac{\alpha_2}{\alpha_1}}\, \left|\|e_i(0)\|^2 - d_i^2\right|\, e^{-\sigma\, t/2} \ =\ c_i\, \left|\|e_i(0)\| - d_i\right|\, e^{-\sigma\, t/2}, \tag{5.117}$$

where $c_i := \frac{\sqrt{m}}{d_i}\sqrt{\frac{\alpha_2}{\alpha_1}}\,(\|e_i(0)\| + d_i)$. By inequality (5.117) we have that every link is exponentially converging to its desired length. This allows us to show that the point-to-set distance ins exponentially decreasing:

$$\begin{aligned} \|e(t)\|_{\mathcal{E}_e} &\leq \sqrt{2\,m}\;\|e(t)\|_{\mathcal{E}_e,\infty} = \max_{i\in\{1,\dots,m\}} c_i\,\big|\|e_i(0)\| - d_i\big|\,\sqrt{2\,m}\,e^{-\sigma\,t/2} && (5.118)\\ &= \max_{i\in\{1,\dots,m\}} c_i\,\sqrt{2\,m}\;\|e_0\|_{\mathcal{E}_e,\infty}\;e^{-\sigma\,t/2} && (5.119)\\ &\leq \max_{i\in\{1,\dots,m\}} c_i\,\sqrt{2\,m}\;\|e_0\|_{\mathcal{E}_e}\;e^{-\sigma\,t/2} && (5.120) \end{aligned}$$

Since the link dynamics are bounded, $\max_{i\in\{1,\dots,m\}} c_i$ is finite and the set $\mathcal{E}_e$ is exponentially stable w.r.t. to the link dynamics. □

Remark 5.4.1. For the local exponential stability result in Corollary 5.4.1 the condition *(iii)* in the definition of a potential function is conservative. It is actually sufficient that the gradient of the potential function V_i satisfies $\omega\,\nabla V_i(\omega) > 0$ for $\omega \neq 0$, that is, V_i is a first and third sector nonlinearity. This guarantees that $\nabla V_i(\omega)$ is strictly monotone increasing in neighborhood of the origin. By the arguments of Lemma 5.4.1 and Corollary 5.4.1 this is again sufficient to establish local exponential stability.

5.4.2 Behavior of the z-Dynamics

We have already mentioned in Subsection 5.2.1 that stability of the set $\mathcal{E}_e$ w.r.t. the link dynamics does not imply that the formation control problem is solved. So far we have only analyzed the behavior of the link dynamics with the initial condition $e_0 = \hat{H}(z_0)$, where $z_0 \in \mathcal{Z}$ was the initial condition of the z-dynamics. We remember the reader that the formation control problem is posed in the state space, where we have the z-dynamics

$$\dot{z} \;=\; -\hat{O}\,\mathrm{diag}\,\{e_i\}\;\boldsymbol{\Psi}(e)\;,\;\; z_0 \in \mathcal{Z}\,. \tag{5.121}$$

The formation control problem requires that the solution $\Phi(t, z_0)$ of the z-dynamics is well defined and converges to a finite point in $\mathcal{E}_z$. Let us first establish a result on existence and uniqueness of the z-dynamics.

Lemma 5.4.2. *If the z-dynamics are obtained by irregular (respectively regular) potential functions, then the solution $\Phi(t, z_0)$ is forward complete $\forall\, z_0 \in \mathcal{Z}$ (respectively $z_0 \in \mathbb{R}^{2n}$).*

Proof. For irregular (respectively regular) potential function and for every initial condition $e_0 = \hat{H}(z_0)$ Theorem 5.3.2 guarantees global existence of the e-dynamics. This and the fact that we can formulate the z-dynamics in terms of the e-dynamics

$$z_i(t) \;=\; z_i(0) + \int_0^t \sum_{j \text{ with } o_{ij}\neq 0} 2\, e_j(\tau)\, \nabla V_j\big(\|e_j(\tau)\|^2 - d_j^2\big)\, d\tau \tag{5.122}$$

guarantee that there is no finite escape time of the z-dynamics. Due to the local Lipschitz property of the right-hand side of the z-dynamics $\forall z \in \mathcal{Z}$ (respectively $\forall z \in \mathbb{R}^{2n}$) uniqueness of the solution $\Phi(t, z_0)$ is also guaranteed and thus the z-dynamics are forward complete $\forall\, z_0 \in \mathcal{Z}$ (respectively $\forall\, z_0 \in \mathbb{R}^{2n}$). □

Note that Lemma 5.4.2 does not guarantee the boundedness of the z-dynamics. Since $e \in \mathcal{E}_e$ implies $\mathbf{\Psi}(e) = 0$, which is also an equilibrium of the z-dynamics, we might be tempted to conclude that convergence of the links to $\mathcal{E}_e$ implies convergence of the positions. This is wrong and is a popular error, which has for example been made in [25]. To see why such a conclusion is misleading, consider the following example.

Example 5.4.1. Consider the following system of coupled ODEs which we will refer to as the e and the z-dynamics:

$$\dot{e} \;=\; -e^2 \quad,\, e(0) = 1 \tag{5.123}$$

$$\dot{z} \;=\; e \quad,\, z(0) = 0 \tag{5.124}$$

Both the z and e-dynamics have the equilibrium $e = 0$. The solution of the e-dynamics is

$$e(t) \;=\; \frac{1}{t+1} \tag{5.125}$$

and indeed converges to the equilibrium $e = 0$. Thus we could conclude that $z(t)$ also converges to some stationary value because the right-hand side of (5.124) converges to zero. But this conclusion is wrong. An integration of the z-dynamics yields

$$z(t) \;=\; \int_0^t \frac{1}{\tau+1}\, d\tau \;=\; \ln|\tau+1|\Big|_0^t \;=\; \ln|t+1|\,. \tag{5.126}$$

We clearly have that $z(t) \underset{t\to\infty}{\to} \infty$, that is, the z-dynamics grow unbounded.

Furthermore, there might be equilibria to the link dynamics which are not equilibria of the z-dynamics. From Theorem 5.3.2 we cannot rule out the possibility that a solution of the link dynamics converges to an equilibrium $\bar{e}$ with the property that for some $i \in \{1, \dots, m\}$

$$\lim_{t\to\infty} 2\,\bar{e}_i(t)\,\nabla V_i\big(\|\bar{e}_i(t)\|^2 - d_i^2\big) \;=\; const. \;\neq\; 0\,. \tag{5.127}$$

By equation (5.122) we then have that the z-dynamics grow linearly and unbounded in time. Indeed it is easy to construct initial conditions where exactly this happens. Let us construct such an initial condition for the directed triangle.

Example 3.1.3. Directed triangle (continued):
From Section 5.2.2 we know that one equilibrium of the link dynamics is given by the set of collinear robots moving with equal velocity vector v determined by $v = e_1\,\psi_1 = e_2\,\psi_2 = e_3\,\psi_3$. Note that v is not necessarily zero. So the robots can converge to a collinear formation which moves with a non-zero velocity $\bar{v}$ and thus we have for la sufficiently large t that $\dot{z}_i = \bar{v}$ or equivalently $z(t) = z_0 + \bar{v}\,t$. In Chapter 7 we will derive the exact region of attraction where this behavior is occurring.

If now in equation (5.122) the terms $2\,e_i(\tau)\,\nabla V_i\big(\|e_i(\tau)\|^2 - d_i^2\big)$ are $\mathcal{L}_1$ signals, then the integral in (5.122) is indeed converging and thus the signal $z_i(t)$ converges to a stationary value. The following theorem uses the exponential stability of the link dynamics to establish that the signal $2\,e_i(\tau)\,\nabla V_i\big(\|e_i(\tau)\|^2 - d_i^2\big)$ is exponentially decreasing and is thus $\mathcal{L}_1$, which again implies that $z(t)$ converges to a stationary value z_*.

Theorem 5.4.2. *Consider a cooperative graph. For every initial condition $z_0 \in \hat{H}^{-1}\left(\Omega(\rho)\right)$ exists an exponentially stable equilibrium point $z_* \in r_{\mathcal{G}}^{-1}(\mathbf{d})$ of the z-dynamics.*

Proof. From our prior conclusions in Corollary 5.4.1 we know that $\forall\, e_0 \in \Omega(\rho)$ exists a constant $\alpha_2 > 0$, such that

$$\left|\nabla V_i\big(\big\|e_i(t)^2 - d_i^2\big\|\big)\right| \;=\; \frac{1}{2}\,\|\mathbf{\Psi}(e(t))\|_\infty^2 \;\leq\; \frac{1}{2}\,\|\mathbf{\Psi}(e(t))\|^2 \tag{5.128}$$

$$\leq \frac{1}{2}\,\alpha_2^2\,m\,\left\|\bar{\mathbf{\Psi}}(e(t))\right\|^2 \leq \frac{1}{2}\,\frac{\alpha_2^3}{\alpha_1}\,m^2\,\left\|\bar{\mathbf{\Psi}}(e_0)\right\|^2\,e^{-\sigma\,t} \tag{5.129}$$

holds $\forall\, i \in \{1,\ldots,m\}$. Thus the gradients of the potential functions are exponentially decreasing. By considering equation (5.117), we can also upper bound the signal $\|e_i(t)\|$ as

$$\|e_i(t)\| \leq c_i\,\left|\|e_i(0)\| - d_i\right|\,e^{-\sigma\,t/2} + d_i\,. \tag{5.130}$$

Consider now for every $i \in \{1,\ldots,m\}$ the vector signal $f_i : \mathbb{R} \to \mathbb{R}^2$ defined as

$$f_i(t) = 2\,e_i(t)\,\nabla V_i\big(\|e_i(t)\|^2 - d_i^2\big)\,. \tag{5.131}$$

Note that its euclidean vector norm, that is the signal $\|f_i(t)\|$, is exponentially decreasing:

$$\|f_i(t)\| = 2\,\left\|e_i(t)\,\nabla V_i\big(\|e_i(t)\|^2 - d_i^2\big)\right\| \tag{5.132}$$

$$\leq 2\,\left(c_i\,\left|\|e_i(0)\| - d_i\right|\,e^{-\sigma\,t/2} + d_i\right)\left(\frac{1}{2}\,\frac{\alpha_2^3}{\alpha_1}\,m^2\,\left\|\bar{\mathbf{\Psi}}(e_0)\right\|^2\,e^{-\sigma\,t}\right) \tag{5.133}$$

Every component of the vector signal $f_i(t)$ is exponentially decreasing and thus $\mathcal{L}_1$. Similar as in equation (5.122) the dynamics of robot i can be written as

$$z_i(t) = z_0 + \int_0^t \sum_{j \text{ with } o_{ij}\neq 0} f_j(\tau)\,d\tau\,. \tag{5.134}$$

Since each $f_j(\tau) \in \mathcal{L}_1$, the integral exists and takes a constant finite value even for $t \to \infty$. Moreover, $z_i(t)$ is bounded and converges exponentially to a constant stationary value z_*, which depends on z_0. By Corollary 5.4.1 the set $\mathcal{E}_e$ is locally exponentially stable, which means that the point to set distance $\|z(t)\|_{\mathcal{E}_z}$ in the z-space is exponentially decreasing. Thus the stationary value z_* is an exponentially stable equilibrium point in $\mathcal{E}_z = r_{\mathcal{G}}^{-1}(\mathbf{d})$. □

We are now ready state our first main result, namely that under the distributed gradient control law from Section 3.2.1 the robots locally converge to a formation.

Theorem 5.4.3. *Main Result I:*
If the sensor graph $\mathcal{G}$ is cooperative, then the gradient control law (3.20) solves the formation control problem for every initial condition $z_0 \in \hat{H}^{-1}\left(\Omega(\rho)\right)$.

Let us illustrate this result at the directed triangle.

Example 3.1.3. Directed triangle (continued):
We remind the reader that, under the gradient control, each robot's strategy is to pursue its leader robot until their distance constraint is satisfied. Now the previous results says the following: The condition $z_0 \in \hat{H}^{-1}(\Omega(\rho))$ means that the robots are initially at positions z_0, such that the initial links $e_0 = \hat{H}\, z_0$ are sufficiently close to the set $\mathcal{E}_e$, that is the link lengths $\|e_i\|$ are sufficiently close the specified link lengths d_i. The question "what is sufficiently close" will be answered in Chapter 7 by geometric arguments. By Theorem 5.4.1, it is clearly necessary that the initial formation $(\mathcal{G}, e_0)$ is infinitesimally rigid, that is, the robots are not allowed to be initially collinear or collocated. For such an initial condition we can guarantee exponential stability of the target formation $\left(\mathcal{G}, r_{\mathcal{G}}^{-1}(\mathbf{d})\right)$, that is, the robots' strategy results in the desired triangular formation.

Figure 5.14 shows a simulation of the directed triangle starting from an initially rigid formation. In this simulation the target formation is specified by an equal sided triangle with side lengths 1, that is, $d_1 = d_2 = d_3 = 1$, and the potential functions are chosen as the squared functions $V_i(\omega) = \frac{\omega^2}{4}$. Thus the dynamics of robot i are simply $\dot{z}_i = e_i \left(\|e_i\|^2 - d_i^2\right)$. Figure 5.14(a) shows the trajectories $z_i(t)$ in the (x, y)-plane with initial conditions $z_i(0) = z_{i0}$, and Figure 5.14(b) the exponentially decreasing function $V(e(t))$. Figure 5.14(c) and Figure 5.14(d) show the x and y-components of each robot, which are exponentially decreasing to a stationary value.

Theorem 5.4.3 solves the formation control problem locally for cooperative sensor graphs. However, this result is only local and do not know the exact region of attraction. Simulation studies show us that the target formation is achieved whenever the initial formation is minimally rigid. For the directed triangle, for example, robots that are initially neither collinear nor collocated always form a triangle with the specified lengths, at least in every simulation. To prove this we use geometric arguments about the invariant sets of the closed-loop dynamics and their stability properties. The following chapter introduces the reader to

the necessary background on differential geometry, which will then help us to confirm our intuition of the directed triangle.

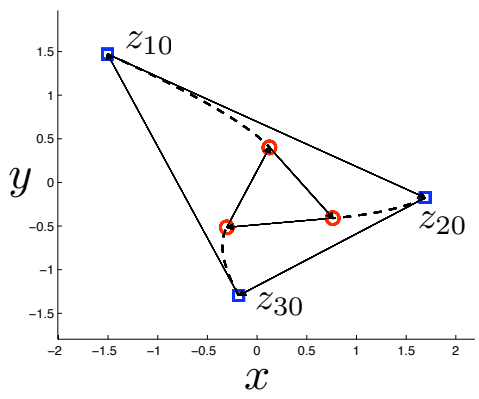

(a) Trajectories in the plane $\mathbb{R}^2$

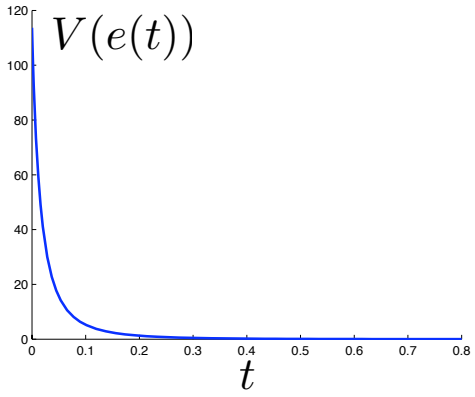

(b) Exponentially decreasing $V(e(t))$

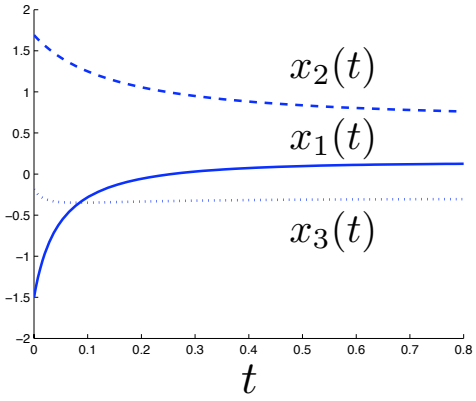

(c) Exponential convergence of $x(t)$

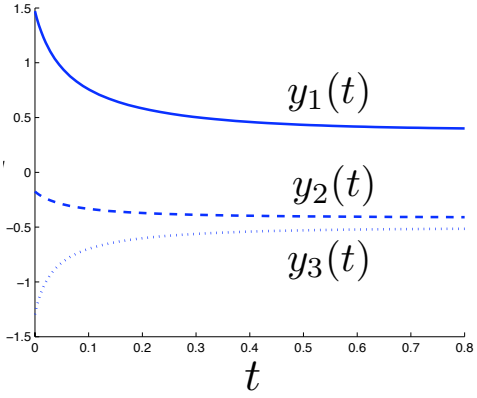

(d) Exponential convergence of $y(t)$

Figure 5.14: Simulation of the directed triangle

Chapter 6

Preliminaries and Definitions III

The results of the last chapter showed that a global stability analysis of the closed-loop link dynamics requires us to deal with the invariant sets of these dynamics. These sets turn out to be submanifolds embedded in the link space. In order to rule out a convergence to these submanifolds we have to argument geometrically both about the submanifolds and the dynamics. This chapter introduces the reader to the necessary background on differential geometry and on the geometric viewpoint of a dynamical system.

6.1 Background on Differential Geometry

Differential geometry is a mathematical discipline that deals with geometric structures called differentiable manifolds and mappings on, of and between these differentiable manifolds. For a rigorous treatment of differentiable manifolds consider any the textbooks [75, 76, 77]. This section gives an intuitive approach to differentiable manifolds and embedded submanifolds.

6.1.1 Differentiable Manifolds

We assume the reader is familiar with the notion of a *vector space*, such as the *Euclidean space* of dimension m. A vector in this space can be represented by an ordered m-tuple of real numbers and we usually refer to it as $\mathbb{R}^m$. The vectors in $\mathbb{R}^m$ are isomorphic to geometric vectors, which are geometric objects quantified with a magnitude and a direction and are

usually depicted as arrows. A multiplication of a vector by real numbers or an addition of vectors leads again to a vector contained in the same vector space. Thus a vector space is closed under linear combinations of its elements. If every vector of $\mathbb{R}^m$ can be obtained by linear combinations of m distinct vectors, we refer to these vectors as being linearly independent and constituting *basis* of the $\mathbb{R}^m$.

Vector spaces are also referred to as *linear spaces* and a differentiable manifold can now be thought of as a nonlinear generalization of a vector space, that is, as a geometric structure that is locally topologically equivalent to $\mathbb{R}^m$. A m-dimensional *differentiable manifold* $\mathcal{M}$ is defined as a topological space with the three following characteristics:

(i) There exists a collection of open sets $U_i \subset \mathcal{M}$ with a countable index i such that $\mathcal{M} = \bigcup_i U_i$.

(ii) There exists a diffeomorphism $\varphi_i : U_i \to \Omega$ where Ω is some open set in $\mathbb{R}^m$.

(iii) For open sets U_i and U_j the map $\varphi_j \circ \varphi_i^{-1} : \varphi_i(U_i \cap U_j) \to \varphi_j(U_i \cap U_j)$ is a diffeomorphism.

The standard terminology is to call a pair $(U_i\,,\,\varphi_i)$ a *chart* and the union of all charts $\bigcup_i (U_i\,,\,\varphi_i)$ an *atlas*. The components of φ_i are referred to as *local coordinates*. These ideas and the characteristics *(i)-(iii)* are illustrated in Figure 6.1.

An example for a two dimensional differentiable manifold $\mathcal{M}$ is the globe. Since we cannot carry a globe around with us all the time, we rather have an atlas, which is a collection of charts $(U_i\,,\,\varphi_i)$. A chart is again a smooth mapping φ_i of an open subset U_i of the globe $\mathcal{M}$ to the two dimensional page $\varphi_i(U_i) \subset \mathbb{R}^2$. Of course all these open sets U_i cover the entire globe and, if we scroll through the pages of the atlas from one chart to another, we can find overlapping sets $U_i \cap U_j$ both in the chart $(U_i\,,\,\varphi_i)$ as $\varphi_i(U_i \cap U_j)$ and in $(U_j\,,\,\varphi_j)$ as $\varphi_j(U_i \cap U_j)$. Since $\varphi_i(U_i \cap U_j)$ and $\varphi_j(U_i \cap U_j)$ can be smoothly attached to each other via the map $\varphi_j \circ \varphi_i^{-1}$ or its inverse, the pages of the atlas are compatible with each other.

Example 6.1.1. 1-sphere S^1: A simple example for a one dimensional differentiable manifold is the unit circle, which is in differential geometry referred to as the 1-sphere

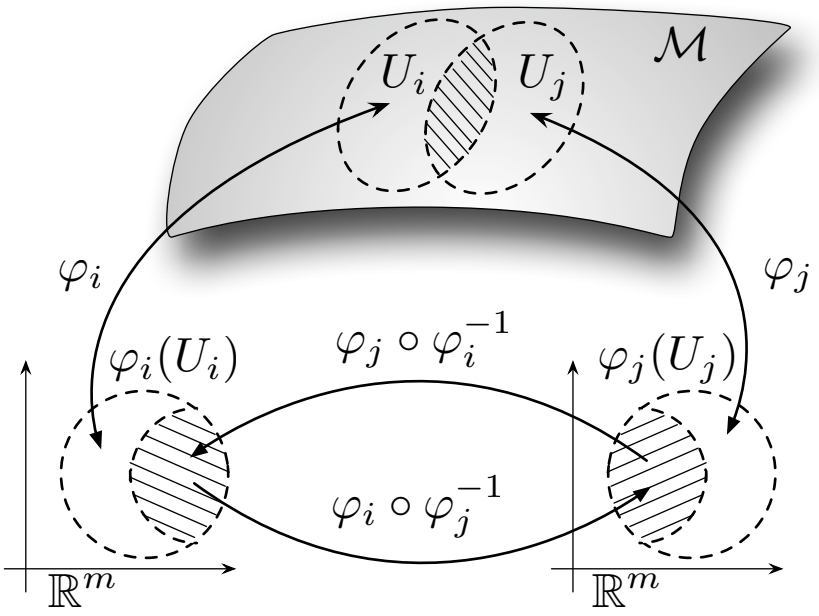

Figure 6.1: Illustration of a m-dimensional manifold $\mathcal{M}$ and two charts

$S^1 := \{x \in \mathbb{R}^2 \,|\, \|x\| = 1\}$ and is shown in Figure 6.2(a). The unit circle can be covered by the two open sets U_1 and U_2 which are shown in Figure 6.2(b) and parametrized by

$$U_1 = \left\{ t \in (0, 2\,\pi) \,\middle|\, [x_1\,,\, x_2]^T = \varphi_1^{-1}(t) = [\cos t\,,\, \sin t]^T \right\} \tag{6.1}$$

$$U_2 = \left\{ \tau \in (-\pi, \pi) \,\middle|\, [x_1\,,\, x_2]^T = \varphi_2^{-1}(\tau) = [\cos \tau\,,\, \sin \tau]^T \right\}, \tag{6.2}$$

where the mappings $\varphi_1 : [\cos t\,,\, \sin t] \mapsto t$ and $\varphi_2 : [\cos \tau\,,\, \sin \tau] \mapsto \tau$ are diffeomorphisms mapping U_1 and U_2 to $\mathbb{R}$. The mapping $t \mapsto \tau$ is also a diffeomorphism, since $\tau = t$ $(0 < t < \pi)$ and $\tau = t - 2\pi$ $(\pi < t < 2\pi)$. Therefore, S^1 is a differentiable manifold and the charts (U_1, φ_1) and (U_2, φ_2) form an atlas.

6.1.2 Tangent and Normal Space

The reader might have already realized that the globe $\mathcal{M}$ is locally always equivalent to a chart $(U_i\,,\, \varphi_i)$. Moreover, at every single point of the globe we can attach a two dimensional page $\varphi_i(U_i)$ of the atlas. At this exact point the page $\varphi_i(U_i)$ will be tangent to the globe.

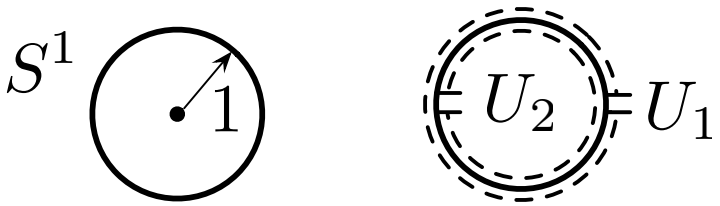

(a) The 1-sphere S^1 (b) Neighbourhoods U_1 and U_2

Figure 6.2: The unit circle S^1 as differentiable manifold

In general we can find for every point p of a m-dimensional differentiable manifold $\mathcal{M}$ a m-dimensional translated vector space which is tangent to the manifold at $p \in \mathcal{M}$. We refer to this vector space as the *tangent space* in a point $p \in \mathcal{M}$ and denote it by $T_p\mathcal{M}$. If the manifold $\mathcal{M}$ is embedded in a higher dimensional space, say $\mathbb{R}^n$, then we associate a second translated vector space with a point $p \in \mathcal{M}$, namely the orthogonal complement of $T_p\mathcal{M}$. This $n-m$ dimensional vector space is called the *normal space* in the point $p \in \mathcal{M}$ and we denote it by $N_p\mathcal{M}$. Together $T_p\mathcal{M}$ and $N_p\mathcal{M}$ span the $\mathbb{R}^n$. A graphical illustration of these two vector spaces is shown in Figure 6.3.

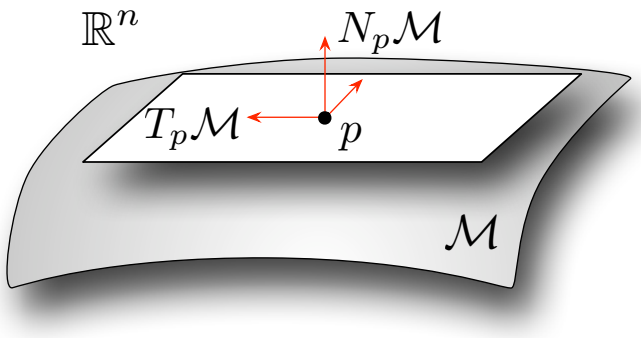

Figure 6.3: Tangent and the normal space of a point $p \in \mathcal{M}$

The tangent and normal space at a point $p \in \mathcal{M}$ can be defined via the local coordinates φ_i. Consider a chart $(U_i\,,\,\varphi_i)$ and a point $p \in U_i \subset \mathcal{M}$, then we have

$$T_p\mathcal{M} \;=\; \mathrm{Im}\left(\left.\frac{\partial \varphi_i^{-1}(x)}{\partial x}\right|_{x=\varphi_i(p)}\right) \quad \text{and} \quad N_p\mathcal{M} \;=\; \{v \in \mathbb{R}^n \,|\, v \perp T_p\mathcal{M}\}\;. \tag{6.3}$$

However, the tangent space can also be defined in an abstract way without local coordinates and is thus independent of the specific chart; likewise the normal space. Sometimes it is helpful to think of the union all tangent and normal spaces at all points of the manifold. That's why we now introduce the notation of a bundle and refer to the sets

$$T\mathcal{M} = \{(p, v) \in \mathcal{M} \times \mathbb{R}^n | \; v \in T_p\mathcal{M}\} \tag{6.4}$$

$$N\mathcal{M} = \{(p, v) \in \mathcal{M} \times \mathbb{R}^n | \; v \in N_p\mathcal{M}\} \tag{6.5}$$

as the *tangent* and the *normal bundle* of the m dimensional manifold $\mathcal{M}$. Both the tangent and the normal bundle are differentiable manifolds of dimension $2m$ respectively $2(n-m)$.

Example 6.1.1. 1-sphere S^1 (continued):
The tangent space of S^1 is obtained at the point $p = [0\,,\,1]^T = \left[\cos\frac{\pi}{2}, \sin\frac{\pi}{2}\right]^T \in U_1 \subset S^1$ as

$$T_pS^1 = \mathrm{Im}\left(\left.\frac{\partial\varphi_1^{-1}(t)}{\partial t}\right|_{t=\varphi_1(p)}\right) = \mathrm{Im}\left(\left.\frac{\partial}{\partial t}\begin{bmatrix}\cos t & \sin t\end{bmatrix}^T\right|_{t=\varphi_1(p)}\right) \tag{6.6}$$

$$= \mathrm{Im}\left(\left.\begin{bmatrix}-\sin t\\ \cos t\end{bmatrix}\right|_{t=\frac{\pi}{2}}\right) = \mathrm{span}\left\{\begin{bmatrix}1\\0\end{bmatrix}\right\}. \tag{6.7}$$

If we embed the circle in the $\mathbb{R}^2$ as shown in Figure 6.4(a), then the normal space is obtained as orthogonal complement of the tangent space. It is for $p = [0\,,\,1]^T \in U_1$ given as

$$N_pS^1 = \left\{v \in \mathbb{R}^2 \,\middle|\, v \perp T_pS^1\right\} = \mathrm{Im}\left(\left.\begin{bmatrix}\cos t\\ \sin t\end{bmatrix}\right|_{t=\varphi_1(p)}\right) = \mathrm{span}\left\{\begin{bmatrix}0\\1\end{bmatrix}\right\}. \tag{6.8}$$

Together T_pS^1 and N_pS^1 clearly span the $\mathbb{R}^2$, which is illustrated in Figure 6.4(b). The tangent bundle (respectively normal bundle) can then be obtained if we construct T_pS^1 (respectively N_pS^1) for every point $p \in U_1 \cup U_2$.

6.1.3 Embedded Submanifolds

Let us go back to vector spaces. Consider the n-dimensional vector space W. A nonempty subset V of W that is closed under linear combinations of its elements is called a *subspace* of

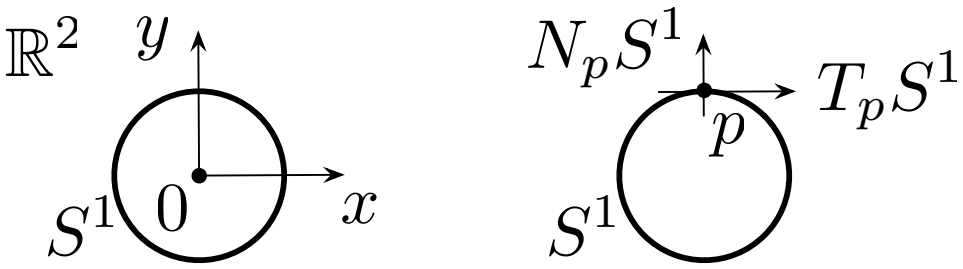

(a) S^1 embedded in $\mathbb{R}^2$ (b) T_pS^1 and N_pS^1

Figure 6.4: The differentiable manifold S^1 embedded in $\mathbb{R}^2$ and its tangent and normal space at $p = [0\,,\,1]^T$

W. The subspace V is a vector space itself. If V has m independent basis vectors, then we say V is a m-dimensional subspace. Now let $A \in \mathbb{R}^{m\times n}$ be a matrix and consider the linear map $A : W \to V$. There are two important subspaces associated with A. One is $\mathrm{Im}\,(A)$, which is a subspace of V, and the other one is $\ker(A)$, which is a subspace of W. The later subspace, $\ker(A)$, can also be written as a pre-image set of the map A, that is,

$$\ker(A) \;=\; \{x \in W \,|\, A\,x = \mathbf{0}\} \;=\; A^{-1}(\mathbf{0})\,. \tag{6.9}$$

Let us now generalize this idea to differentiable manifolds. Similar to spaces and subspaces, an embedded submanifold can be thought of as a differentiable manifold defined on another differentiable manifold and is locally topologically equivalent to a subspace.

For the following definition of an embedded submanifold the author strongly recommends the reader to look at the graphical illustration in Figure 6.5. Let $\mathcal{N}$ be a differentiable manifold with $\dim\mathcal{N} = n$ and let $\mathcal{M} \subset \mathcal{N}$ be a differentiable manifold with $\dim\mathcal{M} = m$. We say that $\mathcal{M}$ is an *embedded submanifold* of $\mathcal{N}$ with dimension $n - m$ if for every $p \in \mathcal{M}$ exists a chart (U, φ) of $\mathcal{N}$ with $p \in U$, such that $\varphi(\mathcal{M}\cap U)$ is a domain of some m-dimensional subspace in $\mathbb{R}^n$, or equivalently, $\mathcal{M} \cap U$ can be expressed in local coordinates as

$$\mathcal{M}\cap U \;=\; \{q \in U \,|\, \varphi_1(q) = \varphi_2(q) = \cdots = \varphi_{n-m}(q) = 0\}\,, \tag{6.10}$$

where φ_i are the components of φ. Thus locally in $\mathcal{M} \cap U$ an embedded submanifold $\mathcal{M}$ is parametrized as the zero level set of a function, just like a subspace in equation (6.9). The

question then arises under which conditions the level set of a function then globally defines an embedded submanifold.

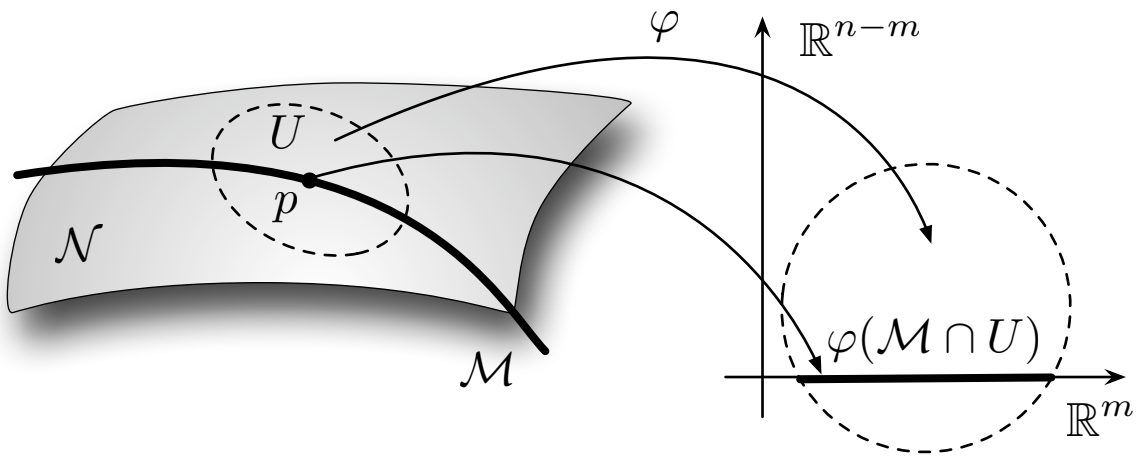

Figure 6.5: Illustration of an embedded submanifold

In order to continue, we have to give some preliminaries on functions on manifolds. Let $\mathcal{N}$ and $\mathcal{M}$ be two differentiable manifolds with the coordinate charts (U_i, φ_i) on $\mathcal{N}$ and (O_i, ψ_i) on $\mathcal{M}$. The mapping $F : \mathcal{N} \to \mathcal{M}$ is said to be differentiable if it is differentiable in local coordinates, that is, for every $p \in U_i$ and $F(p) \in O_i$ the mapping $\psi_j \circ F \circ \varphi_i^{-1}(p)$ is differentiable. The rank of the mapping F at a point $p \in \mathcal{N}$ is defined in local coordinates as

$$\operatorname{rank}(F(p)) \;:=\; \operatorname{rank}\left(\frac{\partial}{\partial p}\left(\psi_j \circ F \circ \varphi_i^{-1}(p)\right)\right). \tag{6.11}$$

If $\mathcal{N}$ and $\mathcal{M}$ are the vector spaces $\mathbb{R}^n$ and $\mathbb{R}^m$, then the charts are simply $(\mathbb{R}^n, I_n)$ and $(\mathbb{R}^m, I_m)$, the map F is differentiable if $\frac{\partial F(p)}{\partial p}$ is continuous, and $\operatorname{rank}(F(p)) = \operatorname{rank}\left(\frac{\partial F(p)}{\partial p}\right)$.

We are now ready to state the pre-image theorem, which allows to parameterize an embedded submanifold as the zero set of a function, just as we do it in (6.9) for a subspace.

Theorem 6.1.1. *Pre-image Theorem ([76], Theorem 5.8): Let $\mathcal{N}$ and $\mathcal{M}$ be two differentiable manifolds, with $\dim\mathcal{N} = n$ and $\dim\mathcal{M} = m$, and let $F : \mathcal{N} \to \mathcal{M}$ be a differentiable mapping. Consider the pre-image set $F^{-1}(q) = \{x \in \mathcal{N} \mid F(x) = q\}$. If $\forall\, p \in \mathcal{N}$*

$\operatorname{rank}(F(p)) = k$, *then for all* $q \in F(\mathcal{N})$ *the pre-image set* $F^{-1}(q)$ *is a closed, embedded submanifold of* $\mathcal{N}$ *with dimension* $n - k$.

In the case that $\mathcal{N} = \mathbb{R}^n$ and $\mathcal{M} = \mathbb{R}^m$, the simply have to check $\operatorname{rank}\left(\frac{\partial F(p)}{\partial p}\right) = k = const.\ \forall\, p \in \mathbb{R}^n$ and obtain that $F^{-1}(q)$ is $n-k$ dimensional, closed, embedded submanifold of $\mathbb{R}^n$. Thus a subspace parametrized by $A\,p = \mathbf{0}$ is a submanifold of dimension $n - \operatorname{rank}(A)$. For nonlinear functions F this condition is very conservative and be relaxed by the following corollary, which can be applied to mappings achieving their maximal rank.

Corollary 6.1.1. *([76], Corollary 5.9) Let* $\mathcal{N}$ *and* $\mathcal{M}$ *be two differentiable manifolds, with* $\dim \mathcal{N} = n$ *and* $\dim \mathcal{M} = m$, *and let* $F : \mathcal{N} \to \mathcal{M}$ *be a differentiable mapping. Assume* $m \leq n$ *and consider the pre-image set* $F^{-1}(q)$. *If for some point* $q \in F(\mathcal{N})$, $\operatorname{rank}(F(p)) = \operatorname{maxrank}(F(p)) = m$ *for all points* $p \in F^{-1}(q)$, *then* $F^{-1}(q)$ *is a closed, embedded submanifold of* $\mathcal{N}$ *with dimension* $n - m$.

Theorem 6.1.1 and Corollary 6.1.1 can be seen as nonlinear extensions of subspaces parametrized by zero sets. If we think of the subspace $A^{-1}(W)$ defined in (6.9) as a hyperplane passing through the origin, we can easily identify its normal vectors as elements of $\operatorname{Im}\left(A^T\right)$ and its tangent vectors as elements of $\ker(A)$. Similar to subspaces the tangent and the normal space of an embedded submanifold can be obtained by the kernel and the image of the function parametrizing it.

Theorem 6.1.2. *([78], p.24 and p.77) Consider the two differentiable manifolds* $\mathcal{N}$ *and* $\mathcal{M}$ *and the differentiable mapping* $F : \mathcal{N} \to \mathcal{M}$, *such that the pre-image set* $F^{-1}(q)$ *is an embedded submanifold of* $\mathcal{N}$. *Its tangent space at a point* $p \in F^{-1}(q)$ *is then given by*

$$T_p F^{-1}(q) \;=\; \ker\left(\left.\frac{\partial F(x)}{\partial x}\right|_p\right), \tag{6.12}$$

and the normal space of $F^{-1}(q)$ *at a point* $p \in F^{-1}(q)$ *is given by*

$$N_p F^{-1}(q) \;=\; \operatorname{Im}\left(\left.\frac{\partial F(x)}{\partial x}\right|_p^T\right). \tag{6.13}$$

Example 6.1.1. 1-sphere S^1 (continued):

Consider the differentiable function $F : \mathbb{R}^2 \to \mathbb{R}$, $F(x) = \|x\|^2$. The 1-sphere $S^1 = \{x \in \mathbb{R}^2 \,|\, \|x\| = 1\}$ can be formulated as the pre-image set $F^{-1}(1)$. If we check the rank of F, we get

$$\operatorname{rank}(F(x)) \;=\; \operatorname{rank}\left(\frac{\partial F(x)}{\partial x}\right) \;=\; \operatorname{rank}\left(\begin{bmatrix} 2\,x & 2\,y \end{bmatrix}\right). \tag{6.14}$$

We have that $\operatorname{rank}(F(x))$ is 1 except at the origin, where $\operatorname{rank}(F(0)) = 0$. Thus the rank is not constant $\forall\, x \in \mathbb{R}^2$. However, we have that $1 \in F(\mathbb{R}^2)$ and $\operatorname{rank}(F(x)) = \operatorname{maxrank}(F(x)) = 1$ for all $x \in F^{-1}(1)$. Therefore by Corollary 6.1.1, $S^1 = F^{-1}(1)$ is an embedded submanifold in $\mathbb{R}^2$ of dimension 2. From Theorem 6.1.2 we obtain the 1-spere's tangent and normal space at the point $p = [0\,,\,1]^T \in S^1$ by

$$T_pS^1 \;=\; T_pF^{-1}(1) \;=\; \ker\left(\frac{\partial F(x)}{\partial x}\Big|_p\right) \;=\; \ker\left(\begin{bmatrix} 0 \\ 2 \end{bmatrix}^T\right) \;=\; \operatorname{span}\left\{\begin{bmatrix} 1 \\ 0 \end{bmatrix}\right\} \tag{6.15}$$

$$N_pS^1 \;=\; N_pF^{-1}(1) \;=\; \operatorname{Im}\left(\frac{\partial F(x)}{\partial x}\Big|_p^T\right) \;=\; \operatorname{Im}\left(\begin{bmatrix} 0 \\ 2 \end{bmatrix}\right) \;=\; \operatorname{span}\left\{\begin{bmatrix} 0 \\ 1 \end{bmatrix}\right\}. \tag{6.16}$$

Now that the reader is familiar with the notion of a manifold, we move on to dynamical systems as seen from the viewpoint of differential geometry.

6.2 Geometric Viewpoint of Dynamical Systems

Similar to optimal control the stability of dynamical systems can also be approached in two ways. We already presented Lyapunov stability theory for sets, where we looked for a function V depending on the state of the system and whose derivative along the systems trajectories is decreasing. In the next chapter we approach the stability of differentiable manifolds in a geometric way. That's why we now give some preliminaries on the geometric viewpoint of dynamical systems, which can be found in the standard textbooks [53, 79, 80].

6.2.1 Vector Fields, Flows and Invariant Manifolds

Let us quickly review the differential geometric viewpoint of the nonlinear system which we already looked at in Section 4.1. We consider the dynamical system

$$\dot{x} \;=\; f(x)\,, \tag{6.17}$$

where the maximum interval of existence is $I_0 = (T_{x0}^-, T_{x0}^+)$ and the initial condition is $x(0) = x_0 \in \mathcal{M} \subset \mathbb{R}^m$. In Section 4.1 we specified the state space $\mathcal{M}$ as the domain where the right-hand side of (6.17) is defined. Let us now assume that $\mathcal{M}$ is an invariant, m-dimensional, differentiable manifold, which is in differential geometry referred to as the *phase space* of (6.17). The right-hand side of (6.17) is called the *vector field* f and is a mapping from a point $p \in \mathcal{M}$ to a vector $f(p) \in \mathbb{R}^m$, or more precisely

$$f \;:\; \mathcal{M} \;\to\; T\mathcal{M} \tag{6.18}$$

$$p \in \mathcal{M} \;\mapsto\; f(p) \in T_p\mathcal{M}\,. \tag{6.19}$$

The map f is illustrated in Figure 6.6.

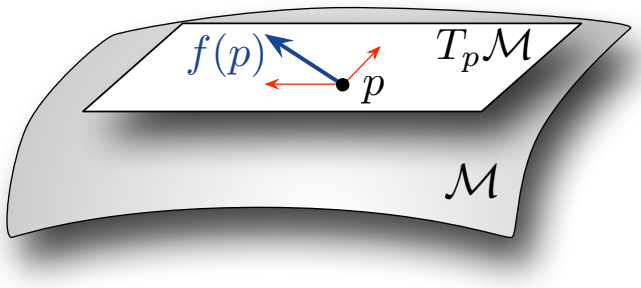

Figure 6.6: The vector field f as mapping $p \in \mathcal{M} \;\mapsto\; f(p) \in T_p\mathcal{M}$

In Section 4.1 we denoted solution of the system (6.17) at time t and for the initial condition $x_0 \in \mathcal{M}$ as the flow $\Phi(t, x_0)$. The flow can also geometrically be defined as a differentiable mapping

$$\Phi \;:\; I_0 \times \mathcal{M} \to \mathcal{M}\,, \tag{6.20}$$

such that the relation $\frac{d}{dt}\ \Phi(\tau, x_0)|_{t=\tau} = f(\Phi(\tau, x_0))$ holds for all $\tau \in I_0$. If we look at f as a direction field defined on the phase space $\mathcal{M}$, then the flow $\Phi(t, x_0)$ corresponds to a smooth curve which starts at $x_0 \in \mathcal{M}$ and evolves on the phase space $\mathcal{M}$, such that $f(p)$ is tangent to the flow $\Phi(t, x_0)$ passing through the point p. This curve in the phase space is usually referred to as the *integral curve* or the *graph* of the dynamical system and the vector field is also called the *phase velocity field* $f(p) = \left.\frac{\partial \Phi(t,p)}{\partial t}\right|_{t=0}$ generating the flow at every point $p \in \mathcal{M}$. This geometrical interpretation of a dynamical system is illustrated in Figure 6.7.

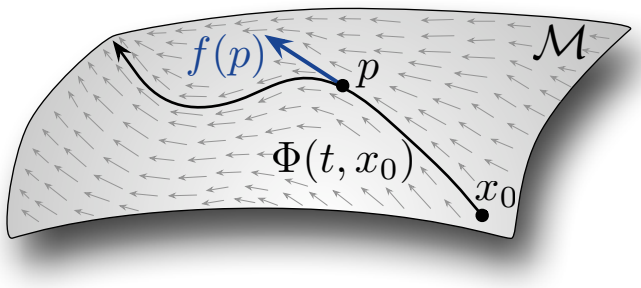

Figure 6.7: Geometrical interpretation of a dynamical system

In Section 4.1 we said that a closed set $\mathcal{N}$ is invariant w.r.t. to the system (6.17) if the flow is "trapped" in $\mathcal{N}$, that is,

$$(\forall\, x_0 \in \mathcal{N})\ \ I_0 = \mathbb{R} \quad \text{and} \quad (\forall\, t \in \mathbb{R})\ \ \Phi(t, x_0) \in \mathcal{N}\,. \tag{6.21}$$

Unfortunately this definition of invariance provides no easy algebraic condition to check whether or not a set $\mathcal{N}$ is invariant. However, if we can identify $\mathcal{N}$ as a differentiable manifold, then $\mathcal{N}$ is invariant if and only if

$$(\forall\, p \in \mathcal{N}) \quad f(p) \in T_p\mathcal{N}\,. \tag{6.22}$$

This becomes immediately clear, if we think of the vector field $f(p)$ as the phase velocity field $\left.\frac{\partial \Phi(t,p)}{\partial t}\right|_{t=0}$. If the flow $\Phi(t, x_0)$ is always in $\mathcal{N}$, then we have that $\forall\, p \in \mathcal{N}$ the phase velocity vector $f(p)$ is in $T_p\mathcal{N}$, and also vice versa. If we have a basis for the normal space $N_p\mathcal{N}$, then equation (6.22) can trivially be rewritten as

$$(\forall\, p \in \mathcal{N}) \quad \mathbf{n}(p)^T\, f(p) \ \ = \ \ 0\,, \tag{6.23}$$

where $\mathbf{n}(p)$ is a matrix whose columns form a basis for $N_p\mathcal{N}$. Equation (6.23) implies that $f(p)$ is orthogonal to the columns of $\mathbf{n}(p)$, which is graphically illustrated in Figure 6.8. We will comeback to this observation in Chapter 7. Note that if the manifold is given as a level set of a function F, then equation (6.23) reduces by Theorem 6.1.2 to the condition $\frac{\partial F(p)}{\partial p} f(p) = 0$ $\forall\, p \in \mathcal{N}$, which is how we would check invariance by the argument $\frac{d}{dt} F(p)\big|_{p\in\mathcal{N}} = 0$.

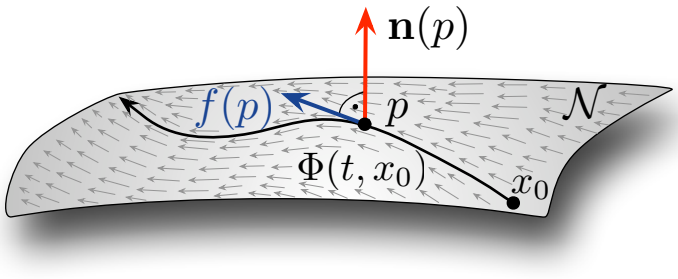

Figure 6.8: For an invariant manifold $\mathcal{N}$ the vector field $f(p)$ is orthogonal to $\mathbf{n}(p) \in N_p\mathcal{N}$

6.2.2 The Geometric Interpretation of Lyapunov's Methods

We conclude this chapter on differential geometry by giving the reader an intuitive understanding about the Lyapunov stability analysis as seen from a differential geometric viewpoint. We consider the system (6.17) and assume that the origin $x = \mathbf{0}$ is an equilibrium point. For the sake of illustration, let state space $\mathcal{M}$ be simply $\mathbb{R}^2$.

In Section 4.1 we presented Lyapunov's *direct method* or also called *second method*, where we looked for a continuously differentiable and positive definite function $V(x)$ whose derivative along trajectories of (6.17) is negative definite:

$$\dot{V}(x) \;=\; \frac{\partial V(x)}{\partial x} f(x) \;=\; \begin{cases} = \; 0 & \text{if } x = 0 \\ < \; 0 & \text{else .} \end{cases} \tag{6.24}$$

If (6.24) holds, then the well known result is the asymptotic stability of the origin. The reader is presumably familiar with the derivation of this result using either ϵ, δ neighbourhoods or comparison functions. Let us now give an heuristic geometric derivation of this condition as it is done in Chapter 2 of [80]. The following arguments are illustrated in Figure 6.9.

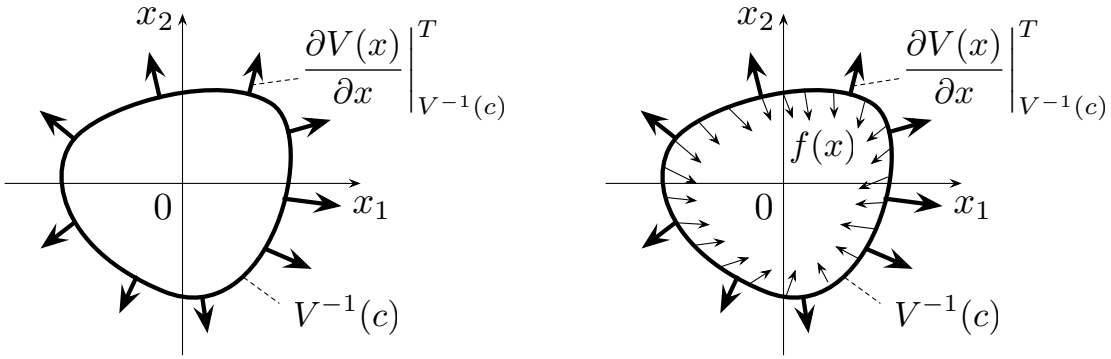

(a) The level set $V^{-1}(c)$ and its normal vector (b) Trajectories pointing inside sublevel set

Figure 6.9: Geometric interpretation of Lyapunov's direct method

Consider a continuously differentiable and positive definite function $V(x)$, which is naturally related to the distance of the point x to the origin. Note that each level set $V^{-1}(c)$ with $c > 0$ defines a closed curve in the plane, or more precisely an 1-dimensional, closed submanifold embedded in $\mathbb{R}^2$. The normal vector of $V^{-1}(c)$ is simply given by $\frac{\partial V(x)}{\partial x}\Big|_{V^{-1}(c)}^{T}$ and is pointing away from the origin in direction of the steepest slope of $V(x)$ as shown in Figure 6.9(a). We want to remind the reader that the vector field $f(x)$ is at every point $x \in \mathbb{R}^2$ tangent to the flow $\Phi(0, x)$. If we want to conclude invariance of the sublevel set bounded by $V^{-1}(c)$, we have to show that the vector field at the boundary $V^{-1}(c)$ is pointing to the inside of this sublevel set. This can simply be checked by saying that the angle between the normal vector $\frac{\partial V(x)}{\partial x}\Big|_{V^{-1}(c)}^{T}$ and the vector field $f(x)$ lies in $(-\frac{\pi}{2}, \frac{\pi}{2})$, or equivalently, that for the inner product holds

$$\left\langle \left[\frac{\partial V(x)}{\partial x}\right]^T, f(x) \right\rangle \Big|_{V^{-1}(c)} = \frac{\partial V(x)}{\partial x} f(x)\Big|_{V^{-1}(c)} < 0\,. \tag{6.25}$$

This condition is illustrated in Figure 6.9(b). If condition (6.25) is satisfied, then the sublevel set bounded by $V^{-1}(c)$ is positively invariant. Since the vector field is pointing strictly inward on the boundary $V^{-1}(c)$, we can assume by continuity of the vector field that the flow $\Phi(t, x)|_{V^{-1}(c)}$ will be at least locally directed towards the origin. Moreover, if we can satisfy condition (6.25) for any nontrivial sublevel set, then we can convince ourselves that the flow $\Phi(t, x)|_{V^{-1}(c)}$ is continuously moving from one sublevel set to another smaller one and will

in the end reach the origin, which implies the asymptotic stability of the origin. But note that checking condition (6.25) for every nontrivial level set is nothing else than Lyapunov's direct method in (6.24), which we essentially just derived by heuristic geometric arguments. This geometric interpretation of Lyapunov's direct method reveals also its clear drawback, namely that we need to find a continuously differentiable and positive definite function $V(x)$ whose sublevel sets are such that the vector field on the boundary is always pointing inside.

With this geometric interpretation of Lyapunov's direct method in mind, we now move on to Lyapunov's *indirect method* or *first method*. This method provides a weaker condition which is obtained from the Lyapunov function $\bar{V}(x) = \frac{1}{2}\, x^T\, P\, x$, where $P \succ 0$. Note that the level sets of $\bar{V}(x)$ are simply ellipsoids or circles for $P = I_2$. Close enough to the origin the vector field $f(x)$ can approximated by its linearization $\frac{\partial f(x)}{\partial x}\Big|_{\mathbf{0}}$. Lyapunov's well known indirect methods states that, if all eigenvalues of $\frac{\partial f(x)}{\partial x}\Big|_{\mathbf{0}}$ are negative, then the system is locally asymptotically stable. This result can be proved if we locally apply Lyapunov's first method with the Lyapunov function $\bar{V}(x)$ on the linearized vector field $\frac{\partial f(x)}{\partial x}\Big|_{\mathbf{0}}$. This results in the equivalent condition, that, if

$$(\exists\, P \succ 0) \quad P\, \frac{\partial f(x)}{\partial x}\bigg|_{\mathbf{0}} + \frac{\partial f(x)}{\partial x}\bigg|_{\mathbf{0}}^{T} P \prec 0 \tag{6.26}$$

holds, then the origin is locally asymptotically stable. The geometric interpretation of Lyapunov's indirect method is as follows. If infinitesimally close to the origin the vector field is pointing to the inside of a set bounded by the ellipsoid $\bar{V}^{-1}(c)$, then we have local asymptotic stability. Unfortunately Lyapunov's indirect method is only local and provides no result if the linear matrix inequality (6.26) is not satisfied.

The reader is now familiar with the geometric interpretation of Lyapunov's first and second method when applied to equilibrium points. In the next chapter, we will extend these geometric ideas to derive a manifold stability theorem, which will be based on the idea stated in (6.25) and will in the end read similar to Lyapunov's indirect method in (6.26).

Chapter 7

Main Result II

The results in Chapter 5 showed that for cooperative graphs the set $\mathcal{E}_e$ is a locally exponentially stable equilibrium set of the link dynamics and thus the robots converge to the target formation. However, this result is only local and restricted to the sublevel set $\Omega(\rho)$. Globally the robots converge to the largest invariant set contained in the set $\mathcal{W}_e$, which we specified in (5.53). Every point $\bar{e} \in \mathcal{W}_e$ is an equilibrium of the link dynamics and we have that either $\bar{e} \in \mathcal{E}_e \subset \mathcal{W}_e$, which is the target formation, or that $\bar{e} \in \mathcal{W}_e \setminus \mathcal{E}_e$. In the second case the matrix $R_{\mathcal{G}}(\bar{e})^T$ has a rank loss, or equivalently $\bar{e} \in \mathcal{Q}$, and thus the formation $(\mathcal{G}, \bar{e})$ is not infinitesimally rigid. Simulation studies show us that for an initially infinitesimally rigid framework $(\mathcal{G}, e_0)$ the solution $\Phi_e(t, e_0)$ converges to $\mathcal{E}_e$ and the robots achieve a formation. For the triangle, for example, we have the intuition that initially not collinear robots will always converge to the specified formation. This chapter provides a tool based on differential geometry, which allows us to confirm our intuition on the triangle.

7.1 Manifold Stability Theorem

Consider an initial condition e_0 of the link dynamics which is not close enough to the equilibrium set $\mathcal{E}_e$ for Theorem 5.4.1 and the following results to apply. The reason therefore is that the corresponding sublevel set $\Omega(V(e_0))$ intersects the set $\mathcal{Q}$, which was defined to be the set where the formation $(\mathcal{G}, e)$ is not infinitesimally rigid. For such an initial condition

we can only guarantee the convergence of $\Phi_e(t, e_0)$ to $\mathcal{W}_e$. The idea to rule out a possible convergence to $\mathcal{W}_e \setminus \mathcal{E}_e \subset \mathcal{Q}$ is graphically illustrated in Figure 7.1 and can be motivated loosely speaking as follows. Suppose we can show that in a neighbourhood of the set $\mathcal{W}_e \cap \mathcal{Q}$

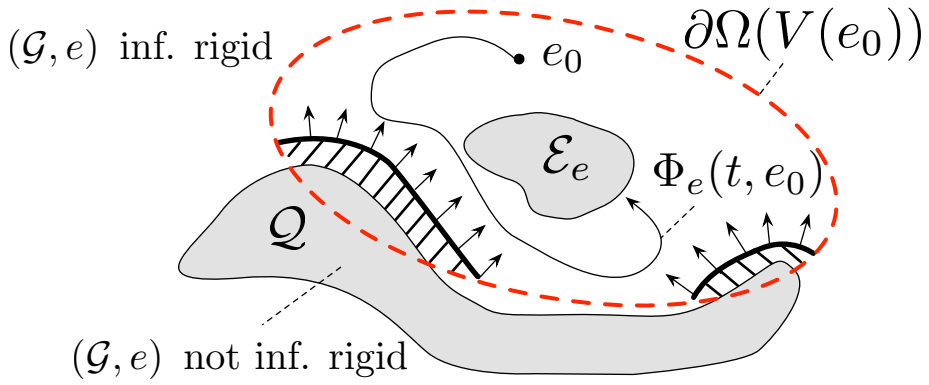

Figure 7.1: An idea to extend the region of attraction

the vector field constituted by the right-hand side of the link dynamics is always pointing away from $\mathcal{W}_e \cap \mathcal{Q}$, then a solution $\Phi_e(t, e_0)$ with $e_0 \notin \mathcal{Q}$ can never converge to $\mathcal{Q}$. Thus the only positively invariant set contained in $\mathcal{W}_e$ to which a solution $\Phi_e(t, e_0)$ can converge to is the set $\mathcal{E}_e$.

7.1.1 In- and Overflowing Invariance

Let us formulate, in terms of differential geometry, the idea that a vector field is pointing away from a set. We consider the dynamical system

$$\dot{x} \;=\; f(x) \tag{7.1}$$

with initial condition $x(0) = x_0 \in \mathcal{M}$, where $\mathcal{M}$ is an invariant m-dimensional manifold. As usual we denote the flow generated by the vector field f as $\Phi(t, x_0)$. In order to define what it means that the vector field f is pointing away from a certain set $\mathcal{N}$, we have to identify an orientation of $\mathcal{N}$, such as a normal vector defined at at every point $p \in \mathcal{N}$. Therefore, we specify the set $\mathcal{N}$ as a closed and invariant n-dimensional submanifold embedded in $\mathcal{M}$.

The specification of $\mathcal{N}$ as an embedded submanifold allows us to identify a normal and a tangential direction relative to $\mathcal{N}$. Moreover, given an $\epsilon > 0$, we can construct a neighbourhood of $\mathcal{N}$ consisting of points $\tilde{p} \in \mathcal{M}$ which are not further than ϵ away from $\mathcal{N}$, that is $\|\tilde{p}\|_{\mathcal{N}} < \epsilon$. Such a neighbourhood can be seen as an embedding of the normal bundle $N\mathcal{N}$ into the relative topology of $\mathcal{M}$ and we define the *tubular* ϵ *neighbourhood* $\mathcal{N}_\epsilon$ as

$$\mathcal{N}_\epsilon \;=\; \{\tilde{p} \in \mathcal{M} |\; \tilde{p} = p + \bar{\epsilon}\, n(p)\,,\; p \in \mathcal{N}\,,\; n(p) \in N_p\mathcal{N}\,,\; \|n(p)\| = 1\,,\; 0 < \bar{\epsilon} < \epsilon\}\;. \tag{7.2}$$

We denote the boundary of the tubular ϵ neighbourhood $\mathcal{N}_\epsilon$ by $\partial\mathcal{N}_\epsilon$ and define it as

$$\partial\mathcal{N}_\epsilon \;=\; \{\tilde{p} \in \mathcal{M} |\; \tilde{p} = p + \epsilon n(p)\,,\; p \in \mathcal{N}\,,\; n(p) \in N_p\mathcal{N}\,,\; \|n(p)\| = 1\}\;. \tag{7.3}$$

Let the closure of $\mathcal{N}_\epsilon$ be denoted by the symbol $\bar{\mathcal{N}}_\epsilon = \mathcal{N}_\epsilon \cup \partial\mathcal{N}_\epsilon$. The manifold $\mathcal{M}$, the embedded submanifold $\mathcal{N}$, its tubular ϵ neighbourhood $\mathcal{N}_\epsilon$, and its closure $\partial\mathcal{N}_\epsilon$ are illustrated in Figure 7.2.

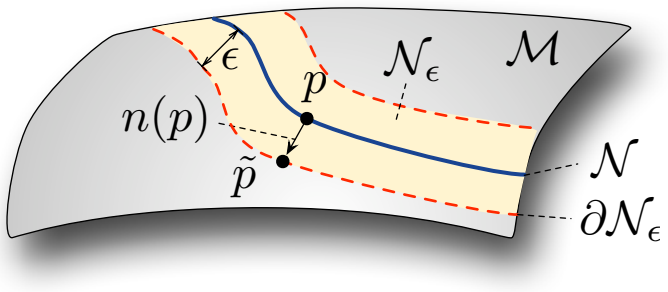

Figure 7.2: Illustration of a tubular neighborhood

Next we define the orientation of the vector field f on $\partial\mathcal{N}_\epsilon$. Consider an $\epsilon > 0$, a point $p \in \mathcal{N}$ and a normal vector $n(p) \in N_p\mathcal{N}$ with $\|n(p)\| = 1$. From this we construct the point $\tilde{p} \in \partial\mathcal{N}_\epsilon$ as $\tilde{p} = p + \epsilon\, n(p)$. Consider the inner product of the vector field f evaluated at $\tilde{p}$ and the normal vector $n(p)$ given by

$$\langle f\,(\tilde{p})\;,\; n(p)\rangle \;=\; \langle f\,(p + \epsilon n(p))\;,\; n(p)\rangle\;. \tag{7.4}$$

If the inner product (7.4) is negative, then the angle defined by $f\,(\tilde{p})$ and $n(p)$ is greater than $\frac{\pi}{2}$. That means that the two vectors point in different half spaces and we say the vector field

$f(\tilde{p})$ is *pointing strictly inward* at $\tilde{p} \in \partial\mathcal{N}_\epsilon$. This case is illustrated in Figure 7.3. Likewise if the inner product (7.4) is positive, then the angle defined by $f(\tilde{p})$ and $n(p)$ is less than $\frac{\pi}{2}$ and the two vectors point in the same half space. We then say the vector field $f(\tilde{p})$ is *pointing strictly outward* at $\tilde{p} \in \partial\mathcal{N}_\epsilon$. Note that the term pointing inward, respectively outward, at $\tilde{p} \in \mathcal{N}_\epsilon$ depends on ϵ, p and $n(p)$. Let us introduce the terms in- and overflowing invariance for the case where the inner product has the same sign for every $p \in \mathcal{N}$ and for every $n(p) \in \mathcal{N}$.

Definition 7.1.1. Consider the dynamical system (7.1) and let $\mathcal{N}$ be a closed, invariant submanifold embedded in $\mathcal{M}$. Let $\epsilon > 0$ and let $\partial\mathcal{N}_\epsilon$ denote the boundary of the tubular ϵ neighbourhood of $\mathcal{N}$.

(i) $\mathcal{N}_\epsilon$ is said to be *inflowing invariant* under (7.1) if

$$(\forall\, p \in \mathcal{N})\ (\forall\, n(p) \in N_p\mathcal{N})\ \ \langle f(p + \epsilon n(p))\ ,\ n(p)\rangle\ <\ 0\,. \tag{7.5}$$

(ii) $\mathcal{N}_\epsilon$ is said to be *overflowing invariant* under (7.1) if

$$(\forall\, p \in \mathcal{N})\ (\forall\, n(p) \in N_p\mathcal{N})\ \ \langle f(p + \epsilon n(p))\ ,\ n(p)\rangle\ >\ 0\,. \tag{7.6}$$

Remark 7.1.1. The terms inflowing and overflowing invariant are taken from *Fenichel Theory*, which was established in [81, 82, 83] and treats the stability properties of differentiable manifolds with boundaries. Unfortunately we do not have manifolds with boundaries and Fenichel Theory is not directly applicable to our problem. The interested reader is referred to [84], where a complete treatment is presented.

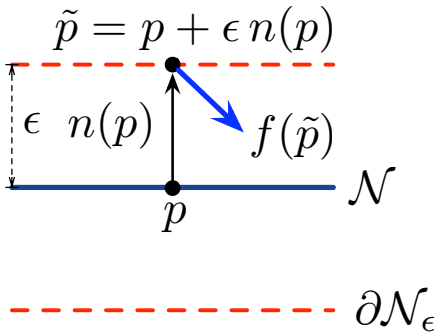

Figure 7.3: The vector field f is pointing strictly inward at $\tilde{p} \in \partial\mathcal{N}_\epsilon$

We can obtain an equivalent definition of in- and overflowing invariance via the flow generated by the vector field f.

Lemma 7.1.1. *Consider the dynamical system (7.1) and let $\mathcal{N}$ be a closed, invariant submanifold embedded in $\mathcal{M}$. Let $\epsilon > 0$ and let $\partial\mathcal{N}_\epsilon$ denote the boundary of the tubular ϵ neighbourhood of $\mathcal{N}$.*

(i) $\mathcal{N}_\epsilon$ is inflowing invariant if and only if for every $x_0 \in \partial\mathcal{N}_\epsilon$ and for all $t > 0$, $\Phi(t, x_0) \in \mathcal{N}_\epsilon$. In either case $\bar{\mathcal{N}}_\epsilon$ is positively invariant.

(ii) $\mathcal{N}_\epsilon$ is overflowing invariant if and only if for every $x_0 \in \partial\mathcal{N}_\epsilon$ and for all $t > 0$, $\Phi(t, x_0) \notin \bar{\mathcal{N}}_\epsilon$. In either case $\bar{\mathcal{N}}_\epsilon$ is negatively invariant.

Proof. Let us first prove (i). Towards this note that $\mathcal{N}$ is a closed set and, since $\mathcal{N}$ has no boundaries (in the sense of edges), the normal space $N_p\mathcal{N}$ is defined $\forall\, p \in \mathcal{N}$. Thus $\mathcal{N}$ is contained in the interior of $\bar{\mathcal{N}}_\epsilon$. Consequently $\bar{\mathcal{N}}_\epsilon$ is the disjoint union of $\mathcal{N}_\epsilon$ and $\partial\mathcal{N}_\epsilon$. Therefore, a trajectory of (7.1) starting outside of $\bar{\mathcal{N}}_\epsilon$ can enter $\mathcal{N}_\epsilon$ only via the boundary $\partial\mathcal{N}_\epsilon$. Let us fix an arbitrary initial condition $x(0) = x_0 \in \partial\mathcal{N}_\epsilon$ and note that the initial orientation of the flow $\Phi(0, x_0)$ is given by the vector field $f(x_0)$. If $\mathcal{N}_\epsilon$ is inflowing invariant, that is, $\forall\, p \in \mathcal{N}$ and $\forall\, n(p) \in N_p\mathcal{N}$ the vectorfield $f(p + \epsilon\, n(p))$ is pointing into $\mathcal{N}_\epsilon$, then

$$(\forall\, t > 0) \quad \Phi(t, x_0) \in \mathcal{N}_\epsilon\,. \tag{7.7}$$

Since $x_0 \in \partial\mathcal{N}_\epsilon$ was arbitrary condition (7.7) holds for all $x_0 \in \partial\mathcal{N}_\epsilon$. Likewise, the condition

$$(\forall\, x_0 \in \partial\mathcal{N}_\epsilon)\ (\forall\, t > 0) \quad \Phi(t, x_0) \in \mathcal{N}_\epsilon \tag{7.8}$$

implies that $\forall\, p \in \mathcal{N}$ and $\forall\, n(p) \in N_p\mathcal{N}$ the vector field $f\,(p + \epsilon\, n(p))$ must point strictly into $\mathcal{N}_\epsilon$. Moreover, if we consider additionally the initial time $t = 0$, then we have that for every $x_0 \in \partial\mathcal{N}_\epsilon$ and for all $t \geq 0$, $\Phi(t, x_0) \in \bar{\mathcal{N}}_\epsilon$, which is the definition positive invariance of $\bar{\mathcal{N}}_\epsilon$ given in Section 4.1. The proof of (ii) is analogous. □

Remark 7.1.2. Lemma 7.1.1 gives an equivalent representation of in- and overflowing invariance via the flow of (7.1). Thus inflowing invariance can loosely speaking be captured by

"for some ϵ trajectories are entering a tubular ϵ neighbourhood of $\mathcal{N}$ with a nonzero normal component and are then bounded within this tubular ϵ neighbourhood" and overflowing invariance by "for some ϵ trajectories are leaving a tubular ϵ neighbourhood of $\mathcal{N}$ with a nonzero normal component and are then bounded away from this tubular ϵ neighbourhood."

Unfortunately the definition of in- and overflowing invariance via the sign of the inner product (7.4) does not provide an easy and checkable condition. The idea to derive a checkable algebraic condition is to contract the tubular ϵ neighbourhood of $\mathcal{N}$ to a thin layer, in fact, such thin layer that the Taylor linearization of the vector field $f(x)$ is valid. Let us motivate this idea in the following example.

Example 7.1.1. Suppose we have given a smooth vector field $f : \mathbb{R}^2 \to \mathbb{R}^2$ and a smooth invariant curve $\mathcal{N}$ in the plane, that is, an invariant 1-dimensional submanifold embedded in $\mathbb{R}^2$. The boundary of a tubular ϵ neighbourhood of the curve $\mathcal{N}$ is given by $\partial\mathcal{N}_\epsilon$ as we defined it in (7.3). The curve and its tubular ϵ neighbourhood are illustrated in Figure 7.4(a).

We would like to conclude inflowing invariance for $\mathcal{N}_\epsilon$, but unfortunately the condition

$$(\forall\, p \in \mathcal{N})\ (\forall\, n(p) \in N_p\mathcal{N})\ \ \langle f\left(p + \epsilon n(p)\right)\,,\, n(p)\rangle \ \ < \ \ 0 \tag{7.9}$$

is not so easy to check. Suppose we contract $\mathcal{N}_\epsilon$ to a thin layer, then the vector field $f(p+\epsilon\, n(p))$ can for a sufficiently a small $\epsilon > 0$ be approximated by a first order Taylor series expansion about a point $p \in \mathcal{N}$:

$$f(p + \epsilon n(p)) \ \ = \ \ f(p) + \epsilon\ \frac{\partial f(x)}{\partial x}\bigg|_p\ n(p) + \mathcal{O}\big(\epsilon^2\big) \tag{7.10}$$

The inner product $\langle f\left(p + \epsilon n(p)\right)\,,\, n(p)\rangle$ can then be evaluated in this thin layer as

$$\begin{aligned}\langle f(p + \epsilon n(p))\,,\, n(p)\rangle \ \ &= \ \ \underbrace{\langle f(p)\,,\, n(p)\rangle}_{=0} + \left\langle \epsilon\ \frac{\partial f(x)}{\partial x}\bigg|_p\ n(p)\,,\, n(p) \right\rangle + \mathcal{O}\big(\epsilon^2\big) &(7.11)\\ &= \ \ \epsilon\, n(p)^T\ \frac{\partial f(x)}{\partial x}\bigg|_p\ n(p) + \mathcal{O}\big(\epsilon^2\big)\,. &(7.12)\end{aligned}$$

The term $\langle n(p)\,,\, f(p)\rangle$ vanishes because $\mathcal{N}$ is an invariant manifold and thus $f(p) \in T_p\mathcal{N}$. The linearized inner product (7.12) corresponds to the angle of the linearized vector field $\frac{\partial f(x)}{\partial x}\Big|_p$ the normal vector $n(p)$. If we can conclude a negative sign of the linearized inner

product for any $p \in \mathcal{N}$ and for any $n(p) \in N_p\mathcal{N}$, then $\mathcal{N}_\epsilon$ should intuitively be inflowing invariant, at least for a sufficiently small ϵ. Note that the normal vector $n(p)$ can have two different orientations. Since the normal vector $\bar{n}(p) = -n(p)$ results in the same linearized inner product (7.12), we need to check only the sign of (7.12) for every $p \in \mathcal{N}$. Moreover, if the linearized vector field is pointing strictly inward, then an intriguing conclusion is that trajectories locally converge to $\mathcal{N}$, as shown in Figure 7.4(b). The following theorem and the following section will confirm our intuition.

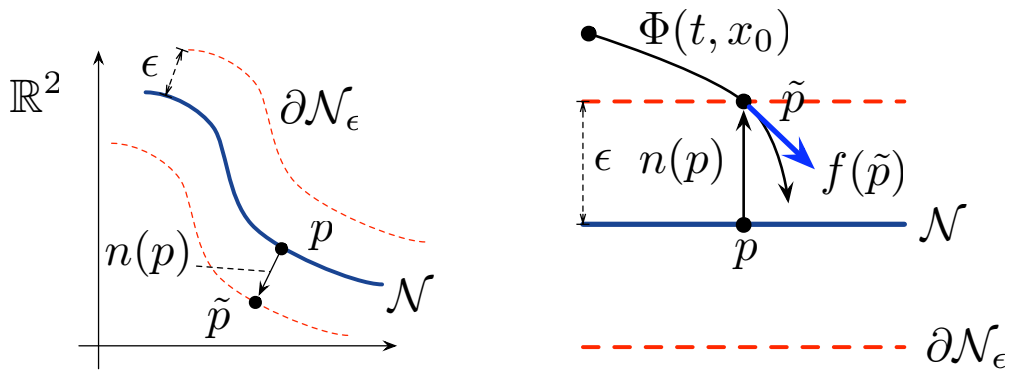

(a) Illustration of the $\mathcal{N}$ and $\partial\mathcal{N}_\epsilon$ (b) Inflowing invariance of $\mathcal{N}_\epsilon$

Figure 7.4: Inflowing invariance of the tubular ϵ neighbourhood smooth curve $\mathcal{N}$ in $\mathbb{R}^2$

The next theorem follows the ideas outlined in Example 7.1.1 and gives a sufficient and checkable condition for in- and overflowing invariance.

Theorem 7.1.1. *Consider system (7.1) with the vectorfield f and assume $f \in \mathcal{C}^2$. Let Ω be a compact set and $\mathcal{N} \subset \Omega$ be a closed, invariant, n-dimensional submanifold embedded in $\mathcal{M}$. Let $\mathbf{n}(p) \in \mathbb{R}^{m\times(m-n)}$ be a matrix whose columns form a basis for $N_p\mathcal{N}$.*

Consider for every $p \in \mathcal{N}$ the symmetric matrix

$$\Gamma(p) \;=\; \mathbf{n}(p)^T \left(\frac{\partial f(x)}{\partial x}\bigg|_p + \frac{\partial f(x)}{\partial x}\bigg|_p^T \right) \mathbf{n}(p) \;\in \mathbb{R}^{(m-n)\times(m-n)}. \tag{7.13}$$

If for every $p \in \mathcal{N}$ the matrix $\Gamma(p)$ is negative definite (respectively positive definite), then there exists $\epsilon^* > 0$ such that for every $\bar{\epsilon}$ with $\epsilon^* \geq \bar{\epsilon} > 0$ the tubular ϵ neighbourhood $\mathcal{N}_{\bar{\epsilon}}$ is inflowing invariant (respectively overflowing invariant).

Proof. In order to avoid too many "−" symbols will prove the overflowing invariant case first. Let $\epsilon > 0$ be arbitrary. We look at a point $\tilde{p} \in \partial\mathcal{N}_\epsilon$. By definition, it has the form

$$\tilde{p} \;=\; p + \epsilon n(p) \tag{7.14}$$

for some $p \in \mathcal{N}$, $n(p) \in N_p\mathcal{N}$ with $\|n(p)\| = 1$. Such a $n(p)$ has the form

$$n(p) \;=\; \sum_{j=1}^{m-n} c_j \, n_j(p) \tag{7.15}$$

where the $n_j(p)$ are columns of $\mathbf{n}(p)$ and $c_j \in \mathbb{R}$. For notational convenience we reformulate equation (7.15) with $\mathbf{n}(p)$ and $\mathbf{c} = [c_1 \, , \, \ldots \, , \, c_n]^T \in \mathbb{R}^{(m-n)\times 1}$ in a compact vector notation:

$$n(p) \;=\; \mathbf{n}(p)\,\mathbf{c} \tag{7.16}$$

The inner product of the vectorfield $f\left(\tilde{p}\right)$ and the normal vector $n(p)$ is given by

$$\begin{aligned}
\left\langle f\left(\tilde{p}\right) \, , \, n(p) \right\rangle \;&=\; \left\langle f\left(p + \epsilon n(p)\right) \, , \, n(p) \right\rangle && (7.17)\\
&=\; \left\langle f\left(p + \epsilon\,\mathbf{n}(p)\,\mathbf{c}\right) \, , \, \mathbf{n}(p)\,\mathbf{c} \right\rangle \, . && (7.18)
\end{aligned}$$

We now expand $f\left(p + \epsilon\,\mathbf{n}(p)\,\mathbf{c}\right)$ to a Taylor series about $p \in \mathcal{N}$ and obtain for the inner product

$$\begin{aligned}
\left\langle f\left(\tilde{p}\right) \, , \, n(p) \right\rangle \;&=\; \left\langle f(p) \, , \, \mathbf{n}(p)\,\mathbf{c} \right\rangle + \left\langle \epsilon \left.\frac{\partial f(x)}{\partial x}\right|_p \mathbf{n}(p)\,\mathbf{c} \, , \, \mathbf{n}(p)\,\mathbf{c} \right\rangle \\
&\quad + \left\langle R_3\left(p, \epsilon\right) \, , \, n(p) \right\rangle && (7.19)\\
&=\; 0 + \epsilon\,\mathbf{c}^T\,\mathbf{n}(p)^T \left.\frac{\partial f(x)}{\partial x}\right|_p \mathbf{n}(p)\,\mathbf{c} + \left\langle R_3\left(p, \epsilon\right) \, , \, n(p) \right\rangle && (7.20)\\
&=\; \frac{\epsilon}{2}\,\mathbf{c}^T\,\mathbf{n}(p)^T \left(\left.\frac{\partial f(x)}{\partial x}\right|_p + \left.\frac{\partial f(x)}{\partial x}\right|_p^T \right) \mathbf{n}(p)\,\mathbf{c} + \left\langle R_3\left(p, \epsilon\right) \, , \, n(p) \right\rangle && (7.21)\\
&=\; \frac{\epsilon}{2}\,\mathbf{c}^T\,\Gamma(p)\,\mathbf{c} + \left\langle R_3\left(p, \epsilon\right) \, , \, n(p) \right\rangle \, , && (7.22)
\end{aligned}$$

where $R_3\left(p, \epsilon\right)$ is the *Lagrange remainder* of the Taylor series expansion ([85], Theorem 4.1). The Lagrange remainder $R_3\left(p, \epsilon\right) \in \mathbb{R}^{m\times 1}$ is a vector where the the ith component $R_{3i}\left(p, \epsilon\right)$ is given by

$$\begin{aligned}
R_{3i}\left(p, \epsilon\right) \;&=\; \frac{1}{2}\left(p + \epsilon\,n(p) - p\right)^T H\left(f_i(\xi)\right)\left(p + \epsilon\,n(p) - p\right) && (7.23)\\
&=\; \frac{\epsilon^2}{2}\,n(p)^T\,H\left(f_i(\xi)\right)\,n(p) && (7.24)
\end{aligned}$$

with $H\left(f_i(\xi)\right)$ denoting the Hessian of the ith entry of the vectorfield f evaluated at some $\xi \in \mathbb{R}^m$ on the line segment

$$\Xi := \left\{ \xi \in \mathbb{R}^m \,|\, \xi \in [p\,,\, p + l\,\epsilon\, n(p)]\,,\, l \in [0,1] \right\}\,. \tag{7.25}$$

By definition $\mathcal{N}_\epsilon$ is overflowing invariant if at $\partial\mathcal{N}_\epsilon$ the vectorfield points in the same direction as the normal vector, with other words, the inner product (7.22) is positive $\forall\, p \in \mathcal{N}$. If the symmetric matrix $\Gamma(p)$ is positive definite, it is clear that we can obtain a positive inner product at every point $p \in \mathcal{N}$ by choosing ϵ sufficiently small at p. Let $\tilde{\epsilon}$ be such a sufficiently small ϵ at $p \in \mathcal{N}$, then we have

$$(\forall\, p \in \mathcal{N})\ (\exists\, \tilde{\epsilon} > 0)\ \ \frac{1}{2}\,\mathbf{c}^T\,\Gamma(p)\,\mathbf{c}\ >\ \frac{1}{\tilde{\epsilon}}\,\left|\langle n(p)\,,\, R_3\left(p, \tilde{\epsilon}\right)\rangle\right|\,. \tag{7.26}$$

We will now give a strictly positive lower bound Γ^* for the left hand side of equation (7.26) and a finite upper bound $\tilde{\epsilon}\,R^*$ for the right hand side of equation (7.26). Note that both these bounds are still dependent on the point p. By assumption we have $\Gamma(p) > 0$ for every $p \in \mathcal{N}$, that is,

$$(\forall\, p \in \mathcal{N})\ (\exists\, \Gamma^* > 0)\ \ \Gamma(p)\ \ \geq\ \ \Gamma^*\, I_n \tag{7.27}$$

$$\Rightarrow\ \ (\forall\, c \in \mathbb{R}^n)\ (\forall\, p \in \mathcal{N})\ (\exists\, \Gamma^* > 0)\ \ \frac{1}{2}\,\mathbf{c}^T\,\Gamma(p)\,\mathbf{c}\ \ \geq\ \ \frac{1}{2}\,\mathbf{c}^T\,\Gamma^*\,\mathbf{c}\,, \tag{7.28}$$

where Γ^* is a strictly positive real number depending on the point $p \in \mathcal{N}$. From standard Taylor series arguments we know that the right hand side of equation (7.26) is upper bounded by the maximum Lagrange remainder of the Taylor series expansion

$$\frac{1}{\tilde{\epsilon}}\,\left|\langle R_3\left(p, \tilde{\epsilon}\right)\,,\, n(p)\rangle\right|\ \ \leq\ \ \frac{1}{\tilde{\epsilon}}\,\left\|R_3\left(p, \tilde{\epsilon}\right)\right\|\,\underbrace{\left\|n(p)\right\|}_{=1} \tag{7.29}$$

$$\leq\ \ \frac{\sqrt{m}}{\tilde{\epsilon}}\,\max_{i=1,\ldots,m}\left|\max_{\xi\in\Xi}\left(\frac{\tilde{\epsilon}^2}{2}\,n(p)^T\,H\left(f_i(\xi)\right)\,n(p)\right)\right|\ =\ \tilde{\epsilon}\,R^*, \tag{7.30}$$

where R^* is a positive finite number depending on the point $p \in \mathcal{N}$. Thus we have

$$(\forall\, p \in \mathcal{N})\ (\exists\, R^* > 0)\ \ \tilde{\epsilon}\,R^*\ \ \geq\ \ \frac{1}{\tilde{\epsilon}}\,\left|\langle R_3\left(p, \tilde{\epsilon}\right)\,,\, n(p)\rangle\right|\,. \tag{7.31}$$

To overcome the obstacle that both Γ^* and R^* are dependent on the point p, we appeal to compactness of the manifold. The manifold $\mathcal{N}$ is a closed subset of the compact set Ω and

therefore itself a compact set. Due to the *Heine-Borel Theorem* ([86], Theorem 3-40) we can cover the manifold $\mathcal{N}$ by a finite number of closed balls $B_{ri}(p_i)$. Therefore, we have

$$\mathcal{N} \;=\; \bigcup_{i=1}^{k} \{B_{ri}(p_i) \cap \mathcal{N}\} \tag{7.32}$$

with k being a finite positive integer. On each of these balls Γ^* and R^* attain their minima and maxima as

$$\Gamma_i^* \;:=\; \min_{p \in B_{ri}(p_i) \cap \mathcal{N}} \Gamma^* \tag{7.33}$$

$$R_i^* \;:=\; \max_{p \in B_{ri}(p_i) \cap \mathcal{N}} R^* \,, \tag{7.34}$$

where Γ_i^* and R_i^* depend on $B_{ri}(p_i) \cap \mathcal{N}$. We define $\epsilon_i^* > 0$ such that

$$\frac{1}{2}\, \mathbf{c}^T\, \Gamma_i^*\, \mathbf{c} \;>\; \epsilon_i^*\, R_i^* \,. \tag{7.35}$$

With this ϵ_i^* the following inequality holds $\forall\, p \in B_{ri}(p_i) \cap \mathcal{N}$

$$\frac{1}{2}\, \mathbf{c}^T\, \Gamma(p)\, \mathbf{c} \;\geq\; \frac{1}{2}\, \mathbf{c}^T\, \Gamma_i^*\, \mathbf{c} \;>\; \epsilon_i^*\, R_i^* \;\geq\; \frac{1}{\epsilon_i^*}\, |\langle R_3\,(p, \epsilon_i^*\,,\, n(p))\rangle| \,, \tag{7.36}$$

and thus we obtain

$$(\exists\, \epsilon_i^* > 0)\;\; (\forall\, p \in B_{ri}(p_i) \cap \mathcal{N}) \;\; \frac{1}{2}\, \mathbf{c}^T\, \Gamma(p)\, \mathbf{c} \;>\; \frac{1}{\epsilon_i^*}\, |\langle R_3\,(p, \epsilon_i^*) \;,\; n(p)\rangle| \,. \tag{7.37}$$

Because the number of balls is finite, we define $\epsilon^* > 0$ as $\epsilon^* := \min\limits_{i=1,\ldots,k} \epsilon_i^*$. Therefore, we have the result

$$(\exists\, \epsilon^* > 0)\;\; (\forall\, p \in \mathcal{N}) \;\; \frac{1}{2}\, \mathbf{c}^T\, \Gamma(p)\, \mathbf{c} \;>\; \frac{1}{\epsilon^*}\, |\langle R_3\,(p, \epsilon^*)\rangle \;,\; n(p)| \,. \tag{7.38}$$

Thus we can choose the strictly positive $\epsilon^* := \min\limits_{i=1,\ldots,k} \epsilon_i^*$ as a uniform bound for which the inner product (7.22) is positive for every $p \in \mathcal{N}$. Clearly, the inner product is then also always positive for every $p \in \mathcal{N}$ if we choose any $\bar{\epsilon}$ smaller than ϵ^*, that is, $\bar{\epsilon} \in (0, \epsilon^*]$. In other words at $\mathcal{N}_{\bar{\epsilon}}$ the vectorfield points in the same direction as the normal vector and thus $\mathcal{N}_{\bar{\epsilon}}$ is overflowing invariant. The proof for the inflowing invariant case is analogous. □

Note that the conditions in Theorem 7.1.1 are not only sufficient for in- and overflowing invariance for some tubular ϵ^* neighbourhood of $\mathcal{N}$, but also for any tubular $\bar{\epsilon}$ neighbourhood with $\epsilon^* \geq \bar{\epsilon} > 0$. We want to remind the reader that in the heuristic geometric derivation of Lyapunov's stability condition in Section 6.2 a sequence of inflowing invariant sublevel sets

led to asymptotic stability. Moreover, in the case of inflowing invariance of a single point $p \in \mathbb{R}^m$ the definiteness condition on the matrix $\Gamma(p)$ defined in (7.13) reduces to

$$\left.\frac{\partial f(x)}{\partial x}\right|_p + \left.\frac{\partial f(x)}{\partial x}\right|_p^T \prec 0\,. \tag{7.39}$$

This is exactly the condition obtained by Lyapunov's indirect method with the Lyapunov function $\bar{V}(x) = \frac{1}{2}\, x^T x$ and which we interpreted as inflowing invariance of an infinitesimally small circle around p. This motivates us to link the properties of in- and overflowing invariance to asymptotic stability.

7.1.2 Relationship of In- and Overflowing Invariance to Stability

We have already shown in Lemma 7.1.1 that in- and overflowing invariance of $\mathcal{N}_\epsilon$ can be related to positive and negative invariance of $\bar{\mathcal{N}}_\epsilon$. Furthermore, the obvious relationship to Lyapunov's direct and indirect method motivates us to prove a local stability result for a manifold $\mathcal{N}$ and its tubular ϵ neighbourhood $\mathcal{N}_\epsilon$ for which Theorem 7.1.1 can be proved.

Theorem 7.1.2. *Consider the system (7.1) and assume it is forward complete. Let $\mathcal{N}$ be a closed, invariant, embedded submanifold and consider its tubular ϵ neighbourhood $\mathcal{N}_\epsilon$ for some $\epsilon > 0$.*

(i) If $\forall\, \bar{\epsilon}$ with $\epsilon \geq \bar{\epsilon} > 0$, $\mathcal{N}_{\bar{\epsilon}}$ is inflowing invariant, then $\mathcal{N}$ is a locally asymptotically stable set with $\bar{\mathcal{N}}_\epsilon$ as guaranteed region of attraction.

(ii) If $\forall\, \bar{\epsilon}$ with $\epsilon \geq \bar{\epsilon} > 0$, $\mathcal{N}_\epsilon$ is overflowing invariant, then $\mathcal{M} \setminus \mathcal{N}$ is invariant and, in particular, $\mathcal{M} \setminus \bar{\mathcal{N}}_\epsilon$ is invariant.

Proof. We prove (i) first. We have already mentioned in the proof of Lemma 7.1.1 that trajectories can only enter or leave $\mathcal{N}_\epsilon$ via $\partial\mathcal{N}_\epsilon$. Therefore, we analyze the dynamics normal to $\mathcal{N}_\epsilon$. First note that inflowing invariance of $\mathcal{N}_\epsilon$ implies that $\bar{\mathcal{N}}_\epsilon$ is positively invariant. Note that for every $\bar{\epsilon} \in (0, \epsilon]$, $\bar{\mathcal{N}}_{\bar{\epsilon}}$ is positively invariant and each $\bar{p} \in \partial\mathcal{N}_{\bar{\epsilon}}$ has the point to set distance $\|\bar{p}\|_{\mathcal{N}} = \bar{\epsilon}$. The condition

$$(\forall\, r > 0)\ (\exists\, \delta > 0)\ \ \|x_0\|_{\mathcal{N}} < \delta \ \ \Rightarrow\ \ (\forall\, t \geq 0)\ \ \|x(t)\|_{\mathcal{N}} < r \tag{7.40}$$

is fulfilled with $\delta = \min\{r\,,\,\epsilon\}$ and thus $\mathcal{N}$ is stable. Since each $\mathcal{N}_{\bar{\epsilon}}$ is inflowing invariant the vectorfield on $\partial\mathcal{N}_{\bar{\epsilon}}$ always points to the inside of $\mathcal{N}_{\bar{\epsilon}}$ and towards $\mathcal{N}$. Due to continuity of the vectorfield there must always exist a tubular neighbourhood of $\partial\mathcal{N}_{\bar{\epsilon}}$ where the vectorfield is pointing towards $\mathcal{N}$. Let us say that each point on this tubular neighbourhood has distance $\Delta\bar{\epsilon}$ to $\partial\mathcal{N}_{\bar{\epsilon}}$. In order to show asymptotic stability we construct the sequence $\{\bar{\epsilon}_i\}$ with $\epsilon = \bar{\epsilon}_0 > \bar{\epsilon}_1 > \cdots > 0$ and $\bar{\epsilon}_i - \bar{\epsilon}_{i+1} < \Delta\bar{\epsilon}$. Then we have

$$\left(\forall\, x(t) \in \mathcal{N}_{\bar{\epsilon}_i} \setminus \mathcal{N}_{\bar{\epsilon}_{i+1}}\right)\ (\exists\, \Delta t_i > 0)\quad x(t + \Delta t_i) \in \mathcal{N}_{\bar{\epsilon}_{i+1}}\,. \tag{7.41}$$

Since the sequence $\{\bar{\epsilon}_i\}$ goes to zero as $i \to \infty$ we have

$$\|x_0\|_{\mathcal{N}} \,<\, \epsilon \quad\Rightarrow\quad \lim_{t\to\infty} \|x(t)\|_{\mathcal{N}} \to 0\,, \tag{7.42}$$

that is, the set $\mathcal{N}$ is asymptotically stable with $\bar{\mathcal{N}}_\epsilon$ as guaranteed region of attraction. The proof of (ii) goes simply via time inversion. Note that an overflowing invariant manifold is inflowing invariant for $t \leq 0$ and thus also asymptotically stable for $t \leq 0$ and with $\bar{\mathcal{N}}_\epsilon$ as region of attraction. Therefore, $\mathcal{M} \setminus \mathcal{N}$ is invariant for $t \geq 0$ and so is $\mathcal{M} \setminus \bar{\mathcal{N}}_\epsilon$. □

Remark 7.1.3. Just as in Section 4.1 the assumption of forward completeness is redundant if $\mathcal{N}$ is additionally compact.

Note that the assumptions of Theorem 7.1.2 can be exactly fulfilled by Theorem 7.1.1. Thus both theorems can be stated in one, which we did not do earlier in order to give the reader a breath between the proofs. Let us now state the final theorem obtained by Theorem 7.1.1 and Theorem 7.1.2. For notational simplicity, we will refer to this theorem in the sequel as *Manifold Stability Theorem.*

Theorem 7.1.3. *Manifold Stability Theorem:*
Consider system (7.1) *with the vectorfield* f *and assume* $f \in \mathcal{C}^2$. *Let* $\Omega \subset \mathcal{M}$ *be a compact invariant set and let* $\mathcal{N}$ *be a closed, invariant, n-dimensional submanifold submanifold embedded in* $\mathcal{M}$ *with* $\mathcal{N} \cap \Omega \neq \emptyset$. *Let* $\mathbf{n}(p) \in \mathbb{R}^{m\times(m-n)}$ *be a matrix whose columns form a basis for* $N_p\mathcal{N}$. *Consider for every* $p \in \mathcal{N} \cap \Omega$ *the symmetric matrix*

$$\Gamma(p) \;=\; \mathbf{n}(p)^T \left(\left.\frac{\partial f(x)}{\partial x}\right|_p + \left.\frac{\partial f(x)}{\partial x}\right|_p^T \right) \mathbf{n}(p) \;\in \mathbb{R}^{(m-n)\times(m-n)}\,. \tag{7.43}$$

(i) If for every $p \in \mathcal{N} \cap \Omega$ the matrix $\Gamma(p)$ is negative definite, then there exists $\epsilon > 0$, such that $\mathcal{N} \cap \Omega$ is a locally asymptotically stable set with $\bar{\mathcal{N}_\epsilon} \cap \Omega$ as guaranteed region of attraction.

(ii) If for every $p \in \mathcal{N} \cap \Omega$ the matrix $\Gamma(p)$ is positive definite, then there exists $\epsilon > 0$, such that $\Omega \setminus \mathcal{N}$ is invariant and, in particular, $\Omega \setminus \bar{\mathcal{N}_\epsilon}$ is invariant.

Proof. Let us prove the more familiar case of asymptotic stability first. The matrix $\Gamma(p)$ is for every p evaluated in the compact set $\mathcal{N} \cap \Omega$ negative definite. That means by Theorem 7.1.1 that there exists an $\epsilon > 0$, such that for every $\bar{\epsilon}$ with $\epsilon \geq \bar{\epsilon} > 0$ the tubular $\bar{\epsilon}$ neighbourhood $\mathcal{N}_{\bar{\epsilon}} \cap \Omega$ is inflowing invariant, that is, the vector field evaluated at $\partial\mathcal{N}_{\bar{\epsilon}} \cap \Omega$ is always pointing strictly into $\mathcal{N}_{\bar{\epsilon}} \cap \Omega$. Note that Ω is an invariant set and by the arguments Theorem 7.1.2 a trajectory $\Phi(t, x_0)$ with initial condition $x_0 \in \bar{\mathcal{N}_\epsilon} \cap \Omega$ asymptotically converges to $\mathcal{N}$. The proof of the overflowing invariant case is analogous. □

If we can fulfill either a positive or negative definiteness condition on the matrix in (7.43) in Theorem 7.1.3, then there exists with $\bar{\mathcal{N}_\epsilon}$ a closed tubular neighbourhood of $\mathcal{N}$, such that either $\mathcal{N}$ is locally asymptotically stable with $\bar{\mathcal{N}_\epsilon}$ as region of attraction or any trajectory starting in $\mathcal{M} \setminus \bar{\mathcal{N}_\epsilon}$ will always be bounded away from $\bar{\mathcal{N}_\epsilon}$. Both cases are illustrated at the example of a smooth curve $\mathcal{N}$ in the plane (Example 7.12) in Figure 7.5.

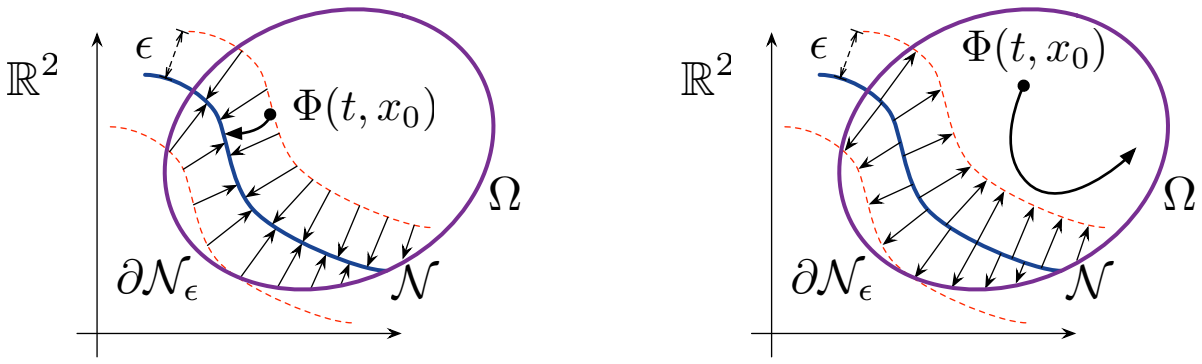

(a) Local asymptotic stability of $\mathcal{N}$

(b) $\mathbb{R}^m \setminus \bar{\mathcal{N}_\epsilon}$ is invariant

Figure 7.5: Local asymptotic stability and repulsiveness of $\mathcal{N}$

Note that in the case in Figure 7.5(b) we can guarantee that the trajectory $\Phi(t, x_0)$ will always be bounded a positive distance $\epsilon > 0$ away from $\mathcal{N}$. If you go back to the idea outlined at the beginning of this section, then Theorem 7.1.2 is exactly the tool we need to in order to prove that the trajectory $\Phi_e(t, e_0)$ will be bounded away from $\mathcal{W}_e \cap \mathcal{Q}$. We will make use of this in the next section, where we derive a global stability result for the directed triangle.

7.2 Global Stability Result for a Directed Triangular Formation

The stability result for the link dynamics in Theorem 5.4.1 is restricted to a sufficiently small sublevel set, and so are the following results including or first main result in Theorem 5.4.3. In this section we make use of the manifold stability theorem (Theorem 7.1.3) in order to arrive at a global stability result. We demonstrate this at the familiar example of the directed triangle (Example 3.1.3) and remark that the same results may also be applicable to more complex formations.

For simplicity we will perform an analysis for regular potential functions $V_i(\omega) = \frac{1}{4}\omega^2$ and later point out the necessary modifications for irregular potential functions. The link dynamics for the directed triangle are then given as in Section 5.2 as

$$\dot{e} = \begin{bmatrix} \dot{e}_1 \\ \dot{e}_2 \\ \dot{e}_3 \end{bmatrix} = \begin{bmatrix} e_2\,\psi_2 - e_1\,\psi_1 \\ e_3\,\psi_3 - e_2\,\psi_2 \\ e_1\,\psi_1 - e_3\,\psi_3 \end{bmatrix} =: f_e(e) \tag{7.44}$$

$$e(0) = e_0 \in \hat{H}\left(\mathbb{R}^6\right), \tag{7.45}$$

where $\psi_i = 2\,\nabla V_i\big(\|e_i\|^2 - d_i^2\big) = \|e_i\|^2 - d_i^2$, the vector field on the right-hand side is denoted by $f_e(e)$ and the state space for the system (7.44) is the link space $\hat{H}\left(\mathbb{R}^6\right)$. The link space is the hyperplane parametrized by $e_1 + e_2 + e_3 = \mathbf{0}$ and is a closed, invariant differentiable manifold of dimension 4. We have already pointed out the different invariant sets of the

link dynamics on page 80. In a first step towards a global stability result we identify these invariant sets as embedded submanifolds of the link space.

7.2.1 The Invariant Sets as Embedded Submanifolds

In general the invariant sets of the link dynamics are given by the set of equal velocities $\mathcal{M}_e$. The set $\mathcal{M}_e$ can be again split up in different invariant sets, among others the desired equilibrium set $\mathcal{E}_e$, where the functions ψ_i take the value zero.

The Target Formation $\mathcal{E}_e$

We noted on page 72 that the target formation $\mathcal{E}_z$ constitutes a three dimensional submanifold embedded in $\mathbb{R}^6$. The corresponding set $\mathcal{E}_e$ in the link space is

$$\mathcal{E}_e \;=\; \left\{ e \in \hat{H}\left(\mathbb{R}^6\right) \,\middle|\, \|e_1\|^2 = d_1^2\,,\; \|e_2\|^2 = d_2^2\,,\; \|e_3\|^2 = d_3^2 \right\} \tag{7.46}$$

and can also be specified as a zero set of the function

$$\begin{aligned} F:\quad & \mathbb{R}^6 \;\to\; \mathbb{R}^5 \\ F(e) \;=\; & \begin{bmatrix} \|e_1\|^2 = d_1^2 \\ \|e_2\|^2 = d_2^2 \\ \|e_3\|^2 = d_3^2 \\ e_1 + e_2 + _3 \end{bmatrix}, \end{aligned} \tag{7.47}$$

that is, $\mathcal{E}_e = F^{-1}(\mathbf{0})$. The Jacobian of $F(e)$ is given by

$$\frac{\partial F(e)}{\partial e} \;=\; \begin{bmatrix} 2\,e_1^T & 0 & 0 \\ 0 & 2\,e_2^T & 0 \\ 0 & 0 & 2\,e_3^T \\ I_2 & I_2 & I_2 \end{bmatrix} \tag{7.48}$$

and has constant rank 5 on $F^{-1}\left(\mathbf{0}\right)$. By Corollary 6.1.1 the target formation $\mathcal{E}_e$ is a closed 1-dimensional submanifold embedded in $\mathbb{R}^6$ and is located on the hyperplane $\hat{H}\left(\mathbb{R}^6\right)$. Spoken

differently, $\mathcal{E}_e$ is a 1-dimensional submanifold embedded in the link space. We obtain the normal space at a point $e \in \mathcal{E}_e$ as

$$N_p\mathcal{E}_e = \mathrm{Im}\left(\left.\frac{\partial F(e)}{\partial e}\right|_{\mathcal{E}_e}\right) = \mathrm{columnspan}\left\{\left.\begin{bmatrix} e_1 & 0 & 0 & I_2 \\ 0 & e_2 & 0 & I_2 \\ 0 & 0 & e_3 & I_2 \end{bmatrix}\right|_{\mathcal{E}_e}\right\}. \tag{7.49}$$

We see that the normal vector of the link space $[I_2\,,\,I_2\,,\,I_2]^T$ is contained in the normal space $N_p\mathcal{E}_e$. Therefore, the other three vectors which form a basis of $N_p\mathcal{E}_e$ can be chosen to be in the in the link space. By linear linear combinations of the columns of $\left.\frac{\partial F(e)}{\partial e}\right|_{e\in\mathcal{E}_e}$ we can obtain the following three vectors

$$\begin{bmatrix} e_1 \\ e_2 \\ e_3 \end{bmatrix} = \begin{bmatrix} e_1 \\ 0 \\ 0 \end{bmatrix} + \begin{bmatrix} 0 \\ e_2 \\ 0 \end{bmatrix} + \begin{bmatrix} 0 \\ 0 \\ e_3 \end{bmatrix} \tag{7.50}$$

$$\begin{bmatrix} e_3 \\ e_2 \\ e_1 \end{bmatrix} = 2\begin{bmatrix} 0 \\ e_2 \\ 0 \end{bmatrix} - \begin{bmatrix} e_1 \\ 0 \\ 0 \end{bmatrix} - \begin{bmatrix} 0 \\ 0 \\ e_3 \end{bmatrix} - e_2\begin{bmatrix} I_2 \\ I_2 \\ I_2 \end{bmatrix} \tag{7.51}$$

$$\begin{bmatrix} e_1 \\ e_3 \\ e_2 \end{bmatrix} = 2\begin{bmatrix} e_1 \\ 0 \\ 0 \end{bmatrix} - \begin{bmatrix} 0 \\ e_2 \\ 0 \end{bmatrix} - \begin{bmatrix} 0 \\ 0 \\ e_3 \end{bmatrix} - e_1\begin{bmatrix} I_2 \\ I_2 \\ I_2 \end{bmatrix}, \tag{7.52}$$

which are all linearly independent and orthogonal to $[I_2\,,\,I_2\,,\,I_2]^T$. Therefore, we can give a different basis for $N_p\mathcal{E}_e$ whose components are either parallel or orthogonal to $[I_2\,,\,I_2\,,\,I_2]^T$:

$$N_p\mathcal{E}_e = \mathrm{Im}\left(\left.\frac{\partial F(e)}{\partial e}\right|_{\mathcal{E}_e}\right) = \mathrm{columnspan}\left\{\left.\begin{bmatrix} e_1 & e_3 & e_1 & I_2 \\ e_2 & e_2 & e_3 & I_2 \\ e_3 & e_1 & e_2 & I_2 \end{bmatrix}\right|_{\mathcal{E}_e}\right\}. \tag{7.53}$$

The tangent space is the orthogonal complement of the normal space and is given by

$$T_p\mathcal{E}_e = \ker\left(\left.\frac{\partial F(e)}{\partial e}\right|_{\mathcal{E}_e}\right) = \mathrm{span}\left\{\left.\begin{bmatrix} J\,e_1 \\ J\,e_2 \\ J\,e_3 \end{bmatrix}\right|_{\mathcal{E}_e}\right\}. \tag{7.54}$$

The Set of Collocated Robots $\mathcal{X}_e$

Another invariant set of the link dynamics (7.44) is the set where each link e_i takes the value zero and thus all three robots are collocated. This is the set

$$\mathcal{X}_e \;=\; \left\{ e \in \hat{H}\left(\mathbb{R}^6\right) \,|\, e_1 = 0\,,\; e_2 = 0\,,\; e_3 = 0 \right\}\,, \tag{7.55}$$

which is simply the origin of the $\mathbb{R}^6$. Similar to the target formation $\mathcal{E}_e$ the set $\mathcal{X}_e$ could be parametrized as zero set of a function, but in this case it is obvious that $\mathcal{X}_e$ is a closed submanifold embedded in $\mathbb{R}^6$, located in the link space and with dimension zero. Thus the tangent space at a point $e \in \mathcal{X}_e$ is an empty space and the normal space can be parametrized by basis vectors which are either parallel or orthogonal to $[I_2\,,\, I_2\,,\, I_2]^T$:

$$N_e\mathcal{X}_e \;=\; \text{columnspan}\left\{ \begin{bmatrix} -I_2 & 0 & I_2 \\ I_2 & -I_2 & I_2 \\ 0 & I_2 & I_2 \end{bmatrix} \right\}\,. \tag{7.56}$$

The Set of Collinear Robots $\mathcal{N}_e$

The general set of equilibria of the directed triangle is the set

$$\mathcal{M}_e \;=\; \left\{ e \in \hat{H}\left(\mathbb{R}^6\right) \,|\, e_1\,\psi_1 = e_2\,\psi_2 = e_3\,\psi_3 \right\}\,, \tag{7.57}$$

which contains $\mathcal{E}_e$ and $\mathcal{X}_e$. The set $\mathcal{M}_e \setminus \{\mathcal{E}_e \cup \mathcal{X}_e\}$ is then the set of collinear robots moving with equal velocity given by $e_1\,\psi_1 = e_2\,\psi_2 = e_3\,\psi_3$. Motivated by this we define the *line set* $\mathcal{N}_z$, that is, the set of all points in the state space $\mathbb{R}^6$ corresponding to collinear robots in the plane. The line set $\mathcal{N}_z$ can be parametrized by

$$\mathcal{N}_z \;=\; \left\{ z \in \mathbb{R}^6 \,\middle|\, \text{rank}\,[e_1\; e_2\; e_3] < 2\,,\, e = \hat{H}\,z \right\}\,. \tag{7.58}$$

Its image $\mathcal{N}_e = \hat{H}\left(\mathcal{N}_z\right)$ in the link space is

$$\mathcal{N}_e \;=\; \left\{ e \in \hat{H}\left(\mathbb{R}^6\right) \,|\, \text{rank}\,[e_1\; e_2\; e_3] < 2 \right\} \;=\; \left\{ e \in \hat{H}\left(\mathbb{R}^6\right) \,|\, \text{rank}\,[e_1\; e_2] < 2 \right\} \tag{7.59}$$

$$\;=\; \left\{ e \in \hat{H}\left(\mathbb{R}^6\right) \,|\, e_1^T\,J\,e_2 \,=\, 0 \right\}\,, \tag{7.60}$$

$$\text{where } J = \begin{bmatrix} 0 & 1 \\ -1 & 0 \end{bmatrix} \text{ is a rotation matrix.}$$

From Example 2.1.2 we know that $\mathcal{N}_e$ is the exactly the set, where the formation $(\mathcal{G}, e)$ looses its rigidity, that is, $\mathcal{N}_e = \mathcal{Q}$. We are interested in the question whether $\mathcal{N}_e$ is a submanifold of the link space. Towards this note that the line set $\mathcal{N}_e$ can be parametrized as zero set of the function

$$\begin{aligned} T: \quad & \mathbb{R}^6 \to \mathbb{R}^3 \\ T(e) &= \begin{bmatrix} e_1^T J\, e_2 \\ e_1 + e_2 + e_3 \end{bmatrix}, \end{aligned} \tag{7.61}$$

that is, $\mathcal{N}_e = T^{-1}(\mathbf{0})$. The Jacobian of $T(e)$ is given by

$$\frac{\partial T(e)}{\partial e} = \begin{bmatrix} -e_2^T J & e_1^T J & 0 \\ I_2 & I_2 & I_2 \end{bmatrix} \tag{7.62}$$

and has constant rank 3 for all $e \in T^{-1}(\mathbf{0}) \setminus \{\mathbf{0}\}$. But note that the Jacobian $\frac{\partial T(e)}{\partial e}$ has a rank loss for $e = \mathbf{0}$, or equivalently for $e \in \mathcal{X}_e$, and thus $\mathcal{N}_e$ is not an embedded submanifold of the link space. However, we can define the set

$$\mathcal{N}'_e = \mathcal{N}_e \setminus \mathcal{X}_e\,, \tag{7.63}$$

which is an open 3-dimensional submanifold of $\mathbb{R}^6$ located in the link space. We obtain the tangent space at a point $e \in \mathcal{N}'_e$ as

$$T_e\mathcal{N}'_e = \ker\left(\frac{\partial F(e)}{\partial e}\Big|_{\mathcal{N}'_e}\right) = \ker\left(\begin{bmatrix} -e_2^T J & e_1^T J & 0 \\ I_2 & I_2 & I_2 \end{bmatrix}\Big|_{\mathcal{N}'_e}\right) \tag{7.64}$$

$$= \operatorname{Im}\left(\begin{bmatrix} e_1 & e_2 + e_3 & e_2 \\ e_2 & -e_3 & e_1 \\ e_3 & -e_2 & -e_1 - e_2 \end{bmatrix}\Big|_{\mathcal{N}'_e}\right). \tag{7.65}$$

We construct the normal space as the orthogonal complement of the tangent space as

$$N_e\mathcal{N}'_e = \ker\left(\begin{bmatrix} e_1^T & e_2^T & e_3^T \\ e_2^T + e_3^T & -e_3^T & -e_2^T \\ e_2^T & e_1^T & -e_1^T - e_2^T \end{bmatrix}\Big|_{\mathcal{N}'_e}\right) = \operatorname{Im}\left(\begin{bmatrix} -J\, e_2 & I_2 \\ -J\, e_3 & I_2 \\ -J\, e_1 & I_2 \end{bmatrix}\Big|_{\mathcal{N}'_e}\right), \tag{7.66}$$

which again consists of basis vectors either parallel or orthogonal to $[I_2\,,\,I_2\,,\,I_2]^T$.

Remark 7.2.1. For a deeper graphical understanding of the set $\mathcal{N}_e'$ it is worth to mention, that the sets $\mathcal{N}_z$ and $\mathcal{X}_z$ can be parametrized easier in different coordinates. The orthogonal coordinate transformation

$$\tilde{z} \;=\; A\,z \quad \text{with} \quad A \;=\; \frac{1}{\sqrt{3}} \begin{bmatrix} \frac{\sqrt{3}}{2} & -\frac{1}{2} & -\frac{\sqrt{3}}{2} & -\frac{1}{2} & 0 & 1 \\ -\frac{1}{2} & -\frac{\sqrt{3}}{2} & -\frac{1}{2} & \frac{\sqrt{3}}{2} & 1 & 0 \\ -\frac{\sqrt{3}}{2} & -\frac{1}{2} & \frac{\sqrt{3}}{2} & -\frac{1}{2} & 0 & 1 \\ -\frac{1}{2} & \frac{\sqrt{3}}{2} & -\frac{1}{2} & -\frac{\sqrt{3}}{2} & 1 & 0 \\ 0 & 1 & 0 & 1 & 0 & 1 \\ 1 & 0 & 1 & 0 & 1 & 0 \end{bmatrix} \tag{7.67}$$

results in the parameterizations

$$\mathcal{E}_z \;=\; \left\{ z \in \mathbb{R}^6 \,\middle|\, \|\tilde{z}_2 - \tilde{z}_1\|^2 = d_1^2\,,\; \|\tilde{z}_3 - \tilde{z}_2\|^2 = d_2^2\,,\; \|\tilde{z}_1 - \tilde{z}_3\|^2 = d_3^2\,, \tilde{z} = A\,z \right\} \tag{7.68}$$

$$\mathcal{X}_z \;=\; \left\{ z \in \mathbb{R}^6 \,|\, \tilde{z}_1 \;=\; \tilde{z}_2 \;=\; \mathbf{0}\,,\; \tilde{z} = A\,z \right\} \tag{7.69}$$

$$\mathcal{N}_z \;=\; \left\{ \tilde{z} \in \mathbb{R}^6 \,|\, \|\tilde{z}_2\| = \|\tilde{z}_1\|\;,\; \tilde{z} = A\,z \right\}. \tag{7.70}$$

Clearly the parameterization in $\tilde{z}$-coordinates does not change the set $\mathcal{E}_z$ since an orthogonal change of coordinates does not change lengths. In contrast, the set $\mathcal{N}_z$ can be expressed simpler by the two diagonals in $(\tilde{z}_1, \tilde{z}_2)$-space and $\mathcal{X}_z$ as the origin in this space, as illustrated in Figure 7.6(a). Clearly $\mathcal{N}_z$ is not a differentiable manifold, but if the origin is subtracted, then $\mathcal{N}_z' = \mathcal{N}_z \setminus \mathcal{X}_z$ is an open differentiable manifold and so is $\mathcal{N}_e' = \hat{H}\,(\mathcal{N}_z')$. A qualitative illustration of $\mathcal{N}_e'$ and $\mathcal{X}_e'$ is given in Figure 7.6(b).

7.2.2 Stability Properties of the Line Set $\mathcal{N}_e$

The stability result in Theorem 5.4.1 says that the set $\mathcal{E}_e$ is locally asymptotically stable for initial conditions in the sublevel set $\Omega(\rho)$, which is small enough to be disjoint with the set of not rigid formations $\mathcal{Q}$. Although this result is at first glance only local, $\Omega(\rho)$ is not an infinitesimally small set. For the directed triangle we can find a strictly positive distance between $\mathcal{E}_e$ and $\mathcal{Q}$, as shown in the next lemma.

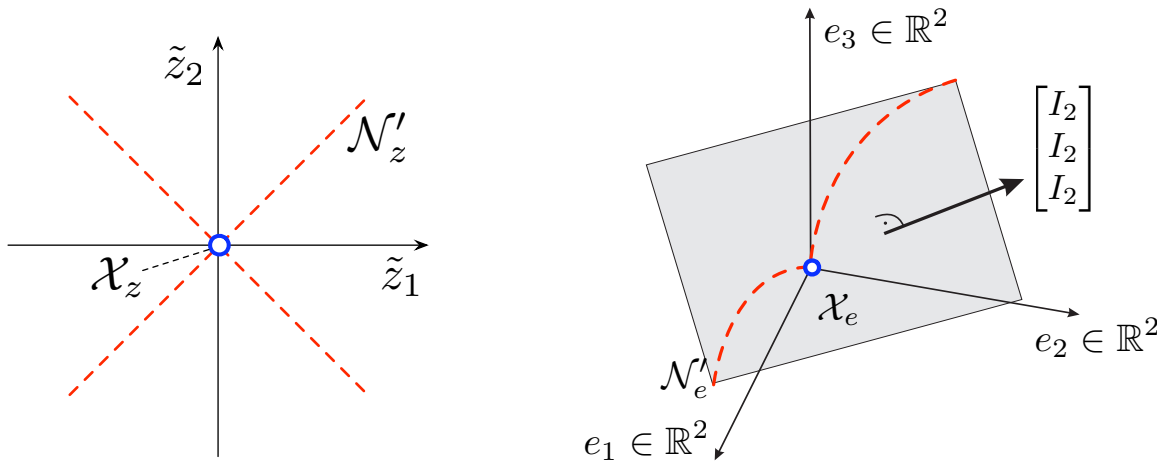

(a) $\mathcal{N}_z$ and $\mathcal{X}_z$ in $\tilde{z}$-coordinates

(b) Qualitative picture of $\mathcal{N}'_e$ and $\mathcal{X}'_e$

Figure 7.6: A qualitative illustration of the line set and the set of collocated robots

Lemma 7.2.1. *There exists a positive distance between $\mathcal{E}_e$ and $\mathcal{N}_e$.*

Proof. The distance between $\mathcal{E}_e$ and $\mathcal{N}_e$ is defined as

$$dist\left(\mathcal{E}_e\,,\,\mathcal{N}_e\right) \;:=\; \inf_{e\in\mathcal{E}_e}\;\inf_{\bar{e}\in\mathcal{N}_e} \|e-\bar{e}\|\;. \tag{7.71}$$

In the set $\mathcal{E}_e$ the triangle inequalities hold, that is, $\forall\, i \in \{1,2,3\}$

$$d_i \;<\; d_{i+1}+d_{i+2} \;\Leftrightarrow\; (\forall\, i\in\{1,2,3\})\;(\forall\, e\in\mathcal{E}_e)\;\; \|e_i\| \;<\; \|e_{i+1}\|+\|e_{i+2}\|\;. \tag{7.72}$$

In the set $\mathcal{N}_e$ one of the following three equalities holds:

$$\|e_1\| \;=\; \|e_2\|+\|e_3\| \tag{7.73}$$

$$\|e_3\| \;=\; \|e_1\|+\|e_2\| \tag{7.74}$$

$$\|e_2\| \;=\; \|e_3\|+\|e_1\|\;. \tag{7.75}$$

In the $(\|e_1\|\,,\|e_2\|\,,\|e_3\|)$-space the set $\mathcal{E}_e$ is a point in the first orthant and the line set $\mathcal{N}_e$ is the union of the three planes defined by the equations (7.73)-(7.75). The equilibrium set $\mathcal{E}_e$ as a point in $(\|e_1\|\,,\|e_2\|\,,\|e_3\|)$-space is by equation (7.72) disjoint with these planes and thus has a positive distance from these planes. The mapping $F:\mathbb{R}^6\to\mathbb{R}^3$, $F\left([e_1\,,\,e_2\,,\,e_3]\right) = [\|e_1\|\,,\,\|e_2\|\,,\,\|e_3\|]$ is continuous and thus $\mathcal{E}_e$ and $\mathcal{N}_e$ also have a positive distance in the (e_1,e_2,e_3)-space. □

Lemma 7.2.1 implies that $\Omega(\rho)$ is not necessarily a small set, but it is also not the entire region of attraction of the set $\mathcal{E}_e$. Simulation studies show us that the exact region of attraction is at least delimited by the line set $\mathcal{N}_e$, which seems to be invariant. The following lemma proves our observation that initially collinear robots stay collinear for all time.

Lemma 7.2.2. *The set $\mathcal{N}_e$ is invariant under the link dynamics.*

Proof. The set $\mathcal{N}_e$ can be split up as $\mathcal{N}_e = \mathcal{N}_e' \cup \mathcal{X}_e$, where $\mathcal{N}_e'$ and $\mathcal{X}_e$ are submanifolds embedded in the link space. For a point $e \in \mathcal{N}_e'$ we choose the normal vector $n(e) = \left[e_2^T J\,,\, e_3^T J\,,\, e_1^T J\right]^T \in \hat{H}\left(\mathbb{R}^6\right)$ as basis for the component of the normal space of $\mathcal{N}_e'$ which lies entirely in the link space. The following calculation shows that the vector field $f_e(e)$ lies in the tangent space of the manifold $\mathcal{N}_e'$ and thus $\mathcal{N}_e'$ is invariant:

$$\begin{aligned}
\left\langle n(e)^T\, f_e(e)\right\rangle\big|_{e\in\mathcal{N}_e} &= \begin{bmatrix} e_2^T J & e_3^T J & e_1^T J \end{bmatrix} \begin{bmatrix} e_1\,\psi_1 \\ e_2\,\psi_2 \\ e_3\,\psi_3 \end{bmatrix}\Bigg|_{e\in\mathcal{N}_e} && (7.76)\\
&= \left[\psi_1\, e_2^T\, J\, e_1 + \psi_2\, e_3^T\, J\, e_2 + \psi_3\, e_1^T\, J\, e_3\right]\big|_{e\in\mathcal{N}_e} && (7.77)\\
&= -\left[(\psi_1+\psi_2+\psi_3)\; e_1^T\, J\, e_2\right] \;=\; 0 && (7.78)
\end{aligned}$$

The invariance of $\mathcal{X}_e$ can either be checked by similar arguments or simply by the fact that $\mathcal{X}_e$ is an equilibrium of the link dynamics. Therefore, $\mathcal{N}_e = \mathcal{N}_e' \cup \mathcal{X}_e$ is invariant. □

In the light of Lemma 7.2.2, the region of attraction of the set $\mathcal{E}_e$ cannot be all of the link space, but is at least delimited by $\mathcal{N}_e$. In the sequel we will show that $\hat{H}\left(\mathbb{R}^6\right) \setminus \mathcal{N}_e$ is the exact region of attraction of $\mathcal{E}_e$. As a first step towards this result, note that the derivative of the sum of the potential functions $V(e)$ results for the directed triangle in the expression

$$\begin{aligned}
\dot{V}(e) &= -\mathbf{\Psi}(e)^T\, R_{\mathcal{G}}(e)\, R_{\mathcal{G}}(e)^T\, \mathbf{\Psi}(e) && (7.79)\\
&= -\left\|e_1\,\psi_1 - e_2\,\psi_2\right\|^2 - \left\|e_2\,\psi_2 - e_3\,\psi_3\right\|^2 - \left\|e_3\,\psi_3 - e_1\,\psi_1\right\|^2 && (7.80)
\end{aligned}$$

and clearly takes the value zero whenever $e \in \mathcal{E}_e$ or $e \in \mathcal{M}_e \setminus \mathcal{E}_e$. Furthermore, note that $\mathcal{M}_e \setminus \mathcal{E}_e = \mathcal{M}_e \cap \mathcal{N}_e$. The next theorem makes directly use of the manifold stability theorem (Theorem 7.1.3) and shows that for every initially rigid formation, the resulting trajectory will be bounded a strictly positive distance away from $\mathcal{M}_e \cap \mathcal{N}_e$.

Theorem 7.2.1. *For every $e_0 \notin \mathcal{N}_e$ exists an $\epsilon > 0$, such that $\forall\, t \geq 0$, $\|\Phi_e(t, e_0)\|_{\mathcal{M}_e \cap \mathcal{N}_e} > \epsilon$.*

The proof of Theorem 7.2.1 uses the parameterizations of $\mathcal{X}_e$ and $\mathcal{N}_e'$ that we derived in the last section. The conditions that we derive from these parameterizations and from the manifold stability theorem are purely algebraic but unfortunately the calculations are lengthy. To simplify the presentation of the proof we want to state three preliminary lemmas.

Lemma 7.2.3. *For every $e_0 \in \hat{H}(\mathbb{R}^6) \backslash \mathcal{X}_e$ exists an $\epsilon > 0$, such that $\hat{H}(\mathbb{R}^6) \backslash \bar{\mathcal{X}}_{e,\epsilon}$ is invariant.*

Proof. Let us calculate the matrix $\Gamma(e)$ from Theorem 7.1.3 for the invariant set $\mathcal{X}_e$. The Jacobian of the vectorfield $f_e(e)$ evaluated on the set $\mathcal{X}_e$ is

$$\left.\frac{\partial f_e(e)}{\partial e}\right|_{\mathcal{X}_e} = \hat{H}\, \frac{\partial}{\partial e} \left.\begin{bmatrix} e_1\, \psi_1 \\ e_2\, \psi_2 \\ e_3\, \psi_3 \end{bmatrix}\right|_{\mathcal{X}_e} = \hat{H}\ \mathrm{diag}\big\{\psi_i\, I_2 + 2\, e_i\, e_i^T\big\}\big|_{\mathcal{X}_e} \tag{7.81}$$

$$= \hat{H}\, \mathrm{diag}\big\{-d_i^2\, I_2\big\} = \begin{bmatrix} d_1^2\, I_2 & -d_2^2\, I_2 & 0_2 \\ 0_2 & d_2^2\, I_2 & -d_3^2\, I_2 \\ -d_1^2\, I_2 & 0_2 & d_3^2\, I_2 \end{bmatrix}. \tag{7.82}$$

We then obtain $\Gamma(e)$ from the symmetric part of

$$n^T\, \left.\frac{\partial f_e(e)}{\partial e}\right|_{\mathcal{X}_e} n = \frac{1}{2} \begin{bmatrix} -I_2 & I_2 & 0_2 \\ 0_2 & -I_2 & I_2 \end{bmatrix} \begin{bmatrix} d_1^2\, I_2 & -d_2^2\, I_2 & 0_2 \\ 0_2 & d_2^2\, I_2 & -d_3^2\, I_2 \\ -d_1^2\, I_2 & 0_2 & d_3^2\, I_2 \end{bmatrix} \begin{bmatrix} -I_2 & 0_2 \\ I_2 & -I_2 \\ 0_2 & I_2 \end{bmatrix} \tag{7.83}$$

$$= \frac{1}{2} \begin{bmatrix} (d_1^2 + 2\, d_2^2)\ I_2 & -(2\, d_2^2 + d_3^2)\ I_2 \\ (d_1^2 - d_2^2)\ I_2 & (d_2^2 + 2\, d_3^2)\ I_2 \end{bmatrix}, \tag{7.84}$$

where the columns of the matrix n form a basis of the normal space of $\mathcal{X}_e$ which is within the link space $\hat{H}(\mathbb{R}^6)$. The matrix $\Gamma(e)$ is then

$$\Gamma(e) = \frac{1}{4} \begin{bmatrix} (2\, d_1^2 + 4\, d_2^2)\ I_2 & (d_1^2 - 3\, d_2^2 - d_3^2)\ I_2 \\ (d_1^2 - 3\, d_2^2 - d_3^2)\ I_2 & (2\, d_2^2 + 4\, d_3^2)\ I_2 \end{bmatrix} = \left[\begin{array}{c|c} \Gamma_{11}(e) & \Gamma_{12}(e) \\ \hline \Gamma_{12}(e)^T & \Gamma_{22}(e) \end{array}\right]. \tag{7.85}$$

Let γ_1 be the angle between the links e_2 and e_3 of the specified triangle, then we get with the law of cosines

$$d_1^2 = d_2^2 + d_3^2 - 2\, d_2\, d_3\, \cos\gamma_1\,. \tag{7.86}$$

Note that with the law of cosines the following equations hold:

$$2d_1^2 + 4d_2^2 > d_1^2 - 3d_2^2 - d_3^2 \quad \Leftrightarrow \quad d_1^2 + 7d_2^2 + d_3^3 > 0 \tag{7.87}$$

$$2d_2^2 + 4d_3^2 > d_1^2 - 3d_2^2 - d_3^2 \quad \Leftrightarrow \quad -d_1^2 + 5d_2^2 + 5d_3^2 = 4d_2^2 + 4d_3^2 + 2d_2 d_3 \cos\gamma_1 > 0\,. \tag{7.88}$$

It is easy to see that

$$\Gamma_{11}(e) \;=\; \frac{1}{4}\left(2\,d_1^2 + 4\,d_2^2\right)\, I_2 \;\succ\; 0\,. \tag{7.89}$$

and with equations (7.87) and (7.88) we can also easily verify that

$$\Gamma_{22}(e) - \Gamma_{12}(e)^T\,\Gamma_{11}(e)^{-1}\,\Gamma_{12}(e) \;\succ\; 0 \tag{7.90}$$

$$\Leftrightarrow \quad \left(2d_1^2 + 4d_2^2\right)\,\left(2d_2^2 + 4d_3^2\right) \;>\; \left(d_1^2 - 3d_2^2 - d_3^2\right)^2\,. \tag{7.91}$$

Therefore, by the *Schur Complement* $\Gamma(e)$ is a positive definite matrix ([87], Theorem 1.12). Thus by Theorem 7.1.2 exists an $\epsilon > 0$, such that $\hat{H}\left(\mathbb{R}^6\right) \setminus \bar{\mathcal{X}}_{e,\epsilon}$ is invariant. □

The following lemma shows a similar result for the set $\mathcal{M}_e \cap \mathcal{N}_e'$.

Lemma 7.2.4. *Consider the open manifold $\mathcal{N}_e'$. For every $e \in \mathcal{M}_e \cap \mathcal{N}_e'$ the linearized vector field $\frac{\partial f_e(e)}{\partial e}\Big|_{\mathcal{M}_e \cap \mathcal{N}_e'}$ is pointing strictly outward of a tubular ϵ neighbourhood of $\mathcal{N}_e'$.*

Before we come to the proof of Lemma 7.2.4, we want to state an algebraic relationship of the gradients of the potential function.

Lemma 7.2.5. *([27], Lemma 5) For any $e \in \mathcal{M}_e \cap \mathcal{N}_e$ we have that $\psi_1 + \psi_2 + \psi_3 < 0$.*

Lemma 7.2.5 can be proved by considering all possible cases of collinear and collocated equilibria of the link dynamics. With this algebraic relationship we can now move on to the proof of Lemma 7.2.4.

Proof of Lemma 7.2.4. The linearized vector field $\frac{\partial f_e(e)}{\partial e}\Big|_{\mathcal{M}_e \cap \mathcal{N}_e'}$ is given by

$$\frac{\partial f_e(e)}{\partial e}\bigg|_{\mathcal{N}_e'} \;=\; \hat{H}\,\frac{\partial}{\partial e}\begin{bmatrix} e_1\,\psi_1 \\ e_2\,\psi_2 \\ e_3\,\psi_3 \end{bmatrix}\bigg|_{\mathcal{N}_e'} \;=\; \hat{H}\,\mathrm{diag}\big\{\underbrace{\psi_i\,I_2 + 2\,e_i\,e_i^T}_{=:\,\Theta_i}\big\}\Big|_{e \in \mathcal{M}_e \cap \mathcal{N}_e'} \tag{7.92}$$

$$= \begin{bmatrix} -\Theta_1 & \Theta_2 & 0_2 \\ 0_2 & -\Theta_2 & \Theta_3 \\ \Theta_1 & 0_2 & -\Theta_3 \end{bmatrix}_{\mathcal{M}_e \cap \mathcal{N}'_e} . \tag{7.93}$$

For notational convenience the argument $e \in \mathcal{M}_e \cap \mathcal{N}'_e$ is left out in the following calculations. If we want to check whether or not the linearized vector field is pointing strictly outward of a tubular ϵ neighbourhood of $\mathcal{N}'_e$, we have to calculate the matrix

$$\Gamma(e) = n(e)^T \left. \frac{\partial f_e(e)}{\partial e} \right| n(e) \tag{7.94}$$

$$= \begin{bmatrix} e_2^T J & e_3^T J & e_1^T J \end{bmatrix} \begin{bmatrix} -\Theta_1 & \Theta_2 & 0_2 \\ 0_2 & -\Theta_2 & \Theta_3 \\ \Theta_1 & 0_2 & -\Theta_3 \end{bmatrix} \begin{bmatrix} -J\, e_2 \\ -J\, e_3 \\ -J\, e_1 \end{bmatrix} \tag{7.95}$$

$$= \begin{bmatrix} e_2^T J & e_3^T J & e_1^T J \end{bmatrix} \begin{bmatrix} \Theta_1 J\, e_2 - \Theta_2 J\, e_3 \\ \Theta_2 J\, e_3 - \Theta_3 J\, e_1 \\ \Theta_3 J\, e_1 - \Theta_1 J\, e_2 \end{bmatrix} \tag{7.96}$$

$$= e_2^T J \Theta_1 J\, e_2 - e_2^T J\, \Theta_2 J\, e_3 + e_3^T J\, \Theta_2 J\, e_3 - e_3^T J\, \Theta_3 J\, e_1 \tag{7.97}$$

$$+ e_1^T J\, \Theta_3 J\, e_1 - e_1^T J\, \Theta_1 J\, e_2 \,, \tag{7.98}$$

where we $n(p)$ is a basis for $N_p \mathcal{N}'_e \cap \hat{H}\left(\mathbb{R}^6\right)$. Let us look closer at the expression $J\, \Theta_i\, J$.

$$J\, \Theta_i\, J = J\, \psi_i\, I_2\, J + 2\, J\, e_i\, e_i^T\, J = -\psi_i\, I_2 + 2\, J\, e_i\, e_i^T\, J \tag{7.99}$$

Note that in $\mathcal{M}_e \cap \mathcal{N}'_e$ the links are collinear and thus we have for any $i, j, k \in \{1, 2, 3\}$ that

$$e_j^T\, J\, \Theta_i\, J\, e_k = -\psi_i\, e_j^T\, e_k + e_j^T\, J\, e_i\, e_i^T\, J\, e_k = -\psi_i\, e_j^T\, e_k \,. \tag{7.100}$$

Therefore, $\Gamma(e)$ simplifies to

$$\Gamma(e) = \left(e_2^T\, \psi_1\, e_1 + e_3^T\, \psi_2\, e_2 + e_1^T\, \psi_3\, e_3\right) - \left(\psi_1\, \|e_2\|^2 + \psi_2\, \|e_3\|^2 + \psi_3\, \|e_1\|^2\right) . \tag{7.101}$$

Now we evaluate the this expression on $\mathcal{M}_e \cap \mathcal{N}'_e$. Remember that for any $e \in \{\mathcal{M}_e \cap \mathcal{N}'_e\}$ the following two properties hold

$$\text{Lemma 7.2.5:} \qquad \psi_1 + \psi_2 + \psi_3 < 0 \tag{7.102}$$

$$\text{Definition of } \mathcal{M}_e\text{:} \qquad e_1\, \psi_1 = e_2\, \psi_2 = e_3\, \psi_3 \,. \tag{7.103}$$

First we evaluate the first term of $\Gamma(e)$ on $\mathcal{M}_e \cap \mathcal{N}'_e$. For any $e \in \{\mathcal{M}_e \cap \mathcal{N}'_e\}$ equation (7.103) holds and therefore the term in the first bracket of $\Gamma(e)$ is zero:

$$e_2^T \psi_1 e_1 + e_3^T \psi_2 e_2 + e_1^T \psi_3 e_3 \;=\; \underbrace{(e_1+e_2+e_3)^T}_{=\mathbf{0}} e_1 \psi_1 \;=\; 0 \tag{7.104}$$

Let us now look at the second term. We split the proof up in two cases, the case where two robots are collocated and the case where non of them are collocated

<u>case 1:</u> $e \in \{\mathcal{M}_e \cap \mathcal{N}'_e\} \cap \mathcal{X}_e^1$: Suppose robot one and robot two are collocated, that is, $e_1 = \mathbf{0}$, or equivalently $e \in \mathcal{X}_e^1$. Thus we have $\psi_1 = -d_1^2 < 0$ and $e_2 = -e_3$. In this case we know from equation (7.103) that $0 = e_2 \psi_2 = e_3 \psi_3 = -e_2 \psi_3$. Thus we obtain

$$\begin{aligned} \Gamma(e) &= -\left(\psi_1 \|e_2\|^2 + \psi_2 \|e_3\|^2 + \psi_3 \|e_1\|^2\right) && (7.105)\\ &= -\big(-d_1^2 \|e_2\|^2 + e_2^T \underbrace{\psi_2 e_2}_{=0} + \mathbf{0}\big) \;=\; d_1^2 \|e_2\|^2 > 0\,. && (7.106) \end{aligned}$$

The proof for $e_2 = 0$ and $e_3 = 0$ is analogous.

<u>case 2:</u> $e \in \{\mathcal{M}_e \cap \mathcal{N}'_e\} \setminus \{\mathcal{X}_e^1 \cup \mathcal{X}_e^2 \cup \mathcal{X}_e^3\}$: Suppose all three robots are collinear but none of them are collocated. Then for every $e \in \{\mathcal{M}_e \cap \mathcal{N}'_e\} \setminus \{\mathcal{X}_e^1 \cup \mathcal{X}_e^2 \cup \mathcal{X}_e^3\}$ exists $x \in \mathbb{R} \setminus \{-1, 0\}$ such that

$$e_2 \;=\; x\, e_1 \qquad \text{and} \qquad e_3 \;=\; -e_1 - e_2 \;=\; -(1+x)\, e_1\,. \tag{7.107}$$

From now on the quantifiers for e and x will be left out. From equations (7.107) and (7.103) follows then

$$\psi_2 \;=\; \frac{\psi_1}{x} \qquad \text{and} \qquad \psi_3 \;=\; -\frac{\psi_1}{1+x}\,. \tag{7.108}$$

If we plug equation (7.108) in equation (7.102) we get the condition

$$\psi_1 \underbrace{\left(1 + \frac{1}{x} - \frac{1}{1+x}\right)}_{=:\,\lambda_1(x)} \;<\; 0 \;\Leftrightarrow\; \operatorname{sign}(\psi_1) = -\operatorname{sign}(\lambda_1(x))\,. \tag{7.109}$$

We can reformulate $\Gamma(e)$ with the scalar x and the relations (7.108) to

$$\begin{aligned}\Gamma(e) &= -2\left(\psi_1 \left\|e_2\right\|^2 + \psi_2 \left\|e_3\right\|^2 + \psi_3 \left\|e_1\right\|^2\right) && (7.110)\\ &= -2\left\|e_1\right\|^2 \left(\psi_1 x^2 + \psi_2 (1+x)^2 + \psi_3\right) && (7.111)\\ &= -2\left\|e_1\right\|^2 \psi_1 \underbrace{\left(x^2 + \frac{(1+x)^2}{x} - \frac{1}{1+x}\right)}_{=:\lambda_2(x)} && (7.112)\end{aligned}$$

We want $\Gamma(e)$ to be positive, which is equivalent to $\operatorname{sign}(\psi_1) \stackrel{!}{=} -\operatorname{sign}(\lambda_2(x))$. But we also know that $\operatorname{sign}(\psi_1) = -\operatorname{sign}(\lambda_1(x))$. Therefore, if

$$\operatorname{sign}(\lambda_1(x)) = \operatorname{sign}(\lambda_2(x)) \tag{7.113}$$

holds, then $\Gamma(e)$ is positive. We can easily check condition (7.113):

$$\lambda_1(x) \cdot \lambda_2(x) = \frac{\left(\left(x+\frac{1}{2}\right)^2 + \frac{3}{4}\right)^3}{x^2\,(1+x)^2} > 0 \tag{7.114}$$

Thus for any $x \in \mathbb{R} \setminus \{-1, 0\}$, $\Gamma(e)$ is positive.

If we summarize both cases we can say that for any $e \in \mathcal{M}_e \cap \mathcal{N}_e'$, $\Gamma(e) > 0$, or equivalently, for any $e \in \mathcal{M}_e \cap \mathcal{N}_e'$ the linearized vector field $\frac{\partial f_e(e)}{\partial e}\Big|_{\mathcal{M}_e \cap \mathcal{N}_e'}$ is pointing strictly outward of a tubular ϵ neighbourhood of $\mathcal{N}_e'$. □

After these extensive algebraic calculations we can use Lemma 7.2.3 and Lemma 7.2.4 to prove Theorem 7.2.1.

Proof of Theorem 7.2.1. Since the sensor graph of the directed triangle is cooperative, we have by Theorem 5.3.2 that for any initial condition e_0 the sublevel set

$$\Omega(V(e_0)) = \left\{ e \in \hat{H}\left(\mathbb{R}^6\right) \,\middle|\, V(e) \leq V(e_0) \right\} \tag{7.115}$$

is a compact and invariant set. The set $\mathcal{M}_e \cap \mathcal{N}_e$ is a closed and invariant set. Thus the set

$$\mathcal{M}_e \cap \mathcal{N}_e \cap \Omega(V(e_0)) \tag{7.116}$$

is also a compact and invariant set. It can be split up into the disjoint sets $\mathcal{M}_e \cap \mathcal{X}_e \cap \Omega(V(e_0))$ and $\mathcal{M}_e \cap \mathcal{N}'_e \cap \Omega(V(e_0))$. By Lemma 7.2.3 we can find an $\epsilon_1 > 0$, such that $\hat{H}\left(\mathbb{R}^6\right) \setminus \bar{\mathcal{X}}_{e,\epsilon_1}$ is invariant.

In order to continue consider an $\epsilon > 0$ and the tubular ϵ neighbourhood of $\mathcal{N}'_e$ at $e \in \{\mathcal{M}_e \cap \mathcal{N}'_e \cap \Omega(V(e_0))\}$, that is, the set

$$\begin{aligned} \mathcal{S}_\epsilon \;=\; & \Big\{ \bar{e} \in \hat{H}\left(\mathbb{R}^6\right) \Big| \; \bar{e} \,=\, e + \bar{\epsilon}\, n(e)\,,\, e \in \{\mathcal{M}_e \cap \mathcal{N}'_e \cap \Omega(V(e_0))\}\;,\; n(e) \in N_e\mathcal{N}'_e\,, \\ & \|n(e)\| = 1\,,\, \bar{\epsilon} \in (0,\epsilon) \Big\}\,. \end{aligned} \tag{7.117}$$

Since $\mathbb{R}^m \setminus \bar{\mathcal{X}}_{e,\epsilon_1}$ is invariant, a solution $\Phi_e(t, e_0)$ with $e_0 \notin \mathcal{N}_e$ cannot enter $\mathcal{N}_e$ via the set $\mathcal{X}_e$, but only via the boundary of the tubular ϵ neighbourhood of $\mathcal{N}'_e$. By Theorem 5.3.2 we also know that the solution $\Phi_e(t, e_0)$ approaches the set $\mathcal{W}_e = \{\mathcal{M}_e \cap \Omega(V(e_0))\}$ as $t \to \infty$. This again implies that, if the trajectory $\Phi_e(t, e_0)$ approaches $\mathcal{N}'_e$, then it must enter $\mathcal{S}_\epsilon$. But by Lemma 7.2.4 we know that the linearized vector field is pointing strictly outward of $\mathcal{S}_\epsilon$ and that the matrix $\Gamma(e)$ of Theorem 7.1.3 is positive definite for every e in the compact invariant set $\mathcal{M}_e \cap \mathcal{N}'_e \cap \Omega(V(e_0))$. By Theorem 7.1.3 this means that there exists an $\epsilon_2 > 0$, such that a solution $\Phi_e(t, e_0)$ with $e_0 \notin \mathcal{N}_e$ cannot enter $\bar{\mathcal{S}}_{\epsilon_2}\ \forall\, t \geq 0$.

The two cases $\mathcal{M}_e \cap \mathcal{X}_e \cap \Omega(V(e_0))$ and $\mathcal{M}_e \cap \mathcal{N}'_e \cap \Omega(V(e_0))$ are illustrated qualitatively in Figure 7.7. If we merge the two cases, we have that

$$(\forall\, e_0 \notin \mathcal{N}_e)\;\; (\forall\, t \geq 0)\;\; \|\Phi_e(t, e_0)\|_{\mathcal{M}_e \cap \mathcal{N}_e} \;>\; \min\{\epsilon_1\,,\, \epsilon_2\}\;, \tag{7.118}$$

which completes the proof. □

7.2.3 The Exact Region of Attraction for $\mathcal{E}_e$

From Chapter 7 we know that locally for $e_{10} \in \Omega(\rho)$, $\Phi_e(t, e_{10})$ converges exponentially to $\mathcal{E}_e$, and globally for $e_{20} \in \hat{H}\left(\mathbb{R}^6\right)$, $\Phi_e(t, e_{20})$ is bounded in $\Omega(V(e_0))$ and converges to either $\mathcal{E}_e$ or to $\mathcal{M}_e \setminus \mathcal{E}_e = \{\mathcal{M}_e \cap \mathcal{N}_e\}$. In the case that $e_{30} \notin \{\Omega(\rho) \cup \mathcal{N}_e\}$, Theorem 7.2.1 shows that the corresponding trajectory $\Phi_e(t, e_{30})$ will always be bounded away from $\mathcal{M}_e \cap \mathcal{N}_e$. These three situations are illustrated in Figure 7.8. If we combine these results, the obvious conclusion is that $\Phi_e(t, e_{30})$ is bounded and has to converge to $\mathcal{E}_e$, and while doing so, $\Phi_e(t, e_{30})$ has to enter

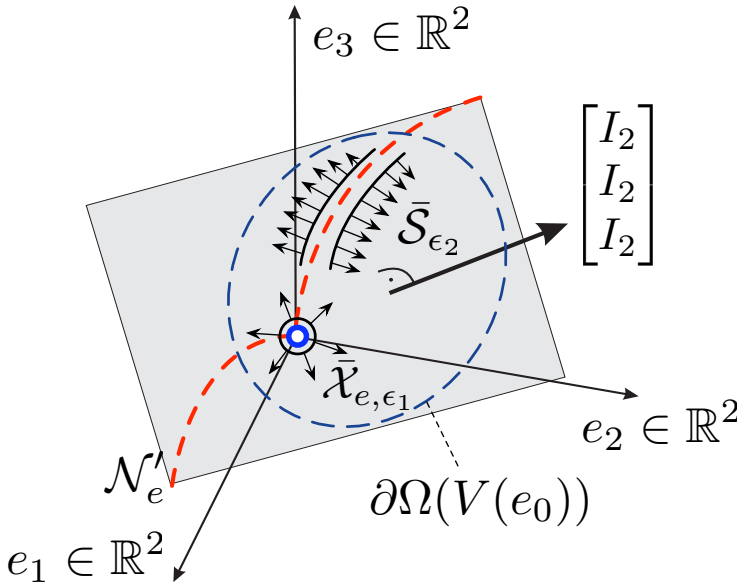

Figure 7.7: Overflowing invariance of $\bar{\mathcal{S}}_{\epsilon_2}$ and $\bar{\mathcal{X}}_{e,\epsilon_1}$

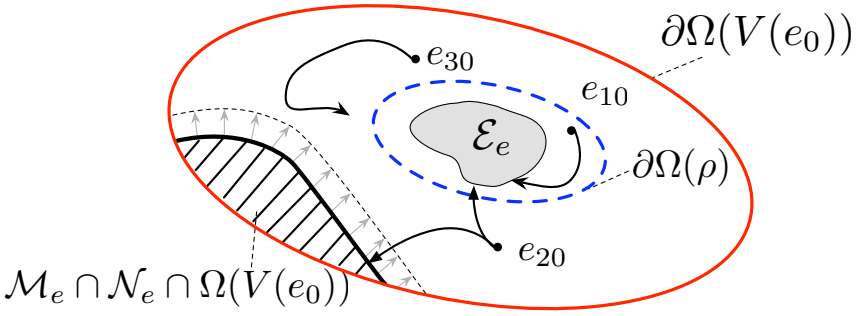

Figure 7.8: Possible trajectories arising from the results in Chapter 7 and Theorem 7.2.1

$\Omega(\rho)$ in a finite time. Let us first establish a lemma which states a finite time convergence of $\Phi_e(t, e_{30})$ to $\Omega(\rho)$

Lemma 7.2.6. *Consider an initial condition $e_0 \in \hat{H}(\mathbb{R}^6) \setminus \{\Omega(\rho) \cup \mathcal{N}_e\}$. The corresponding solution $\Phi_e(t, e_0)$ of the link dynamics enters $\Omega(\rho)$ in finite time.*

Proof. As usual the sum of all potential functions $V(e)$ is a Lyapunov function candidate $V(e)$ and its derivative along trajectories is

$$\dot{V}(e) \;=\; -\|e_1\,\psi_1 - e_2\,\psi_2\|^2 - \|e_2\,\psi_2 - e_3\,\psi_3\|^2 - \|e_3\,\psi_3 - e_1\,\psi_1\|^2\,. \tag{7.119}$$

Clearly $\dot{V}(e)$ is zero iff $e \in \mathcal{M}_e = \mathcal{E}_e \cup \{\mathcal{M}_e \cap \mathcal{N}_e\}$. By Theorem 7.2.1 we have that $\forall\, t \geq 0$, $\Phi_e(t, e_0)$ is bounded away from $\mathcal{M}_e \cap \mathcal{N}_e$ and thus we have that $\dot{V}(e)$ is zero if and only if $\Phi_e(t, e_0) \in \{\mathcal{M}_e \setminus \mathcal{N}_e\} = \mathcal{E}_e$. Therefore, $V\big(\Phi_e(t, e_0)\big)$ is always decreasing $\forall\, t \geq 0$.

We know show that there is a finite time in which $V\big(\Phi_e(t, e_0)\big) \leq \rho$, or equivalently, in which $\Phi_e(t, e_0)$ enters $\Omega(\rho)$. By Theorem 7.2.1 we can define δ as follows:

$$(\forall\, e_0 \notin \mathcal{N}_e) \quad \delta := \inf_{t \geq 0} \|\Phi_e(t, e_0)\|_{\mathcal{M}_e \cap \mathcal{N}_e} > 0\,. \tag{7.120}$$

Consider the two sets

$$\Lambda \;=\; \left\{ e \in \hat{H}\left(\mathbb{R}^6\right) \setminus \{\Omega(\rho) \setminus \partial\Omega(\rho)\} \,\middle|\, \|e\|_{\mathcal{M}_e \cap \mathcal{N}_e} \geq \delta \right\} \tag{7.121}$$

$$\Omega(V(e_0)) \;=\; \left\{ e \in \hat{H}\left(\mathbb{R}^6\right) \,\middle|\, V(e) \leq V(e_0) \right\}. \tag{7.122}$$

For every initial condition $e_0 \in \hat{H}(\mathbb{R}^6)$, $\Omega(V(e_0))$ is a compact and invariant set (Theorem 5.3.2) and Λ is a closed set, which is disjoint with $\mathcal{M}_e$. The sets are illustrated in Figure 7.9.

Let us assume that there exists no finite time in which a solution $\Phi_e(t, e_0)$ with $e_0 \in \Lambda$ converges to the interior of $\Omega(\rho)$, that is, $\Phi_e(t, e_0) \in \Lambda \;\; \forall\, t \in [0, \infty)$. Note that in addition $\Phi_e(t, e_0)$ is $\forall t \geq 0$ bounded in the compact set $\Lambda \cap \Omega(V(e_0))$. This allows us to bound $\dot{V}(e(t))$ uniformly from above by a strictly negative number, namely

$$\sigma \;=\; -\min_{e \in \Lambda \cap \Omega(c)} \left[\|e_1\,\psi_1 - e_2\,\psi_2\|^2 + \|e_2\,\psi_2 - e_3\,\psi_3\|^2 + \|e_3\,\psi_3 - e_1\,\psi_1\|^2\right] \;<\; 0\,. \tag{7.123}$$

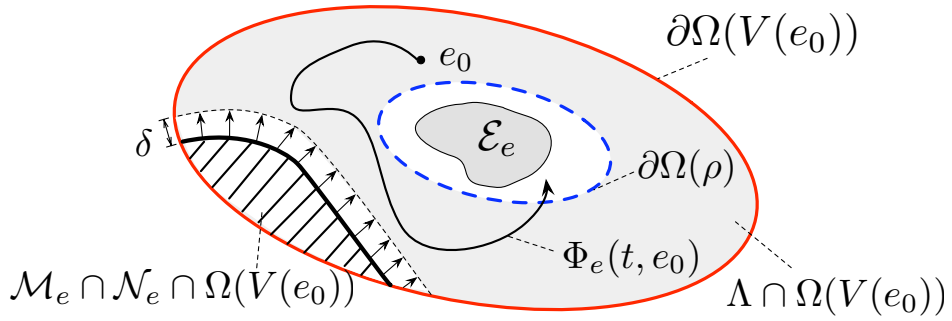

Figure 7.9: A trajectory with $e_0 \notin \{\Omega(\rho) \cup \mathcal{N}_e\}$ enters $\Omega(\rho)$ in a finite time

Thus we have

$$(\forall\, t \geq 0) \;\; \dot{V}(e(t)) \;\leq\; -\sigma \;\;\Rightarrow\;\; (\forall\, t \geq 0) \;\; V(e(t)) \;\leq\; V(e(0)) - \sigma\, t\,. \tag{7.124}$$

But this is impossible because $V(e(t))$ is nonnegative. Thus our assumption is wrong and $\Phi_e(t, e_0)$ enters $\Omega(\rho)$ in finite time, as shown in Figure 7.9. □

We are now ready to show that $\hat{H}\,(\mathbb{R}^6) \setminus \mathcal{N}_e$ is the exact region of attraction of the target formation $\mathcal{E}_e$ and that any trajectory starting off $\mathcal{N}_e$ converges exponentially to $\mathcal{E}_e$.

Theorem 7.2.2. *The target formation $\mathcal{E}_e$ is exponentially stable w.r.t. to the link dynamics and with $\hat{H}\,(\mathbb{R}^6) \setminus \mathcal{N}_e$ as exact region of attraction.*

Proof. By the preceding lemma we know that for an initial condition $e_0 \in \hat{H}\,(\mathbb{R}^6) \setminus \mathcal{N}_e$ the corresponding solution $\Phi_e(t, e_0)$ enters $\Omega(\rho)$ in a finite time. By Corollary 5.4.1 we know that the set $\mathcal{E}$ is exponentially stable with $\Omega(\rho)$ as guaranteed region of attraction. Therefore, the set $\mathcal{E}$ is asymptotically stable w.r.t. to the link dynamics, the region of attraction is given by $\hat{H}\,(\mathbb{R}^6) \setminus \mathcal{N}_e$, and the overall convergence rate is exponential. The set $\hat{H}\,(\mathbb{R}^6) \setminus \mathcal{N}_e$ is the exact region of attraction for $\mathcal{E}_e$ since $\mathcal{N}_e$ is an invariant set which is disjoint with $\mathcal{E}_e$. □

The overall picture, as we derived it in this chapter, is as follows: A trajectory of the link dynamics with $e_0 \notin \{\Omega(\rho) \cup \mathcal{N}_e\}$ is bounded within $\Omega(V(e_0))$, is bounded a distance δ away from $\mathcal{M}_e \cap \mathcal{N}_e \cap \Omega(V(e_0))$, enters $\Omega(\rho)$ in a finite time, and then converges exponentially to

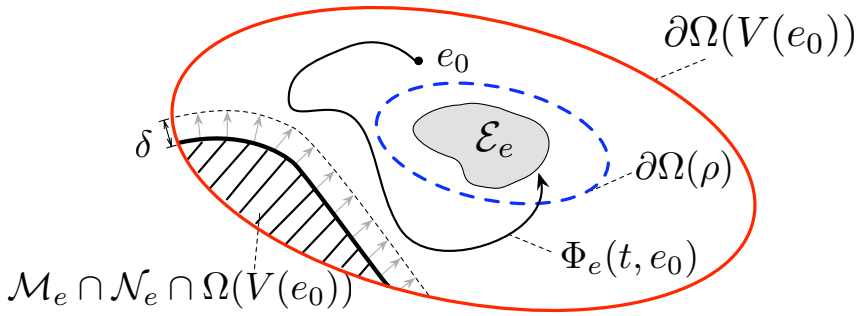

Figure 7.10: A possible trajectory of the link dynamics with $e_0 \notin \{\Omega(\rho) \cup \mathcal{N}_e\}$

the target formation $\mathcal{E}_e$. Such a trajectory is illustrated in Figure 7.10. Note that this Figure is slightly different from the Figure 7.1 at the beginning of this chapter. The main difference is that Figure 7.1 implies that for an initially rigid formation $(\mathcal{G}, e_0)$, the corresponding trajectory $\Phi_e(t, e_0)$ is always be bounded away a fixed distance from the set $\mathcal{Q}$, which is the set of not rigid formations. The set $\mathcal{Q}$ corresponds in the case of the directed triangle to the set $\mathcal{N}_e$. If we want to fulfill the scenario illustrated in Figure 7.1, then we have to show additionally that a trajectory resulting from an initial condition $e_0 \notin \mathcal{N}_e$ is bounded a strictly positive distance away from $\mathcal{N}_e$.

Theorem 7.2.3. *For every $e_0 \in \hat{H}(\mathbb{R}^6) \setminus \mathcal{N}_e$ exists an $\epsilon > 0$, such that $\|\Phi_e(t, e_0)\|_{\mathcal{N}_e} > \epsilon$ $\forall\, t \geq 0$.*

Proof. By Lemma 7.2.6 we know that for every $e_0 \in \hat{H}(\mathbb{R}^6) \setminus \mathcal{N}_e$ exists a $T > 0$ such that for all $t \geq T$, $\Phi_e(t, e_0) \in \Omega(\rho)$. We also know that $\mathcal{N}_e$ is invariant. Therefore, for all $t \in [0, T]$ the trajectory $\Phi_e(t, e_0)$ cannot be in $\mathcal{N}_e$, because then $\Phi_e(t, e_0)$ is in $\mathcal{N}_e$ $\forall\, t \geq 0$.

In order to continue note that $\Phi_e(t, e_0)$ is bounded within the compact sublevel set $\Omega(V(e_0))$. The set $\mathcal{N}_e \cap \Omega(V(e_0))$ is compact and also the trajectory $\Phi_e(t, e_0)$ with $t \in [0, T]$ is itself a compact set, as shown in Figure 7.11. Consider a sequence $\{e_{t_i}\}$ in the latter set and another sequence $\{n_i\}$ in $\mathcal{N}_e \cap \Omega(V(e_0))$. Each of theses sequences is contained in a compact set and, by the Bolzano-Weierstrass theorem ([86], Theorem 3-13), each has an

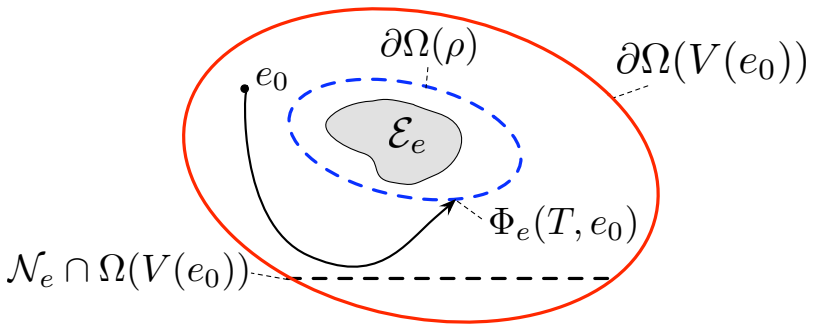

Figure 7.11: The compact sets $\mathcal{N}_e \cap \Omega(V(e_0))$ and $\Phi_e(t, e_0)$ with $t \in [0, T]$

accumulation point in this compact set. The two accumulation points of the these sequences are either identical, which means that the trajectory $\Phi_e(t, e_0)$ and $\mathcal{N}_e \cap \Omega(V(e_0))$ intersect, or they are a positive distance apart. As already mentioned before, the trajectory $\Phi_e(t, e_0)$ cannot intersect the invariant set $\mathcal{N}_e$ and thus we have that for $e_0 \in \hat{H}(\mathbb{R}^6) \setminus \mathcal{N}_e$ exists an $\epsilon > 0$ such that $\|\Phi_e(t, e_0)\|_{\mathcal{N}_e} > \epsilon \ \forall\, t \geq 0$. □

If we combine the exact region of attraction of $\mathcal{E}_e$ with Theorem 5.4.2, which gave us the exponential stability of the z-dynamics, we can conclude that initially not collinear robots are never collinear $\forall\, t \geq 0$, converge exponentially to the specified triangular formation, and become stationary. In the case that the robots are initially collinear, Lemma 7.2.2 says that they will stay collinear $\forall\, t \geq 0$. This is our second main result, which we formulate in terms of rigidity, because we have the intuition that this result can be generalized to more complicated setups beyond the directed triangle.

Theorem 7.2.4. *Main Result II:*
Consider the directed triangle (Example 3.1.3) and the gradient control law (3.16) obtained from the potential function $V_i(\omega) = \frac{1}{4}\omega^2$. *Iff the initial formation* $(\mathcal{G}, e_0)$ *is infinitesimally rigid, the formation is infinitesimally rigid* $\forall\, t \geq 0$ *and the robots will converge exponentially to a finite limit point in the target formation* $\left(\mathcal{G}, r_{\mathcal{G}}^{-1}(\mathbf{d})\right)$.

Theorem 7.2.4 is a global result for the directed triangle, in the sense that it gives the

exact region of attraction for the target formation $\left(\mathcal{G}, r_{\mathcal{G}}^{-1}(\mathbf{d})\right)$. Our second main result seems to be very obvious, but the extension of the local result in the sublevel set $\Omega(\rho)$ to a global stability result is by no means straightforward. However, the global analysis gives us a deeper insight in the problem and we can give the exact region of attraction not only for the target formation in general, but also for its disjoint components.

We have already mentioned on page 36 that the target formation specified by the side lengths is not unique and defines two triangles with different orientation. One of these triangles has the orientation $e_1^T J\, e_2 < 0$ (clockwise) and the other $e_1^T J\, e_2 > 0$ (counterclockwise). The set $e_1^T J\, e_2 = 0$ corresponds to the set of collinear robots and is invariant. Therefore, if the robots have initially a (counter)clockwise orientation, that is, $e_1(0)^T J\, e_2(0) \underset{(>)}{<} 0$, then this orientation is invariant and the robots converge to the target formation with this orientation.

7.2.4 Remarks to the Global Stability Analysis

This short section completes and concludes the global stability analysis performed in this chapter and points out alternative proof techniques

Behavior of Collinear Robots

The question is still open, how a trajectory resulting from initially collinear robots will evolve. For completeness we answer this question briefly and approach it in the link space. Note that, if $e_0 \in \mathcal{N}_e$, then the trajectory $\Phi_e(t, e_0)$ is bounded within $\Omega(V(e_0))$ (Theorem 5.3.2) and remains on the invariant set $\mathcal{N}_e$ for all time (Lemma 7.2.2). If $e_0 \in \mathcal{N}_e'$, then $\Phi_e(t, e_0)$ is always bounded away from $\mathcal{X}_e$ (Lemma 7.2.3) and will converge to the largest invariant set contained in

$$\mathcal{M}_e \cap \mathcal{N}_e' \cap \Omega(V(e_0)) \;=\; \{e \in \Omega(V(e_0)) \cap \mathcal{N}_e' \,|\, e_1\,\psi_1 = e_2\,\psi_2 = e_3\,\psi_3\}\;. \tag{7.125}$$

If the target formation is specified, such that $d_1 \neq d_2 \neq d_3$, then a point $\bar{e}$ in the limit set of $\Phi_e(t, e_0)$, which is a subset of $\mathcal{M}_e \cap \mathcal{N}_e' \cap \Omega(V(e_0))$, has the property $\bar{e}_i\,\bar{\psi}_i \neq 0$. Thus the steady state velocity of each robot is not zero and the robots do not converge to a stationary collinear point. In the other case where, for example, $d_1 = d_2 = d > 0$ are the specified

lengths for link e_1 and link e_2, a possible collinear limit point is for example $\bar{e} = [\bar{e}_1\,,\,\bar{e}_2\,,\,\mathbf{0}]^T$ with $\|\bar{e}_1\| = d = \|\bar{e}_2\|$. This point is an equilibrium of both the link and the z-dynamics and an analysis based on linearization shows that its region of attraction is a thin set of measure zero, in fact it is a single trajectory. Summarizing we can say that a generic and collinear initial condition will almost always result in collinear robots which are moving with a constant speed along the line where they are assembled.

Modifications for Irregular Potential Functions

In the case of irregular potential functions Lemma 7.2.3 is trivially satisfied because the robots will always be bounded away from $\mathcal{X}_e$. Since Lemma 7.2.5 is also satisfied for irregular potential functions ([28], Lemma 5), Lemma 7.2.4 and the resulting Theorem 7.2.1 can be proved analogously. All the other results follow from Theorem 7.2.1, just as in the case of the regular potential function $V_i(\omega) = \frac{1}{4}\,\omega^2$. Therefore, irregular potential functions do not provide additional difficulties in the global stability analysis of the directed triangle.

Alternative proof techniques of Theorem 7.2.1

The result that initially not collinear robots always converge the the specified triangle has also been shown by [25, 27, 28] using a different approaches. These references also used the function $V(e)$ as either a Lyapunov function or in the context of the invariance principle. The natural obstacle that these references stumble on is that $\dot{V}(e) = 0$ does not imply $e \in \mathcal{E}_e$ or a convergence $\Phi(t, e_0) \to \mathcal{E}_e$. An additional result similar to Theorem 7.2.1 has to be shown, which is basically an instability result of the line set $\mathcal{N}_e$.

We established this result via the manifold stability theorem (Theorem 7.1.3) via a linearization of the vector field. Alternatively we could have looked for a Lyapunov function which is related to the distance to the line set $\mathcal{N}_e$ and which is always increasing close to $\mathcal{N}_e$. A natural candidate for such a Lyapunov function is the function parametrizing $\mathcal{N}_e$, namely $F(e) = e_1^T\,J\,e_2$. Reference [25] and [27, 28] performed such an approach using either the area of the triangle or $\det\big[e_1\,,\,e_2\big]$ as Lyapunov function. Note that both functions are equivalent

to our function $F(e)$. This approach results very quickly in Theorem 7.2.1 and proves it way easier than the manifold stability theorem, which involves extensive algebraic calculations and which would fail if the linearization takes the value zero.

But similar to the case of stability of an equilibrium point $x = \mathbf{0}$, where the function $\|x\|^2$ is rarely a suitable Lyapunov function, a function similar to $F(e)$ has to be found first. Our approach is superior in the sense that it provides an algebraic test, which depends on the vector field only and not on an additional Lyapunov function. However, since we have to evaluate a definiteness condition of a state dependent matrix, it is questionable whether or not the manifold stability theorem can be applied successfully to more complicated formations, where the linearization of the vector field could take the value zero and where invariant sets are either no manifolds at all or have more complicated parametrizations than $e_1^T J\, e_2 = 0$. At the end of the next and final chapter, we present an idea for a possible extension of the manifold stability theorem, which possibly simplifies its application.

Chapter 8

Conclusions

8.1 Summary of Results

This thesis studies the formation control problem for autonomous robots. In Chapter 3 the formation control is specified as a stabilization problem of an infinitesimally rigid target formation by distributed control. We propose a general control law that is capable of solving this stabilization problem and that depends on the graph matrices only.

In Chapter 5 we approach the formation control problem as a set stabilization problem in the link space and relate it for an undirected sensor graph to an optimal control problem. In order to extend the idea of a common optimal goal to directed sensor graph, we introduce the notion of a cooperative graph via a dissipation equality and identify some cooperative and non-cooperative graphs. For cooperative graphs we derive a local exponential stability result of the target formation together with a guaranteed region of attraction.

Finally in Chapter 7, we derive a stability and instability theorem for differentiable manifolds, which allows us to obtain the exact region of attraction for the benchmark example of the directed triangle.

The main results and contributions of this thesis are as follows:

- Formulation of a potential function based formation control law for directed sensor graphs in dependence of the incidence and the outgoing edge matrix of the graph.

- Identification of an inverse optimal control problem for undirected sensor graphs, which is related to graph rigidity and to stability of the target formation.
- Extension of the inverse optimality result to directed sensor graphs via the definition of a cooperative graph in a dissipation equality.
- Identification of directed cycles and directed open chain graphs as cooperative graphs.
- Proof of the exponential stability of the target formation for cooperative graphs together with a guaranteed region of attraction that depends on rigidity of the formation.
- Derivation of a manifold stability and instability theorem based on linearization.
- Global stability analysis of three robots interconnected in a directed cyclic graph which should form a triangular formation.

8.2 Future Work

The results of this thesis could be extended in different ways. A very interesting system theoretic question arising from Chapter 3 is the following: All the referenced formation and consensus control laws which match the setup of Figure 3.4 consider either kinematic points or double integrators as dynamics of the autonomous robots. If each robot has now more complicated or higher order dynamics the question arises whether the very same controller $u = -\hat{O}\, C\left(\hat{H}\, z\right)$ also stabilizes the multi-robot system. Is it possible to derive an either geometric or dissipativity based parameterization of the system class of a single robot for which the the controller $u = -\hat{O}\, C\left(\hat{H}\, z\right)$ stabilizes the overall system? Reference [24], for example, shows that strict passivity of each robot is a sufficient but also conservative condition for the stability of the overall system. Such a study would be of great importance in order to extend the results of this thesis and the mentioned references to real world models of autonomous robots.

The results of Chapter 5 can be extended as follows. We showed that the distributed gradient control law is an inverse optimal control, that means, it can be related to an optimal control problem. But probably also a converse theorem may realizable, that is, to set up an optimal formation control problem whose solution is a distributed control stabilizing the robots to the target formation. The recent result [88] shows under which conditions the solution of an LQR problem is a distributed control law corresponding to a certain interconnection structure and may serve as a starting point.

The definition of a cooperative graph in Chapter 5 is such that the robots' closed-loop dynamics behave as if the graph was undirected. This definition is quite restrictive, as we can see from the necessary condition in Lemma 5.3.2, and could be extended to capture a wider class of directed graphs. To give an example, the graph in Figure 2.1 has the property that the derivative of $V(e)$ along the trajectories of the link dynamics is

$$\dot{V}(e) \;=\; -\mathbf{\Psi}(e)^T\, R_{\mathcal{G}}(e)\, R_{\mathcal{G}}(e)^T\, \mathbf{\Psi}(e) + 2\,\left(e_1\,\nabla V_1 - e_4\,\nabla V_4\right)\, e_5\,\nabla V_5\,, \tag{8.1}$$

where we omitted the argument in the gradients of the potential functions. The definition of a cooperative graph may be extendable, for example, with an additional weighting of the single links, to capture the graph in Figure 2.1. Since simulation studies show us that the robots converge either to the target formation or to a non-rigid formation, an extended definition of a cooperative graph should in particular identify the set $\mathcal{W}_e$ as the positive limit set of the link dynamics.

Another idea to attack the formation control problem from the optimal control side is not to look for an underlying optimality principle of the overall system. From a game theoretic viewpoint the formation control problem may also be modeled as a non-cooperative game. Figure 5.9, for example, can be seen as a modified version of the pursuer-evader game [89] where the robots correspond to the players. The main difference to the the classical pursuer-evader game is, of course, that robot 2's strategy is not to escape from robot 1. Thus in a game theoretic approach the first questions to answer are the identification of the players and their strategies. So far the idea of game theory has only entered formation control in [90], but unfortunately with the use of global coordinates and without an analytical solution.

The global stability analysis in Chapter 7 based on linearization has both advantages and disadvantages compared to a Lyapunov based analysis. The main drawback of Theorem 7.1.3 are the conservativeness of the result and the complicated calculations in its application. By considering not the tubular neighbourhood of a manifold but rather an ellipsoidal neighbourhood, it may be possible to derive the conditions of Lyapunov's first method (equation (6.26)) for manifolds, which are less conservative and probably result in easier calculations.

Of course, the most prestigious problem to attack in the field of formation control, is a global stability result similar to Theorem 7.2.4, but for any infinitesimally rigid target formation. Obviously such a result is extremely hard to prove, if it is feasible at all.

Summarizing we can say, that multi-robot systems in general, and formation control in particular, constitute a wide and active research area with lots of interesting and promising problems, that are challenging both in fundamental theory and in their applications.

Glossary

$\hat{A}$	$:= A \otimes I_2$	25
$\bar{A}$	$:= \mathcal{A} \cup \partial\mathcal{A}$	52
circ	circulant matrix	92
D	domain where the right-hand side of a dynamical system is defined	51
$\mathcal{E}_e$	target formation as equilibrium of the link dynamics	73
$\mathcal{E}_z$	target formation as equilibrium of the z-dynamics	72
$F(A)$	image of the set A under the mapping F	7
$(\mathcal{G}, z)$	framework	21
$(\mathcal{G}, e)$	formation	25
$\mathcal{G}$	(sensor) graph	17
H	incidence matrix of a directed graph	18
H_u	incidence matrix of an undirected graph	20
$\hat{H}(\mathcal{Z})$	link space for dynamics obtained by irregular potential functions	72
I_n	identity matrix of $\mathbb{R}^n$	25
$\mathbf{1}$	vector of appropriate dimension with a 1 in each component	19
$\mathbf{I}_2$	$:= \mathbf{1} \otimes I_2$	43
I_0	maximum interval of existence of a dynamical system	51
m	number of edges, respectively links in the graph	17
$\mathcal{M}_e$	equilibria of the link dynamics, set of equal velocities	79
n	number of nodes in the graph, respectively number of robots	17
$\nabla f(x)$	$:= \left[\frac{\partial f(x)}{\partial x_1)}, \ldots, \frac{\partial f(x)}{\partial x_2}\right]$	38

$\mathcal{N}_\epsilon$	tubular ϵ neighbourhood of the embedded submanifold $\mathcal{N}$	124
$\partial\mathcal{N}_\epsilon$	boundary $\mathcal{N}_\epsilon$	125
$\bar{\mathcal{N}}_\epsilon$	$:= \mathcal{N}_\epsilon \cup \partial\mathcal{N}_\epsilon$	125
N_i	neighbour set of node i	17
$\|x\|$	$:= \|x\|_2 = \sqrt{\sum_i x_i^2}$, standard euclidean norm	22
$\|x\|_\infty$	$:= \|x\|_\infty = \max_i \|x_i\|$, infinity norm	73
$\mathcal{N}_z$	line set in the z-space	139
$\mathcal{N}_e$	line set in the e-space	139
$\mathcal{N}'_e$	$:= \mathcal{N}_e \setminus \mathcal{X}_e$	140
O	outgoing edge matrix	20
$\Omega(c)$	sublevel set of the function V	11
$\Omega(V(e_0))$	invariant sublevel set for cooperative graphs	88
$\mathcal{Q}$	set of not rigid formations	98
$r_\mathcal{G}(z)$	rigidity function of the framework $(\mathcal{G}, z)$	21
$\frac{\partial r_\mathcal{G}(z)}{\partial z}$	rigidity matrix of the framework $(\mathcal{G}, z)$	23
$v(e)$	rigidity function of the formation $(\mathcal{G}, e)$	26
$R_\mathcal{G}(e)$	$:= \operatorname{diag}\left\{e_i^T\right\} \hat{H}_u$, rigidity matrix of the formation $(\mathcal{G}, e)$	26
$\left(\mathcal{G}, v^{-1}(\mathbf{d})\right)$	$= \left(\mathcal{G}, r_\mathcal{G}^{-1}(\mathbf{d})\right)$, target formation	26
U	ingoing edge matrix	20
$V^{-1}(c)$	level set/pre-image set of the function V	9
$\mathcal{W}_e$	positive limit set of link dynamics for cooperative graphs	88
$\mathcal{X}_e$	set of collocated robots in the e-space	79
$\mathcal{X}_e^i$	$:= \left\{ e \in \hat{H}\left(\mathbb{R}^{2n}\right) \middle\vert\ e_i = \mathbf{0} \right\}$	72
$\mathcal{X}_z$	set of collocated robots in the z-space	72
$\mathcal{X}_z^i$	$:= \left\{ z \in \mathbb{R}^{2n} \middle\vert\ e_i = \mathbf{0}\,,\ e = \hat{H}\, z \right\}$	69
$\mathcal{Z}$	state space for dynamics obtained by irregular potential functions	69

List of Figures

Bibliography

[1] A. Okubo. Dynamical aspects of animal grouping: Swarms, schools, flocks and herds. *Advances in Biophysics*, 22:1–94, 1986.

[2] S. Hubbard, B. Barak, and S. Sigurdson. A model of the formation of fish schools and migrations of fish. *Ecological Modeling*, 174:35–37, 2004.

[3] D. Grunbaum and A. Okubo. Modelling social animal aggregations. *Fontiers in Theoretical Biology*, (296-325), 1994.

[4] S. Janson, M. Middendorf, and M. Beekman. Honey bee swarms: How do scouts guide a swarm of uniformed bees. *Animal Behavior*, 70(1):349–358, 2005.

[5] D. J. Low, K. M. Passino, and M. M. Polycarpou. Following the crowd. *Nature*, 407:465–466, 2000.

[6] T. Viscek. A question of scale. *Nature*, page 421, 411.

[7] C. W. Reynolds. Flocks, herds and schools: A distributed behavorial model. *Computer Graphics*, 27:171–194, 1987.

[8] J. Lin, S. A. Morse, and B.D.O. Anderson. The multi-agent rendezvous problem. *Proceedings of the 42nd IEEE Conference on Decision and Control*, 2:1508–1513, 2003.

[9] J. Lin, S. A. Morse, and B.D.O. Anderson. The multi-agent rendezvous problem - the asynchronous case. *Proceedings of the 43rd IEEE Conference on Decision and Control*, 2:1926–1931, 2004.

[10] J.A. Marshall, Z. Lin, M. Broucke, and B. Francis. Pursuit strategies for autonomous agents. *Lecture Notes in Control and Information Sciences*, pages 137–151, November 2004.

[11] J.A. Marshall, M. Broucke, and B. Francis. Unicycles in cyclic pursuit. *Proceedings of the 2004 American Control Conference, Boston, Massachusetts USA*, 2004.

[12] Z. Lin, B. Francis, and M. Maggiore. State agreement for continuous-time coupled nonlinear systems. *SIAM Journal of Control and Optimization*, 49:622–629, April 2004.

[13] J. Cortes, S. Martinez, and F. Bullo. Robust rendezvous for mobile autonomous agents via proximity graphs in arbitrary dimensions. *IEEE Transactions on Automatic Control*, 51(8), 2006.

[14] J. Cortés, S. Martinez, T. Karatas, and F. Bullo. Coverage control for mobile sensing networks. *IEEE Transactions on Robotics and Automation*, 20(2):243–255, 2004.

[15] K. Laventall and J. Cortés. Coverage control by robotic networks with limited-range anisotropic sensory. *Proceedings of the 2008 American Control Conference, Seattle, Washington USA*, pages 2666–2671, 2008.

[16] A. Kwok and S. Martínez. Coverage control with unicycles via hybrid modeling. *Proceedings of the 2008 American Control Conference, Seattle, Washington USA*, pages 2672–2677, 2008.

[17] J. M. Hendrickx and B.D.O. Anderson. Directed graphs for the analysis of rigidity and persistence in autonomous agent systems. *unpublished manuscript, to appear in International Journal of of Robust and Nonlinear Control*.

[18] H. G. Tanner, A. Jadbabaie, and G.J. Pappas. Stable Flocking of Mobile Agents, Part II: Dynamic Topology. *42nd IEEE Conference on Decision and Control, Maui Hawaii*, December 2003.

[19] T. Eren, P. N. Belhumer, B.D.O. Anderson, and S.A. Morse. A framework for maintaining formations based on rigidity. *Proceedings of the IFAC World Congress*, Barcelona Spain 2002.

[20] R. Olfati-Saber and R. M. Murray. Distributed cooperative control of multiple vehicle formations using structural potential functions. *15th IFAC World Congress , Barcelona, Spain*, July 2002.

[21] C. Yu, J. M. Hendrickx, B. Fidan, B.D.O. Anderson, and V.D. Blondel. Three and higher dimensional autonomous formations: Rigidity, persistence and strutural persistence. *Automatica*, 43(3):387–402, March 2007.

[22] B. D.O. Anderson, C. B. Yu, B. Fidan, and J. M. Hendrickx. Control and information architectures for formations. *Proceedings of the 2006 IEEE International Conference on Control Applications, Munich Germany.*

[23] H. G. Tanner, A. Jadbabaie, and G.J. Pappas. Stable Flocking of Mobile Agents, Part I: Fixed Topology. *42nd IEEE Conference on Decision and Control, Maui Hawaii*, pages 2010–2015, December 2003.

[24] M. Arcak. Passivity as a Design Tool for Group Coordination. *IEEE Transactions on Automatic Control*, 52(8):1380–1390, 2007.

[25] S. Smith, M. Broucke, and B. Francis. Stabilizing a multi-agent system to an equilateral polygon formation. *MTNS*, 2006.

[26] Stabilization of infinitesimally rigid formations of multi-robot networks. L. Krick and M. Broucke and B. Francis. *International Journal of Control*, Submitted January 2008.

[27] M. Cao, C. Yu, S.A. Morse, B.D.O. Anderson, and S. Dasgupta. Controlling a Triangular Formation of Mobile Autonomous Agents. In *The 46th IEEE Conference on Decision and Control (CDC), New Orleans, LA, USA*, pages 3603–3608, December 2007.

[28] M. Cao, C. Yu, S.A. Morse, B.D.O. Anderson, and S. Dasgupta. Generalized Controller for Directed Triangle Formations. In *The 17th International Federation of Automatic Control World Congress (IFAC), Seoul, Korea*, July 2008. preprint.

[29] B.D.O. Anderson, C. Yu, S. Dasgupta, and S.A. Morse. Control of three co-leader formation in the plane. *System and Control Letters*, pages 573–578, 2007.

[30] M. Cao, B.D.O. Anderson, S.A. Morse, and C. B. Yu. Control of acyclic formations of mobile autonomous agents. *preprint*, 2008.

[31] J. Xu. *Theory and Applications of Graphs*. Springer, 2003.

[32] N. Biggs. *Algebraic Graph Theory*. Cambridge University Press, 2nd edition, 1993.

[33] B. Roth. Rigid and flexible frameworks. *American Mathematical Monthly*, 88(1):6–21, 1981.

[34] T. Tay and W. Whiteley. Generating isostatic frameworks. *Structural Toplogy*, 11:21–69, 1985.

[35] B.D.O. Anderson, C.B. Yu, and F. Baris. Information architecture and control design for rigid formations. *Proceedings of the 26th Chinese Control Conference*, pages 2–10, 2007.

[36] T. Eren, W. Whiteley, B.D.O. Anderson, S.A. Morse, and P. N. Belhumer. Information structures to secure control of rigid formations with leader-follower architecture. *American Control Conference, Portland, Oregon USA*, pages 2966–2970, June 8-10 2005.

[37] R. Olfati-Saber and R. M. Murray. Graph rigidity and distributed formation stabilization of multi-vehicle systems. *Proceedings of the 41st Conference on Decision and Control, Las Vegas, Nevada USA*, December 2002.

[38] T. Jordàn J. Bang-Jensen. On persistent directed graphs. *Networks*, to appear, 2007.

[39] T.H. Cormen, C.E. Leiserson, R.L. Rivest, and C. Stein. *Introduction to Algorithms*. MIT Press, 2001.

[40] H. Sira-Ramírez and S. K. Agrawal. *Differentially Flat Systems*. Marcel Dekker, 2004.

[41] Z. Lin, M. Broucke, and B. Francis. Local control strategies for groups of mobile autonomous agents. *IEEE Trans. Automatic Control*, pages 622–629, 2004.

[42] Z. Lin, B. Francis, and M. Maggiore. Necessary and sufficient graphical conditions for formation control of unicycles. *IEEE Trans. Automatic Control*, pages 121–127, 2005.

[43] B. Francis. Course Notes ECE1635, Distributed Control of Autonomous Agents, University of Toronto. 2007.

[44] L. Krick. Application of Graph Rigidity in Formation Control of Multi-Robot Networks. Master Thesis supervised by M. Broucke and B. Francis, University of Toronto, 2007.

[45] H. Bai, M. Arcak, and J. T. Wen. Group coordination when the reference velocity is available only to the leader: an adaptive design. In *Proceedings of the 2007 American Control Conference*, pages 5400–5405, New York, NY, 2007.

[46] H. Bai, M. Arcak, and J. T. Wen. Adaptive motion coordination: Using velocity feedback to achieve parameter convergence. *Proceedings of the 2008 American Control Conference, Seattle, Washington USA*, pages 759–764, 2008.

[47] H. Ando, Y. Oasa, and M. Yamashita. Distributed memoryless point convergence algorithm for mobile robots with limited visibility. *IEEE Transactions on Robotics and Automation*, 15(5), 1999.

[48] J. Dold. Digital Control of Mobile Robots in Formation. Diploma Thesis supervised by B. Francis, University of Toronto, 2007.

[49] H. Khalil. *Nonlinear Systems*. Prentice Hall, 3rd edition, 2000. International edition.

[50] W. Hahn translated by A. P. Baartz. *Stability of Motion*. Springer, 1967.

[51] N.P. Bathia and G.P. Szegö. *Stability Theory of Dynamical Systems*. Springer, 1970.

[52] N. Rouche, P. Habets, and M. Laloy. *Stability Theory by Lyapunov's Direct Method*. Springer, 1977.

[53] D.V. Anosov and V. I. Arnol'd. *Dynamical System I*. Springer, 1985.

[54] A. N. Michel, K. Wang, and B. Hu. *Qualitative Theory of Dynamical Systems. The Role of Stability-Preserving Mappings*. MAIK Nauka/Interperiodica distributed exclusively by Springer Science+Business Media LLC., New York, NY, USA, 2nd edition, 2000.

[55] Y. Lin, E. D. Sontag, and Y. Wang. A smooth converse lyapunov theorem for robust stability. *SIAM J. Control Optim.*, 34(1):124–160, 1996.

[56] Y. Lin, E. Sontag, and Y. Wang. Lyapunov-function characterizations of stability and stabilization for parameterized families of systems. *Decision and Control, 1993., Proceedings of the 32nd IEEE Conference on*, 3:1978–1983, December 1993.

[57] A. E. Bryson Jr. and Y.-C. Ho. *Applied Optimal Control*. Hemisphere Publishing Cooperation, revised printing 2005 edition, 1975.

[58] T. L. Vincent and W. Jervis. *Nonlinear Optimal Control Systems*. John Wiley and Sons, Inc., 1997.

[59] S. S. Sastry. Lectures in optimal control and dynamic games. *Coure Notes EECS290A, Advanced Topics in Control Theory, University of Berkeley, California*, 1966.

[60] L.S. Pontryagin, V.G. Boltyanskii, R.V. Gamkrelidze, and E.F. Mishchenko. *The Mathematical Theory of Optimal Processes*. Wiley, New York, 1962.

[61] R. Bellman. *Dynamic Programming*. Princeton University Press, 1957.

[62] M. Athans and P. L. Falb. *Optimal Control: An Introduction to the Theory and its Applications*. McGraw-Hill, 1966.

[63] P.P. Varaiya. *Lecture Notes on Optimization*. New York, Van Nostrand Reinhold, 1972. http://paleale.eecs.berkeley.edu/~varaiya/papers_ps.dir/NOO.pdf.

[64] A. Melikyan, A. Akhmetzhanov, and N. Hovakimyan. On initial value and terminal value problems for hamilton–jacobi equation. *Systems and Control Letters*, 56:714–721, 2007.

[65] R.F. Hartl and S.P. Sethi. A note on the free terminal time transversality condition. *Zeitschrift für Operations Research*, 27:203–208, 1983.

[66] C.I. Byrnes and C.F. Martin. An integral-invarianc principle for nonlinear systems. *IEEE Transactions on Automatic Control*, 40(6):983–994, June 1995.

[67] R. L. Eberhart. Stability of optimal control systems. *Proceedings of the 36th Conferrence on Decision and Control, San Diego, California USA*, December 1997.

[68] R. Sepulchre, M. Janković, and P. Kokotović. *Constructive Nonlinear Control*. Springer, 1997. http://montefiore.ulg.ac.be/services/stochastic/pubs/1997/SJK97a.

[69] R. A. Freeman and P.V. Kokotović. Inverse optimality in robust stabilization. *SIAM J. Control and Optimization*, 34(4):1365–1391, July 1996.

[70] R. A. Freeman and P.V. Kokotović. *Robust Nonlinear Control: State Space and Lyapunov Techniques*. Springer, 1996.

[71] S. MacLane and G. Birkhoff. *Algebra*. AMS Chelsea Publishing, American Mathematical Society, Providence, Rhode Island, 1999.

[72] R. Boudarel, J. Delmas, and P. Guichet. *Dynamic Programming and its Application to Optimal Control*. Acadmic Press, 1971.

[73] J.C. Willems. Dissipative dynamical systems part i: General theory. *Archive for Rational Mechanics and Analysis*, 45:321–351, January 1972.

[74] R. Bhatia. *Matrix Analysis*. Springer, 1997.

[75] M. Spivak. *Differential Geometry*, volume 1. Publish or Perish, Inc., 1977.

[76] W. M. Boothby. *An Introduction to Differentiable Manifolds an Riemanian Geometry*. Academic Press Inc., 1986.

[77] F. W. Warner. *Foundations of Differentiable Manifolds and Lie Groups*. Springer, 1994.

[78] V. Guillemin and A. Pollack. *Differential Topology*. Prentice-Hall, 1974.

[79] V. I. Arnol'd. *Ordinary Differential Equations*. Springer, 1992.

[80] S. Wiggins. *Introduction to Aplied Nonlinear Dynamical Systems and Chaos*. Springer, 2nd edition, 2000.

[81] N. Fenichel. Persistence and smoothness of invariant manifolds for flows. *Ind. Univ. Math. J.*, 21:193–125, 1971.

[82] N. Fenichel. Asymptotic stability with rate conditions. *Ind. Univ. Math. J.*, 23:1109–1137, 1974.

[83] N. Fenichel. Asymptotic stability with rate conditions ii. *Ind. Univ. Math. J.*, 26:81–93, 1971.

[84] S. Wiggins. *Normally Hyperbolic Invariant Manifolds in Dynamical Systems*. Springer, 1991.

[85] L.J. Corwin. *Multivariable Calculus*. CRC Press, 1982.

[86] T. M. Apostol. *Mathematical Analysis*. Addison-Wesley Publishing Company Inc., 1957. 4th printing, 1964.

[87] F. Zhang. *The Schur Complement and its Applications*. Springer, 2005.

[88] N. Motee, A. Jadbabaie, and B. Bamieh. On decentralized optimal control and information structures. *Proceedings of the 2008 American Control Conference, Seattle, Washington USA*, 2008.

[89] R. Isaacs. *Differential Games*. Courier Dover Publications, 1965.

[90] D. Gu. A differential game approach to formation control. *IEEE Transactions on control systems technlogy*, 16(1):85–93, 2008.